



BETTER SHIPS, BLUE OCEANS

Propeller design review and exploratory studies

Report No. : 32992-1-POW
Date : February 2023
Version : 1.0
Final Report

Propeller design review and exploratory studies

MARIN order No. : 32992
MARIN Project Manager : John Huisman

Number of pages : 147

Ordered by : DYKSTRA NAVAL ARCHITECTS
Kruithuisstraat 21
1018 WJ AMSTERDAM

Order document : Email dated 2 September 2022,
Quotation "220826 Quotation 32992 SHIPS_POW_v2.0.pdf"
Reference : Project ZERO

Reported by : ir. T.J. Huisman
Reviewed by : dr. ir. E.J. Foeth

Version	Date	Version description
0.3	23-12-2022	Draft Report
0.4	16-01-2023	Final Draft Report
1.0	26-01-2023	Final Report

MANAGEMENT SUMMARY

Dykstra Naval Architects commissioned MARIN to study the two thrusters for the sailing yacht ZERO. The objective was to determine the performance of both thrusters generating of power while sailing, and, the performance during propulsion.

A feasibility study was performed whether the computational tool PROCAL as used for propeller design is also suited to compute the performance in terms of thrust and power in the envisioned range of operation of the propellers during regeneration. This study showed that PROCAL was suited with sufficient accuracy.

Propeller manufacturer Hundested provided preliminary designs of both propellers and thrusters via DYKSTRA. The first objective of this project was to assess the performance of both Hundested thrusters and propellers in both propulsion and regeneration mode according to the operational scenarios as provided by Dykstra.

Three CFD computations were performed using RANS-BEM to obtain the wake fields of the ship and thrusters both in regeneration and propulsion. For propulsion the wake field was determined both with feathered and working front propeller. CFD computations were performed using RANS-BEM on both thrusters to determine the open water characteristics, both in propulsion and regeneration mode.

Polynomials as function of propeller pitch and advance coefficient for both propulsion and regeneration mode were determined, for both the front and aft thruster. This polynomial can be integrated into the performance prediction programs.

Using the polynomials, based on the usage scenarios, operational conditions were determined in terms of propeller pitch and propeller rotational speed for both propulsion and regeneration. It was shown that hydrodynamically it is more efficient to propel or regenerate with a lightly driven front or aft propeller, respectively.

Using computational tools MARIN analysed the performance of the propeller designs in terms of powering, regeneration and cavitation behaviour. The HUNDESTED propellers are cavitating both in propulsion at 12 knots and regeneration at 16 knots. At 12 knots propulsion, the propeller hull excitation with a pressure fluctuation of 2.0 kPa clearly exceeds the usual limit of 1.0 kPa. The computations show that the propellers could need some adjustment in terms of the camber distribution to better balance the cavitation margins. The cavitation performance in propulsion is strongly related via the camber and pitch distributions to the cavitation performance while regenerating.

The second objective of this project was to provide propeller design support. Therefore, exploratory design studies were performed to provide further design directions for the final design of the propellers. It was shown that improvements of about 3% in power regeneration were possible while the propulsive performance could be improved by about 1%, whilst also improving the cavitation behaviour. It was found that improving on the power consumption in propulsion is in general also beneficial for the power regeneration during sailing.

Finally, it is recommended to adapt the geometry of the strut of the thrusters, which were shown to be sensitive to flow separation which hampers the propeller performance in terms of cavitation and shaft excitation forces during propulsion.

CONTENTS	PAGE
MANAGEMENT SUMMARY	ii
1 INTRODUCTION.....	1
1.1 PHASE 1: Applicability of PROCAL	1
1.2 PHASE 2: Design review.....	1
1.2.1 Wake field computations	1
1.2.2 Open water characteristics.....	2
1.2.3 Analysis and assessment of operational performance	2
1.3 PHASE 3: Multi-objective design exploration	2
2 DESIGN INPUT.....	3
2.1 Geometry	3
2.2 Operational scenarios.....	4
2.3 Hull resistance	4
3 COMPUTATIONAL METHODS.....	5
3.1 REFRESCO.....	5
3.2 PROCAL.....	6
3.3 RANS-BEM.....	7
3.4 PROPART	7
4 APPLICABILITY OF PROCAL.....	9
5 RESULTS AND DISCUSSION	10
5.1 Open water computations.....	10
5.1.1 Propulsion polynomial.....	10
5.1.2 Regeneration polynomial	11
5.2 CFD computations	12
5.3 Propeller analysis, feathered.....	18
5.4 Propeller analysis, propulsion.....	19
5.4.1 Pressure distributions.....	20
5.4.2 Cavitation inception	22
5.4.3 Cavitation behaviour	24
5.4.4 Underwater radiated noise	26
5.4.5 Radial loading distribution	26
5.4.6 Hull pressure excitation.....	27
5.4.7 Thrust variation	28
5.4.8 Discussion points	29
5.5 Propeller analysis, regeneration	30
5.5.1 Pressure distributions.....	32
5.5.2 Cavitation inception.....	34
5.5.3 Cavitation behaviour	36
5.5.4 Underwater radiated noise	38
5.5.5 Radial loading distribution	39
5.5.6 Hull pressure excitation.....	40
5.5.7 Thrust variation	41
5.5.8 Discussion points	41
5.6 Propeller analysis, other requirements, bollard pull	42
6 EXPLORATORY DESIGN OPTIMISATION	43
6.1 Selected design conditions.....	43
6.2 Geometry parametrisation	43
6.3 Optimisation approach.....	45

6.4	Optimisation results aft propeller	46
6.5	Optimisation results front propeller	50
6.6	Discussion points.....	53
7	CONCLUSIONS AND RECOMMENDATIONS	54
Table pages		T1 – T2
Figure pages		F1 – F57
APPENDIX I : List of symbols		A1.1 – A1.8
APPENDIX II : Procedures of model tests.....		A2.1 – A2.10
DOCUMENTATION SHEETS:	PROCAL	
	ReFRESCO	
	Propeller Design Support & Evaluation	

1 INTRODUCTION

By email dated June 8, 2020, Dykstra Naval Architects contacted MARIN. In a video call on June 11, 2020, Dykstra Naval Architects requested MARIN to provide a quotation for a study into the usage of the propeller for the generation of power while sailing with wind propulsion. The objective was to show the balance and trade-offs between the propulsion and generation mode using multi-objective optimisation.

Following up, in a video call on August 24, 2022, Dykstra Naval Architects requested MARIN to provide an update to the quotation. The project has evolved and named *Project ZERO*. Hundested was selected as propeller manufacturer. The sailing yacht will be equipped by two CPP pushing thrusters without ducts, a smaller one before the keel optimised for regeneration, and a larger unit after the keel optimised for propulsion. Hundested provided preliminary designs of both the propellers and the thrusters for evaluation and design checks by MARIN.

By email, dated September 2, 2022, DYKSTRA commissioned MARIN to perform this work according to MARIN quotation "220826 Quotation 32992 SHIPS_POW_v2.0.pdf".

Power will be regenerated while the azimuth thruster is turned around. The propeller is now operating in its so-called third quadrant with - from the propellers point of view - a negative rate of revolutions and negative ship speed. In this third quadrant the camber of the blade profiles and shape of the propeller pitch is more favourable than with the thruster in its propulsion position and with the propeller trailing in the flow. Operating in the third quadrant means that the trailing and leading edge switch and the propeller will require more or less symmetric blade profiles if the propeller is also to be used for propulsion.

The goal is to assess the performance of both propellers in propulsion and regeneration modes.

1.1 PHASE 1: Applicability of PROCAL

A feasibility check needs to be performed whether the computational tool PROCAL as used for propeller design is suited to compute the performance in terms of thrust and power in the envisioned range of operation of the propellers. Validation will be performed with recently conducted 4-quadrant measurements of the F-series. If this succeeds, PROCAL can be used for the analysis of propulsion and generation.

1.2 PHASE 2: Design review

Hundested provided via Dykstra preliminary designs of both the propellers and the thrusters for evaluation and design checks by MARIN.

The first goal of this project is to assess the performance of both Hundested thrusters and propellers in both propulsion and regeneration according to the operational scenarios as provided by Dykstra. The following subsections describe the required scope of work to achieve this goal.

1.2.1 Wake field computations

The wake field of the ship at the location of both thrusters is required, which may include the boundary layer of the ship, and for the aft thruster the wake from the keel, (feathered) front propeller and thruster. MARIN computed the effective wake fields to capture the effect of the front propeller on the aft propeller in both propulsion mode and regeneration mode.

Using a RANS-BEM computations, the effective wake field for the rear propeller will be determined with the thruster in pushing mode. A double body CFD approach will be used for simplicity. DYKSTRA provided the resistance characteristics of the ship.

The front propeller will be considered both in propulsion and feathered position. The feathered mode will probably be the most common mode for propulsion.

In addition to the required effective wake field in behind-ship situation, this computation gives the difference between the open water performance and the in-behind performance of the thruster, which provides the propulsion factors.

1.2.2 Open water characteristics

Using the RANS-BEM approach, open water characteristics of the thrusters and the propellers will be computed for both the first and third quadrant of operation. The computations provide the thruster resistance and propeller torque and thrust. The pressure distributions on the thruster bodies were studied. These computations also give the effective wake field from the pushing thruster.

1.2.3 Analysis and assessment of operational performance

The propeller design evaluation involves a study into the feasibility of the propeller designs provided by Hundested, by calculations and comparison to MARIN's database and MARIN's experience. For each condition MARIN will advise the client regarding the:

- propeller performance in terms of thrust (or drag) and torque;
- cavitation characteristics and cavitation noise (if any), both in terms of sheet cavitation and tip vortex cavitation, and the risk of cavitation erosion;
- hull-pressure excitation;
- cavitation-inception speed and characteristics;
- possible points of improvement on both propellers.

If the proposed design propellers show room for improvement, MARIN will provide the design suggestions to the propeller manufacturer. Since the main work involves preparations, setup of the computations and checks, updated propeller designs can be evaluated relatively quickly at reduced cost.

1.3 PHASE 3: Multi-objective design exploration

Based on the preliminary designs by Hundested, a further design scan will be done by the multi-objective propeller optimisation toolbox PropArt. Thousands of geometry variants will be assessed with PROCAL computations, steadily converging towards the optimum.

PropArt searches for the best propeller geometry as a function of the specified objectives and constraints, such as the limits on the spindle torque and propeller cavitation. The propeller will be fully parametrised in pitch, camber, thickness, skew and chord and blade profiles. The optimisation study will show the trade-off between propulsion and generation.

The second objective of this project is to provide propeller design support. This will be done using explorative studies towards the optimum blade shape of the propellers.

2 DESIGN INPUT

2.1 Geometry

Both propellers were included in the 3D model of the ship as shown in Figure 2-1. The propellers were also supplied in tabular format.

Table 2-1: Summary of supplied input files.

3D model of the ship, including propellers	24-00 Linesplan 3D Lns 087 Keel05 Rudd04 Thr02.3dm
Front propeller	SPS286 Forward unit Blade design 14-09-2022.xlsx
Aft propeller	SPS386 Aft unit Blade design 13-09-2022.xlsx
Scenarios and ship resistance	Operational scenarios for prop optimization.pdf

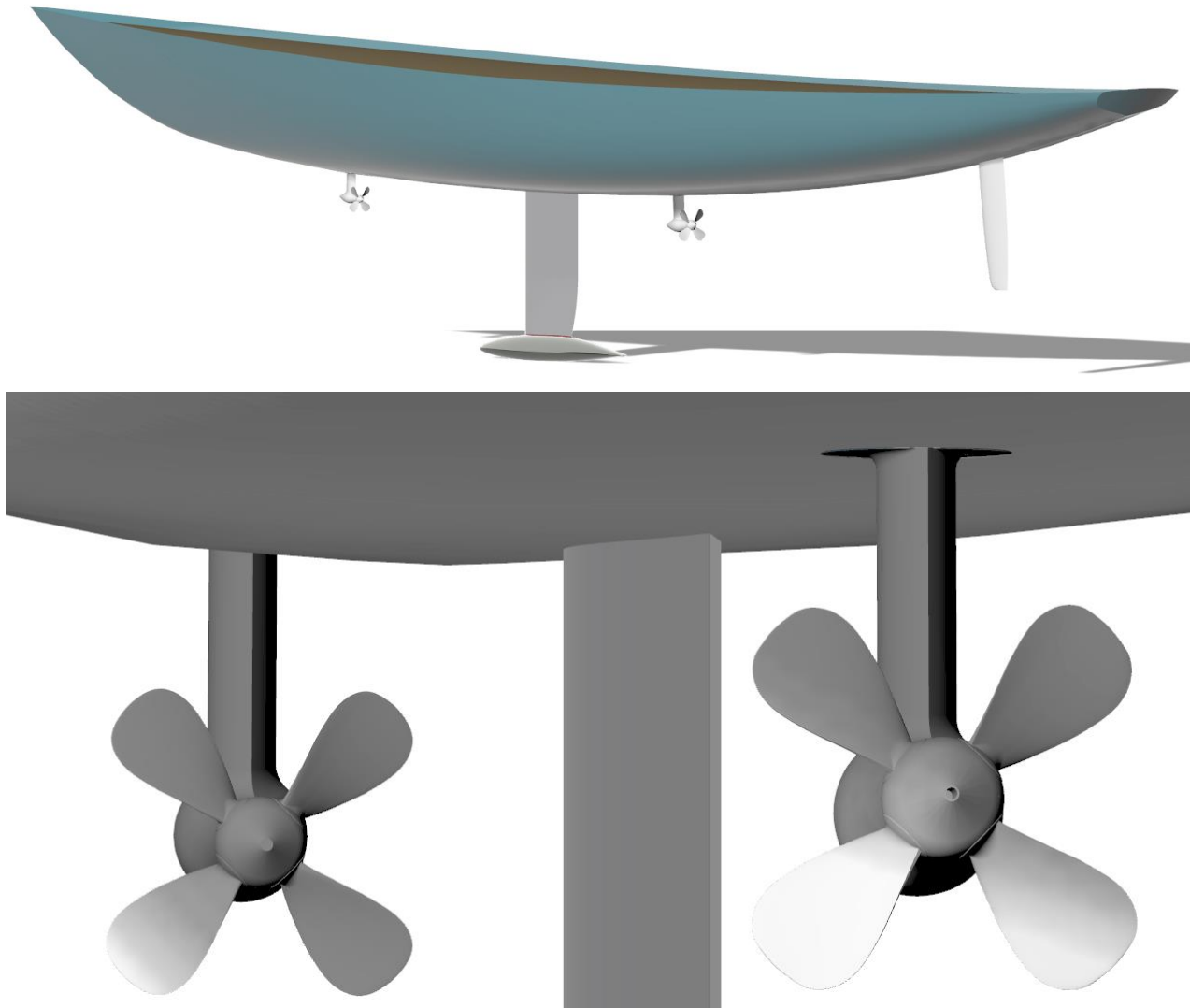


Figure 2-1: Renderings of yacht ZERO with HUNDESTED thrusters front and aft.

2.2 Operational scenarios

Operational scenarios were provided by Dykstra. The ship is powered by sails and propellers which can be used in different combinations.

CHARTER MODE

1. Maximum regeneration with both props at 16 knots ship speed with an expected total power generation of 250 kW.
2. Intermediate speed motoring for short stretches, delivered by one or two propeller; to be investigated what combination is best. Ship speed of 12 knots, at an approximate power of 380 kW.

CROSSING / DELIVERY MODE

3. Regeneration mode with both props active at 14 knots ship speed with expected total power generation of 125 kW.
4. Light regeneration by the front propeller only and the aft propeller probably feathered. The ship speed is 10 knots and the regenerated power is 20 kW. At ship speeds over 10 knots, the aft propeller would probably be used for regeneration as well.
5. Free sailing with both propellers feathered at a ship speed of 8 knots.
6. Motorsailing on the aft propeller, front propeller either feathered or lightly driven to reduce drag. The ship speed is 10 knots and the total propulsion power is 50 kW.
7. Economic motoring for maximum range (no wind) on the aft propeller, with the front propeller either feathered or lightly driven to reduce drag. Ship speed is 8 knots, at an approximate power of 100 kW.

OTHER REQUIREMENTS

8. Maximum power on both propellers in bollard pull condition in order to sail away from a lee-shore.

Two more scenarios were provided by Dykstra. However, during discussions it was agreed to leave the analyses for those two scenarios out of the scope of work.

9. Manoeuvring, using the thrusters sideways.
10. Crash stop (by changing pitch).

2.3 Hull resistance

The following information regarding the hull resistance was provided by Dykstra:

Vs [kts]	Resistance [kN]	Windage TWS=0 [kN]	Total [kN]
6	7.55	0.69	8.2
8	11.6	1.23	12.8
10	18.8	1.92	20.7
12	29.5	2.77	32.3
14	44.0	3.76	47.8
16	71.5	4.92	76.4

Drag additions for rudder and various small items were added already by DYKSTRA.

3 COMPUTATIONAL METHODS

3.1 REFRESCO

MARIN performed simulations with the RANS solver ReFRESCO, see www.refresco.org. It solves the incompressible viscous flows based on the Navier-Stokes equations. Double-body simulations are used which use a steady approach, converging the simulation until the flow features and forces stabilise. The results are presented in the form of pressure coefficient and friction coefficient ratio on the hull surface and the velocity and headloss in the flow.

The pressure coefficient is defined as:

$$C_p = \frac{P - P_{hs}}{\frac{1}{2} * \rho * V_s^2}$$

With:

P	= pressure in [Pa]
P_{hs}	= hydrostatic pressure in [Pa]
ρ	= water density in [kg/m ³],
V_s	= ship speed in [m/s]

The friction coefficient ratio is defined as:

$$C_{f,ratio} = \frac{C_f}{C_{f,ref}}$$

With C_f , the local skin friction coefficient, defined by:

$$C_f = \frac{\tau}{\frac{1}{2} * \rho * V_s^2}$$

Where τ is the shear stress, in [Pa]. The reference flat-plate skin friction coefficient $C_{f,ref}$ is defined by:

$$C_{f,ref} = 0.37 \times \log_{10}(R_{e,l})^{2.584}$$

Where $R_{e,l}$ is the local Reynolds number:

$$R_{e,l} = \frac{\rho V_s \Delta_x}{\mu}$$

With Δ_x the distance from the bow to the local point in [m] and μ the water viscosity in [kg.s/m].

The 3D flow features are presented using slices of normalised X velocity, head loss and X vorticity. Regions of reversed flow are given as well (regions where the flow follows the ship). The headloss gives a clear impression of the energy loss in the wake of the ship and is defined as follows:

$$H_l = 1 - \left(\left(\frac{\|\vec{V}\|}{V_s} \right)^2 + C_p \right)$$

The normalised X Velocity is defined as follows:

$$u = \frac{V_x}{V_s}$$

Where V_x is the X velocity component in [m/s]

The X Vorticity is defined as follows:

$$\omega_x = \Omega_x \times \frac{L_{pp}}{V_s}$$

Where Ω_x is the X component of the vorticity vector.

3.2 PROCAL

Propeller computations were done with PROCAL, a boundary element method (BEM) which computes the inviscid flow around the propeller within the ship's wake field. Besides efficiency, the calculations give the pressure distribution and the extent and dynamics of the sheet cavitation developing on the propeller blades. PROCAL has been developed by MARIN within the Cooperative Research Ships (CRS) framework. The input for PROCAL is an operational condition in terms of speed and rotation rate.

Although the tip vortex is not computed in PROCAL, separate models are used to compute the strength of the tip vortex and inception and noise. The Empirical cavitating Tip Vortex (ETV) model is used which is an engineering model developed at MARIN.

PROCAL can be used to predict the cavitation inception buckets for sheet-cavitation and tip-vortex cavitation for both pressure-side and suction-side cavitation. A range of propeller loading coefficients is computed with PROCAL providing the pressure distributions on the propeller blade, while the ETV model provides an estimate of the cavitation inception of the tip vortices, which are usually the dominant types of cavitation in terms of inception speed.

PROCAL was used with a computational mesh including the actual hub shape. PROCAL takes the effective wake field from the RANS-BEM coupling, described further in Section 3.3, such that the flow including the suction effect of the propellers is included. The effective wake methodology ensures that the inflow is similar as compared to (more computationally expensive and more laborious) full RANS computations with sliding interface in which the propeller is fully modelled in a viscous flow simulation. Although details of interaction of tip vortices is not captured, the mean flow which governs the propeller performance is computed sufficiently accurate. The method is widely used and sufficiently validated.

The results are presented using the normalised pressure coefficient CPN and cavitation inception number σ_N , which are defined as:

$$\text{CPN} = \frac{p - (p_a + \rho g h_s)}{\frac{1}{2} \rho n^2 D^2} \quad \sigma_N = - \frac{p_v - (p_a + \rho g h_s)}{\frac{1}{2} \rho n^2 D^2}$$

with p pressure, p_a the atmospheric pressure, $\rho g h_s$ the hydrostatic pressure at the shaft, p_v the vapour pressure, ρ water density, n rotational speed and D the propeller diameter. Using this definition, CPN can directly be compared with the cavitation number σ_N in the calculations. If $-\text{CPN}$ exceeds σ_N , or if $p = p_v$, inception of cavitation will occur after which the cavitation extent is computed. When at a location the pressure drops below the vapour pressure, cavitation will occur.

The results in terms of propulsion are reported in terms of the advance coefficient J , thrust coefficient K_T and torque coefficient K_Q , as further provided in the appendices.

For power regeneration, the results are presented as function the hydrodynamic pitch angle β which is defined as

$$\beta = \arctan \frac{V}{0.7\pi n D}$$

The propeller thrust and torque, are made non-dimensional by the relative resultant velocity at 0.7R radius and defined as,

$$V_r = \sqrt{V^2 + (0.7\pi n D)^2}$$

The propeller thrust coefficient is defined as:

$$C_T = \frac{T}{\left(\frac{1}{2} \rho V_r^2\right) \frac{\pi}{4} D^2}$$

The propeller torque coefficient is defined as:

$$C_Q = \frac{Q}{\left(\frac{1}{2}\rho V_r^2\right) \frac{\pi}{4} D^3}$$

The regeneration efficiency is defined as

$$\eta_{regen} = \frac{P}{VT} = \frac{C_Q}{C_T} \frac{2}{0.7 \tan(\beta)}$$

Finally, the power coefficient is defined as

$$C_P = \frac{P}{P_{flow}} = \frac{2C_Q \left(1 + \frac{1}{(\tan \beta)^2}\right)}{0.7 \tan \beta}$$

with propeller power $P = 2\pi nQ$ and flow power $P_{flow} = \frac{1}{2}\rho V^3 \frac{\pi}{4} D^2$

3.3 RANS-BEM

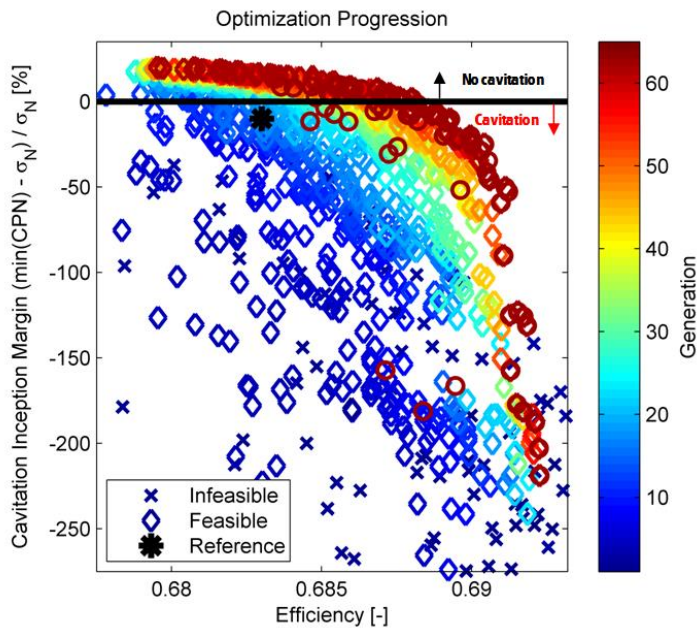
In RANS-BEM the flow around the thruster housing is calculated by means of RANS, while the flow around both propellers is calculated by means of the boundary element method (BEM) PROCAL. Doing so, the mutual interaction between the hull, thruster and propeller is calculated. In the RANS simulations the action of the propeller is represented by force fields that follow from PROCAL calculation of the propeller. The PROCAL calculation requires the effective inflow to the propeller. These effective wake fields follow from the total velocity field according to RANS minus the propeller induced velocities according to a previous PROCAL calculation. This iterative process is repeated until converged.

This method is successfully validated with RANS-RANS sliding interface computations and model tests. The RANS-BEM approach is attractive in terms of cost and computational effort compared to a sliding interface approach.

3.4 PROPART

Within MARIN and the CRS, the multi-objective optimisation method PropArt has been developed for propeller design optimisation studies. A parametric propeller geometry is coupled to an optimisation algorithm. PROCAL computations are performed for a large number of propeller geometries with varying radial distributions. After the PROCAL computations, often in multiple design conditions, the performance is evaluated in terms of cavitation behaviour, efficiency and strength requirements. PropArt contains the implementation of the EU EROCAV design guidelines to judge the risk of cavitation erosion.

A propeller design is always a compromise and by using optimisation techniques, the best balance between the objectives can be demonstrated using Pareto front plots as shown in the following figure. All dots in the figure represent a particular propeller design. As the design process advances, better propellers are created. This is shown in the figure as going from the earlier designs in blue to the latest ones in red. The Pareto front is given by the propellers represented by the dark red dots. This figures demonstrates that the margin against cavitation cannot be improved without compromising efficiency.



Example of optimisation case with final Pareto front in red. Both the margin against cavitation and efficiency were to be maximised.

In an early phase of the project, the results of a propeller design optimisation study can provide the opportunity for the client to develop a challenging but achievable set of design criteria for the propeller design.

A propeller design by MARIN is often used as a benchmark and for comparison with other propeller designs from the industry, therewith serving as a quantification of the quality of the designs in terms of the imposed design objectives and constraints. The MARIN propeller then acts a competing reference for any third-party propeller designs, but can also be selected as the final propeller to be installed on the ship.

Propeller design optimisations focus at the minimisation of sheet cavitation, correct strength of the tip-vortex and avoidance of cavitation erosion, while achieving high efficiency.

The radial distributions chord, skew, rake, pitch, camber and thickness will be given freedom, after which the computational framework creates thousands of geometries, converging towards the best possible propeller designs. Then, the best propeller will be selected from the Pareto Front for further study.

4 APPLICABILITY OF PROCAL

A feasibility check was performed whether the computational tool PROCAL as used for propeller design and analysis is suited to compute the performance in terms of thrust and power in the envisioned range of operation of the propellers, also including regeneration in the third quadrant.

Similarly to the tuning that is done for propulsion (PROCAL is tuned on the database of propellers at MARIN), also tuning was done for regeneration, based on the recent F-series.

The differences between regeneration and propulsion mode with regards to the accuracy of PROCAL is comparable. The prediction of PROCAL in the operational area (CQ between 0.05 and 0.2, increasing with pitch) is generally within few percent accurate with respect to the model tests.

Outside the normal operational range, when the propeller is either highly loaded or very lowly loaded, the prediction of PROCAL deviates due to the occurrence of strong vortices leading edge vortices which are not captured by PROCAL. This effect is visible both in propulsion and regeneration.

In terms of regeneration efficiency the trends and levels are well predicted by PROCAL. At low CP, however, there is some larger deviation. The results are regarded as remarkably good. The efficiency curves in propulsion mode show similar comparison.

Note that PROCAL treats regeneration as negative, thereby providing negative thrust, negative power, negative circulation and suction side is regarded pressure side during post-processing.

5 RESULTS AND DISCUSSION

5.1 Open water computations

CFD computations using RANS-BEM were performed on a set of 20 conditions for both the aft and front thruster in open water without the ship to determine the open water characteristics in terms of thrust and torque as function of advance ratio. The resistance of the thruster and the effective inflow in the propeller follow from the RANS computation, while the propeller thrust and torque are computed by the BEM computation with PROCAL. Figure 5-1 gives a visualisation.

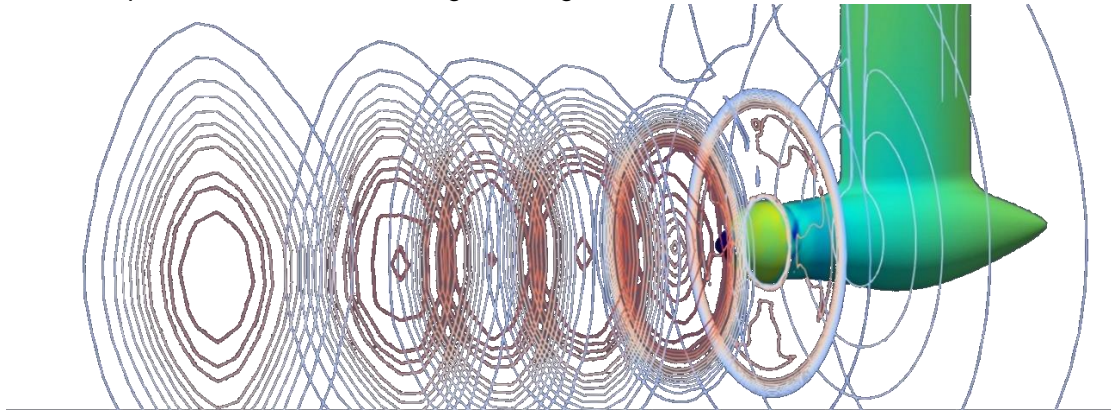
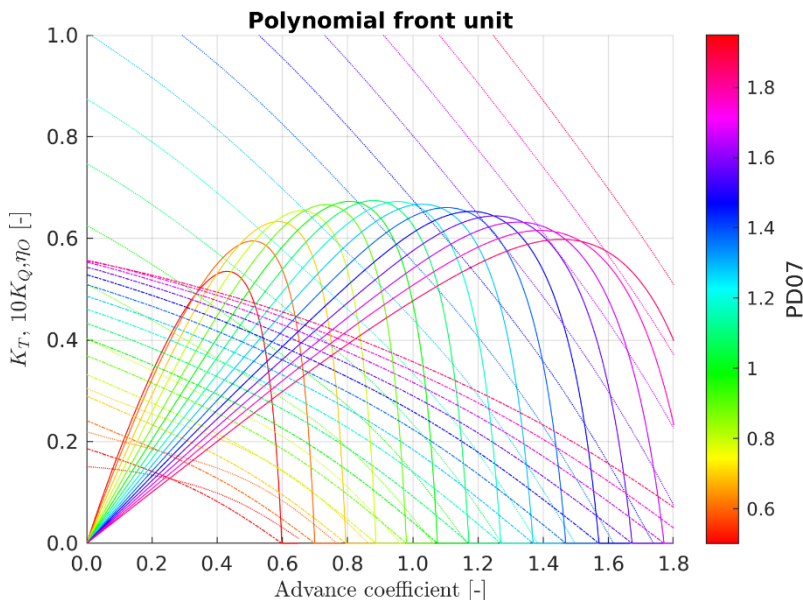


Figure 5-1: Visualisation of velocity slices with low and high velocity in blue and red, respectively.

5.1.1 Propulsion polynomial

For the analysis of the scenarios a reduced factorial polynomial was created based on PROCAL computations at different J value and different pitch. The set of 20 RANS-BEM computations was analysed, which was further used to compute a set of 600 PROCAL computations for both the front and aft propeller. A MARIN standard and maybe in this case somewhat conservative correlation allowance was used to correct the thruster force from CFD to account for bolts, anodes, gaps, roughness and other factors.

The polynomial is presented on page T1. Both the unit thrust coefficient K_{T_u} and the propeller thrust coefficient K_{T_p} are provided as well as the power coefficient K_Q . The thruster performance K_{T_u} is visualised in Figure 5-2. For the front unit in a P07/D range of 0.5 to 1.95 and for the aft unit in a P07/D range of 0.5 to 1.8 with steps of 0.1.



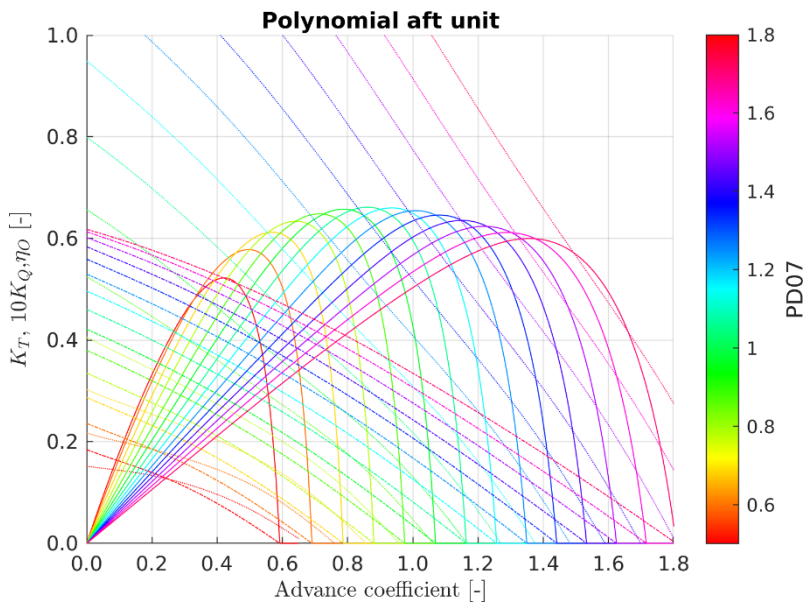


Figure 5-2: Polynomial description of the open water performance of the thruster.

5.1.2 Regeneration polynomial

The Hundested propellers were extensively computed with RANS-BEM and PROCAL in the third quadrant for a range of beta and pitch. A reduced factorial polynomial was made for both the front and aft unit, as given in the table on page T2. The polynomial was optimised to capture the peak efficiency and peak CP correctly and is intended to be used in that area of operational only. This polynomial should be evaluated for beta in radians minus pi. For pitch the polynomial is usable between $P_{0.7}/D = 0.5$ and $P_{0.7}/D = 2.4$. Both the unit thrust and the propeller thrust are provided. Figure 5-3 provides a visualisation of the polynomial as function of propeller pitch, in steps of 0.05.

The corresponding efficiency and CP are plotted in Figure 5-4. There are subtle differences between the front and aft unit, both due to the propeller design, the design pitch and the resistance of the thruster body and strut. At higher pitch the differences become higher, where the larger resistance (due to more flow separation) of the front thruster (dimensionless) yields lower efficiency.

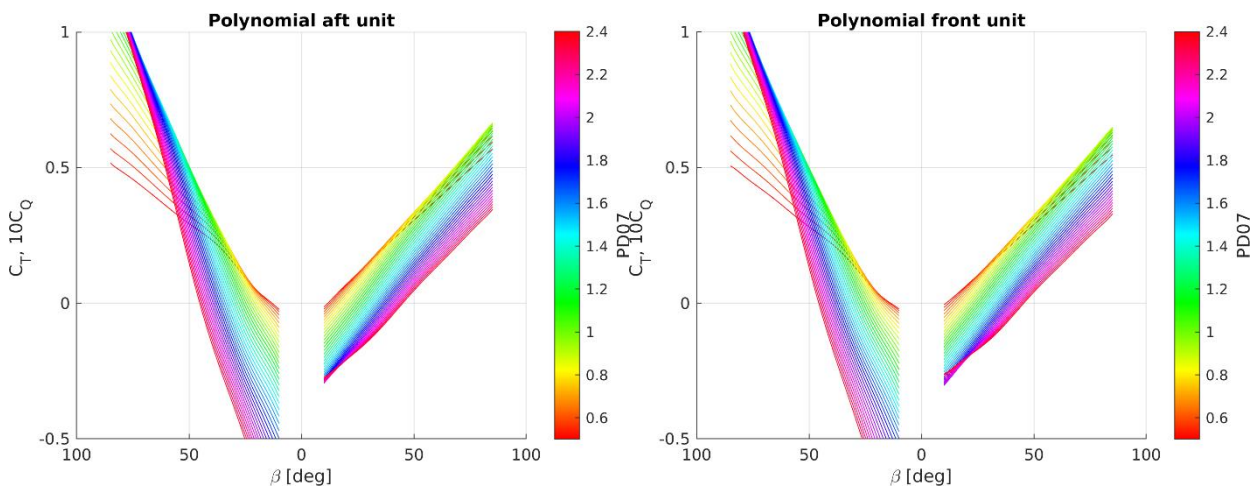


Figure 5-3: Polynomial of C_T and C_Q for the aft and front unit.

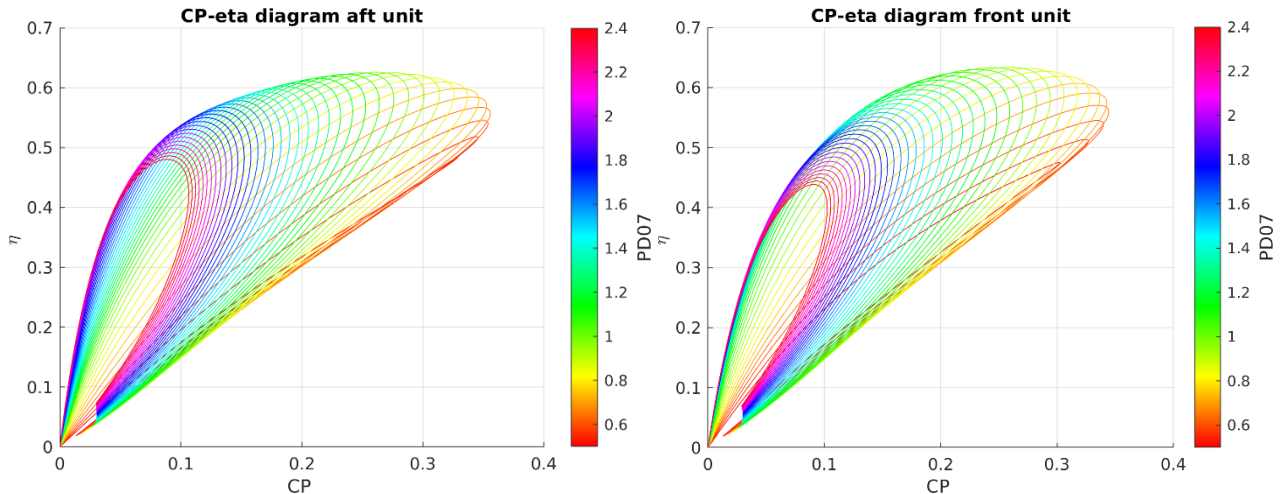


Figure 5-4: Polynomial presentation of the regeneration power and efficiency for the aft and front unit.

5.2 CFD computations

Three CFD computations were performed using the RANS-BEM approach:

1. 12 knots, both propellers working, as shown in Figure 5-5 and on pages F1 to F7.
2. 12 knots, front propeller feathered, as shown in Figure 5-6 and on pages F8 to F14.
3. 16 knots, both propellers regenerating, as shown in Figure 5-7 and Figure 5-8 and on pages F15 to F21.

Figure 5-5 shows the axial velocity profiles V_x . The ship sails at 12 knots, represented by $V_x = 1.0$. Both the front and aft propeller accelerate the flow. The boundary layer of the ship is also becoming visible near the aft part of the hull. Using some preliminary assumptions the rotation rates were chosen. The propellers are in design pitch. The resulting thrust share is 70/30 for the aft and front propeller, respectively.

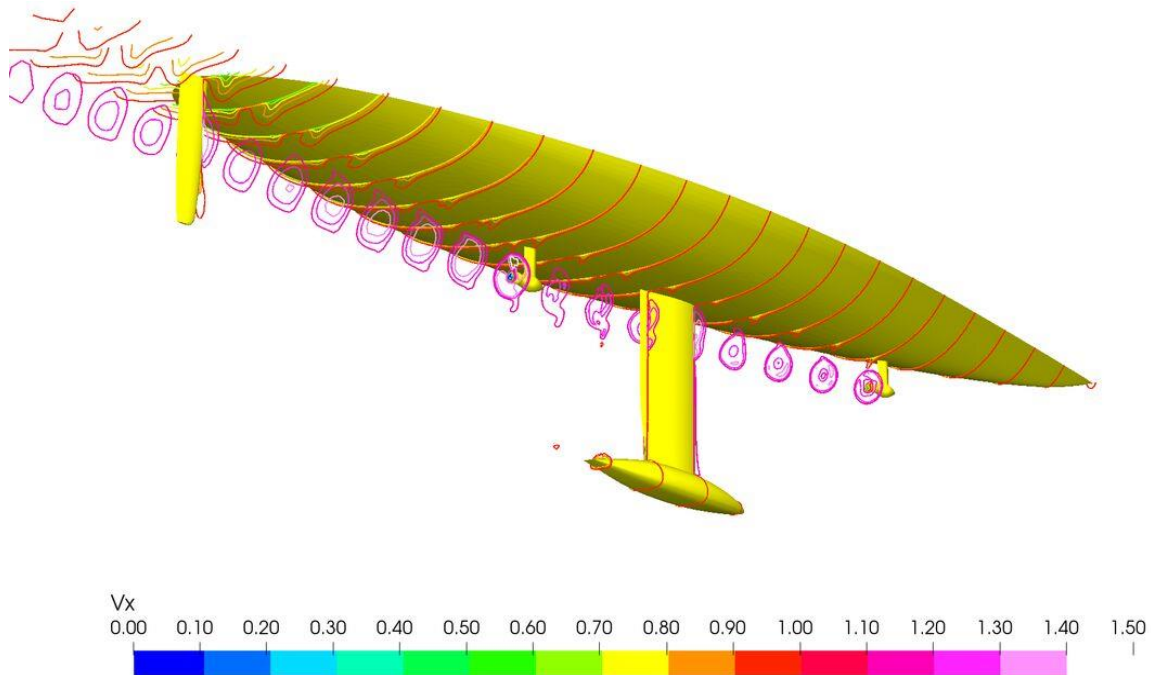


Figure 5-5: Velocity profiles at 12 knots with working aft and front propeller.

Figure 5-6 also shows the velocity V_x at 12 knots, however, with feathered propeller which is not acceleration, but deceleration the flow somewhat. In comparison with Figure 5-5, the aft propeller accelerates the flow more since the total thrust is now delivered by the aft propeller only.

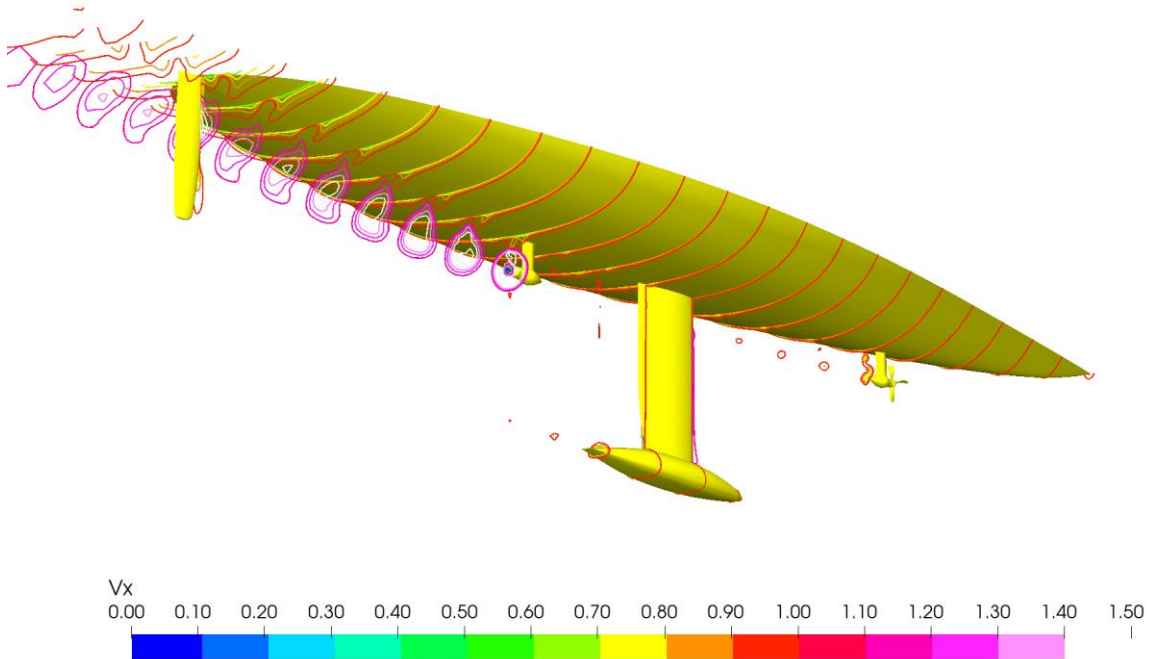


Figure 5-6: Velocity profiles at 12 knots with working aft and feathered front propeller.

Figure 5-7 also shows the V_x , now at a ship speed of 16 knots, while both propeller are regenerating. In regeneration, the propeller decelerate the flow to about half of the ship speed directly after the propeller. As shown, the slipstream from the front propeller mixed rather quickly with the higher velocity surrounding flow, providing inflow towards the rear propeller at about 90% of the ship speed. Using preliminary computations, the pitch and rotation rate of the propellers were chosen such that 250 kW would be generated, approximately, again with 70/30 share between aft and front propeller, respectively.

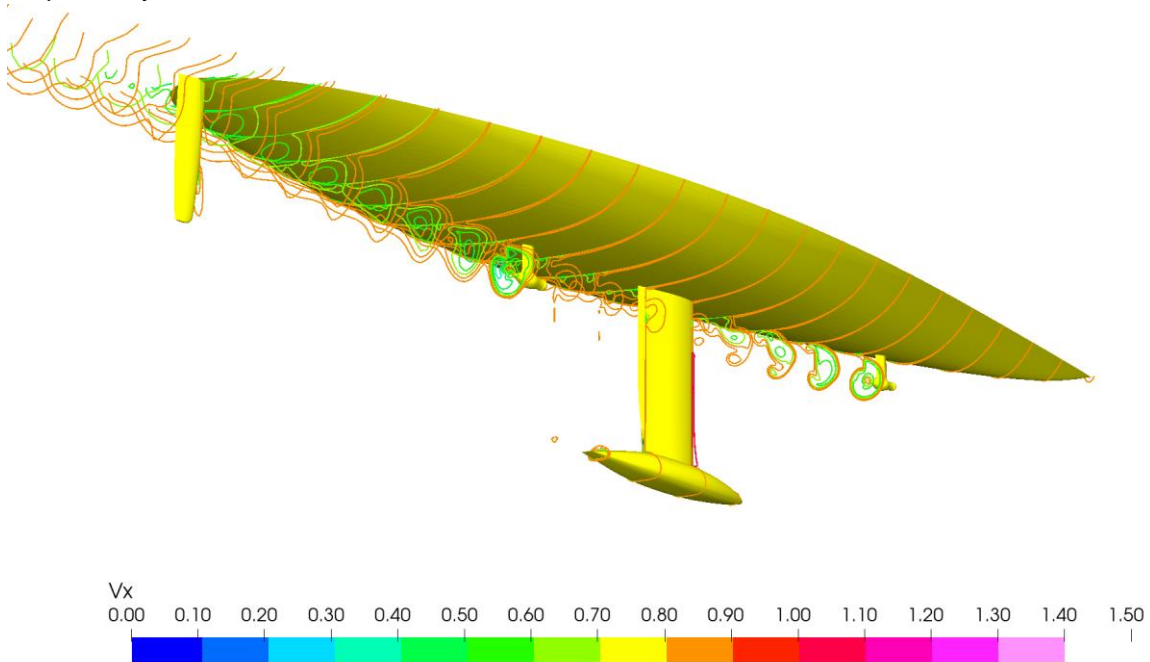


Figure 5-7: Velocity profiles at 16 knots with both propellers regenerating

Figure 5-8 shows the headloss during regeneration. The definition of headloss has been given in section 3.1. The headloss gives a clear impression of the energy loss in the wake of the ship, with in blue low energy loss and in red high energy loss. The energy loss directly behind the propellers is obvious.

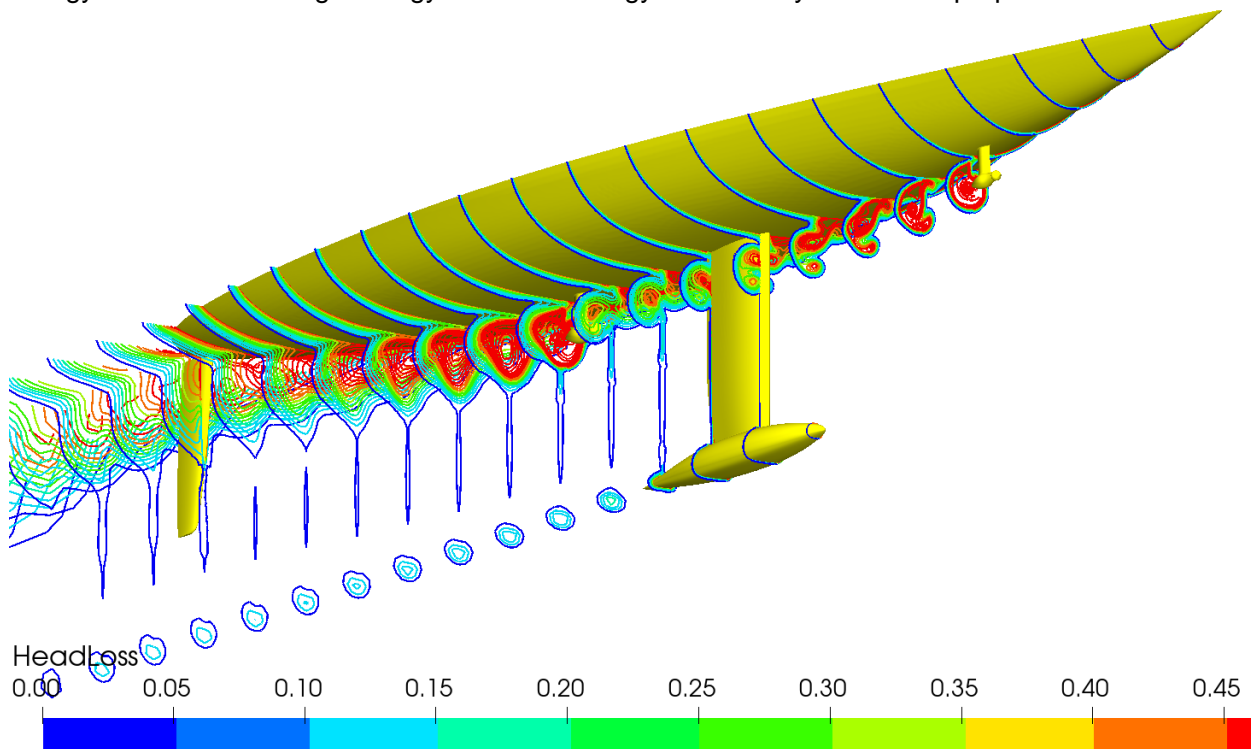


Figure 5-8: Headloss due to the regenerating propellers.

To capture the flow from the front towards aft propeller in all detail, the computational mesh between the front and rear propeller was refined, as shown in Figure 5-9. After the aft thruster, the grid was not refined anymore.

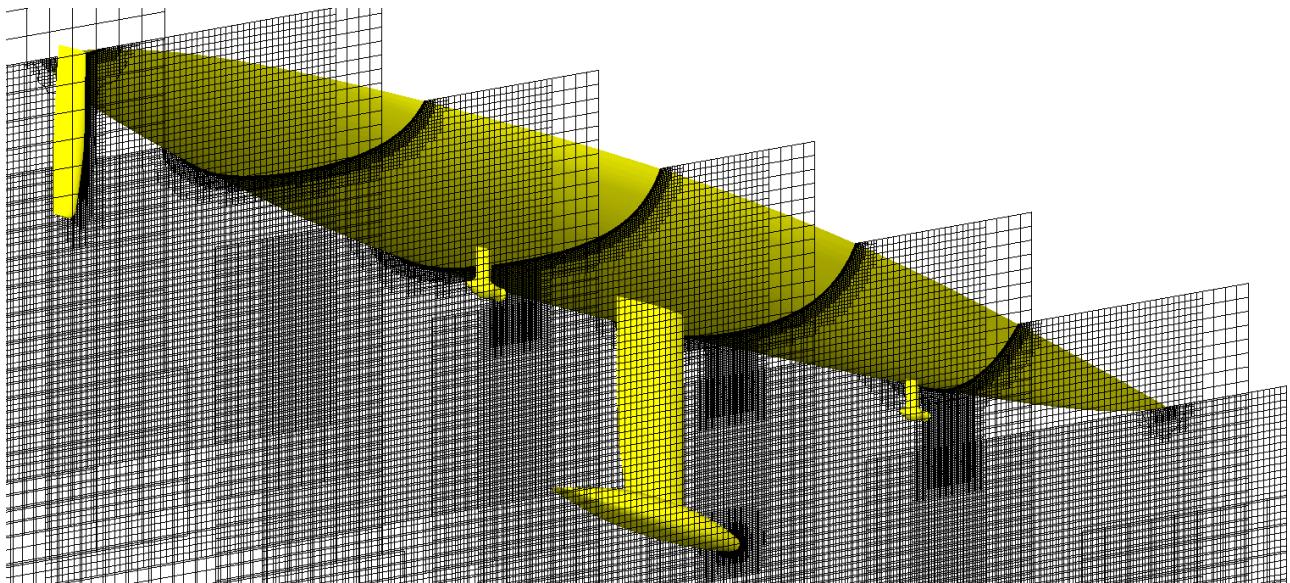


Figure 5-9: Visualisation of mesh density and refinement zones.

In propulsion mode the propellers encounter the influence of a reversed flow area at the trailing edge of the struts, as visualised in Figure 5-10. Although the reversed flow does not extent towards the propeller, the wake field of the propeller is more influenced by the strut than normal. The front thruster has slightly more extent of the reversed flow, probably due the slightly larger thickness over chord ratio and less suction effect from the propeller.

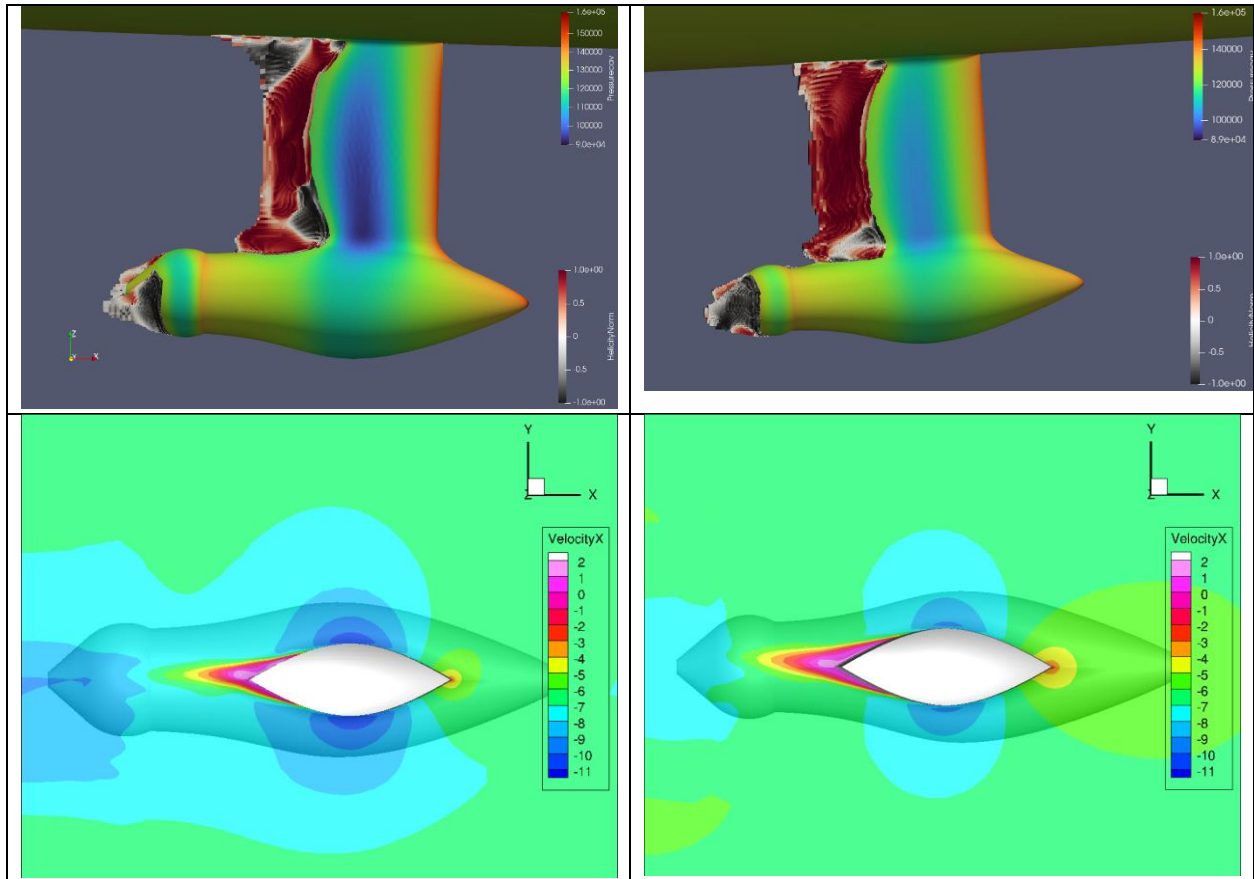


Figure 5-10: Reversed flow on the aft thruster (left) and front thruster (right) in propulsion at 12 knots, both propeller working (reversed flow in grey/red in the top figure, in purple to red in bottom figure).

The wake fields of the flow encountered by the propellers are given in Figure 5-11 and Figure 5-12, for the front propeller is feathered and in propulsion mode, respectively.

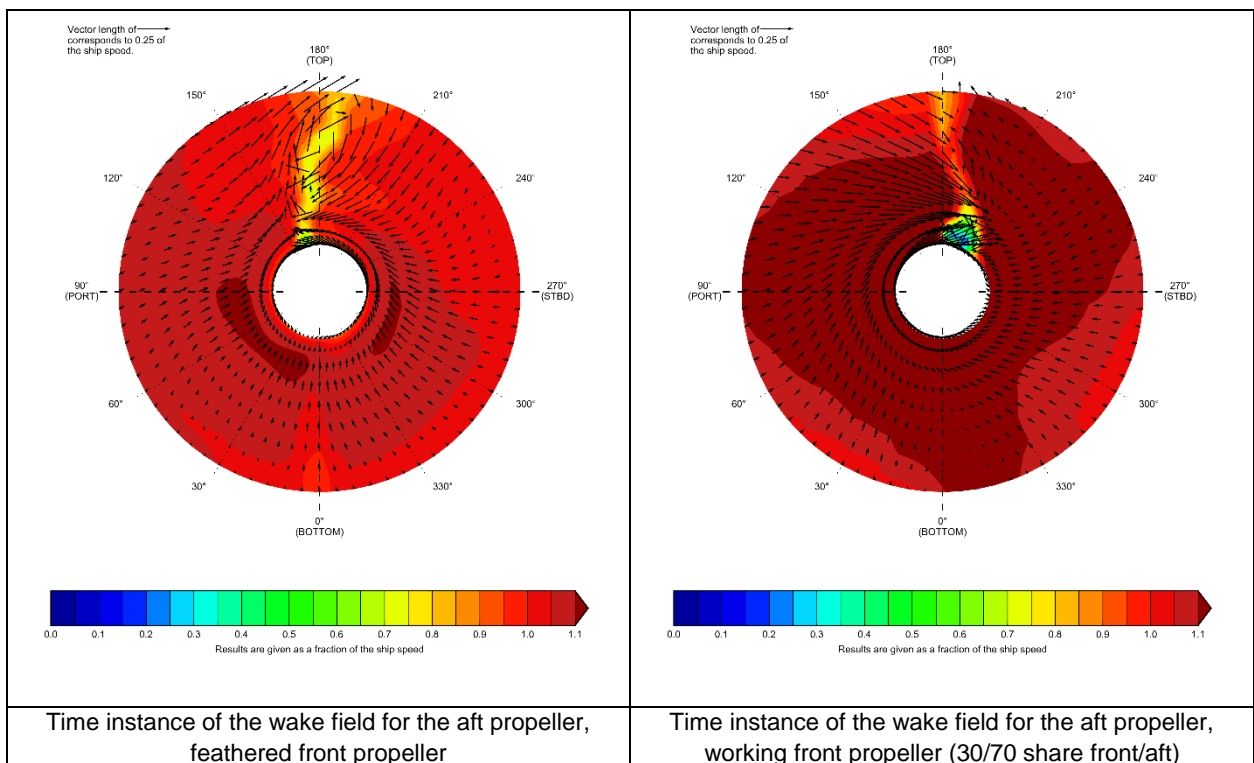


Figure 5-11: Wake fields of the aft propeller at 12 knots ship speed.

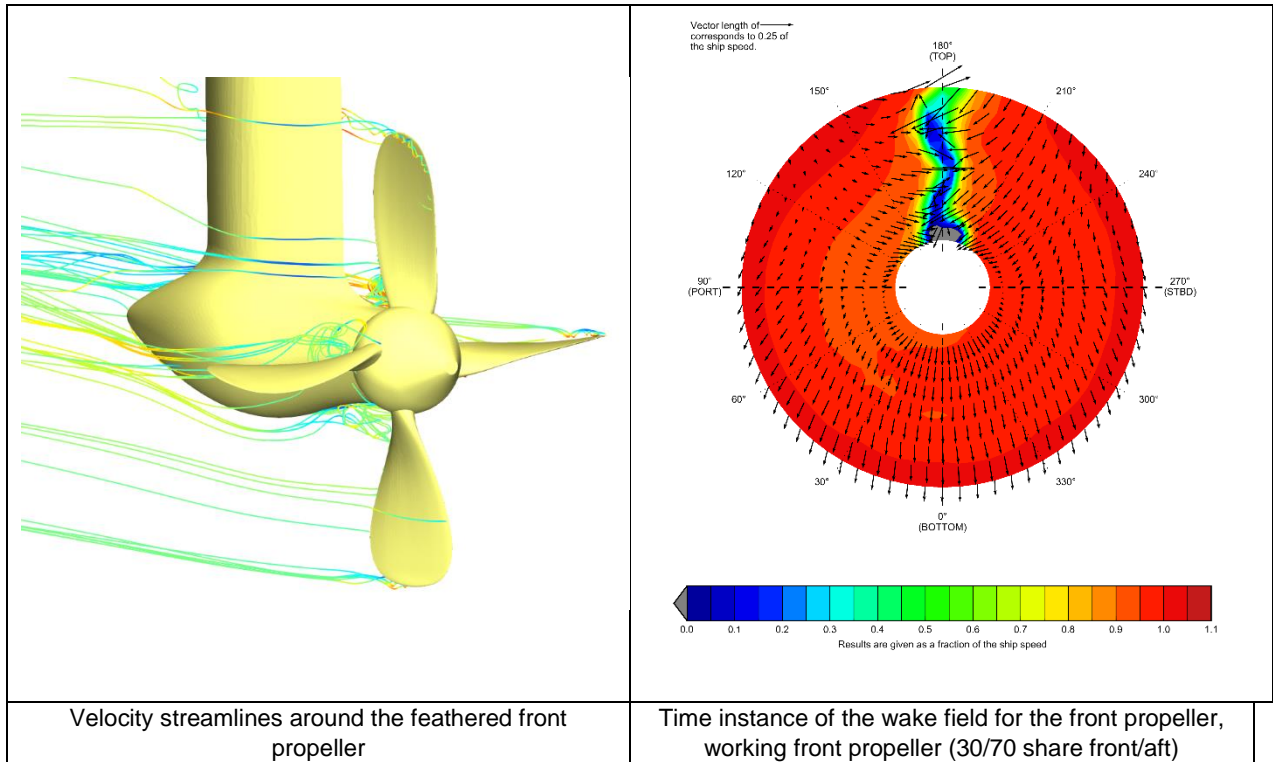


Figure 5-12: Wake field of the front propeller at 12 knots ship speed.

In regeneration mode, the front propeller encounters - apart from some stagnation of the strut - a clean inflow. The aft propeller, however, is influenced by the flow from the front propeller, as shown in Figure 5-7. The wake fields are visualised in Figure 5-12. The aft propeller encounters much more variation in the inflow compared to the front propeller during the regeneration.

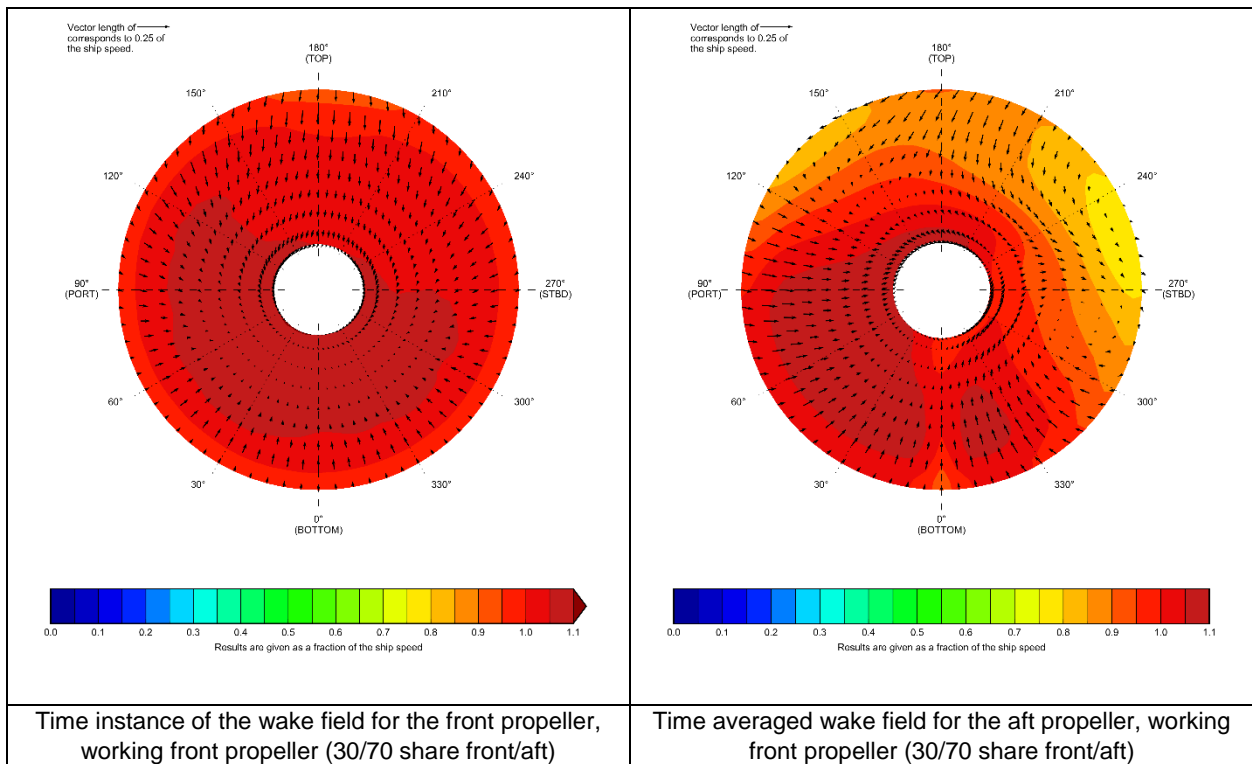


Figure 5-13: Wake field of the aft and front propeller at 16 knots ship speed in regeneration mode.

As noted in the subscript for the wake of the aft propeller in Figure 5-12, the wake for the aft propeller was averaged over 25 evaluations shown in Figure 5-14.

The wake into the aft propeller originates from a complex flow process involving mixing of the slipstream of the front propeller with low velocities and the surrounding higher velocity flow. All kind of vortices are present, which makes this a highly unsteady process. This leads to variations in the velocity distributions which the aft propeller encounters, as shown by Figure 5-14.

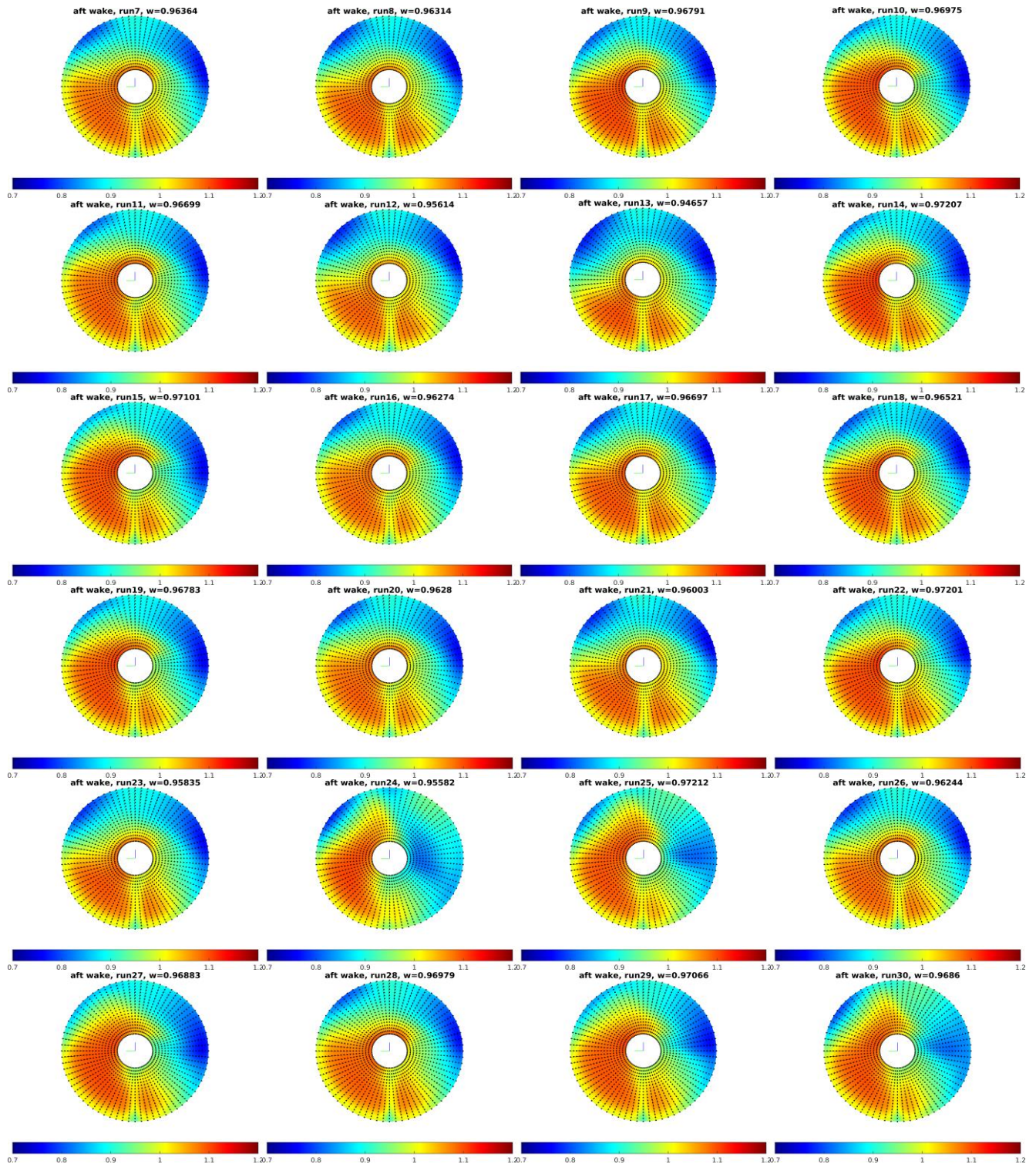


Figure 5-14: Evaluations of the wake field of the aft propeller in regeneration mode.

Due to the variation in the wake field the power absorption will have a variation also; in the computations power absorption variations up to 10% are encountered. It is recommended to take this into account for the controllers and engine settings. Secondly, also the drag varies which may lead to velocity variations, depending on the eigenfrequencies. Note that this is the worst-case scenario in which the ship encounters no drift. In practise the slipstream from the front propeller may likely pass the rear propeller and then these variations would not occur.

5.3 Propeller analysis, feathered

Using PROCAL the propellers were computed for their feathering performance in:

1. Trailing edge forward and pod forward.
2. Trailing edge forward and pod backward.
3. Leading edge forward and pod forward.
4. Leading edge forward and pod backward.

The results are presented in Figure 5-15. There are differences, both due the difference of blade design (primarily the design pitch and thickness) between the propellers, and differences in the operating mode due to velocity and pressure field over the torpedo unit and the difference between the leading edge and trailing edge.

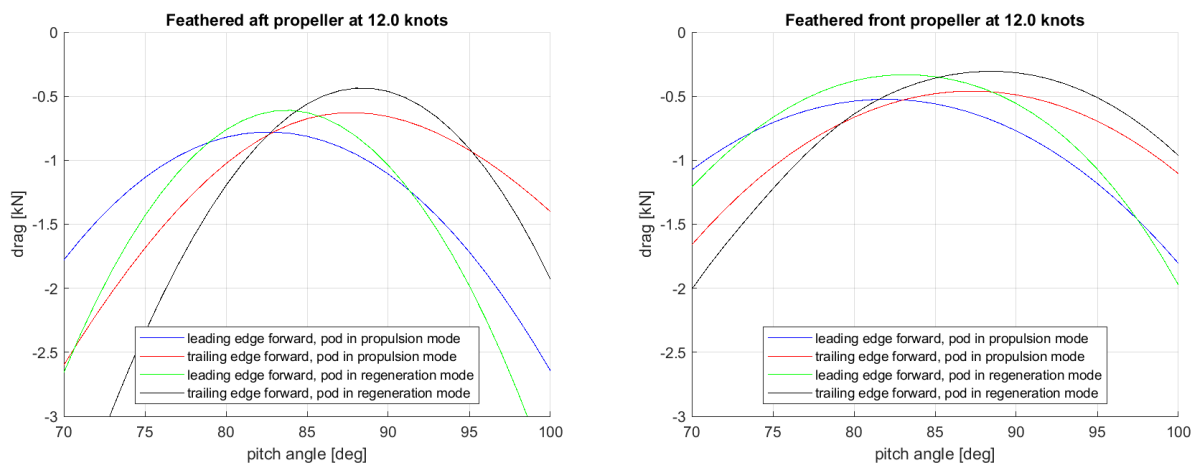


Figure 5-15: Investigation in best feathering mode and corresponding angle.

The trailing edge forward with the pod in regeneration mode would be the best option for feathering. At the neutral angle of 88 degrees, the drag D_F for both propellers can be estimated by:

$$D_F = \frac{5.2 * D^2 * V^2}{1000} [kN]$$

in which D [m] the propeller diameter and V the ship speed [m/s].

In addition to the drag of the feathered propeller, the thrusters have a resistance in feathered mode too and this drag of the thrusters is largely influenced by the separation zone. Also corrections for roughness and mechanical parts and anodes have been added. On average, the drag for regeneration and propulsion position is similar because of the symmetry of the strut. For the aft and front unit the drag can be estimated by $0.10V^2$ and $0.043V^2$ respectively.

In scenario 5, the ship is powered by the wind at 8 knots ship speed, both propellers are feathered. Hence, the total drag of the feathered units is about 2.7 kN.

5.4 Propeller analysis, propulsion

Three scenarios deal with the propulsion of the ship:

- Scenario 2. Intermediate speed motoring for short stretches at 12 knots.
- Scenario 6. Motor sailing on the aft propeller at 10 knots, with total power $P_D = 50$ kW.
- Scenario 7. Economic motoring at 8 knots.

The front propeller can either be feathered or lightly driven to reduce the drag, both options were investigated for the three scenarios.

Table 5-1: Powering prediction for different propulsion scenarios.

		driven front propeller				feathered front propeller		
		motoring	motoring*	motor sailing	economic motoring	motoring	motor sailing	economic motoring
PD aft	@0.7	1.051	1.051	1.357	1.012	0.927	1.313	0.956
PD front	@0.7	1.586	1.200	1.936	1.632			
VS	KNOTS	12.00	12.00	10.00	8.00	12.00	10.00	8.00
R	kN	32.3	32.3	5.1	12.8	32.3	4.8	12.8
Rfeather	kN					1.6	1.1	0.7
front TH	front/aft	0.121	0.250	0.000	0.087			
THDF aft	1-R/TH	0.050	0.050	0.050	0.050	0.045	0.045	0.045
THDF front	1-R/TH	0.050	0.050	0.050	0.050			
WT aft		-0.049	-0.103	0.000	-0.036	0.000	0.000	0.000
WT front		0.000	0.000	0.000	0.000			
ETA-Rs		1.000	1.000	1.000	1.000	1.000	1.000	1.000
N aft	RPM	344.4	339.8	177.4	229.4	382.4	185.9	242.7
N front	RPM	224.7	313.3	129.5	138.2			
PD aft	kW	299.1	263.4	44.2	80.5	346.5	50.0	91.1
PD front	kW	41.2	78.7	5.8	8.8			
PD	kW	340.3	342.1	50.0	89.3	346.5	50.0	91.1
THu aft	kN	29.9	25.5	5.3	12.3	35.4	6.2	14.1
THu front	kN	4.1	8.5	0.0	1.2	-1.6	-1.1	-0.7
THu	kN	34.0	34.0	5.3	13.5	33.8	5.0	13.4
THp aft	kN	32.2	28.0	6.7	13.3	37.6	7.5	15.1
THp front	kN	5.5	10.0	0.9	1.8	-0.3	-0.2	-0.1
KQ aft		0.0323	0.0296	0.0349	0.0294	0.0273	0.0344	0.0281
KQ front		0.0489	0.0345	0.0362	0.0447			
KTu aft		0.175	0.153	0.117	0.162	0.168	0.124	0.166
KTu front		0.137	0.147	0.000	0.104			
KTp aft		0.188	0.168	0.148	0.175	0.178	0.151	0.178
KTp front		0.183	0.172	0.090	0.157			
CTp aft		0.786	0.607	0.222	0.747	1.025	0.257	0.921
CTp front		0.185	0.384	0.000	0.119			
SIGN aft		3.38	3.47	12.75	7.62	2.74	11.61	6.81
SIGN front		12.32	6.36	37.11	32.57			
ETA-O aft		0.648	0.659	0.621	0.651	0.631	0.634	0.639
ETA-O front		0.614	0.670	0.000	0.551			
ETA-D		0.586	0.583	0.521	0.590	0.575	0.493	0.579

*condition for the optimisation as reported in Chapter 6.

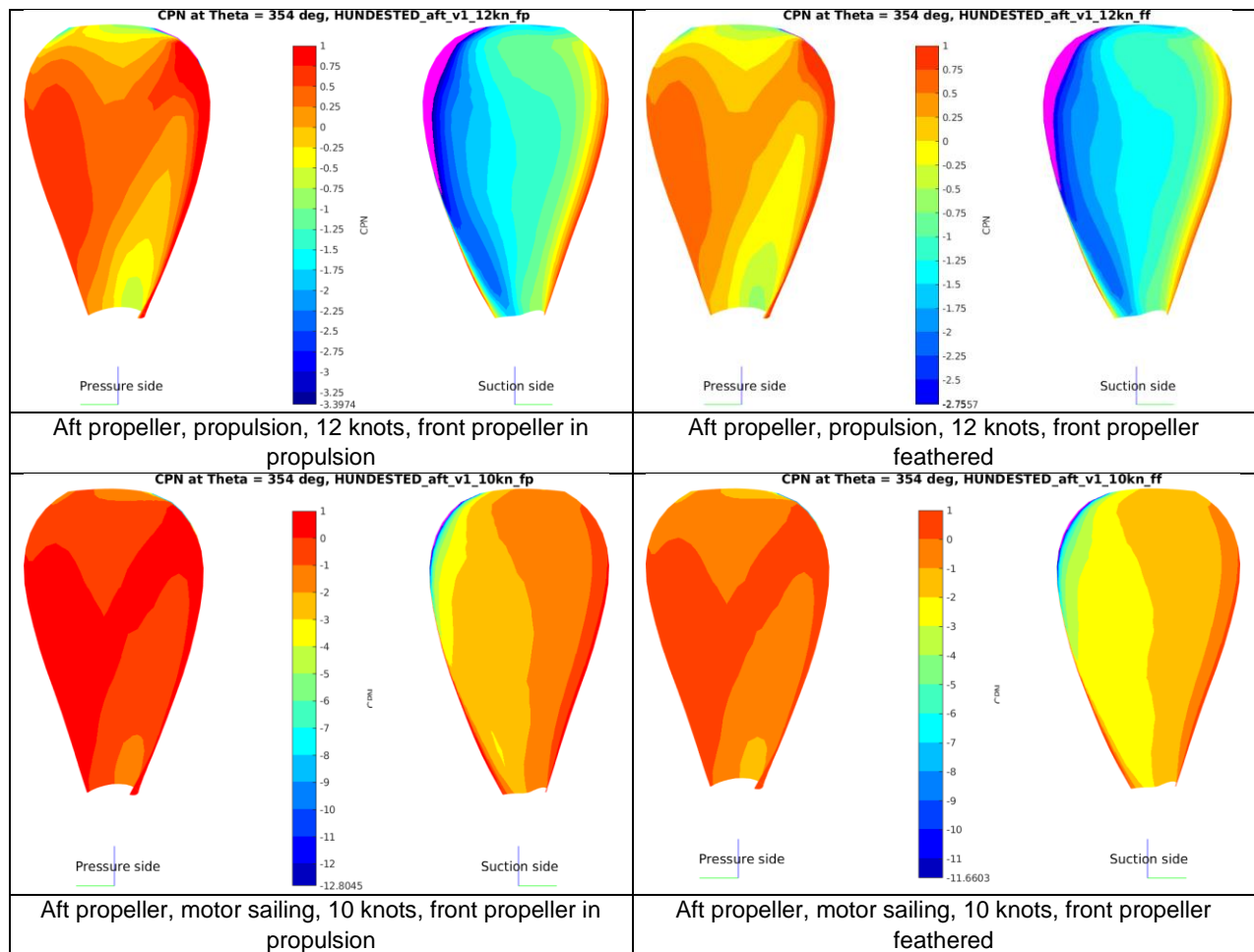
Using the provided resistance of the ship, the results from the CFD computations (see section 5.1) and the polynomial speed-power predictions were done based on K_T/J^2 identity. The results are given in Table 5-1. The relative relative efficiency is assumed to be one. The thrust share between the front and aft propeller and the pitch of both were optimised to minimise either the total power consumption or to maximise the delivered thrust.

The results show that -from a propulsion hydrodynamics point of view - it is preferred to sail with a lightly driven front propeller instead of a feathered front propeller. Note that there could be drawbacks mechanically and electrically when a propeller is lightly driven which are beyond the scope of this work.

5.4.1 Pressure distributions

Contour plots are provided by Figure 5-16 and Figure 5-17 at the blade position in which the lowest pressures occur on the blades. The pressure coefficient CPN is visualised, ranging from high pressure in red, to low pressure in dark blue where $-CPN$ equals the cavitation number σ_N . Pressure below the vapour pressure, or CPN lower than σ_N , is indicated in magenta, in which area cavitation will be formed and then spread over the blade.

For the 12 knots condition the figures on pages F22 to F27 and F28 to F34 provide the contour plots for all blade angles for the aft and front propeller, respectively.



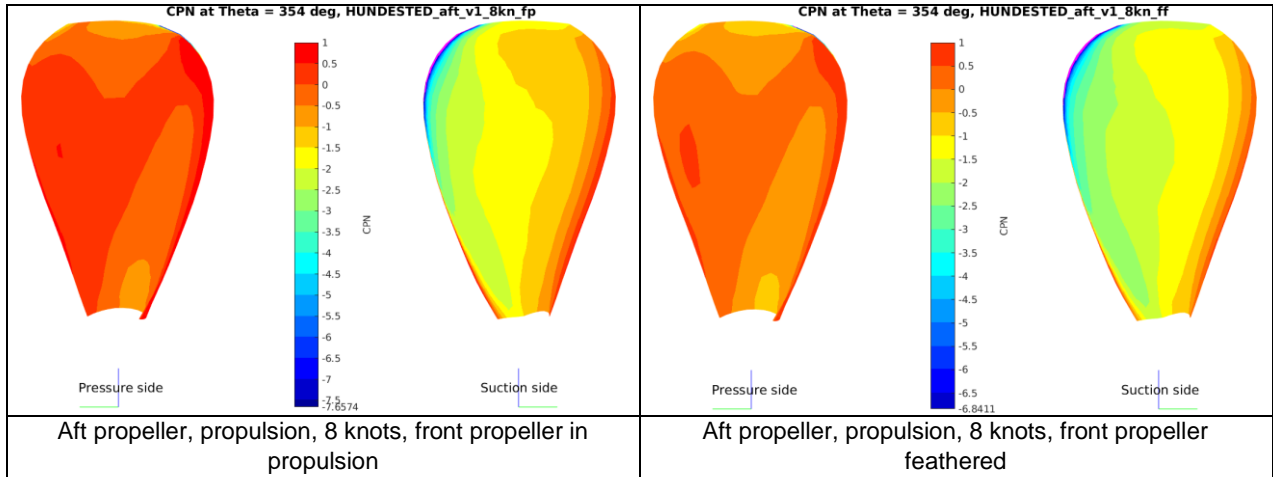


Figure 5-16: Pressure contours for the aft propeller (non-cavitating computation).

As shown, all conditions show pressures below the vapour pressure along the upper part of the leading edge. There is a sharp-peaked suction pressure which will lead to cavitation. Cavitation computations are provided in section 5.4.3. Near the root or at the mid chord of the blade, there is sufficient margin against cavitation.

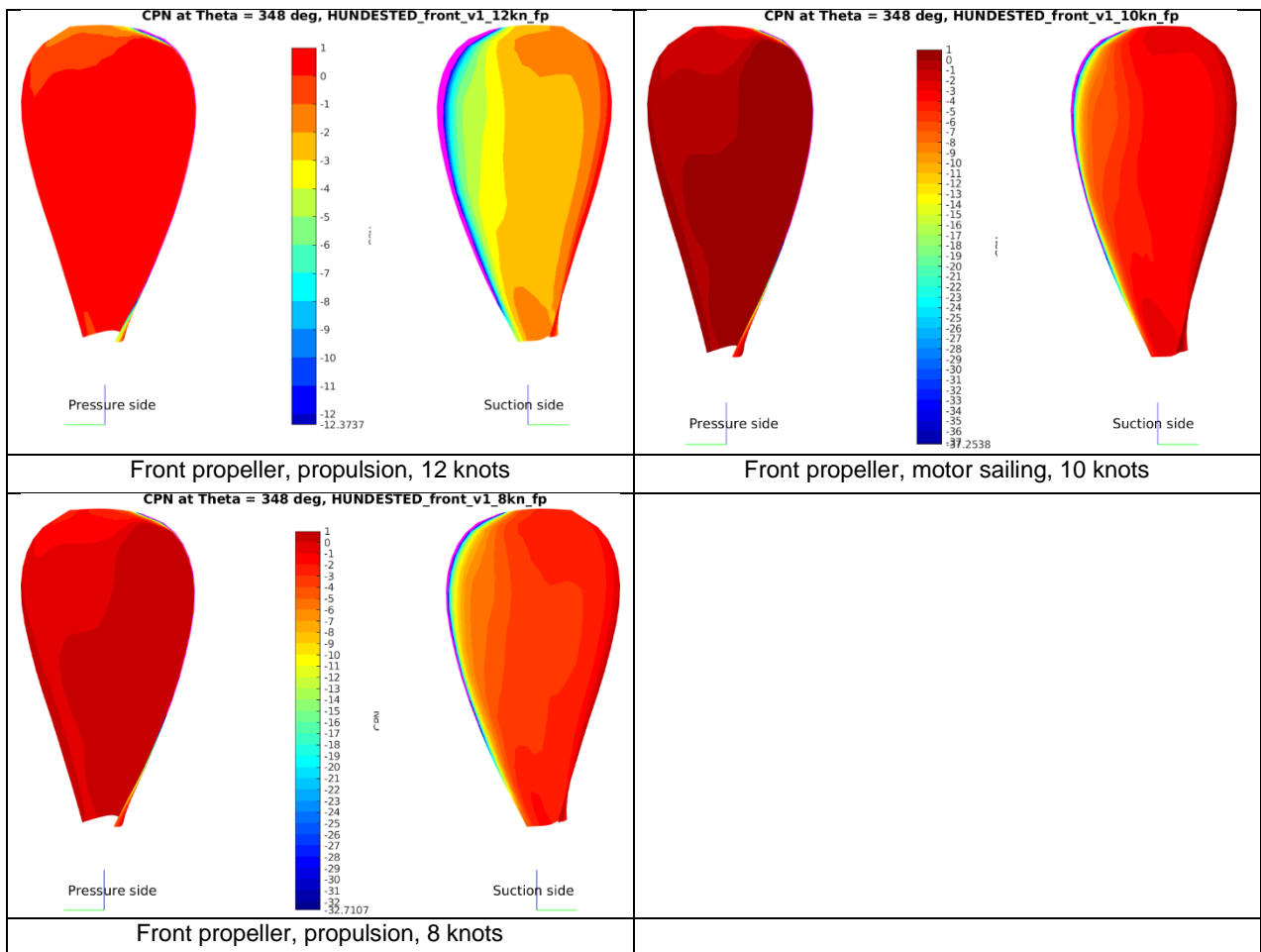


Figure 5-17: Pressure contours for the front propeller (non-cavitating computation).

The minimum pressures as function of propeller radius are provided in Figure 5-18. This figure indicates that in the 12 knots conditions the propeller starts to cavitate already at a low radius between 0.5 and 0.6.

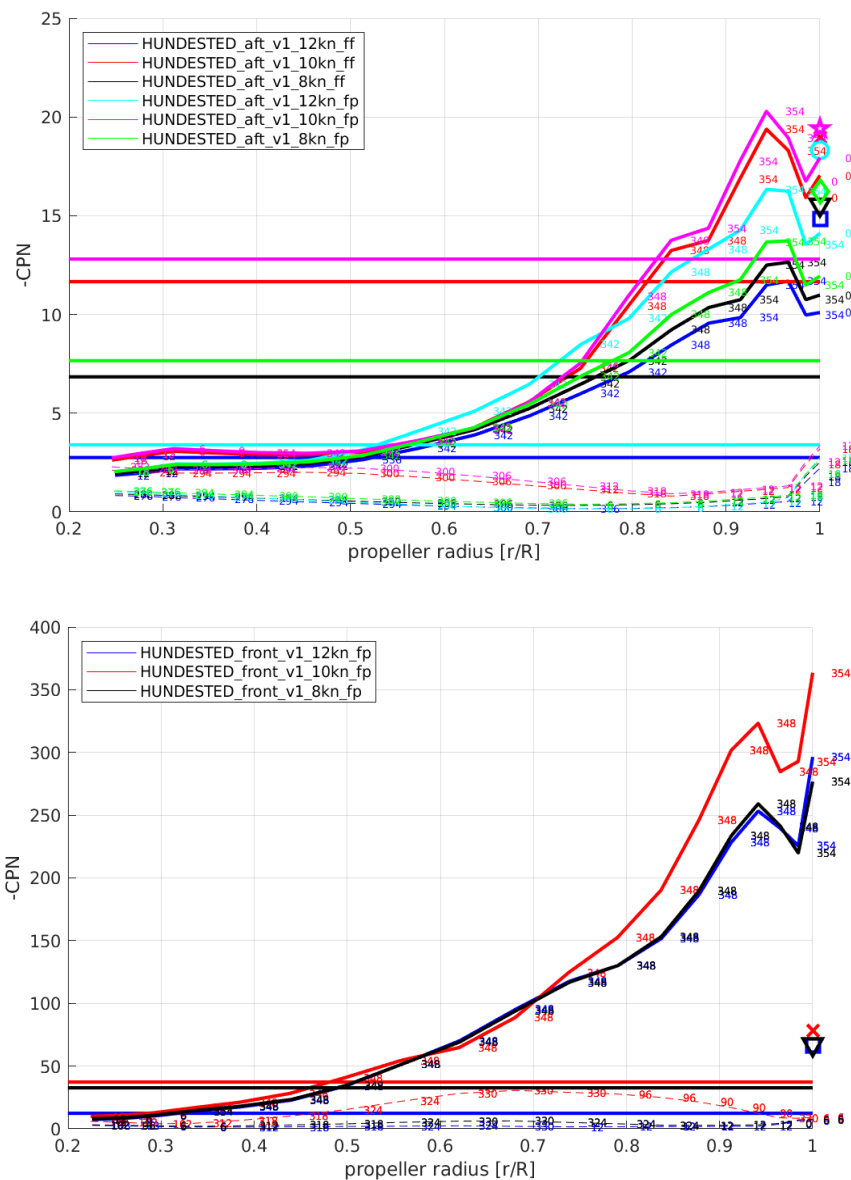


Figure 5-18: Minimum pressure coefficient as function of propeller radius for the aft propeller (top) and front propeller (bottom). The horizontal lines indicate the cavitation inception limit. The solid lines represent the suction-side pressure-peak and the dashed lines the pressure-side pressure-peak. The markers give the pressure coefficient of the core of the tip vortex.

5.4.2 Cavitation inception

In terms of cavitation-inception characteristics, Figure 5-19 and Figure 5-20 provide the cavitation inception lines for the aft and front propeller, respectively. For sheet cavitation, the cavitation inception is determined on the propeller within the interval of the specified propeller radii as given in the title of the plots.

The operational points are provided by the small cross markers. Additionally, for the 12 knots condition (with feathered front propeller for the aft propeller), the operational curve (σ_N , K_T) as function of ship speed is also given.

The two sets of lines per condition indicate pressure side cavitation with low pressure in terms of CPN at low K_T and suction side cavitation with low pressure in terms of CPN at high K_T . The cavitation bucket

is the area between both lines. The numbers near the inception lines provide the angle in degrees in which the pressure is critical with 0 degrees the top position.

The pressure coefficient -CPN occurring on the propeller can directly be compared with the cavitation number σ_N . Cavitation occurs when $-CPN > \sigma_N$, i.e., if the cavitation inception lines would be above the operational points.

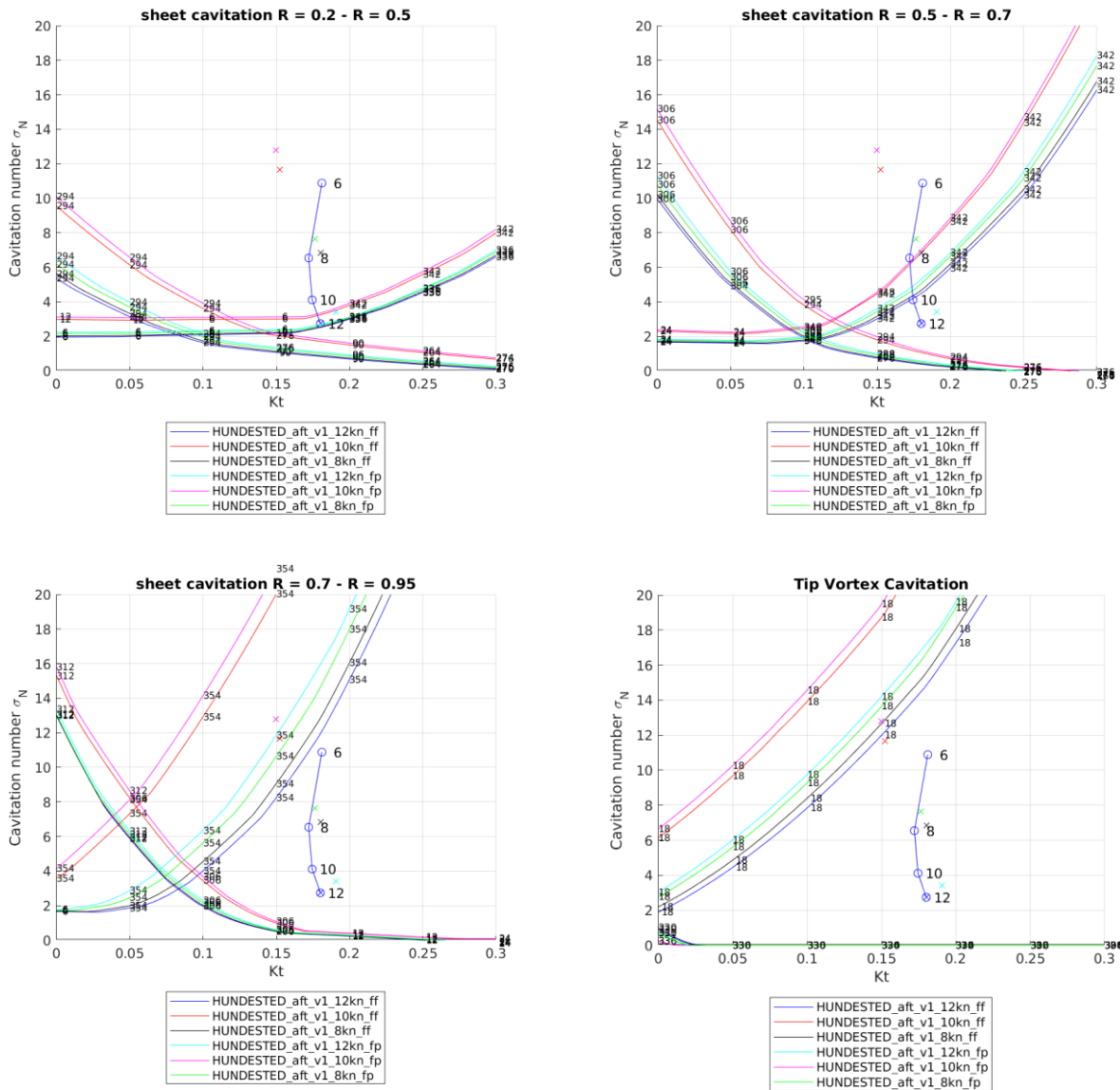


Figure 5-19: Computed sheet cavitation inception diagrams for the aft propeller.

The differences in the inception curves are dominated by the pitch setting in each condition. Therefore, the inception lines of the 8 and 12 knots conditions are very similar. The cavitation bucket becomes smaller with increasing pitch, although usually the operational point is also at lower rpm which positions the operational point higher in the diagram.

For high pitch settings the cavitation is dominated by sheet cavitation at the higher radii, while at lower pitch tip vortex cavitation is the first occurring form of cavitation.

For the aft propeller, the margins against pressure-side cavitation are very large. This would call for an increase in camber to rebalance suction- and pressure side cavitation.

For the front propeller the cavitation inception is difficult to interpret or to base conclusions on. First recommendation would be to improve the separation from the strut, such that the propeller encounters less disturbed inflow.

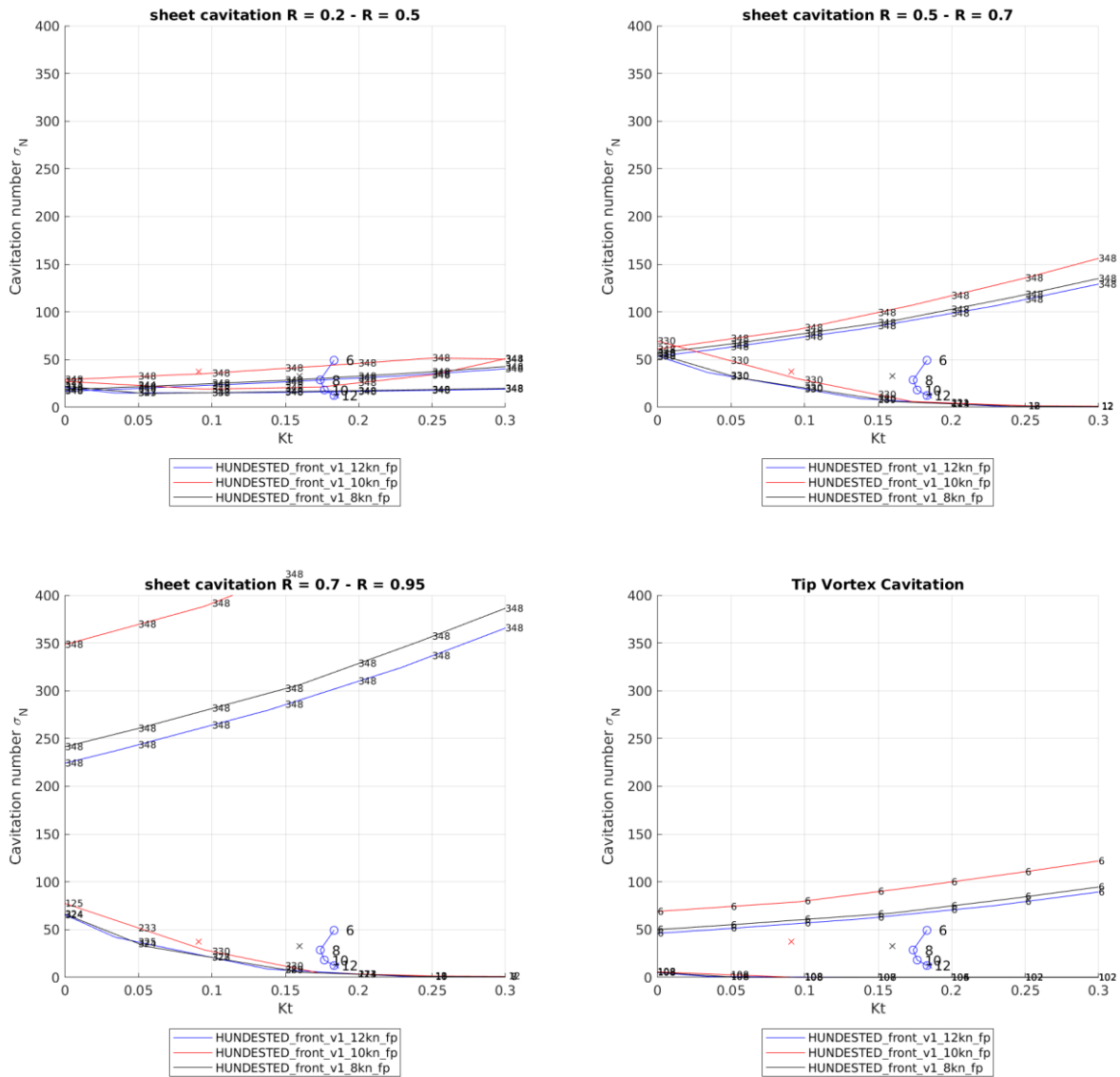


Figure 5-20: Computed sheet cavitation inception diagrams for the front propeller.

5.4.3 Cavitation behaviour

Figure 5-21 provides sketches of the cavitation behaviour which are obtained from cavitation computations. In black the contour of the cavitation and propeller is given. A green colour indicates suction side sheet cavitation with favourable shape with regards to the risk on cavitation erosion. A red colour indicates suction side sheet cavitation with risk on cavitation erosion. In blue colour the non-erosive growing phase is shown. In purple pressure side sheet cavitation is presented, but is not present in the current design.

The 12 knots conditions are also shown on figure pages F35 and F36 for multiple blade angles during the rotation in the wake field.

At 12 knots condition, both the aft and front propeller show a potentially erosive sheet cavitation, which occurs primarily due to the adverse inflow from the strut of the thruster. At lower speeds also cavitation occurs, although the cavitation extent is clearly less.

It is advised to pay attention to the design of the strut of the thruster such that less adverse flow would be obtained. Possibly, also the design of the propeller could be adapted to avoid erosive shapes of cavitation.

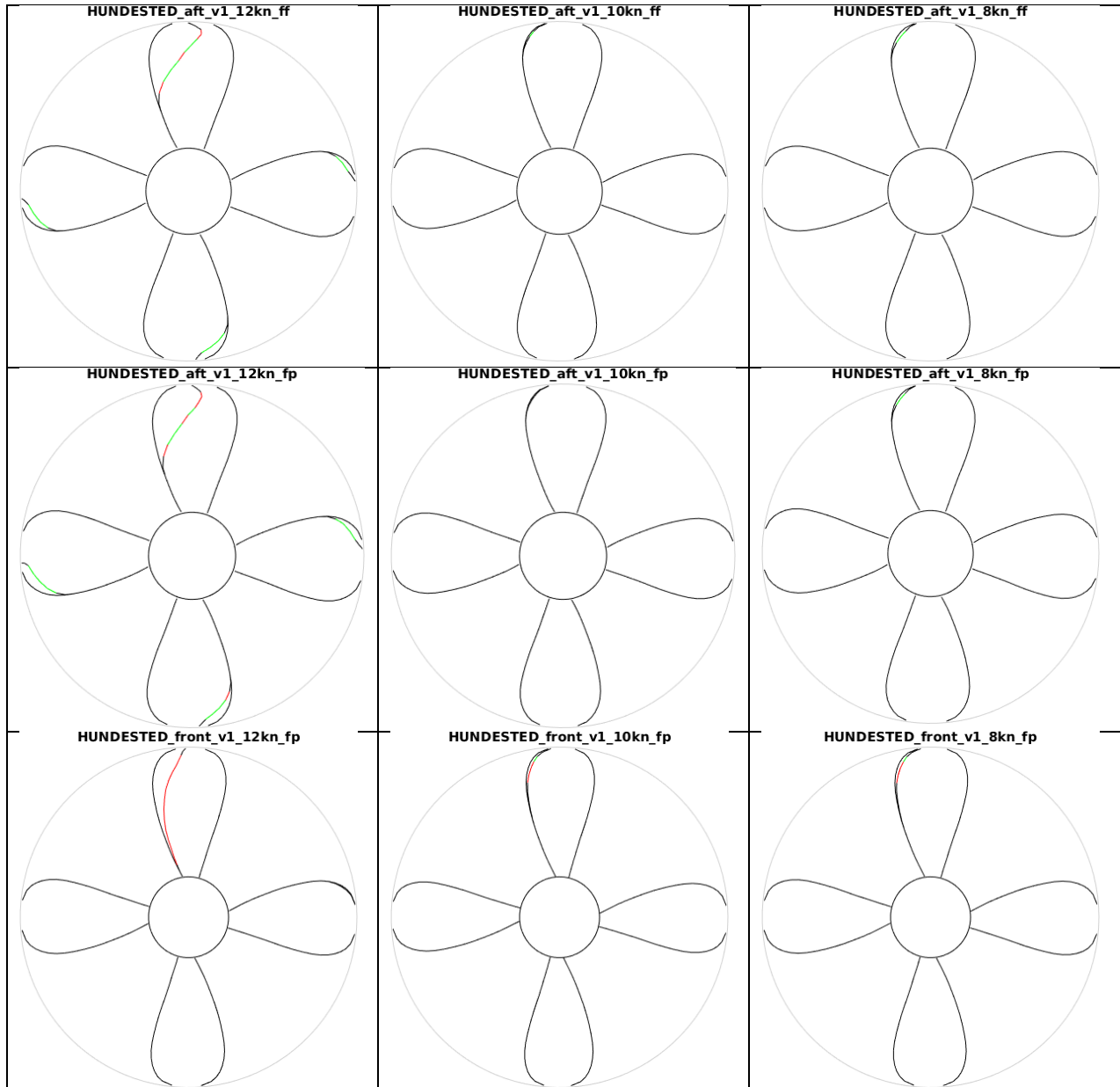


Figure 5-21: Computed cavitation behaviour of the aft propeller (top two rows) and front propeller (bottom row) at 12 knots in propulsion.

5.4.4 Underwater radiated noise

The estimate of the total underwater radiated noise is provided by Figure 5-22. Although sheet cavitation is present as well in the 12 knots conditions, the noise of the tip vortex is dominant. For reference, the level of the DNV Quiet 11 knots notation is presented. As shown, the current propellers exceed this level at 12 knots.

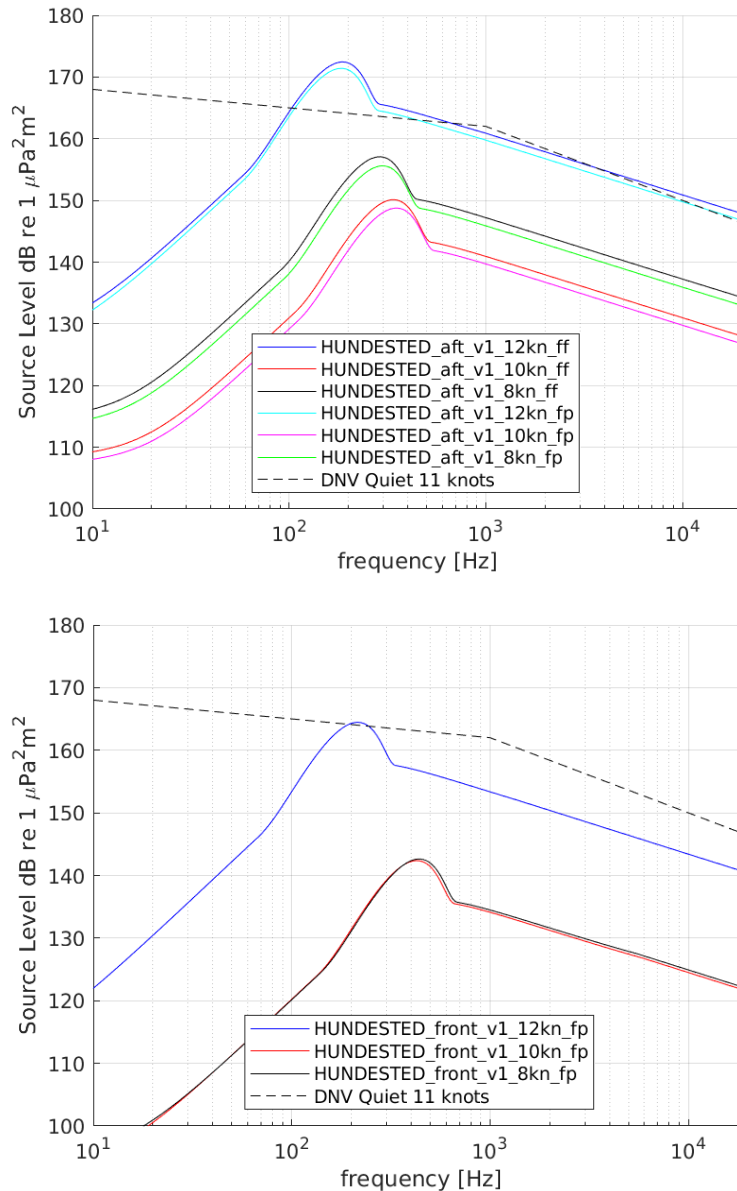


Figure 5-22: Under water radiated noise predictions for the aft propeller (top) and front propeller (bottom).

5.4.5 Radial loading distribution

For the prediction of the inception of the tip vortices and the underwater radiated noise predictions the circulation strength at the tip was used as a measure of the strength of the tip vortices.

Therefore, for more insight, the distribution of the circulation over the propeller radius is given in Figure 5-23 and Figure 5-24. The solid line indicates the mean circulation, while the cross-marked and square-marked lines indicate the maximum and minimum circulation in the wake field respectively. A silent propeller would have a value of around 0.03 at $r/R = 0.95$. As shown, the circulation near the tip exceeds this value.

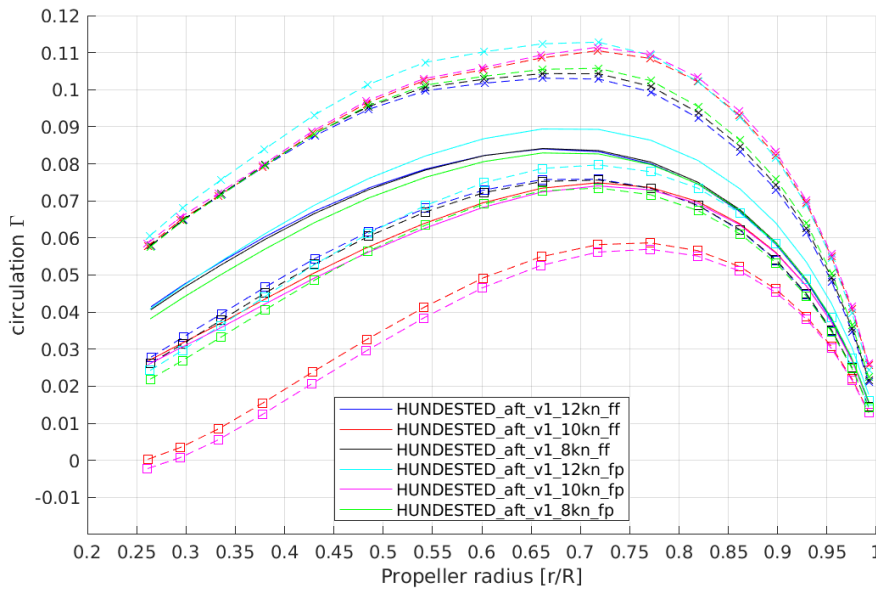


Figure 5-23: Radial distribution of the circulation for the aft propeller

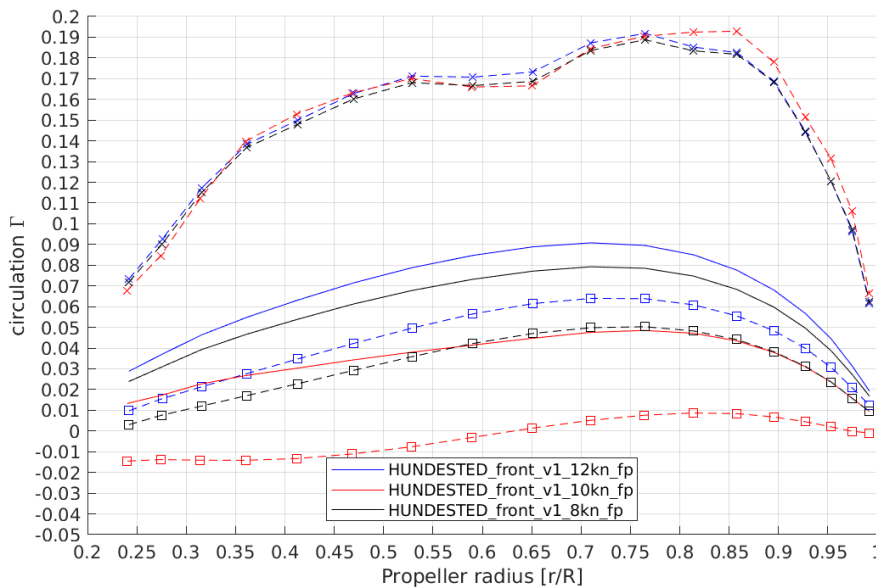


Figure 5-24: Radial distribution of the circulation for the front propeller.

5.4.6 Hull pressure excitation

Figure 5-25 gives the results of the computations on hull pressure fluctuations as induced by the propeller and the cavitation on the propeller. For reference, a level of 1.0 kPa is commonly regarded as the upper limit for yachts, although some parties also require 0.75 kPa at maximum. At 12 knots these criteria are exceeded. Especially the 12 knots condition with the aft propeller exceeds these criteria, due to the amount of cavitation.

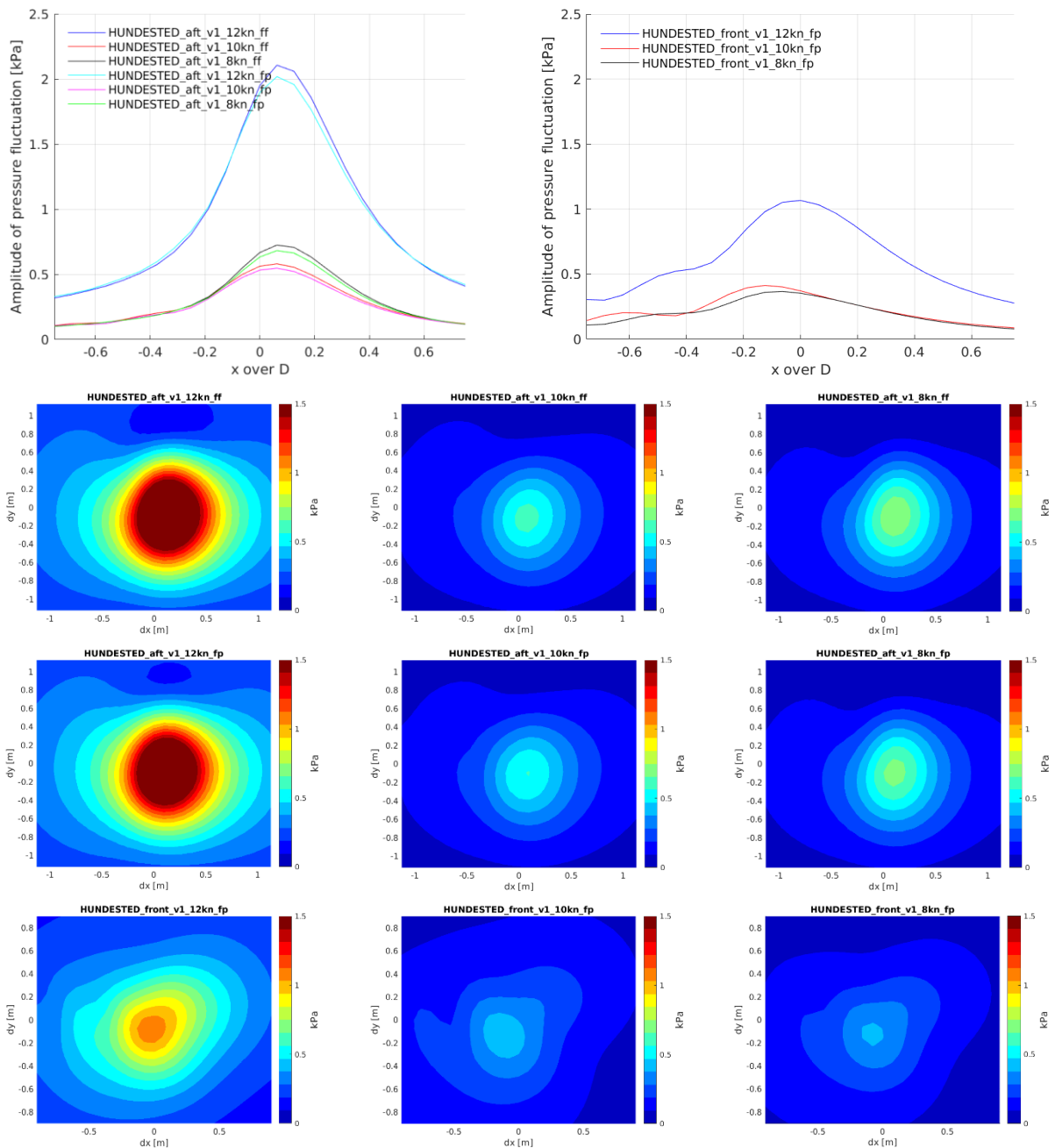


Figure 5-25: Computation of propeller-induced hull pressure fluctuation at the first blade harmonic frequency for both propellers.

5.4.7 Thrust variation

The dimensionless blade and shaft forces are reported in Figure 5-26 for the aft propeller. The blade force acts on the CPP mechanism, while the shaft force excites the unit and its foundation. The smallest shaft force variation for 12 knots condition with feathered front propeller already exceeds 5%, which is commonly used for yachts and cruise vessels. Although the absolute values are smaller, the variation in thrust for motor sailing is significant. Note also the sharp slope in the blade force between 315 and 350 degrees, where the propeller blade passes the wake peak of the strut. At 180 degrees the influence of the wake of the keel is clearly visible.

The (dimensionless) force fluctuations for the front propeller are significantly larger, as shown in Figure 5-27. This may also give an effect on the efficiency of the propeller. At some point in the 10 knots motor sailing condition the thrust of one blade becomes even negative which worsens the total efficiency of a full rotation. This effect is not incorporated in the powering predictions.

Actual nuisance from thrust variations largely depends on the frequency and transfer functions within the ship.

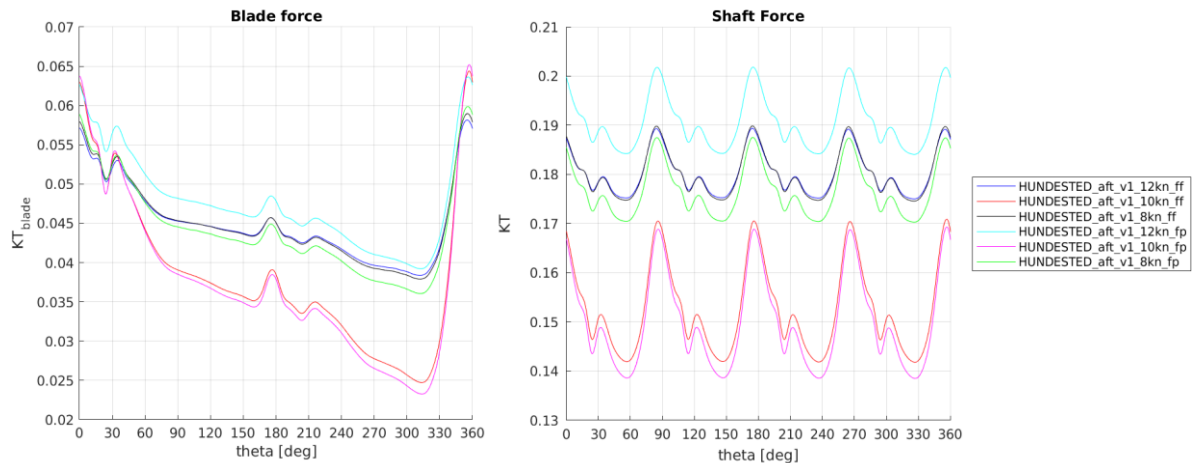


Figure 5-26: Blade and shaft forces for the aft propeller.

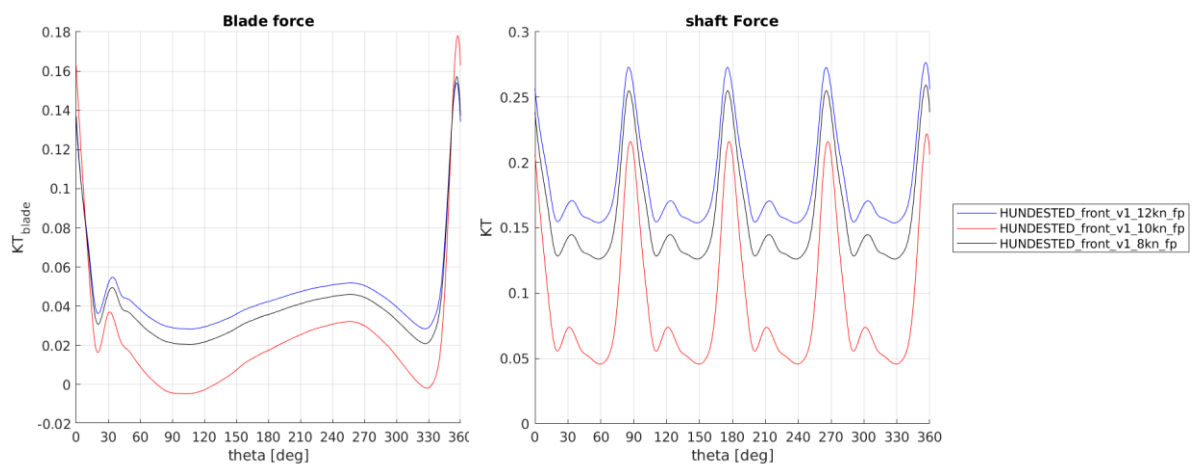


Figure 5-27: Blade and shaft forces for the front propeller.

5.4.8 Discussion points

It is advised to pay attention to the design of the strut of the thruster such that less adverse flow would be obtained. This would help in avoiding the unsteady behaviour of the cavitation and the large thrust variations.

It is also advised to remove the sensitivity of the propeller to suction side sheet cavitation by increasing the camber in the tip region. This is possible as the margin against pressure side cavitation is large.

5.5 Propeller analysis, regeneration

For regeneration the propellers were analysed in three scenarios:

- Scenario 1. Max regeneration at 16 knots, 250 kW
- Scenario 3. 14 knots, 125 kW
- Scenario 4. Front propeller only at 10 knots, 20 kW

Using the polynomial, and assuming that the sails deliver sufficient power to maintain the ship speed, Table 5-2 summarises the performance data of both propellers in each of the three scenarios. The pitch and rpm of both propeller were optimised such that the efficiency of the combination of both propellers is optimal. Note that the assumption is being made that the wake fraction of the aft propeller is constant, despite the varying load on the front propeller. In view of probable drift of the ship, the probability that the slipstream of the front propeller interacts with the aft propeller is not large, and this assumption is justified and the data can be regarded on the conservative side.

Table 5-2: Performance data during regeneration.

			<i>max P</i>	<i>max ETA</i>			
V	KNOTS	16.0	16.0	16.0	14.0	10.0	10.0
PD front	@0.7	0.806	0.659	0.936	0.976	1.121	0.959
PD aft	@0.7	0.831	0.643	1.021	1.101	2.159	feathered
w front		0.004	0.004	0.004	0.004	0.004	0.004
w aft		0.027	0.027	0.027	0.027	0.027	
thdf front		-0.010	-0.010	-0.010	-0.010	-0.010	-0.010
thdf aft		0.015	0.015	0.015	0.015	0.015	
VA front	m/s	8.20	8.20	8.20	7.17	5.12	5.12
VA aft	m/s	8.01	8.01	8.01	7.01	5.01	
VR front	m/s	17.84	18.31	17.16	14.83	10.12	10.65
VR aft	m/s	17.17	18.16	15.89	13.41	7.06	
beta front	rad	0.477	0.464	0.498	0.505	0.531	0.502
beta aft	rad	0.485	0.457	0.528	0.550	0.788	
CTu front		-0.108	-0.123	-0.096	-0.092	-0.078	-0.094
CQ front		-0.121	-0.121	-0.116	-0.113	-0.099	-0.114
CTp front		-0.096	-0.111	-0.083	-0.078	-0.063	-0.080
CTu aft		-0.114	-0.125	-0.103	-0.101	-0.058	
CQ aft		-0.128	-0.119	-0.132	-0.134	-0.084	
CTp aft		-0.101	-0.114	-0.087	-0.082	-0.031	
TH front	kN	-19.8	-23.6	-16.2	-11.6	-4.6	-6.1
THp front	kN	-17.7	-21.5	-14.1	-10.0	-3.7	-5.2
-PD front	kW	101.1	110.1	85.1	53.4	14.6	20.0
THu aft	kN	-30.8	-37.9	-24.1	-16.7	-2.7	-1.7
THp aft	kN	-26.9	-34.0	-19.9	-13.5	-1.4	-0.4
-PD aft	kW	148.9	165.7	118.6	71.6	5.4	
-PD	kW	250.0	275.8	203.8	125.0	20.0	20.0
THu	kN	-50.7	-61.5	-40.3	-28.3	-7.3	-7.9
N front	RPM	360.3	372.2	342.8	295.1	198.5	212.2
N aft	RPM	276.2	296.4	249.7	208.0	90.6	
ETA front		0.620	0.566	0.637	0.637	0.618	0.638
ETA aft		0.586	0.532	0.599	0.596	0.392	
ETA		0.599	0.545	0.615	0.613	0.535	0.493
CP front		0.312	0.340	0.263	0.246	0.185	0.253
CP aft		0.295	0.328	0.235	0.211	0.044	

Table 5-2 shows that it is more efficient to have both propellers regenerating instead of feathering the aft propeller, similarly to the conclusion that was found for propulsion. The total efficiency depends on the ability and efficiency of the mechanical and electrical systems.

The optimal power share and corresponding pitch and rotation rates were investigated, primarily to check the behaviour of the polynomial. Figure 5-28 shows interesting behaviour presenting the performance as function of power regeneration for a ship speed of 16.0 knots, optimised for the total efficiency of the front and rear propeller combined. At low power generation the front propeller takes most of the share due to its higher efficiency via its favourable wake fraction and thrust deduction factor. For higher power generation, the rear propeller is required to work harder.

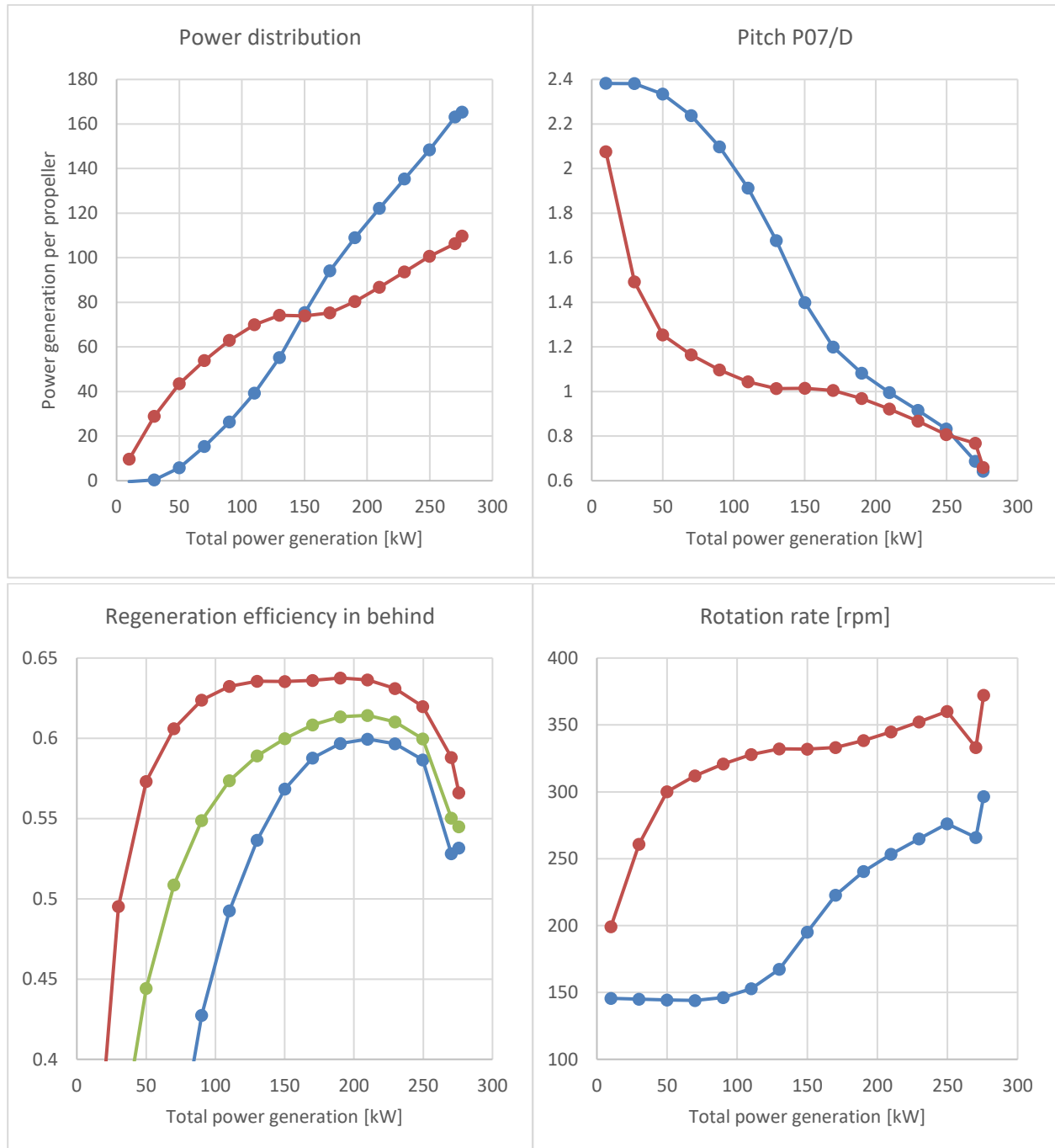


Figure 5-28: Additional insight in the power share and corresponding pitch and rotation rates at 16.0 knots ship speed. In blue the aft and red the front propeller, while green represents the total.

5.5.1 Pressure distributions

Contour plots are provided by Figure 5-16 and Figure 5-17. The pressure coefficient CPN is visualised, ranging from high pressure in red, to low pressure in dark blue where $-CPN$ equals the cavitation number σ_N . Pressure below the vapour pressure, or CPN lower than σ_N , is indicated in magenta.

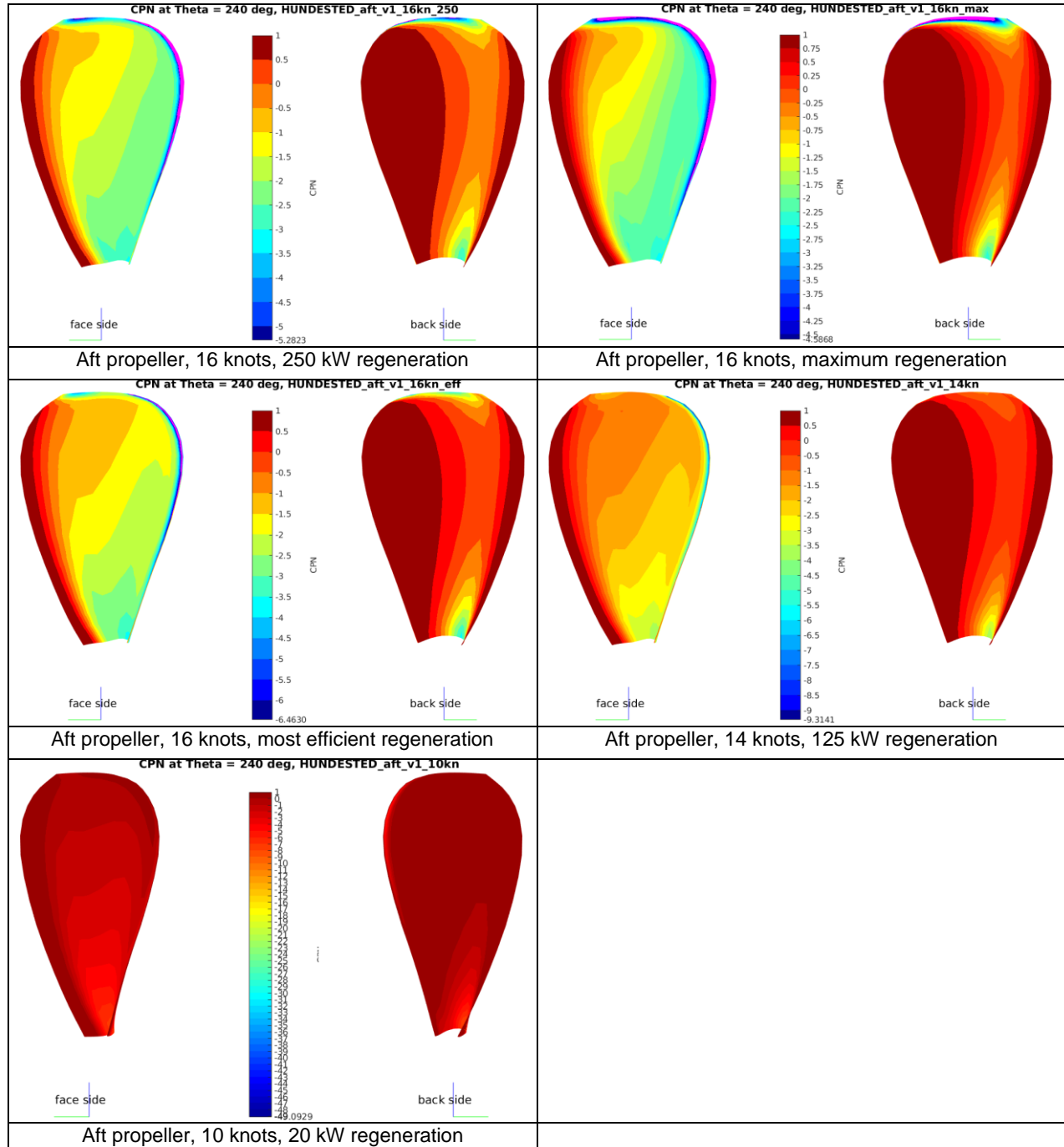


Figure 5-29: Pressure contours for the aft propeller during regeneration (non-cavitating computation).

All conditions show pressures below the vapour pressure along the upper part of the leading edge. There is a sharp-peaked suction pressure which will lead to cavitation. Cavitation computations are provided in section 5.4.3. At the mid chord of the blade, there is sufficient margin against cavitation. Near the root, at the leading edge (in regeneration) there is an area of low pressures, but only for the aft propeller in maximum regeneration mode there occurs some minor root cavitation.

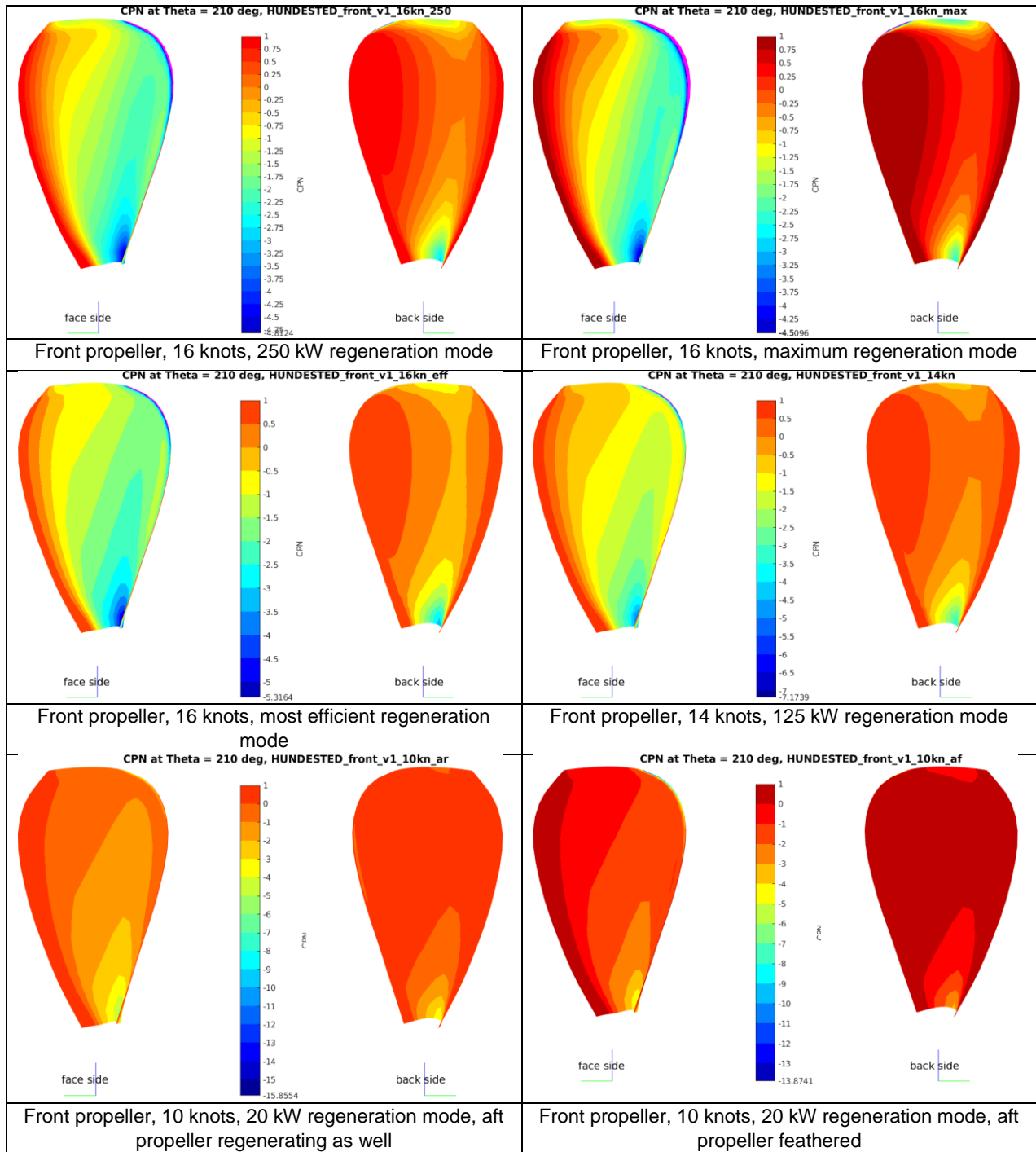


Figure 5-30: Pressure contours for the front propeller during regeneration (non-cavitating computation).

For the 16 knots condition in 250 kW regeneration mode, the figures on pages F37 to F42 and F43 to F48 provide the contour plots for all blade angles for the aft and front propeller, respectively.

The minimum pressures as function of propeller radius are provided in Figure 5-18. This figure indicates that in the 16 knots conditions the propellers cavitates in the tip regions only, except for the aft propeller in maximum regeneration mode which features some minor blade root cavitation.

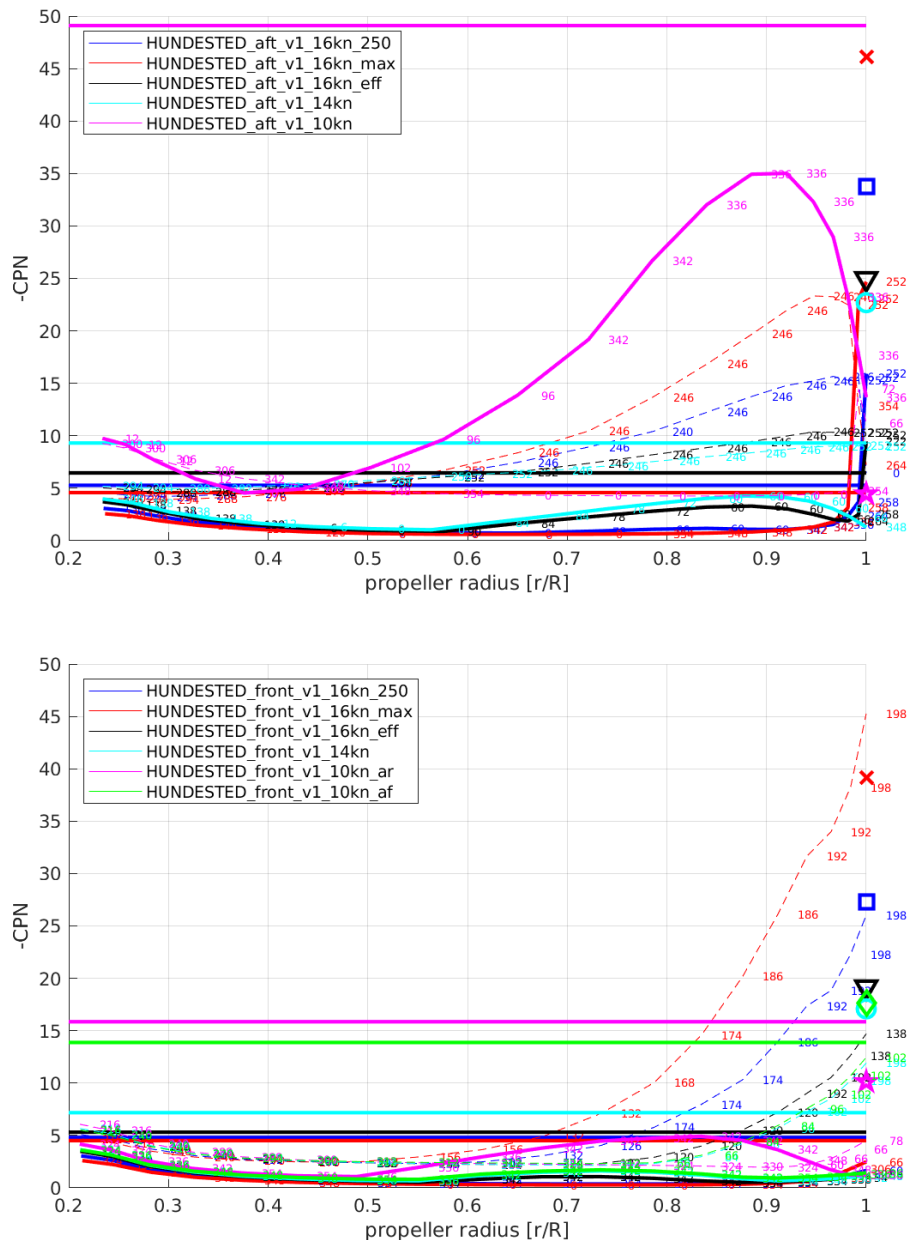


Figure 5-31: Minimum pressure coefficient as function of propeller radius for the aft propeller (top) and front propeller (bottom) during regeneration. The horizontal lines indicate the cavitation inception limit. The solid lines represent the suction-side back-side pressure-peak and the dashed lines the face-side pressure-peak. The markers give the pressure coefficient of the core of the tip vortex.

5.5.2 Cavitation inception

Figure 5-19 and Figure 5-20 provide the cavitation inception lines for the aft and front propeller, respectively. For sheet cavitation, the cavitation inception is determined on the propeller within the interval of the specified propeller radii as given in the title of the plots.

The operational points are provided by the small cross markers. The two sets of lines per condition indicate face cavitation (in regeneration this is the suction-side) with low pressure in terms of CPN at low K_T and back cavitation (in regeneration this is the pressure-side) with low pressure in terms of CPN at high K_T . The cavitation bucket is the area between both lines. The numbers near the inception lines provide the angle in degrees in which the pressure is critical with 0 degrees the top position.

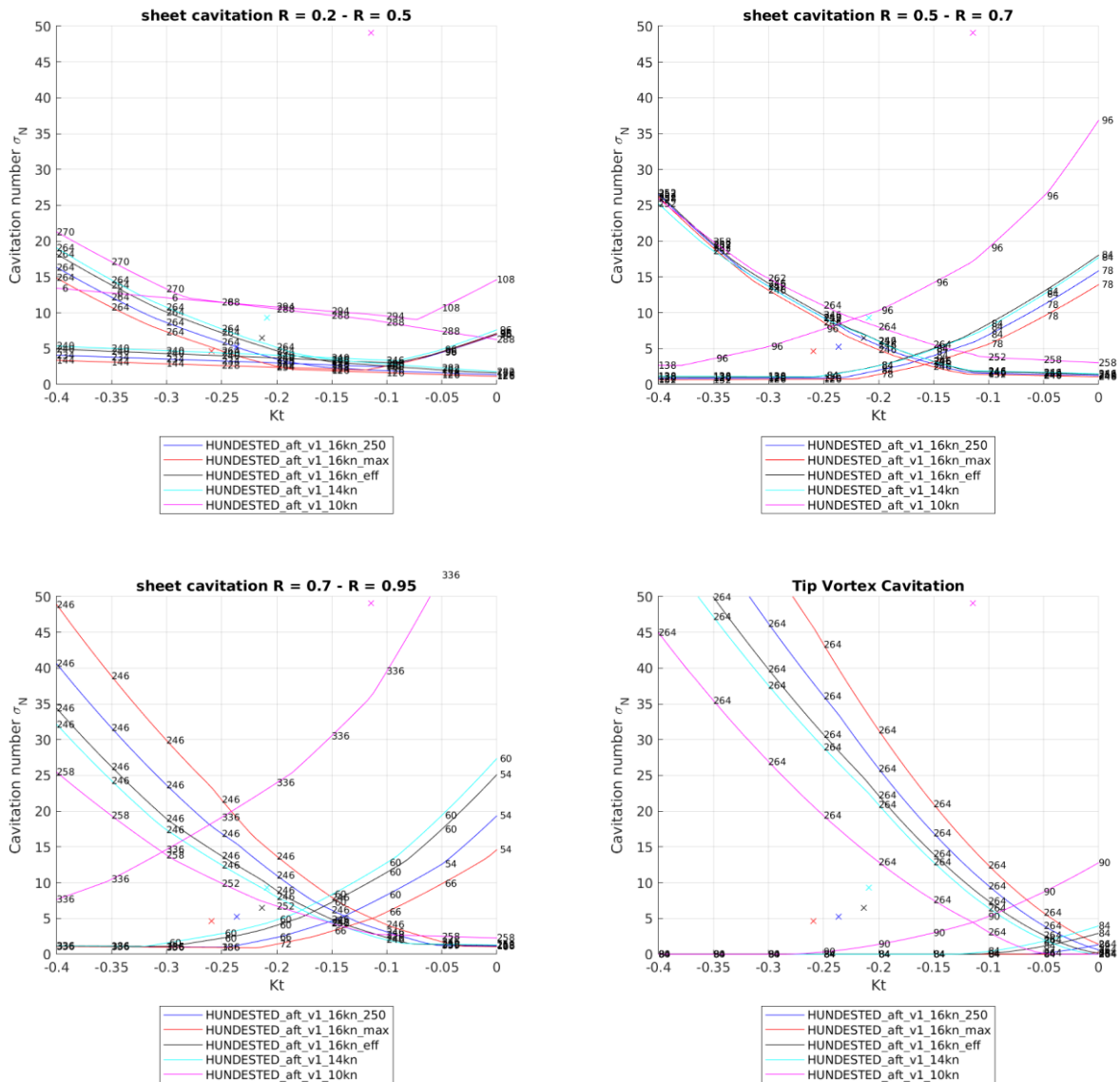


Figure 5-32: Computed sheet cavitation inception diagrams for the aft propeller during regeneration.

The differences in the inception curves are dominated by the pitch setting in each condition. Therefore, some inception lines are very similar. As shown, the cavitation bucket becomes smaller with increasing pitch, although usually the operational point is also at lower rpm which positions the operational point higher in the diagram.

The margins against back cavitation are very large. This would vote for an increase in camber to balance the suction- and pressure side cavitation more properly.

Some minor blade root cavitation is predicted for the 16 knots condition for both max regeneration and 250kW regeneration. The front propeller is slightly more sensitive to blade root cavitation compared to the aft propeller.

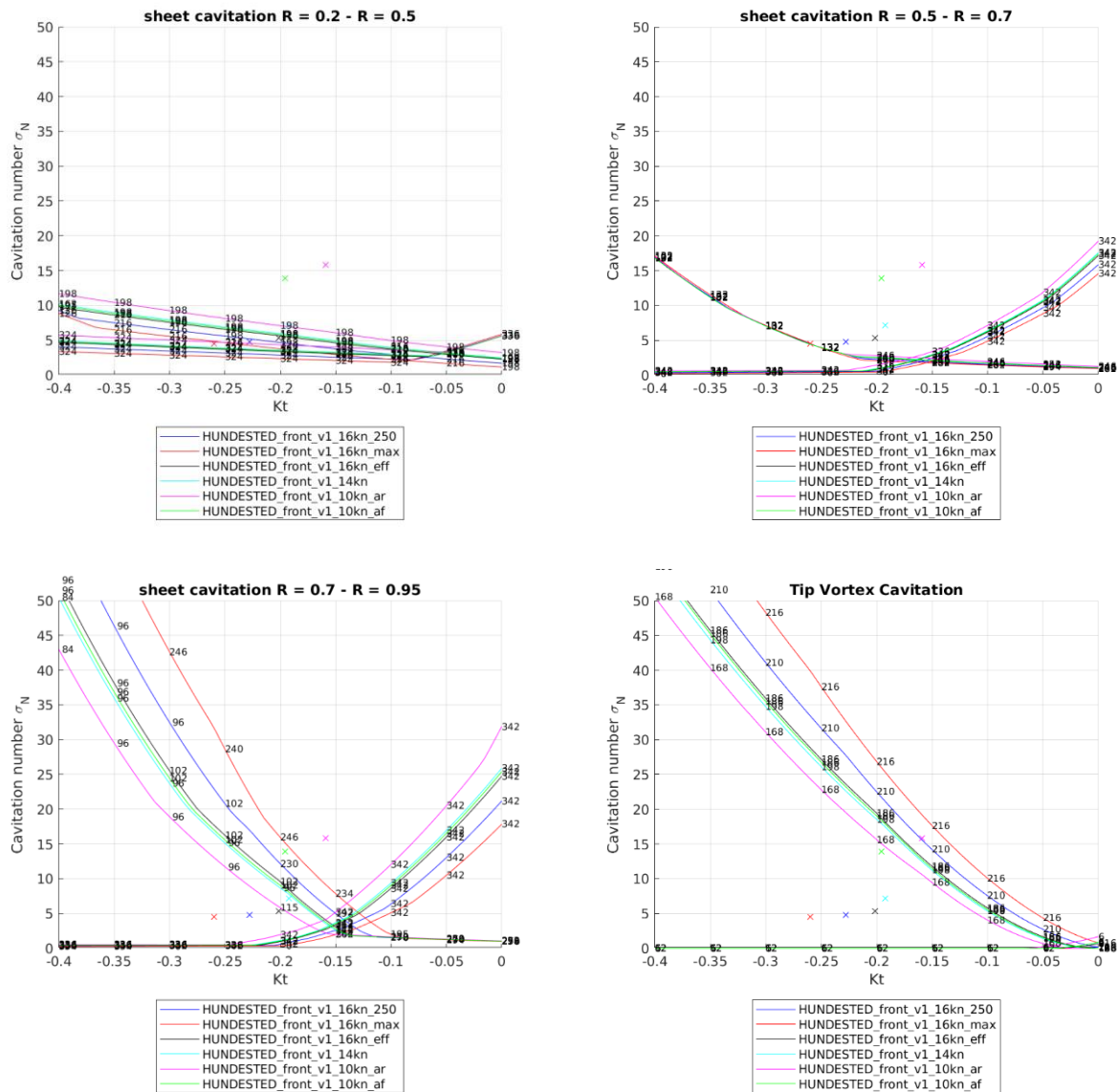


Figure 5-33: Computed sheet cavitation inception diagrams for the front propeller during regeneration.

5.5.3 Cavitation behaviour

Figure 5-21 provides sketches of the cavitation behaviour which are obtained from cavitation computations. In black the contour of the cavitation and propeller is given. Due to the regeneration, the cavitation occurs on the face side which is presented in purple.

Sheet cavitation occurs at 16 knots on the suction side (face side of propeller during regeneration), on both the front and aft propeller. The cavitation behaves stable and probably non-erosive, except for aft propeller in the scenario of maximum regenerating at 16 knots. Here the flow over the tip becomes very complex with too much interaction between the pressure distribution of the back and face side of the propeller blade.

The 16 knots conditions are also shown on figure pages F49 to F51 for multiple angles in the wake field.

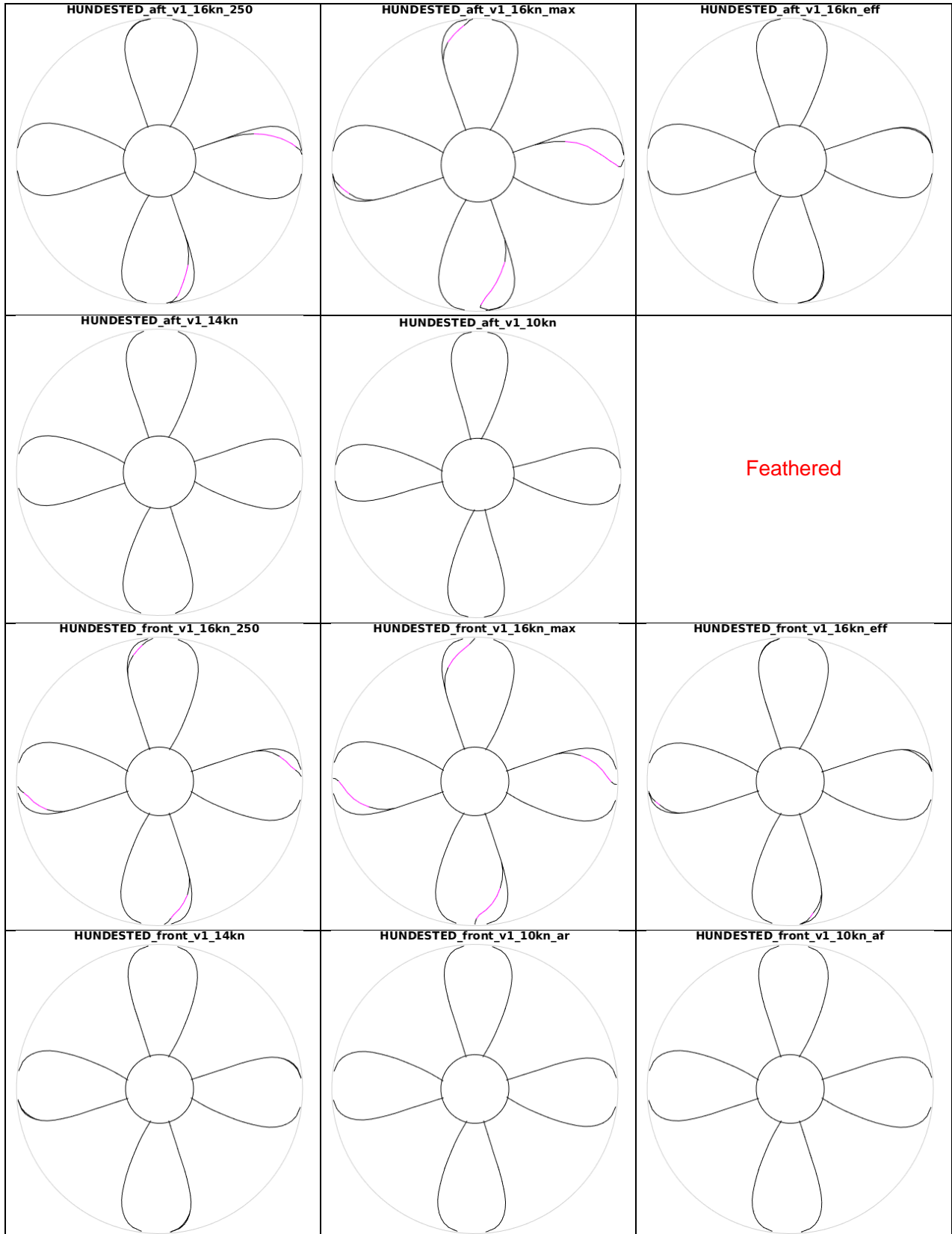


Figure 5-34: Computed cavitation behaviour of the aft propeller (top two rows) and front propeller (bottom row) during regeneration.

5.5.4 Underwater radiated noise

The estimate of the total underwater radiated noise is provided by Figure 5-22. The levels for 10 and 14 knots (almost) coincide on a base level. Although sheet cavitation is present in the 16 knots condition for 250 kW and max power regeneration, the noise of the tip vortex is dominant. For reference, the level of the DNV Quiet 11 knots notation is presented. As shown, the current propellers only exceed this level at 16 knots while regeneration maximum power. The front and aft propeller have similar levels, although the front propeller dominates the aft propeller.

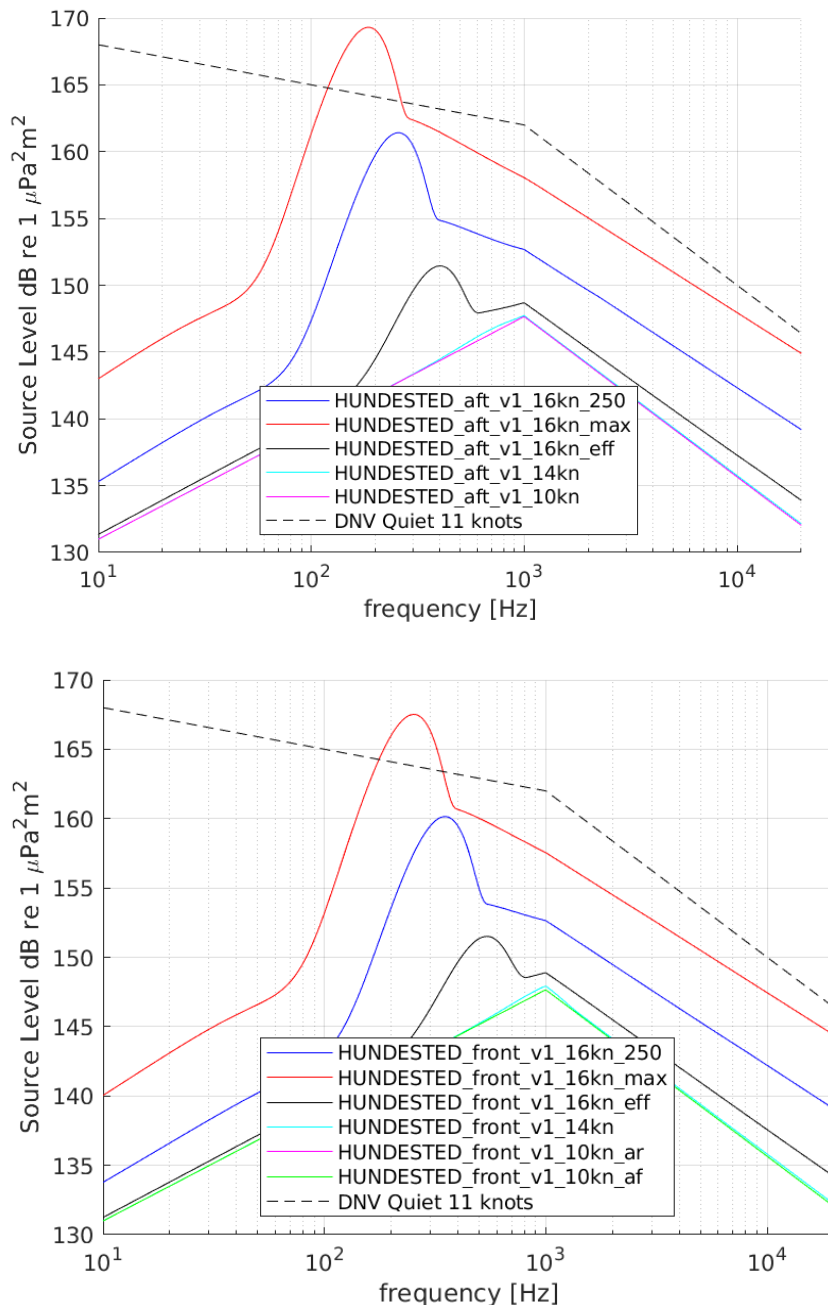


Figure 5-35: Underwater radiated noise predictions for the aft propeller (top) and front propeller (bottom) during regeneration.

5.5.5 Radial loading distribution

For the prediction of the inception of the tip vortices and the underwater radiated noise predictions the circulation was used. The circulation near the propeller tip can be regarded as a measure of the strength of the tip-vortices.

Therefore, for more insight, the distribution of the circulation over the propeller radius is given in Figure 5-23 and Figure 5-24. The solid line indicates the mean circulation, while the cross-marked and square-marked lines indicate the maximum and minimum circulation in the wake field respectively. As shown, the circulation near the tip is predominantly present which indicates that the propeller is not tip unloaded during regeneration.

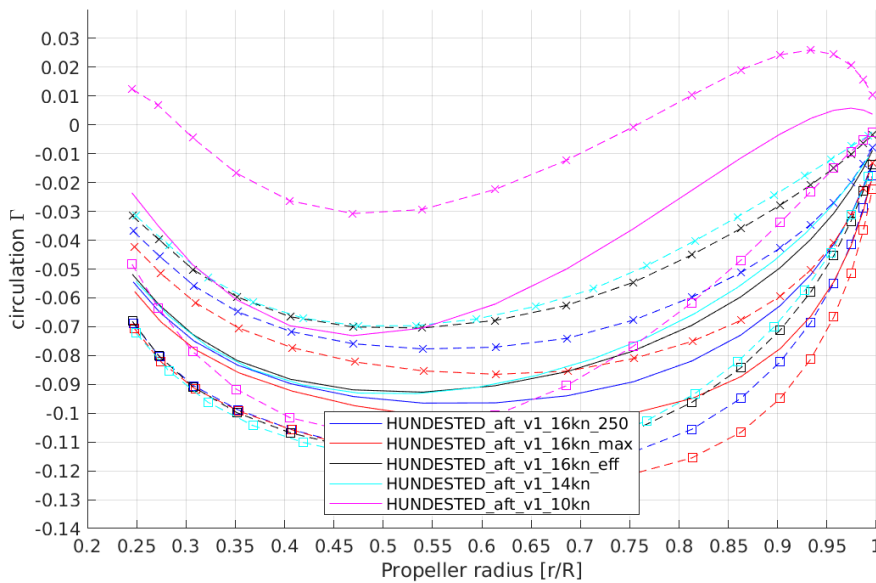


Figure 5-36: Radial distribution of the circulation for the aft propeller in regeneration.

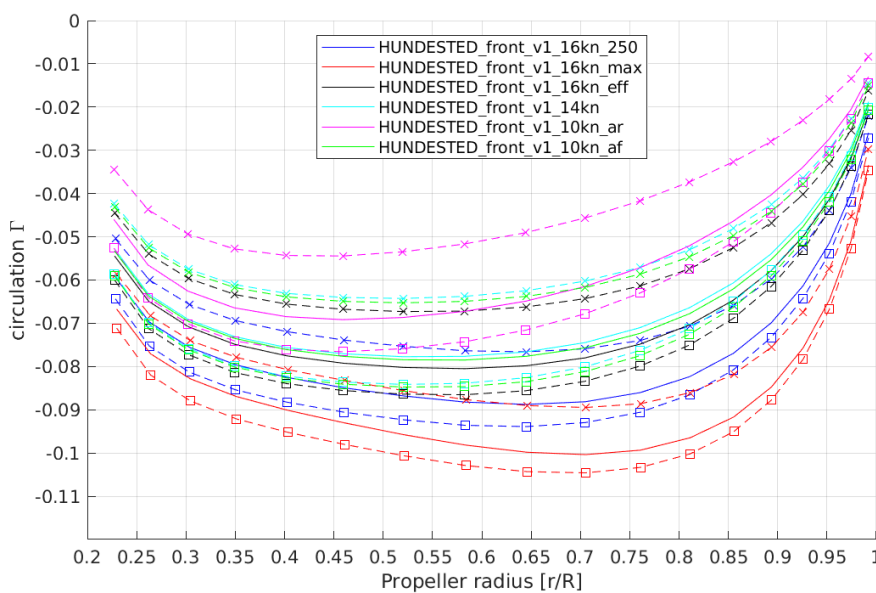


Figure 5-37: Radial distribution of the circulation for the front propeller in regeneration.

5.5.6 Hull pressure excitation

Figure 5-25 gives the results of the computations on hull pressure fluctuations as induced by the propeller and the cavitation on the propeller. For reference, a level of 1.0 kPa is commonly regarded as the upper limit for yachts, although some parties also require 0.75 kPa at maximum, which is only approached by the aft propeller at 16 knots in maximum regeneration.

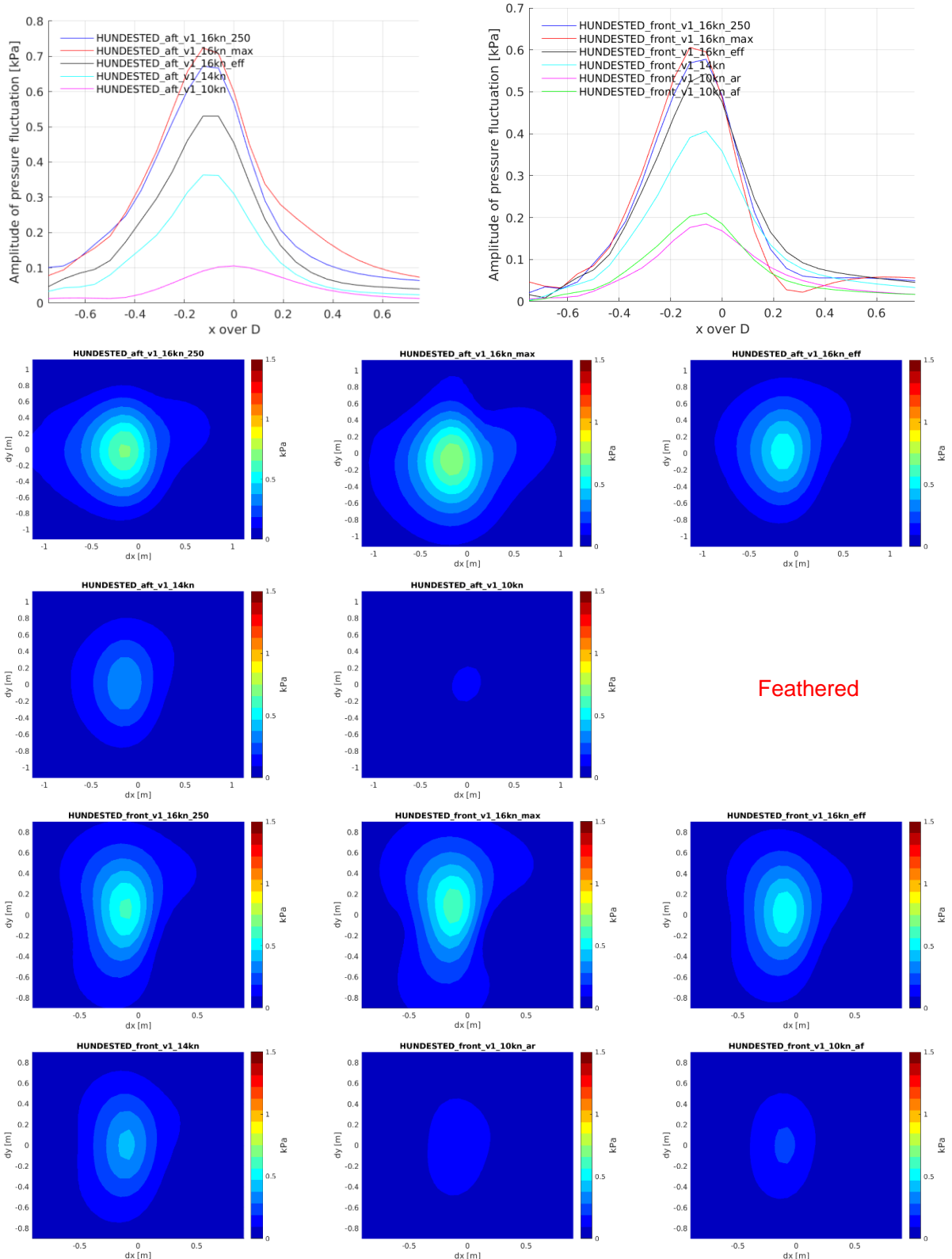


Figure 5-38: Computation of propeller-induced hull pressure fluctuation at the first blade harmonic frequency for both propellers in regeneration.

5.5.7 Thrust variation

The dimensionless blade and shaft forces are reported in Figure 5-39 and Figure 5-40 for the aft and front propeller, respectively. The wake from the aft propeller is relatively more complicated which gives also some more variation in the blade force. The shaft force variation, however, is quite limited. There are no indications for any issues due to thrust variations in that sense.

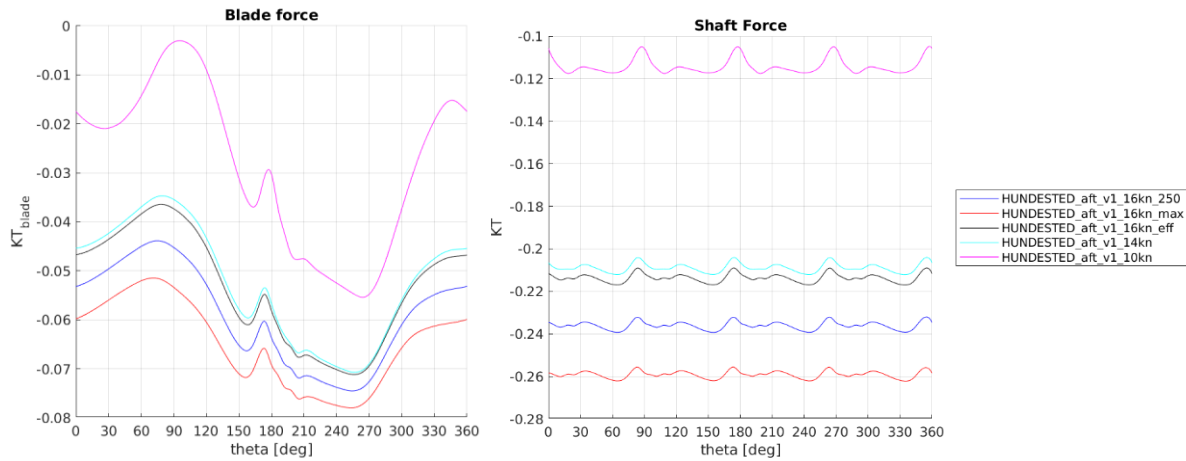


Figure 5-39: Blade and shaft forces for the aft propeller.

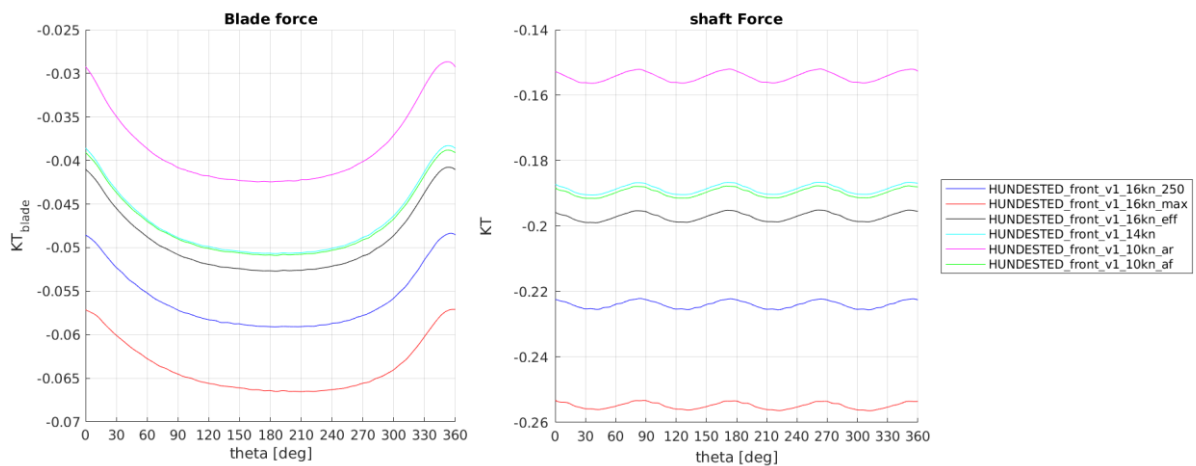


Figure 5-40: Blade and shaft forces for the front propeller.

5.5.8 Discussion points

It is advised to increase the maximum camber of the propellers to minimise the amount of cavitation which occurs at 16 knots in regeneration mode.

5.6 Propeller analysis, other requirements, bollard pull

Scenarios 8 to 10 deal with bollard pull, manoeuvring and crash stop, of which the bollard pull is the most relevant scenario in terms of propeller design. If the bollard pull is successful, other manoeuvring conditions are usually no problem. The crash stop is very dependent on the ship mass and other aspects and is usually tackled in a simulation using standard B-series data, which is outside the scope of the current propeller design review.

In bollard pull it is assumed that the propeller will absorb maximum power of 400 kW and 300 kW at the maximum rotation rate of 400 rpm and 500 rpm for the aft and front propellers, respectively. Using the polynomials, this gives a pitch $P_{0.7/D}$ of 0.671 and 0.719, and a bollard pull of 59.7 kN and 41.8 kN for the aft and front propeller respectively, assuming a commonly used thrust deduction factor of 0.05.

Cavitation during bollard pull is usually very stable and not critical in terms of erosion. PROCAL neglects the effect of vortices, which is why the outline colours red.

Too much cavitation could lead to thrust breakdown, from which the propellers do not yet suffer, although the margins are not large, especially for the front propeller.

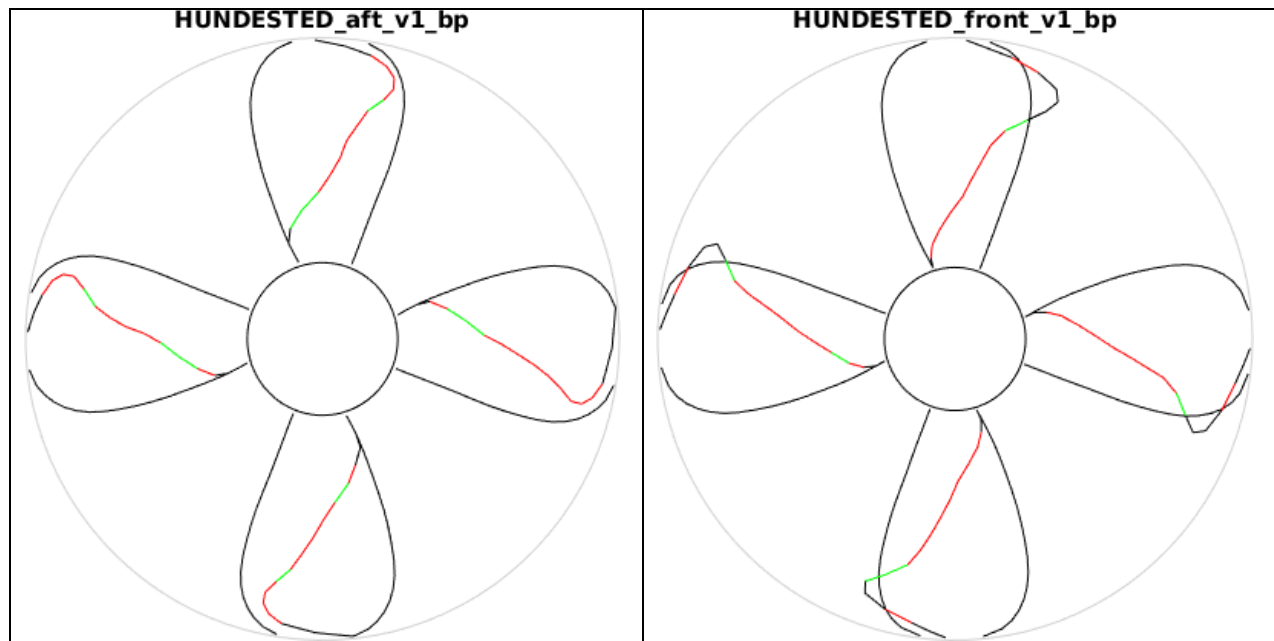


Figure 5-41: Cavitation extent during bollard pull at maximum power, maximum rotation rate.

6 EXPLORATORY DESIGN OPTIMISATION

6.1 Selected design conditions

For the design optimisation, an improved wake field for propulsion was assumed, as shown in Figure 6-1. The wake field was taken similar for the aft and front unit.

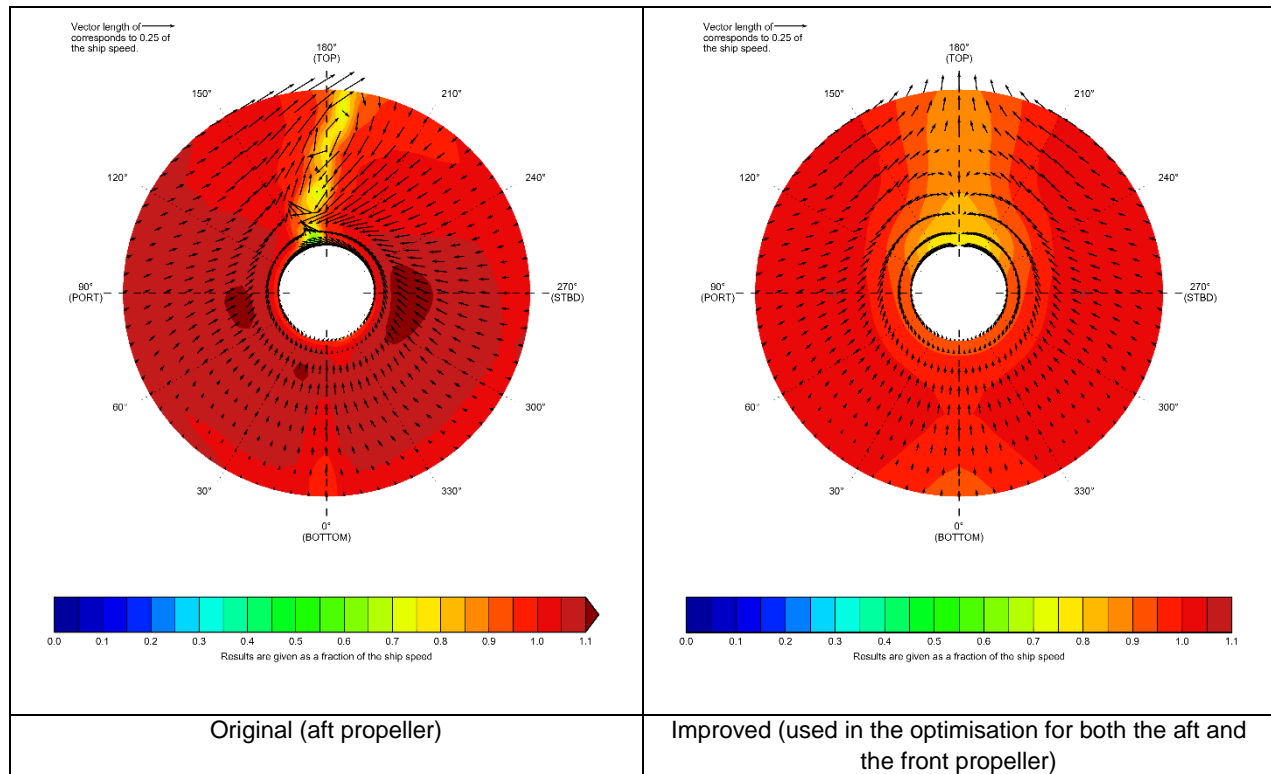


Figure 6-1: Assumed improved wake field for optimisation purposes.

The most demanding conditions were selected to be used in the optimisation. These conditions originate from the charter mode, scenarios 1 and 2.

- For propulsion, the condition is the 12.0 knots condition, delivered by both propellers. For the optimisation, this condition is defined in propeller thrust TH_p , as given in Table 5-1). at that speed. At this thrust, the objective is to minimise the consumed power. In this condition, the cavitation behaviour should be acceptable. For the front propeller, would it be used during propulsion, it should be suited for this. There, a more realistic pitch of $P_{0.7}/D = 1.2$ was selected at a thrust share of 25%. This condition was also presented in Table 5-1.
- For regeneration the condition is the 250 kW regeneration at 16 knots ship speed. For the optimisation, this condition is defined in the propeller drag TH_p , as given in Table 5-2. At this drag, the objective is to maximise the regenerated power. A constraint is that cavitation behaviour should be acceptable.

6.2 Geometry parametrisation

The geometry of the propellers was fully parametrised in both the radial and chordwise geometry distributions using Bezier curves, as shown in Figure 6-2 to Figure 6-6. The distributions for rake and maximum thickness follow a similar recipe.

The control points of the Bezier curves serve as the optimisation variables. Quite some variations are possible. The task of the optimiser is to find the most optimal distributions.

Especially for the blade profiles (chordwise camber and thickness distributions) the parametrisation was adapted with the purpose of regeneration in mind. The basis profile is symmetric in terms of thickness and camber. The optimiser will select the direction to tune, either favourable for regeneration or propulsion, or both simultaneously.

In total the parametrisation consist of 58 design variables, which makes this a very extensive optimisation problem. The blade profiles are defined at the root and a mid-radii (also a design variable) and the tip, in between which the profiles are interpolated.

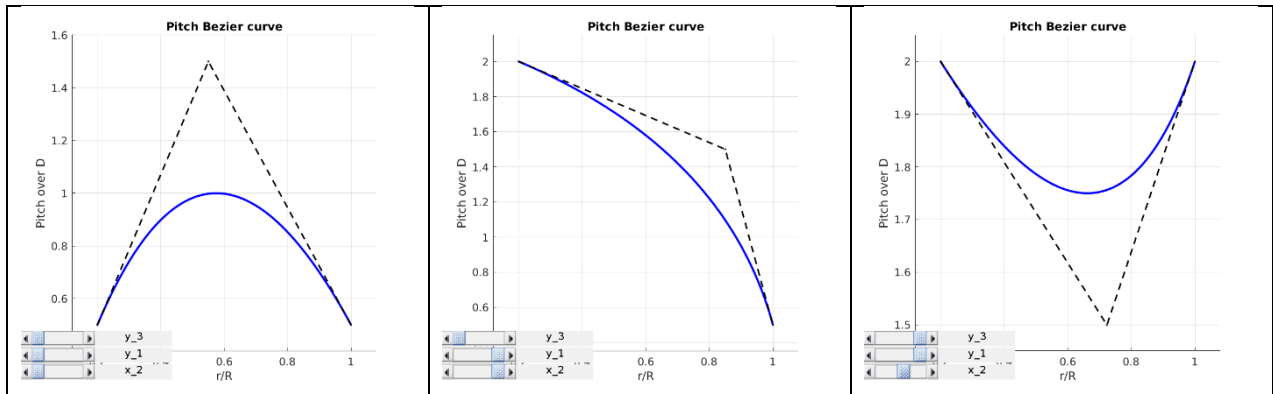


Figure 6-2: Bezier parametrisation of the radial pitch distribution (3 variations shown).

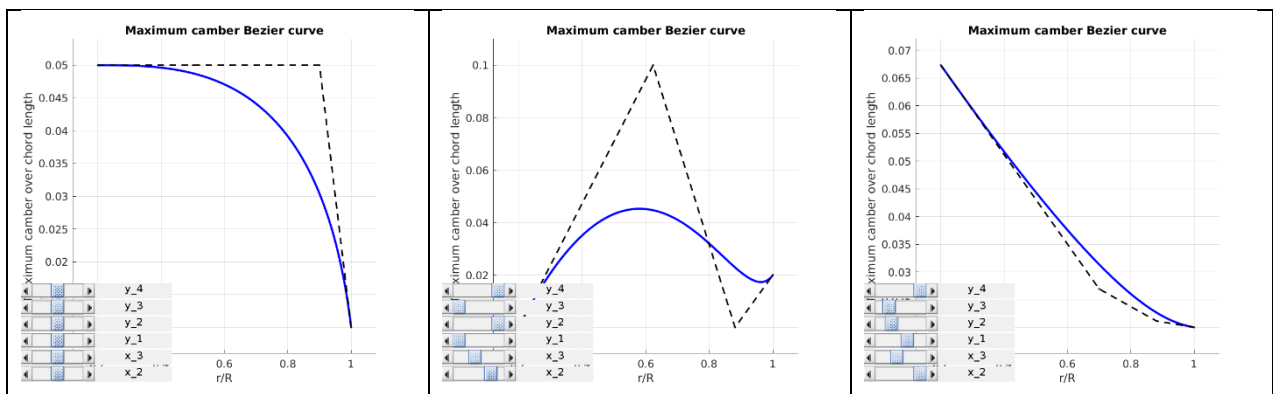


Figure 6-3: Bezier parametrisation of the radial camber distribution (3 variations shown).

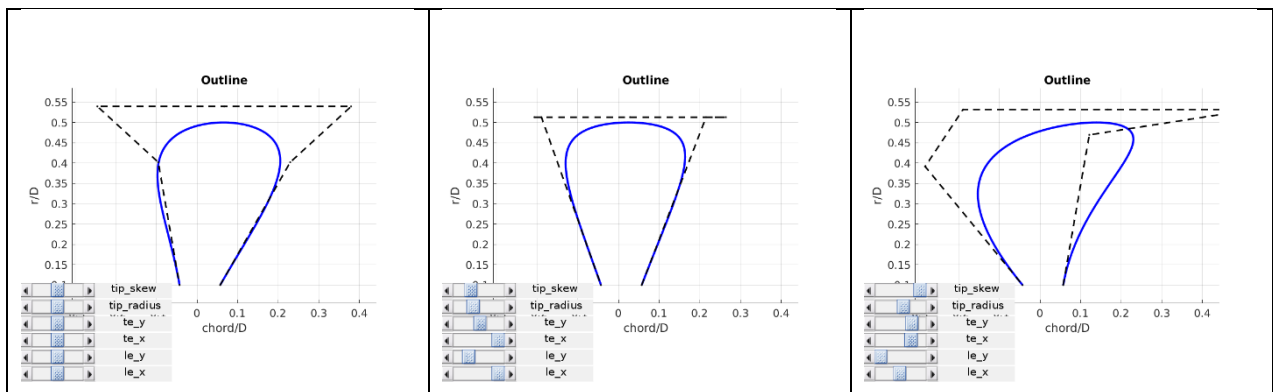


Figure 6-4: Bezier parametrisation of the radial outline (skew and chord) distribution (3 variations shown).

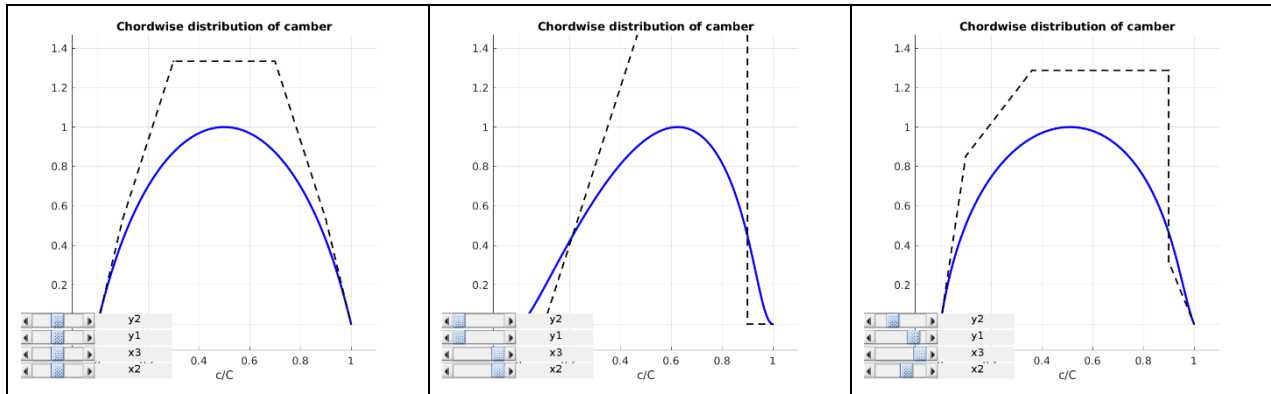


Figure 6-5: Bezier parametrisation of the chordwise distribution of camber (3 variations shown).

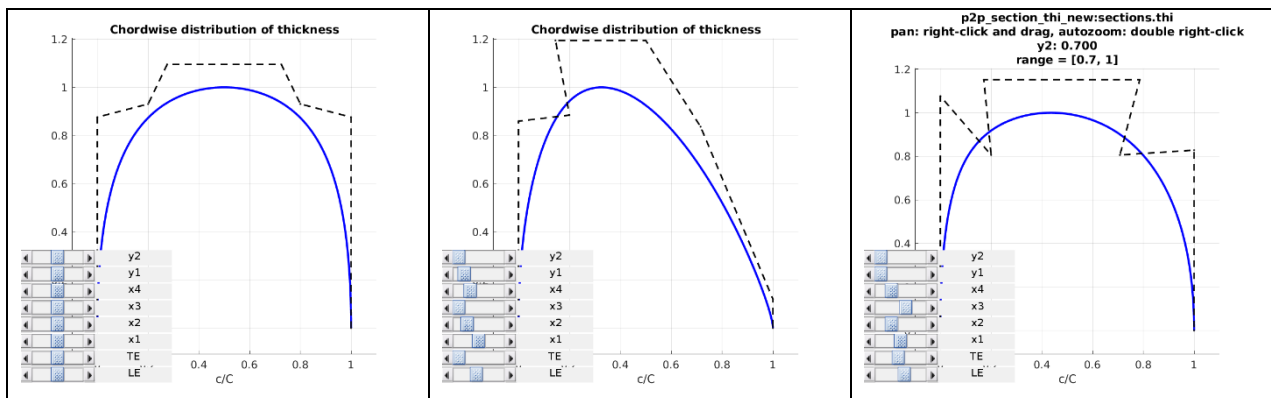


Figure 6-6: Bezier parametrisation of the chordwise distribution of thickness (3 variations shown).

6.3 Optimisation approach

In the optimisation the level of the radial distribution of propeller pitch is modified such that at the specified rotation rate the propeller drag equals the specified value. This design pitch is set in regeneration mode. The rotation rate is a variable during the optimisation, which thus allows freedom in the design pitch as well. For propulsion, the pitch is set, by rotating the entire blade along the spindle axis.

In total 6 PROCAL computations are done for each individual; 3 in generation mode and 3 in propulsion mode. One to set the pitch, one in an overloaded situation and one to analyse flow separation which is done using a steady (averaged) computation.

Based on the results, the optimisation objectives are evaluated. Several constraints were evaluated and applied to the optimisation algorithm, such as sufficient thickness to comply to class rules, avoidance of flow separation near the trailing edges and certain minimum cavitation margins to avoid root cavitation and mid-chord bubble cavitation for instance.

The diameters of the propellers were not part of the scope of the optimisation. The polynomials as created in this project provide a powerful means to optimise this again, if required.

The optimisation was approached initially for the aft propeller only. Different stages were done, each stage continuing upon the results of the previous stage with updated settings in terms of design space, constraints and objectives.

6.4 Optimisation results aft propeller

The first stage is initialised with a random population of propellers and focused on the optimisation of the power objectives. The optimisation was run until the performance of the propellers matched the design from Hundested. The results of the first stage of optimisation are shown in blue to red in Figure 6-7. The reference Hundested propeller is given as a black circle. Only a small Pareto front was found which indicates that improving on the power consumption in propulsion is in general also beneficial for the power regeneration during sailing.

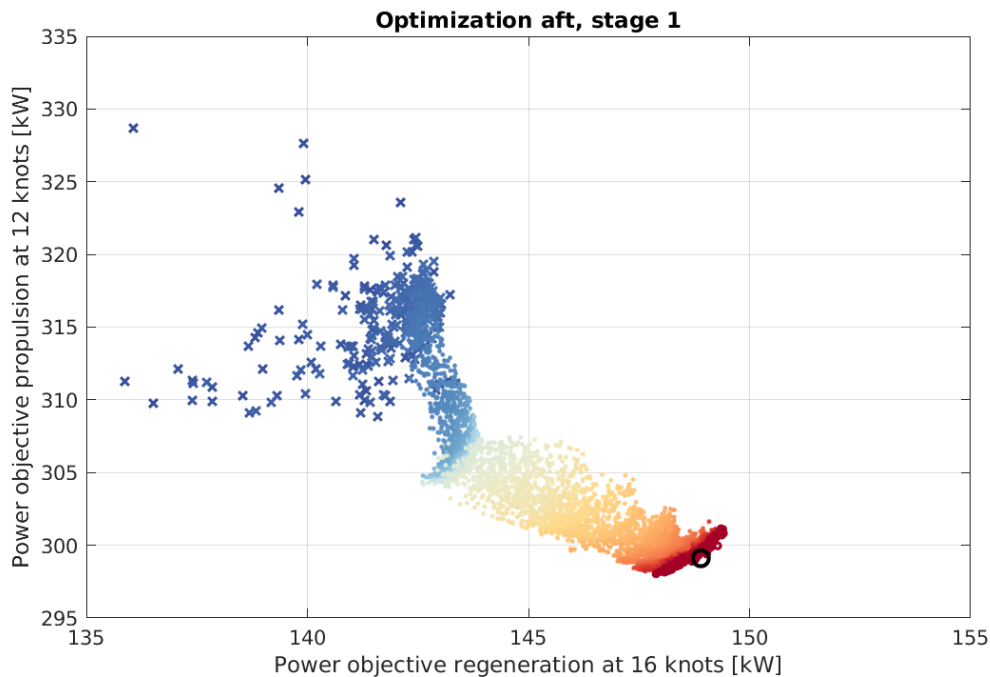


Figure 6-7: First stage of optimisation.

After this stage of optimisation the cavitation margins were optimised in a three-objective optimisation study. The results are shown in Figure 6-8, zoomed towards the Pareto Front, from which it becomes clear that there is a clear trade-off between power and cavitation margins. The optimisation done such that a positive cavitation margin is required, which means no cavitation in the design points. The Hundested design does not fulfil this criterion and is therefore not shown in the graphs. Instead, the black line indicates the power level of the Hundested design. As shown, it seems to be possible to improve on the regeneration power while improving the cavitation behaviour as well.

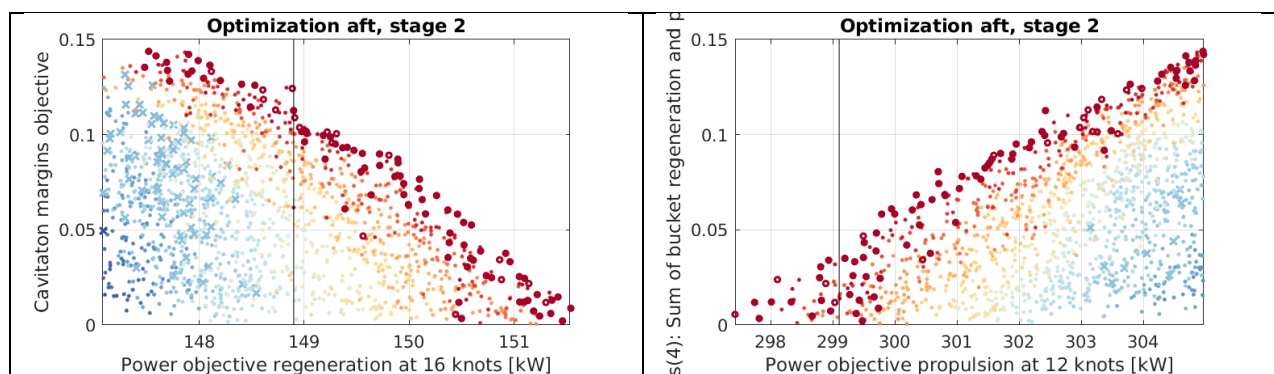


Figure 6-8: Second stage of optimisation.

The third and final stage of optimisation is again optimisation for the power objectives with a chosen value for the cavitation margins and a minimum regeneration power of 150 kW. It was considered that a small cavitation is sufficient and chosen at a value of 0.02 in the plots above

This stage was again approached using several iterative sub stages to also further optimise the cavitation performance. The sub stages are not reported. The total optimisation took almost 1000 generations of 96 propeller individuals to converge towards the final Pareto Front as shown in red, which took about 3 weeks of optimisation time. The results are shown in Figure 6-9, including also the final Pareto Front of stage 2 in dark blue.

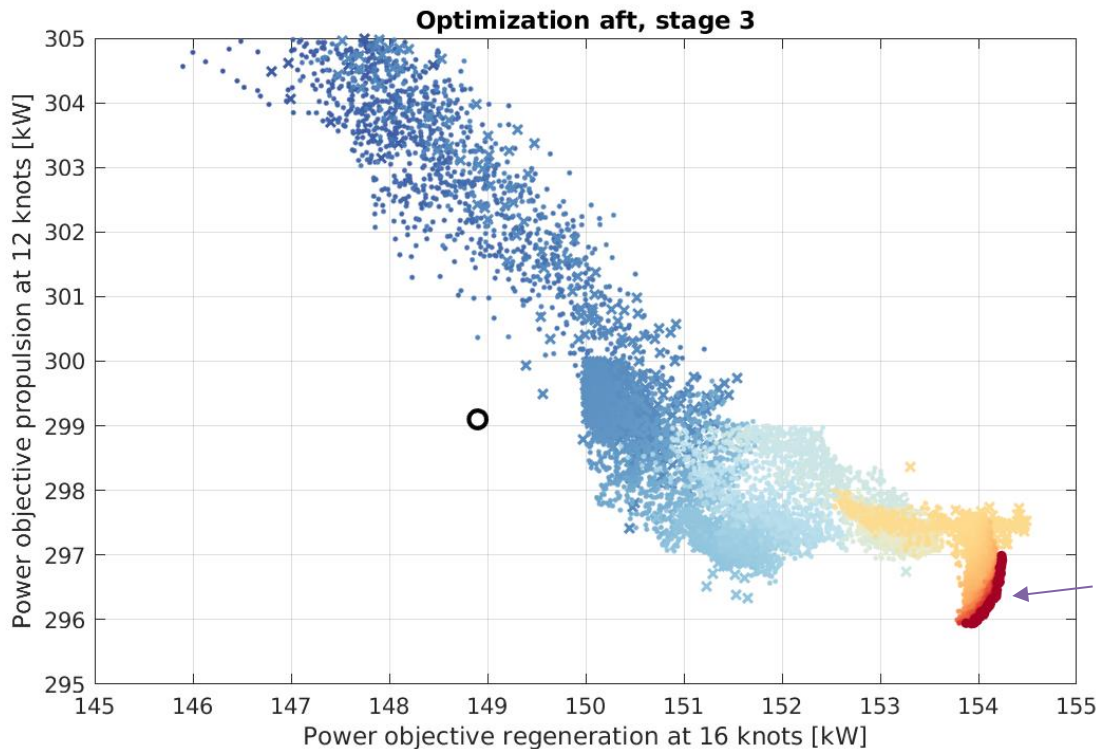


Figure 6-9: Final stage optimisation results for the aft propeller.

The final propeller for further analysis was chosen at the location of the front indicated by the purple arrow in Figure 6-9. The final rotation rate in regeneration was optimised towards 274.9 RPM, compared to 276.2 RPM and a pitch $P07/D = 0.909$ compared to $PD07/D = 0.831$, for the new design and the HUNDESTED design, respectively. As shown in Figure 6-9, the optimised propeller is about 1% more efficient in propulsion at 12 knots and about 3.5% more efficient during regeneration at 16 knots with 250 kW in total.

The optimised aft propeller is visualised in Figure 6-10. Geometrical details are provided on figure pages F52 to F54, note that the blade profiles are presented not to scale to clearly show the differences with the HUNDESTED design. The aft propeller was optimised towards a quite common propeller for propulsion, except for the skew and rake distribution. Also the blade profiles are not very uncommon, they are clearly not standard profiles. In addition, the trailing edge for propulsion has been designed as leading edge for regeneration.

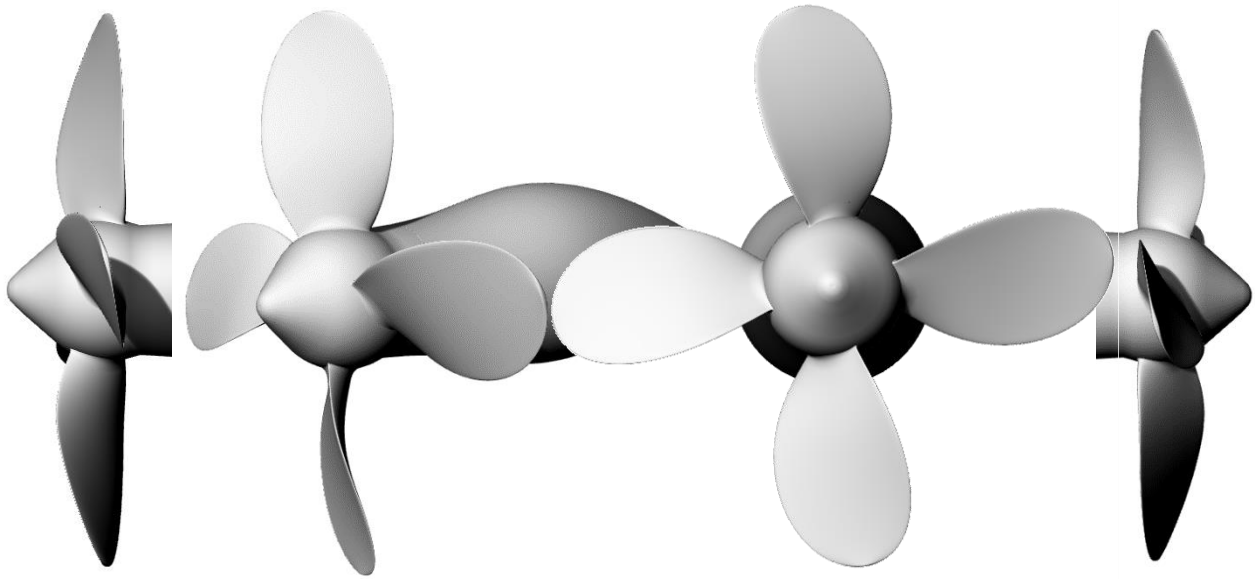


Figure 6-10: Rendered views on the optimised aft propeller.

The cavitation performance is summarised and compared with Figure 6-11 which is directly related to Figure 5-18 and Figure 5-31, although the propeller has been analysed in a modified wake field for propulsion. Figure 6-11 shows that:

- The optimised propeller has a slightly increased tip vortex inception for both conditions (the large marker at the tip at $r/R = 1$ is positioned at lower pressure). Nonetheless, Figure 6-12 shows that the developed tip vortex noise is slightly lower for the optimised propeller.
- The minimum pressure lines of the optimised propeller are below the horizontal line, which means that no sheet cavitation would be developing on the optimised propeller in both conditions.

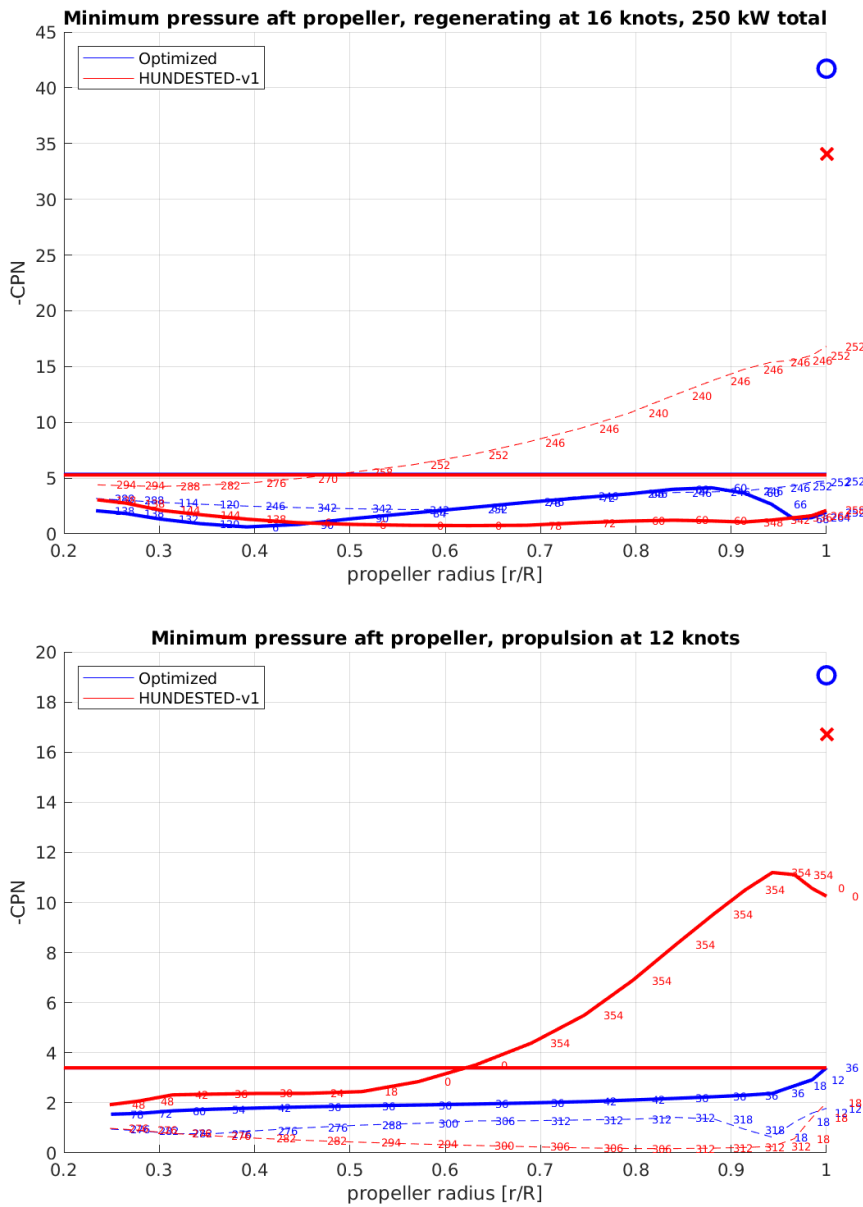


Figure 6-11: Minimum pressures on the propeller blades, optimised versus HUNDESTED-v1.

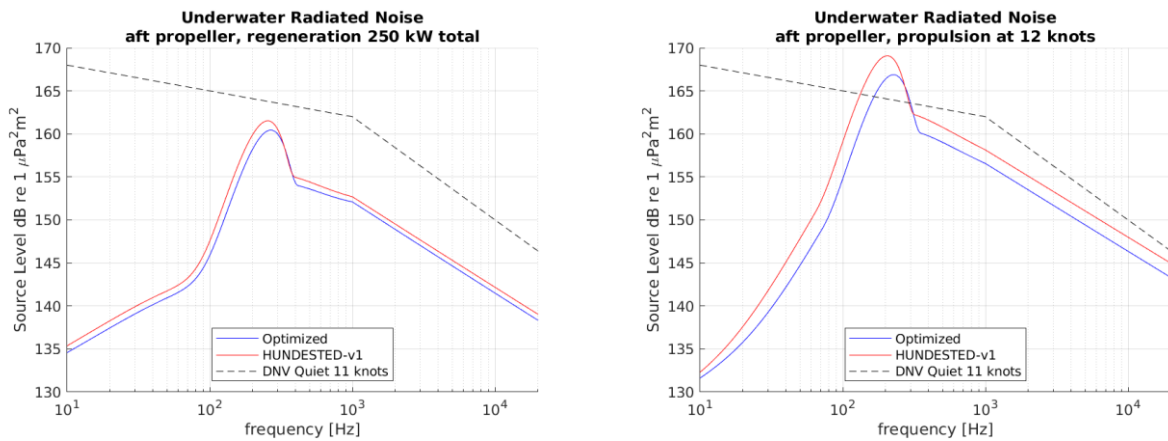


Figure 6-12: Underwater radiated noise predictions for the aft propeller, optimised versus HUNDESTED-v1.

6.5 Optimisation results front propeller

The front propeller is much lower loaded in propulsion compared to the aft propeller. In addition, the wake field during regeneration is cleaner. This makes the design of the front propeller different compared to the aft propeller.

A similar approach was followed for the front propeller as for the aft propeller, although the front propeller was initialised with the Pareto front of stage 2 of the aft propeller optimisation.

Again several sub iterations were performed for further improved cavitation performance and finally, the Pareto front was found, as shown in Figure 6-13. This optimisation is composed of another 800 generations of propeller designs. Again the Pareto Front is very small indicating that improving on the power consumption in propulsion is in general also beneficial for the power regeneration during sailing.

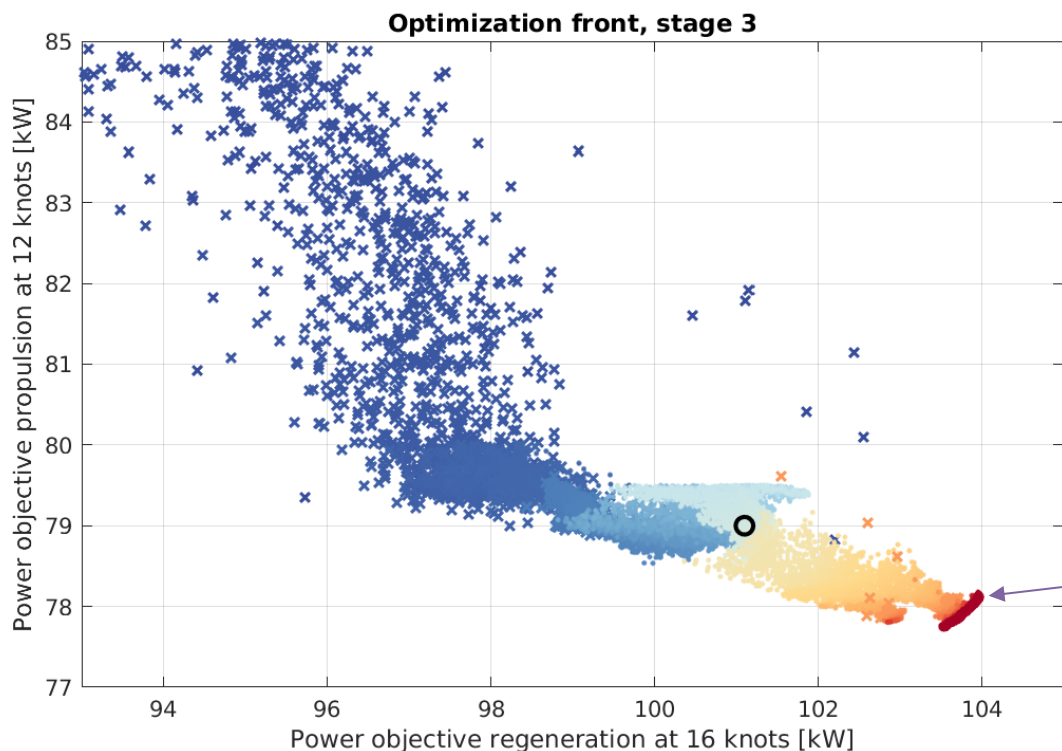


Figure 6-13: Final stage optimisation results for the front propeller.

The final propeller for further analysis was chosen at the location of the purple arrow in Figure 6-13. The final rotation rate in regeneration was optimised towards 340.7 RPM, compared to 360.3 RPM and a pitch $P07/D = 0.924$ compared to $PD07/D = 0.806$, for the new design and the HUNDESTED design, respectively. As shown in Figure 6-9, the optimised propeller is about 1% more efficient in propulsion at 12 knots and about 2.9% more efficient during regeneration at 16 knots with 250 kW in total.

The optimised aft propeller is visualised in Figure 6-14.

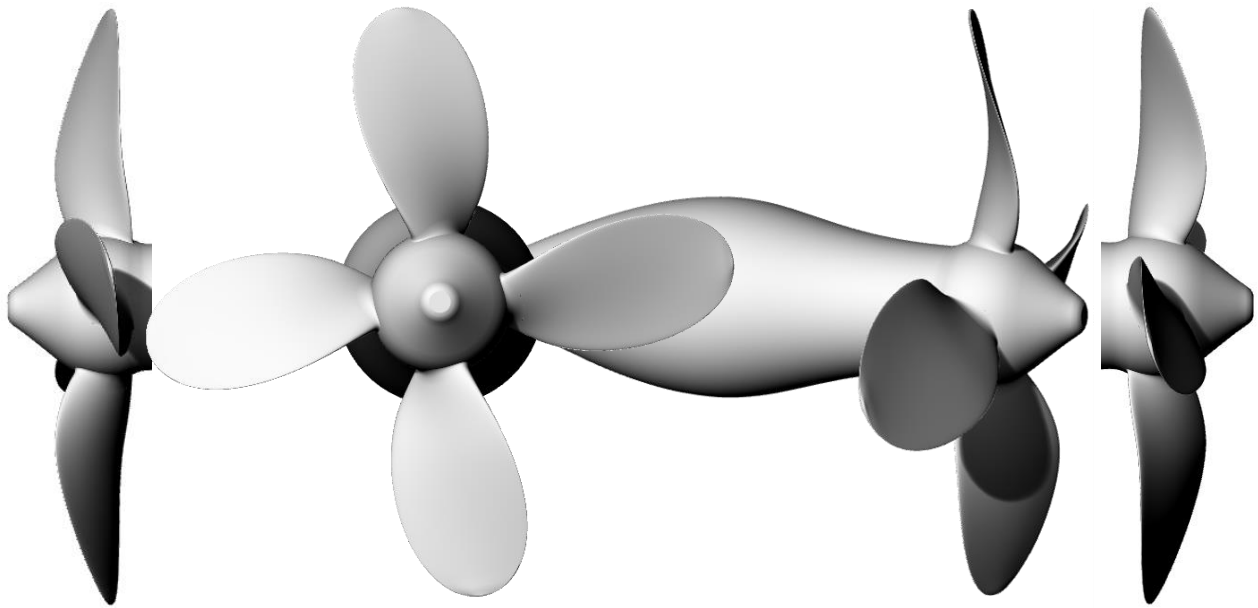


Figure 6-14: Rendered views on the optimised front propeller.

Geometrical details are provided on figure pages F55 to F57. Note that the blade profiles are presented not to scale to clearly show the differences with the HUNDESTED design. The front propeller was also optimised towards a quite common propeller for propulsion in terms of pitch and camber distribution, but the skew and rake distribution clearly differ. Also the blade profiles are more uncommon, as if mirrored, optimised for cavitation performance in regeneration mode. Most probably, the thickness in the tip can be reduced if the propeller would additionally be optimised for weight, which is left to final consideration and not within the scope of the current work.

Although the front propeller is even more tailored to power regeneration, the efficiency gain with respect to the HUNDESTED propeller is less than the gain obtained for the aft propeller. This is due to the wake adaptation of the aft propeller to the less uniform wake in regeneration and would be accounted for in the relative rotative efficiency if the propulsion coefficients would be properly split out.

In addition, it was seen during the optimisation that the location of the maximum camber does not affect the efficiency of the propeller significantly. Cavitation performance is influenced, however, which is why the aft propeller has the position of camber shifted backward in propulsion mode. The front propeller is more critical in regeneration for cavitation, which is why the position of camber is shifted backward in regeneration mode instead.

The cavitation performance is summarised and compared with Figure 6-15 which shows that:

- The optimised propeller has a slightly increased tip vortex strength for both conditions (the large marker at the tip at $r/R = 1$ is positioned at lower pressure). Nonetheless, Figure 6-16 shows that the developed tip vortex noise is slightly lower for the optimised propeller during regeneration.
- The minimum pressure lines of the optimised propeller are below the horizontal line, which means that no sheet cavitation would be developing on the optimised propeller in both conditions.

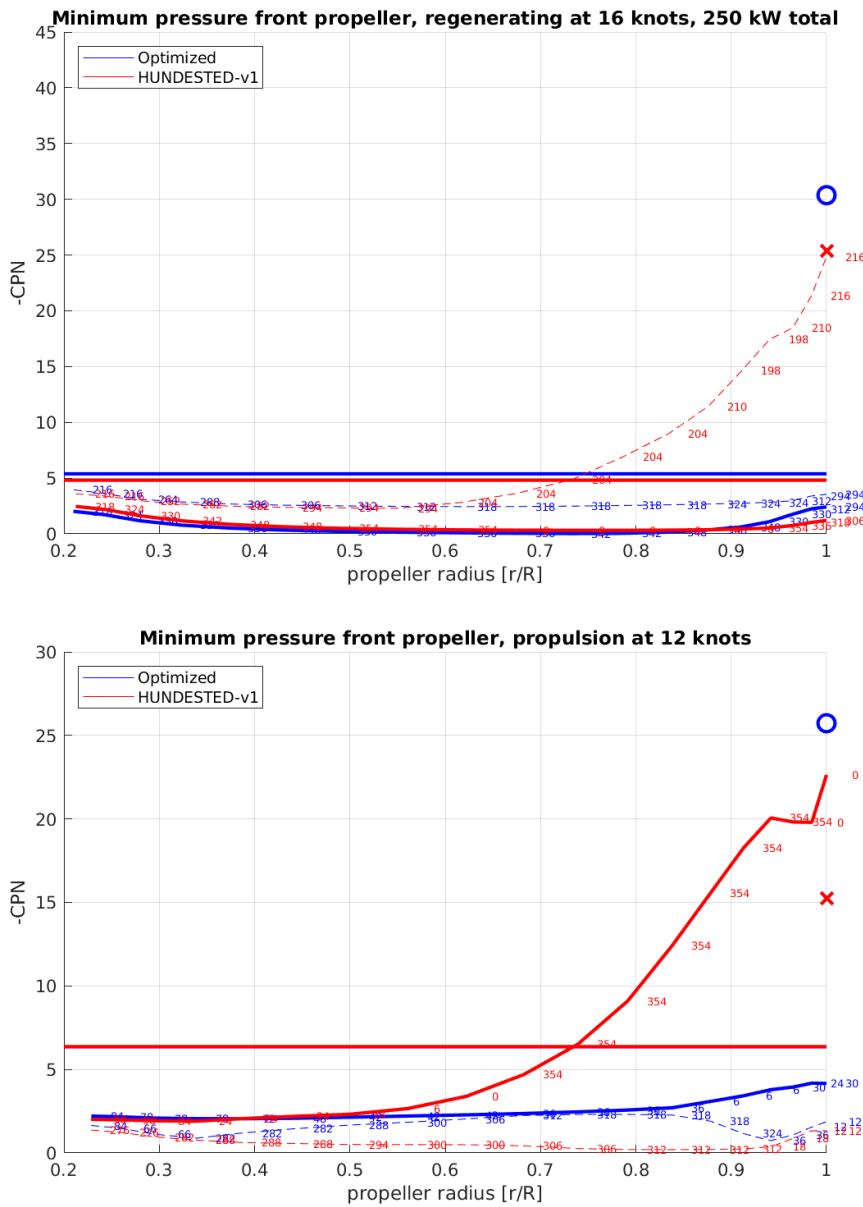


Figure 6-15: Minimum pressures on the propeller blades, optimised versus HUNDESTED-v1.

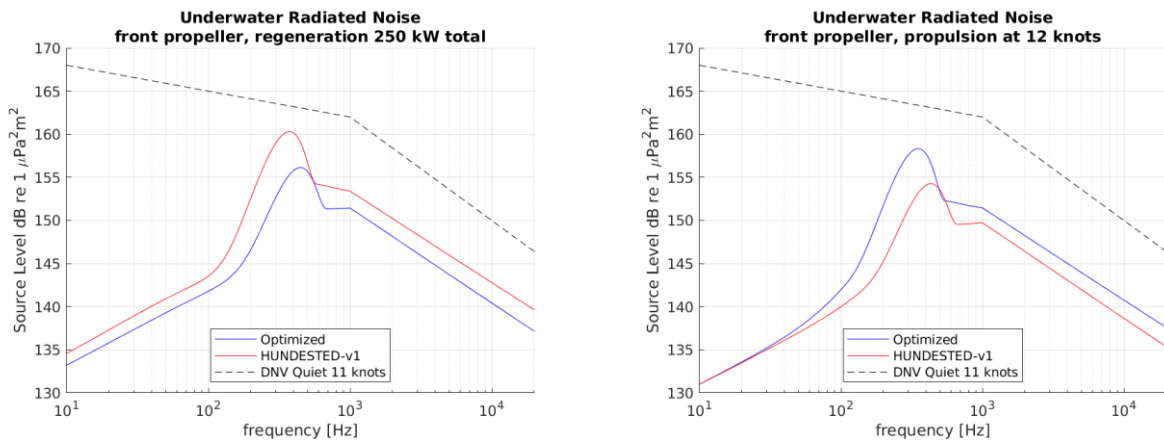


Figure 6-16: Underwater radiated noise predictions for the front propeller, optimised versus HUNDESTED-v1.

6.6 Discussion points

Using propeller optimisation studies it was shown that improvements up to 3.5% in terms of regeneration efficiency are possible. Larger savings might be possible at the cost of loss in bollard pull and increased cavitation extent, larger hull pressure levels and more underwater radiated noise. In MARIN's opinion the currently optimised propellers feature a good balance between efficiency and cavitation nuisance in view of the yacht type of application which comes normally with high comfort standards.

A normal propeller features an anti-singing edge at the trailing edge. In view of the usage of the trailing edge in regeneration it is not advised to apply an anti-singing edge, although this increases the risk on propeller singing in propulsion. Propeller singing in regeneration remains a risk.

The propellers encounter a large variety in design conditions, both in beta value and pitch settings. This should ideally be taken into account in the optimisation. This increases however the complexity of the optimisation to another level and was regarded outside the scope of the current work.

The same extensive analysis of optimised propeller as was done for the HUNDESTED propellers was regarded out of scope of work as well for this exploratory optimisation study.

7 CONCLUSIONS AND RECOMMENDATIONS

The following conclusions summarise the findings of the present project:

Three CFD computations were performed using RANS-BEM to obtain the wake field of the ship and thrusters both in regeneration and propulsion. In propulsion the wake field was determined both with feathered and working front propeller. CFD computations were performed using RANS-BEM on both thrusters to determine the open water characteristics, both in propulsion and regeneration mode. Polynomials as function of propeller pitch and advance coefficient for both propulsion and regeneration were determined, for both the front and aft thruster. These polynomials can be integrated in the performance prediction programs. Using the polynomials, based on the usage scenarios, operational conditions were determined in terms of propeller pitch and propeller rotational speed for both propulsion and regeneration.

- It was shown that from a propulsion-hydrodynamic point of view it is more efficient to propel or regenerate with lightly driven front or aft propeller, respectively.

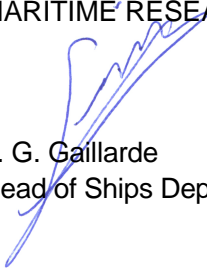
Using computational tools MARIN analysed the performance of the propeller designs in terms of powering, regeneration and cavitation behaviour.

- The HUNDESTED propellers show quite some cavitation, both in propulsion at 12 knots and regeneration at 16 knots. At 12 knots propulsion, the propeller hull excitation with a pressure fluctuation of 2.0 kPa clearly exceeds the usual limit of 1.0 kPa. The computations show that the propellers could need some adjustment in terms of the camber distribution to better balance the cavitation margins. The cavitation performance in propulsion is strongly related via the camber and pitch distributions to the cavitation performance in regeneration.
- Exploratory design studies were performed to provide design directions for the final design of the propellers. It was shown that improvements of about 3% in power regeneration were possible while the propulsive performance could be improved by about 1% and improving the cavitation behaviour as well. It was found that improving on the power consumption in propulsion is in general also beneficial for the power regeneration during sailing. No large trade-offs were found.

It is recommended to adapt the geometry of the strut of the thrusters, which were shown to be sensitive to flow separation which hampers the propeller performance in terms of cavitation and shaft excitation forces during propulsion.

The conclusions and recommendations do not supersede the more detailed comments made in the report.

Wageningen, February 2023
MARITIME RESEARCH INSTITUTE NETHERLANDS


Ir. G. Gaillarde
Head of Ships Department

TABLES

powers		aft			front		
Pitch	J	Ktu	Ktp	Kq	Ktu	Ktp	Kq
P07/D							
0	0	0.2461	0.1066	0.0132	-0.1456	-0.2383	0.0551
1	0	-1.6510	-0.7191	-0.0363	0.5169	1.0812	-0.3371
2	0	5.7629	3.3215	0.0390	1.0634	-0.2604	0.8590
3	0	-7.6503	-4.4126	0.1338	-2.3396	-0.7863	-0.9502
4	0	5.3662	3.0606	-0.1209	1.9545	1.0018	0.6197
5	0	-1.9295	-1.0883	0.0435	-0.7588	-0.4677	-0.2136
6	0	0.2768	0.1536	-0.0065	0.1115	0.0767	0.0295
0	1	-1.1569	0.2511	-0.1948	2.9679	2.7238	-0.2581
1	1	7.2609	-2.8333	1.8448	-16.3683	-15.0910	2.5227
2	1	-21.8810	6.6561	-6.1525	32.4317	29.6888	-8.2695
3	1	32.2410	-7.9649	9.5213	-32.1622	-28.7939	12.4019
4	1	-25.0015	4.9216	-7.6316	16.8753	14.3755	-9.5103
5	1	9.7718	-1.4650	3.0519	-4.4164	-3.4021	3.6201
6	1	-1.5120	0.1634	-0.4802	0.4461	0.2777	-0.5416
0	2	1.1849	-0.3101	-0.2945	-8.8969	-6.3085	-0.4222
1	2	-6.1008	8.6453	-1.5890	50.9026	36.0061	-1.2866
2	2	25.3466	-28.4718	13.9832	-113.1927	-78.2505	12.3496
3	2	-55.3152	35.5647	-30.7101	121.9286	78.6672	-25.8492
4	2	57.0917	-19.5726	29.4466	-66.4372	-36.3873	23.5389
5	2	-27.1732	4.2274	-13.0489	16.9781	5.9358	-9.9444
6	2	4.8346	-0.1379	2.1887	-1.4966	0.1660	1.5955
0	3	-2.8445	-4.4088	2.2114	5.4570	3.0470	2.1204
1	3	-6.6857	0.1508	-10.8554	-40.1227	-25.3618	-7.9454
2	3	27.0529	32.2064	12.0865	117.3282	79.5451	6.8210
3	3	-5.1537	-49.8668	6.0486	-150.7340	-99.3796	5.3559
4	3	-34.6590	23.7878	-17.7818	88.6456	48.9862	-11.1342
5	3	29.0465	-0.7007	10.1818	-21.1832	-4.9586	5.8048
6	3	-6.7267	-1.3901	-1.8599	1.0934	-1.6018	-1.0017
0	4	8.4123	9.2674	-1.3723	1.8672	1.5685	-2.0153
1	4	-9.9168	-24.5598	12.3985	-20.3440	-17.9470	8.8749
2	4	-38.6119	1.5124	-23.5781	9.1562	5.1495	-10.8420
3	4	75.0483	39.8282	12.7854	40.9510	42.8576	2.0569
4	4	-36.5398	-31.0709	2.0937	-45.3190	-41.7200	3.0179
5	4	-0.6958	4.7989	-2.7439	12.8832	8.7496	-1.2335
6	4	2.8607	1.1113	0.3489	-0.1636	0.9737	0.0332
0	5	-7.4055	-4.8402	-1.2621	5.5226	5.2234	0.6840
1	5	35.2899	28.8157	-3.6692	13.5363	13.2450	-6.5948
2	5	-41.5823	-44.6707	17.1367	-49.9188	-48.5045	12.4353
3	5	-1.2612	13.9296	-15.1993	37.5331	31.7482	-5.8422
4	5	19.9574	9.7024	2.0530	-1.4781	4.0721	-1.3706
5	5	-6.9096	-4.9534	0.9498	-3.5039	-5.0415	1.0055
0	6	-2.8203	-3.3019	2.3805	-8.1588	-7.8501	1.2515
1	6	-1.0374	3.7739	-7.0491	18.0143	18.0079	-1.9861
2	6	22.2169	13.9508	1.8196	-6.6519	-3.4677	-3.4829
3	6	-22.7494	-18.4010	6.0351	-12.1891	-15.9613	5.7387
4	6	6.9703	6.4299	-2.8312	6.1313	7.2821	-1.8817
0	7	1.4644	0.8912	0.1667	0.4831	0.1890	-0.2752
1	7	-9.3922	-8.1774	2.7347	-3.6879	-4.8706	2.8729
2	7	9.8421	9.5378	-5.8317	10.6375	12.1711	-3.7221
3	7	-3.7166	-3.9304	2.3027	-4.5525	-5.0551	1.2449
0	8	1.3087	1.2863	-0.6186	0.3380	0.6505	-0.5010
1	8	-1.7907	-1.9594	1.8351	-3.4347	-3.7258	0.9129
2	8	1.2362	1.4026	-0.8175	1.6735	1.7784	-0.3816
0	9	0.0629	0.0922	-0.2036	0.5529	0.5367	-0.0651
1	9	-0.2900	-0.3285	0.1203	-0.2820	-0.2861	0.0530
0	10	0.0426	0.0457	-0.0028	-0.0008	0.0010	-0.0035

POLYNOMIAL FOR THE PERFORMANCE OF THE AFT AND FRONT UNIT IN PROPULSION AS FUNCTION OF PITCH AND ADVANCE COEFFICIENT

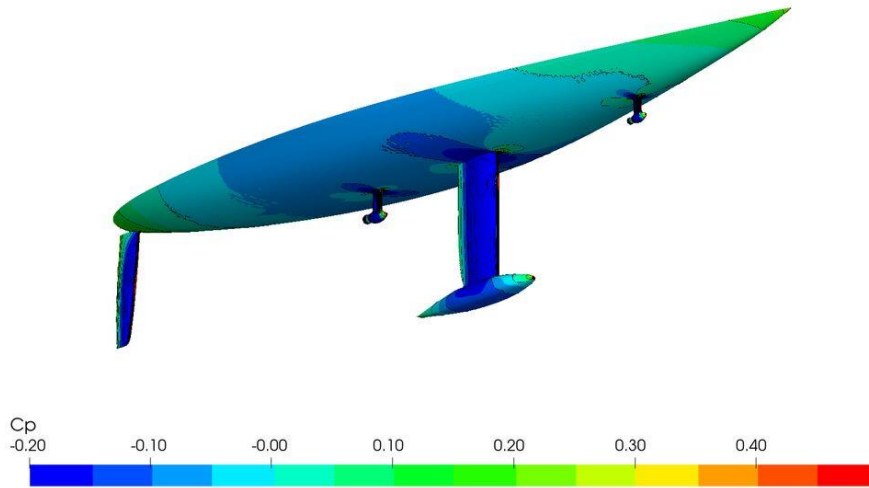
powers		aft			front		
Pitch	Beta - π	Ctu	Ctp	10Cq	Ctu	Ctp	10Cq
P07/D	[rad]						
0	0	-0.92	0.70	-1.31	0.41	-0.29	-0.55
0	1	13.13	-6.67	5.76	-11.39	-1.38	9.90
0	2	-65.77	34.80	16.67	75.15	11.60	-62.80
0	3	149.06	-133.24	-212.10	-262.28	-43.98	194.40
0	4	-166.82	328.07	768.30	538.12	85.84	-369.99
0	5	56.65	-516.52	-1544.15	-691.54	-86.65	467.22
0	6	82.72	531.01	1945.74	578.24	36.83	-383.69
0	7	-118.57	-356.22	-1567.47	-315.05	7.59	197.10
0	8	66.68	150.38	780.77	107.36	-14.86	-64.28
0	9	-18.19	-36.28	-218.15	-20.67	5.84	15.47
0	10	1.99	3.82	26.05	1.73	-0.78	-2.57
1	0	1.19	-2.95	7.94	1.92	2.77	-0.40
1	1	-24.07	18.32	-50.80	8.14	-1.95	-11.94
1	2	145.49	-33.51	131.41	-81.63	-8.69	98.35
1	3	-332.48	69.15	-124.24	329.42	73.76	-259.25
1	4	403.49	-145.01	-11.55	-658.45	-192.18	409.10
1	5	-278.30	197.68	81.79	733.54	245.06	-511.65
1	6	89.31	-162.77	-42.44	-491.07	-168.40	454.19
1	7	8.94	80.76	16.48	200.57	62.15	-218.82
1	8	-14.60	-22.27	-13.10	-45.87	-10.66	36.78
1	9	2.79	2.54	4.28	4.23	0.39	2.75
2	0	1.02	5.78	-16.94	-8.81	-8.03	5.19
2	1	6.75	-34.97	105.19	28.62	16.03	-10.24
2	2	-106.92	46.38	-266.31	-50.53	-31.70	-53.51
2	3	251.95	-25.52	294.04	-38.96	28.07	152.14
2	4	-273.36	22.01	-76.07	231.74	35.01	-83.24
2	5	178.14	-33.74	-89.24	-273.21	-93.38	-21.32
2	6	-76.54	25.47	51.16	146.64	73.03	-24.54
2	7	18.12	-9.58	6.91	-40.84	-25.70	60.98
2	8	-1.20	1.74	-6.42	5.57	3.78	-21.56
3	0	-3.17	-6.11	16.36	11.59	9.54	-10.29
3	1	14.05	36.40	-98.58	-46.74	-19.41	38.85
3	2	24.95	-52.45	237.24	115.55	32.25	-24.15
3	3	-92.95	22.53	-284.59	-133.53	-54.28	-80.72
3	4	84.63	4.81	155.06	39.59	49.76	96.51
3	5	-33.50	-4.32	-10.35	25.53	-16.56	13.08
3	6	9.01	1.15	-25.74	-14.33	0.45	-57.03
3	7	-2.04	-0.60	8.06	0.83	0.04	19.34
4	0	2.31	3.25	-8.18	-7.27	-5.87	8.02
4	1	-13.41	-19.49	46.32	28.10	10.72	-34.80
4	2	8.35	31.32	-97.99	-63.52	-8.09	56.19
4	3	16.25	-17.98	104.47	78.92	11.18	-18.14
4	4	-17.98	1.59	-60.62	-41.41	-13.97	-35.17
4	5	3.77	0.50	20.72	4.91	5.64	35.81
4	6	0.50	0.37	-3.56	1.42	-0.21	-9.63
5	0	-0.70	-0.82	2.07	2.23	1.83	-2.71
5	1	4.56	5.06	-11.29	-7.77	-3.16	11.55
5	2	-5.94	-8.77	20.90	14.42	0.21	-22.04
5	3	0.77	5.74	-16.53	-16.16	1.32	20.94
5	4	2.07	-0.87	4.76	8.53	0.49	-10.35
5	5	-0.74	-0.26	-0.16	-1.60	-0.58	2.02
6	0	0.08	0.08	-0.21	-0.27	-0.23	0.32
6	1	-0.56	-0.51	1.19	0.83	0.39	-1.12
6	2	0.95	0.96	-2.20	-1.11	0.10	1.57
6	3	-0.59	-0.72	1.70	0.85	-0.47	-0.93
6	4	0.12	0.19	-0.45	-0.25	0.20	0.22

POLYNOMIAL FOR THE PERFORMANCE OF THE AFT AND FRONT UNIT IN REGENERATION AS FUNCTION OF PITCH AND BETA.

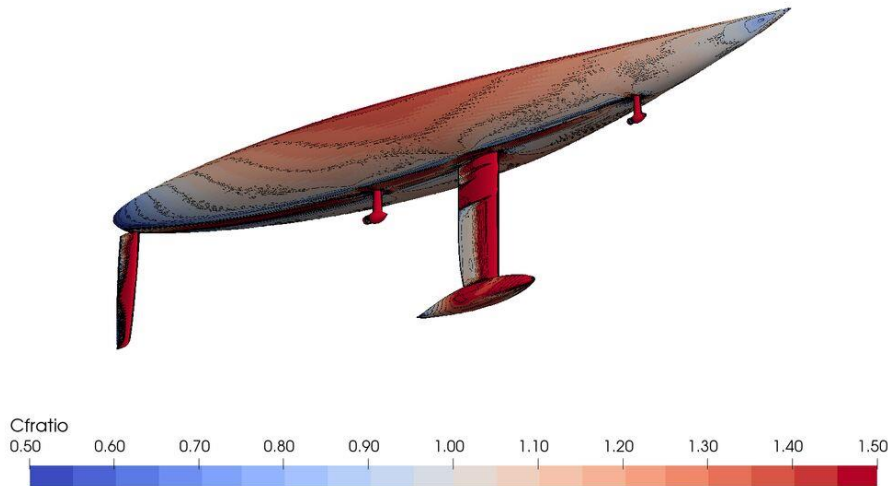
FIGURES

SHIP ID	: C2352	Draught Fore (Tf)	: 1.924 m
Water depth	: infinite	Draught Aft (Ta)	: 1.924 m
Thrust coeff	: -ct-	Dyn. sinkage	: 0.000 m
Scale	: 1	Dyn trim	: 0.00 deg
Turb model	: K_OMEGA (SST_2003)	Speed	: 12.00 kn

12 KNOTS, MOTORING, FRONT PROPELLER WORKING



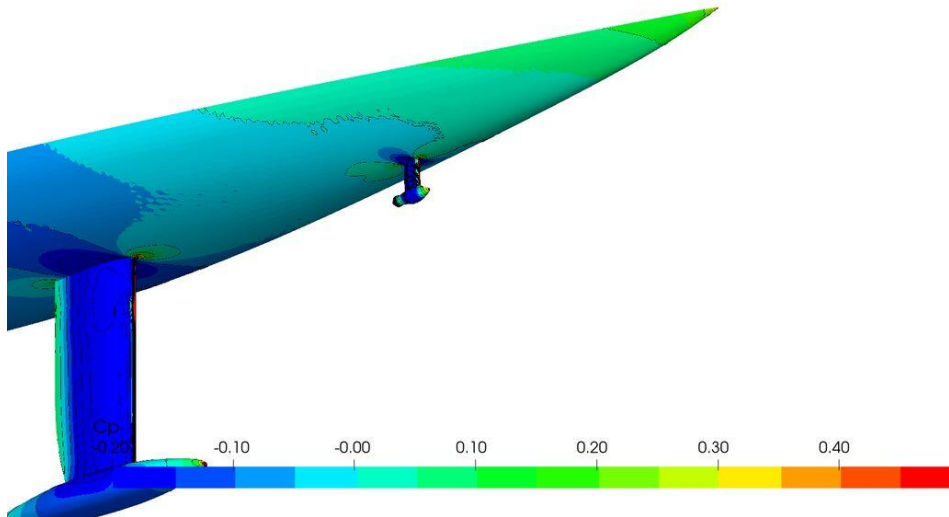
Dynamic pressure coefficient distribution on the hull, oblique underwater view from the bow



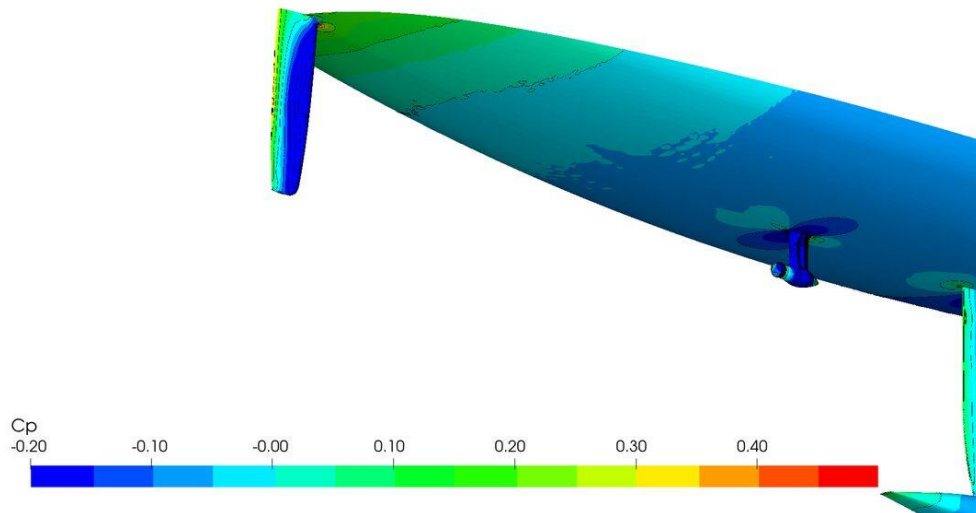
Local skin friction to flat plate friction ratio, oblique underwater view from the bow

SHIP ID	: C2352	Draught Fore (Tf)	: 1.924 m
Water depth	: infinite	Draught Aft (Ta)	: 1.924 m
Thrust coeff	: -ct-	Dyn. sinkage	: 0.000 m
Scale	: 1	Dyn trim	: 0.00 deg
Turb model	: K_OMEGA (SST_2003)	Speed	: 12.00 kn

12 KNOTS, MOTORING, FRONT PROPELLER WORKING



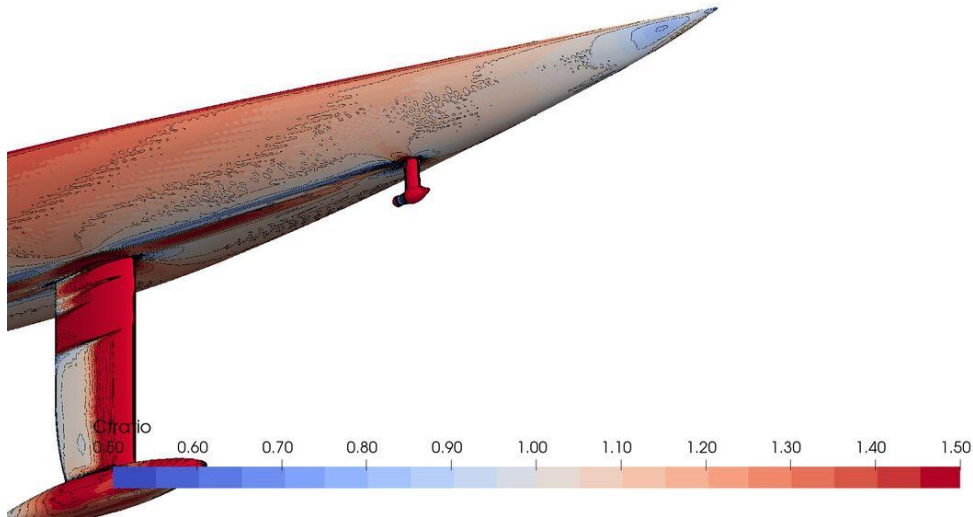
Dynamic pressure coefficient distribution on the hull, oblique underwater view on the bow



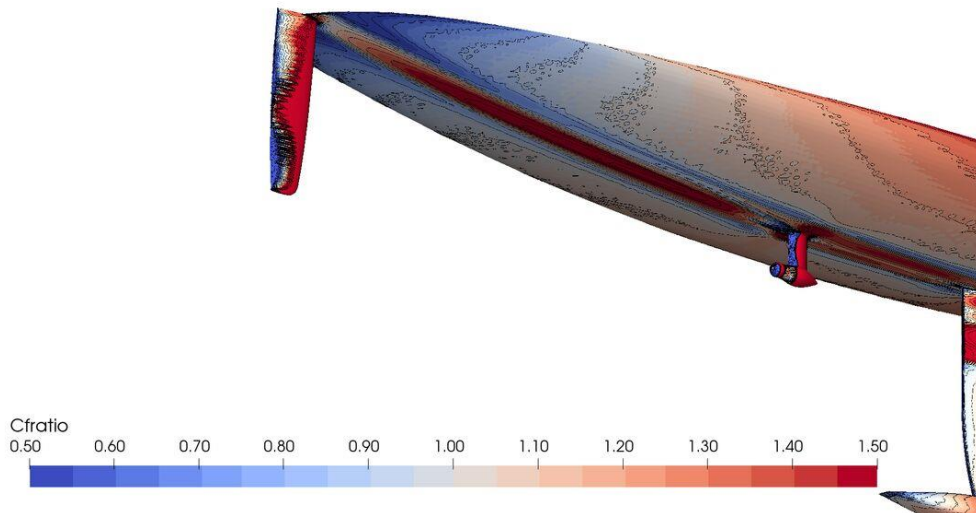
Dynamic pressure coefficient distribution on the hull, oblique underwater view on the stern

SHIP ID	: C2352	Draught Fore (Tf)	: 1.924 m
Water depth	: infinite	Draught Aft (Ta)	: 1.924 m
Thrust coeff	: -ct-	Dyn. sinkage	: 0.000 m
Scale	: 1	Dyn trim	: 0.00 deg
Turb model	: K_OMEGA (SST_2003)	Speed	: 12.00 kn

12 KNOTS, MOTORING, FRONT PROPELLER WORKING



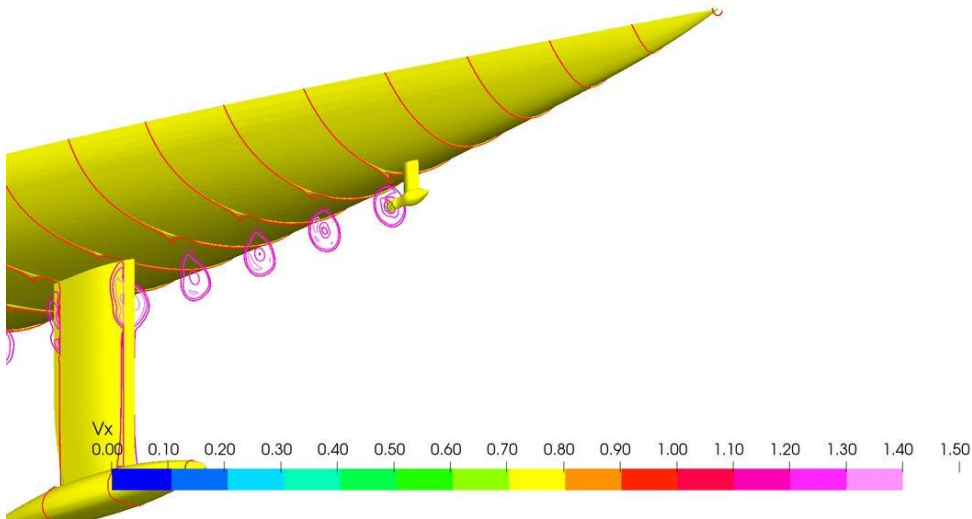
Local skin friction to flat plate friction ratio, oblique underwater view on the bow



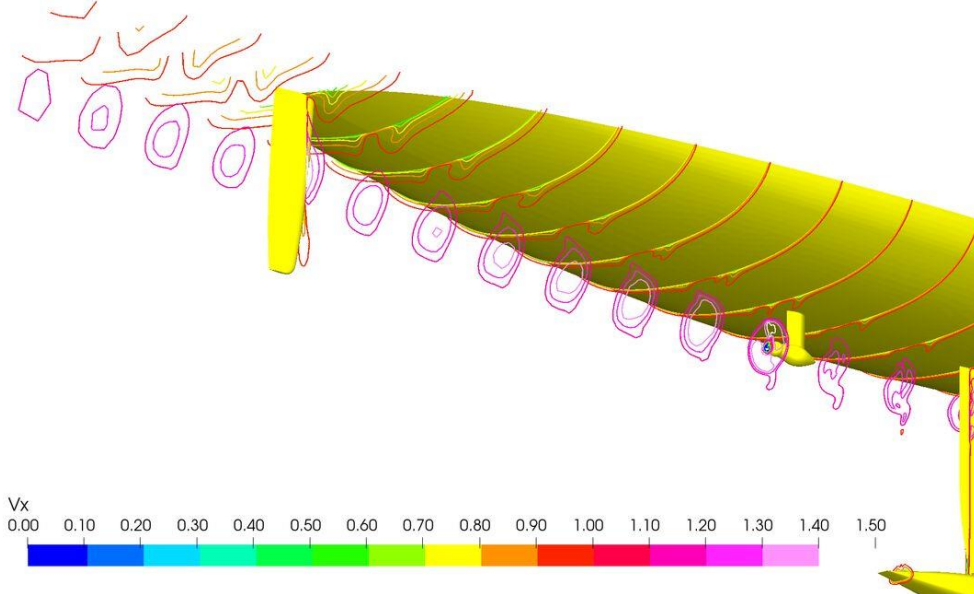
Local skin friction to flat plate friction ratio, oblique underwater view on the stern

SHIP ID	: C2352	Draught Fore (Tf)	: 1.924 m
Water depth	: infinite	Draught Aft (Ta)	: 1.924 m
Thrust coeff	: -ct-	Dyn. sinkage	: 0.000 m
Scale	: 1	Dyn trim	: 0.00 deg
Turb model	: K_OMEGA (SST_2003)	Speed	: 12.00 kn

12 KNOTS, MOTORING, FRONT PROPELLER WORKING



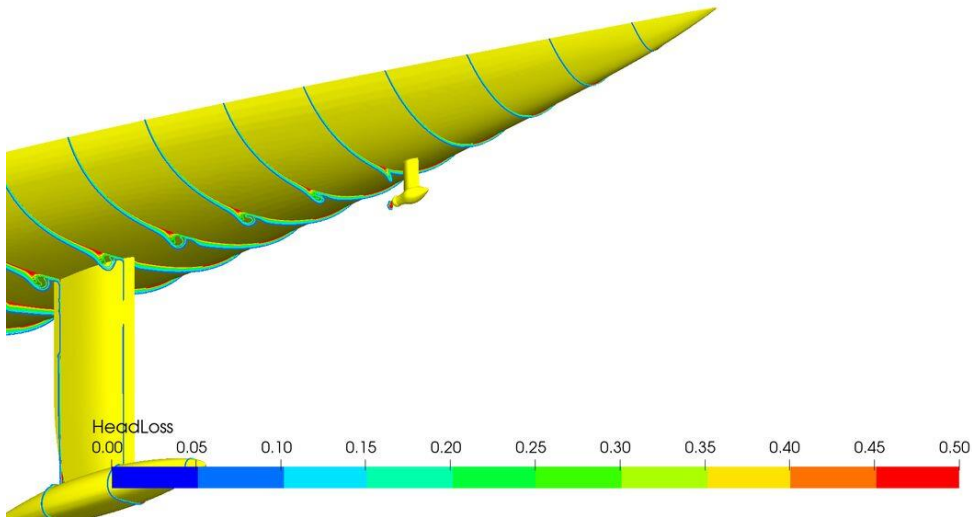
Slices of axial velocity, oblique underwater view on the bow



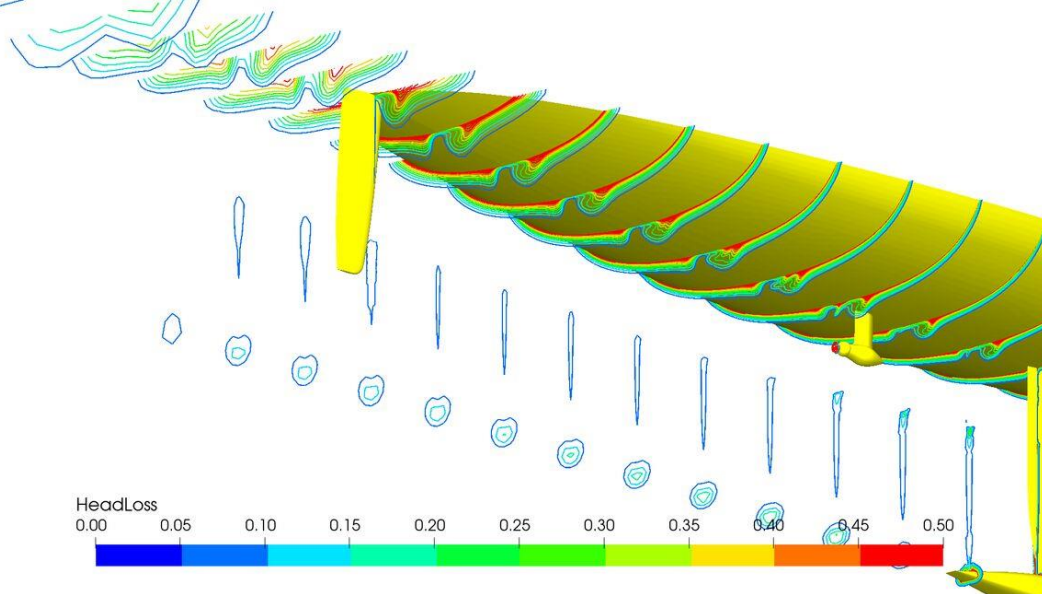
Slices of axial velocity, oblique underwater view on the stern

SHIP ID	: C2352	Draught Fore (Tf)	: 1.924 m
Water depth	: infinite	Draught Aft (Ta)	: 1.924 m
Thrust coeff	: -ct-	Dyn. sinkage	: 0.000 m
Scale	: 1	Dyn trim	: 0.00 deg
Turb model	: K_OMEGA (SST_2003)	Speed	: 12.00 kn

12 KNOTS, MOTORING, FRONT PROPELLER WORKING



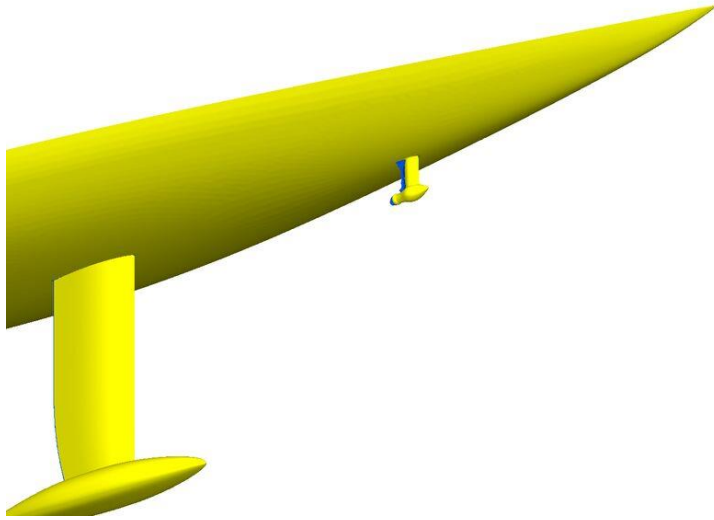
Slices of head loss, oblique underwater view on the bow



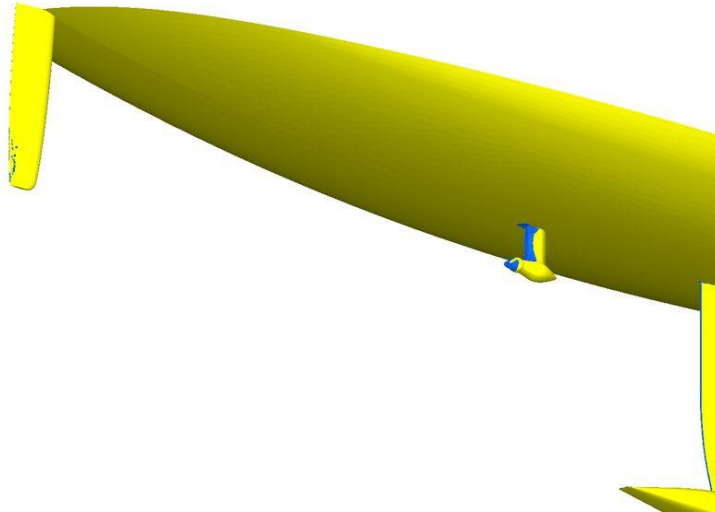
Slices of head loss, oblique underwater view on the stern

SHIP ID	: C2352	Draught Fore (Tf)	: 1.924 m
Water depth	: infinite	Draught Aft (Ta)	: 1.924 m
Thrust coeff	: -ct-	Dyn. sinkage	: 0.000 m
Scale	: 1	Dyn trim	: 0.00 deg
Turb model	: K_OMEGA (SST_2003)	Speed	: 12.00 kn

12 KNOTS, MOTORING, FRONT PROPELLER WORKING



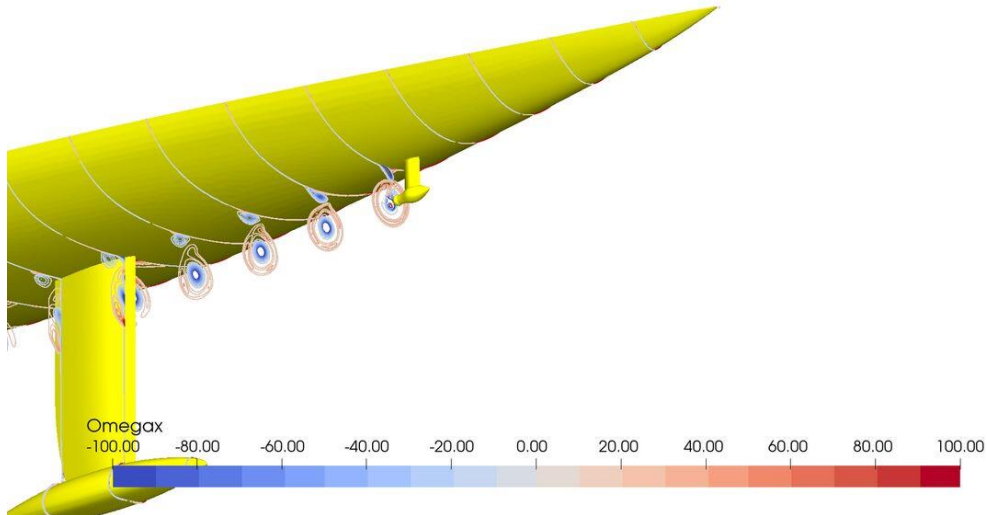
Reversed flow regions, oblique underwater view on the bow



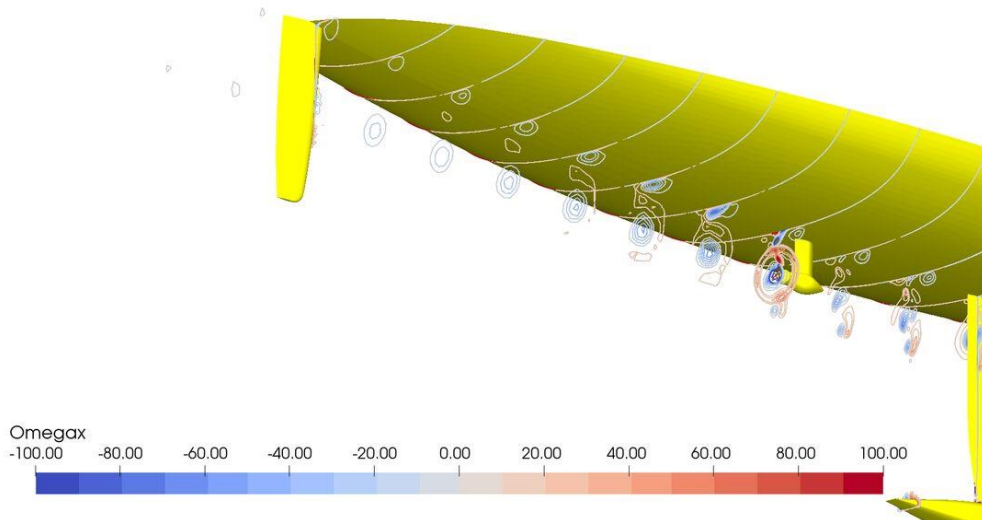
Reversed flow regions, oblique underwater view on the stern

SHIP ID	: C2352	Draught Fore (Tf)	: 1.924 m
Water depth	: infinite	Draught Aft (Ta)	: 1.924 m
Thrust coeff	: -ct-	Dyn. sinkage	: 0.000 m
Scale	: 1	Dyn trim	: 0.00 deg
Turb model	: K_OMEGA (SST_2003)	Speed	: 12.00 kn

12 KNOTS, MOTORING, FRONT PROPELLER WORKING



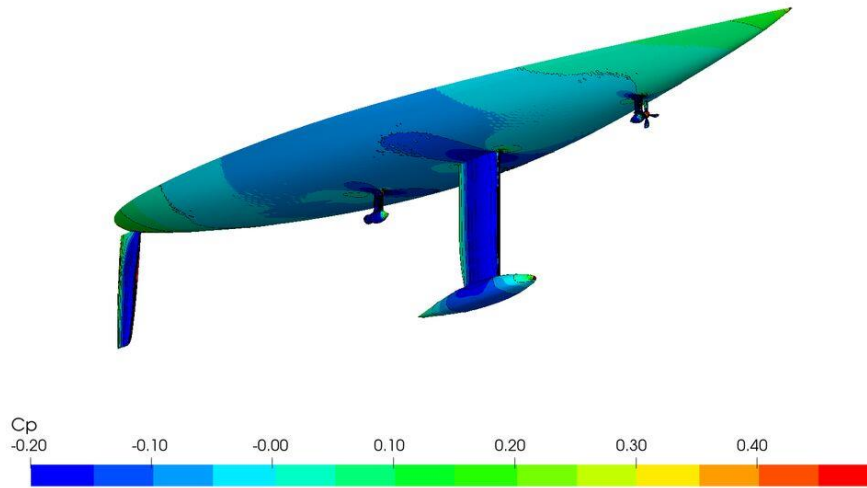
Slices of axial vorticity, oblique underwater view on the bow



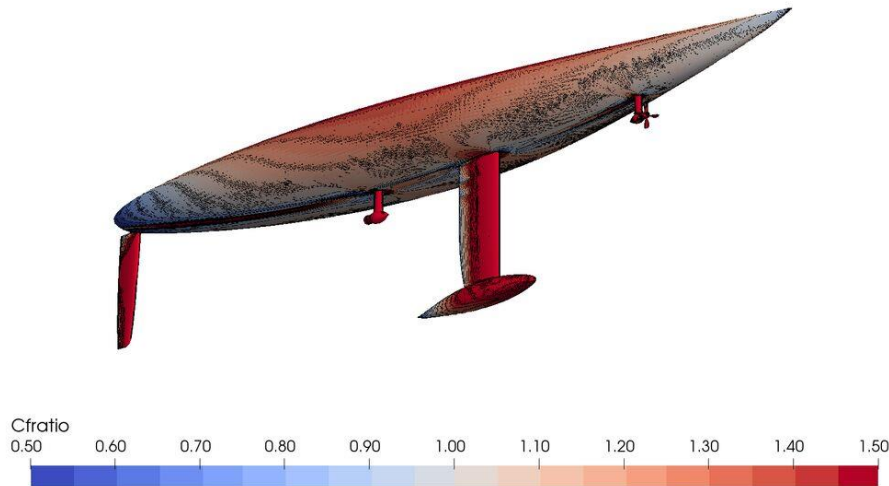
Slices of axial vorticity, oblique underwater view on the stern

SHIP ID	: C2352	Draught Fore (Tf)	: 1.924 m
Water depth	: infinite	Draught Aft (Ta)	: 1.924 m
Thrust coeff	: -ct-	Dyn. sinkage	: 0.000 m
Scale	: 1	Dyn trim	: 0.00 deg
Turb model	: K_OMEGA (SST_2003)	Speed	: 12.00 kn

12 KNOTS, MOTORING, FRONT PROPELLER FEATHERED



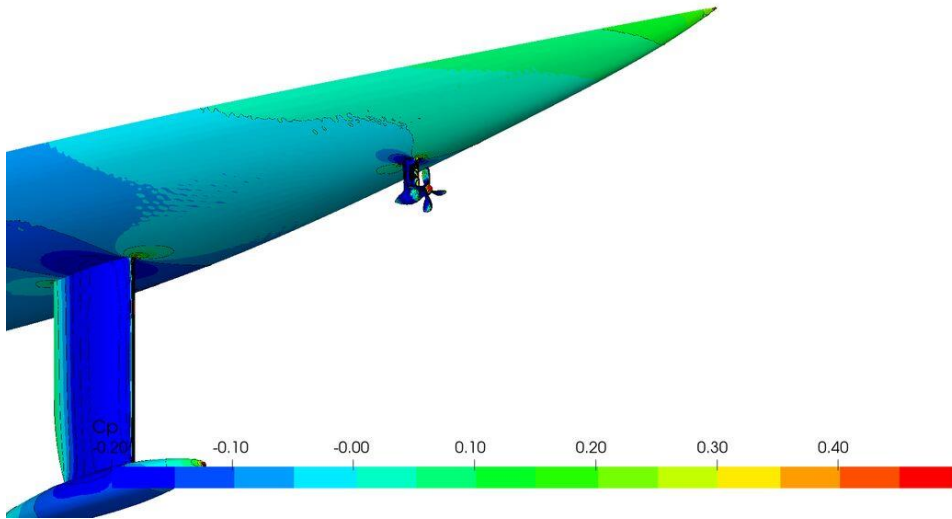
Dynamic pressure coefficient distribution on the hull, oblique underwater view from the bow



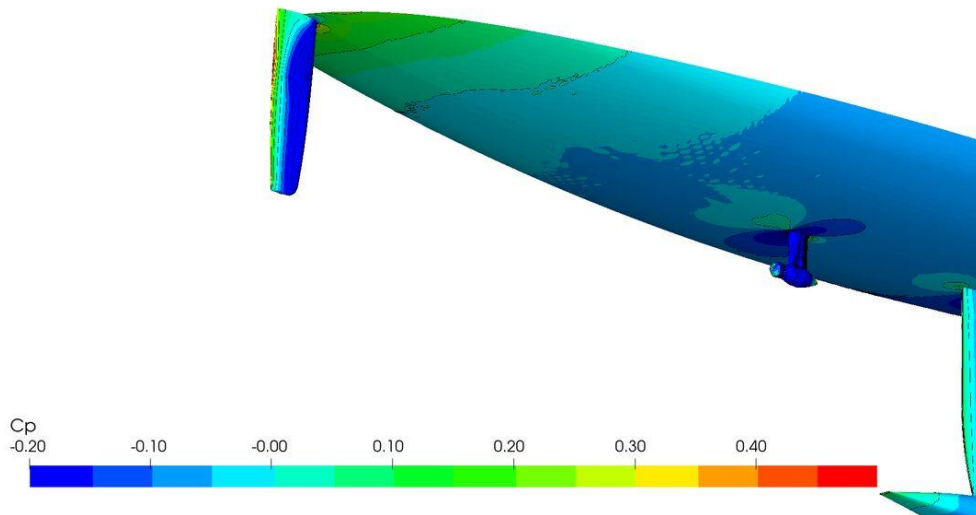
Local skin friction to flat plate friction ratio, oblique underwater view from the bow

SHIP ID	: C2352	Draught Fore (Tf)	: 1.924 m
Water depth	: infinite	Draught Aft (Ta)	: 1.924 m
Thrust coeff	: -ct-	Dyn. sinkage	: 0.000 m
Scale	: 1	Dyn trim	: 0.00 deg
Turb model	: K_OMEGA (SST_2003)	Speed	: 12.00 kn

12 KNOTS, MOTORING, FRONT PROPELLER FEATHERED



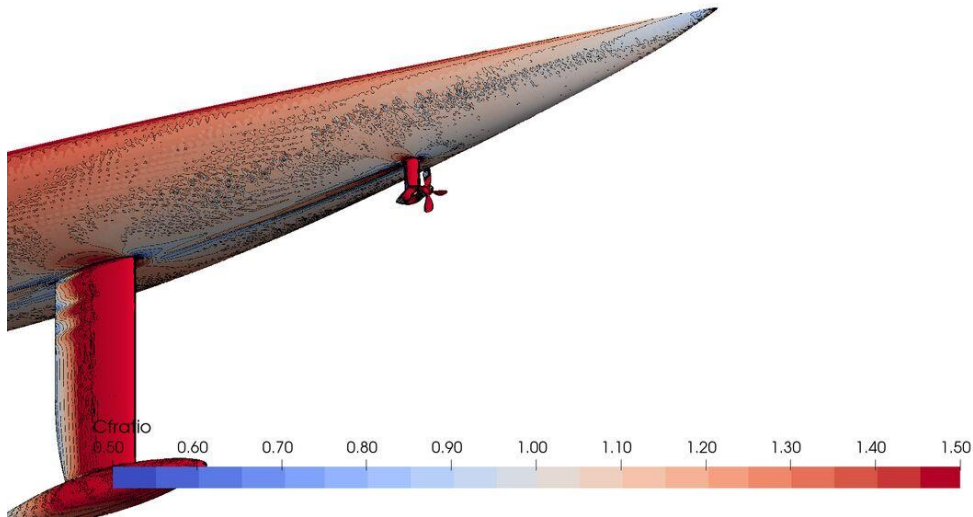
Dynamic pressure coefficient distribution on the hull, oblique underwater view on the bow



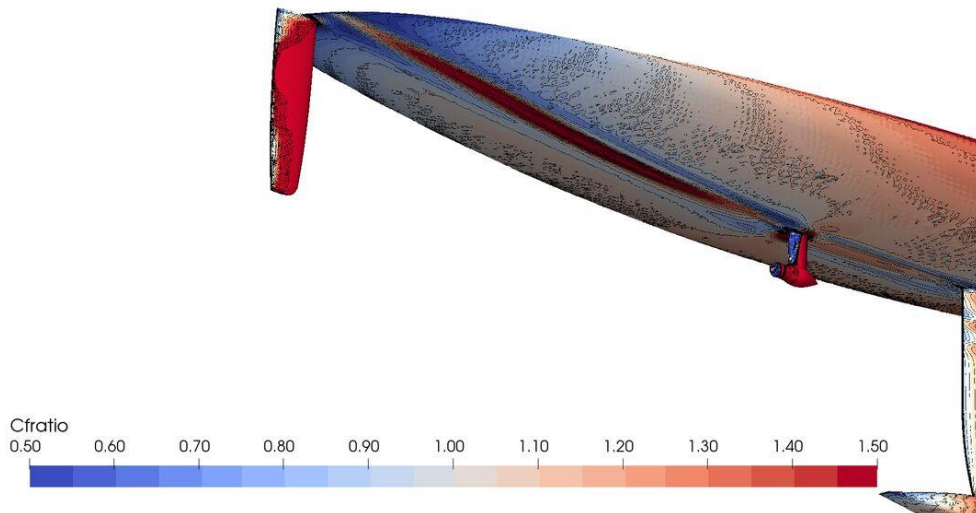
Dynamic pressure coefficient distribution on the hull, oblique underwater view on the stern

SHIP ID	: C2352	Draught Fore (Tf)	: 1.924 m
Water depth	: infinite	Draught Aft (Ta)	: 1.924 m
Thrust coeff	: -ct-	Dyn. sinkage	: 0.000 m
Scale	: 1	Dyn trim	: 0.00 deg
Turb model	: K_OMEGA (SST_2003)	Speed	: 12.00 kn

12 KNOTS, MOTORING, FRONT PROPELLER FEATHERED



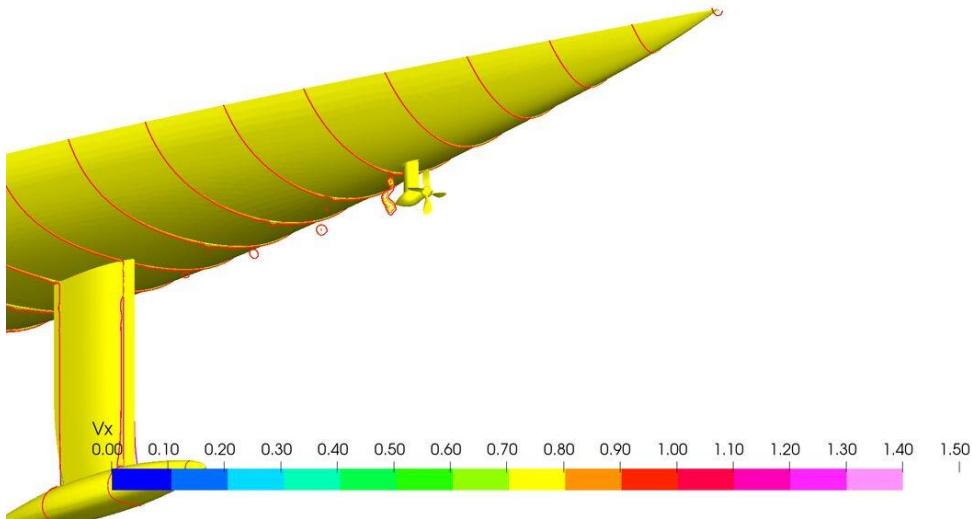
Local skin friction to flat plate friction ratio, oblique underwater view on the bow



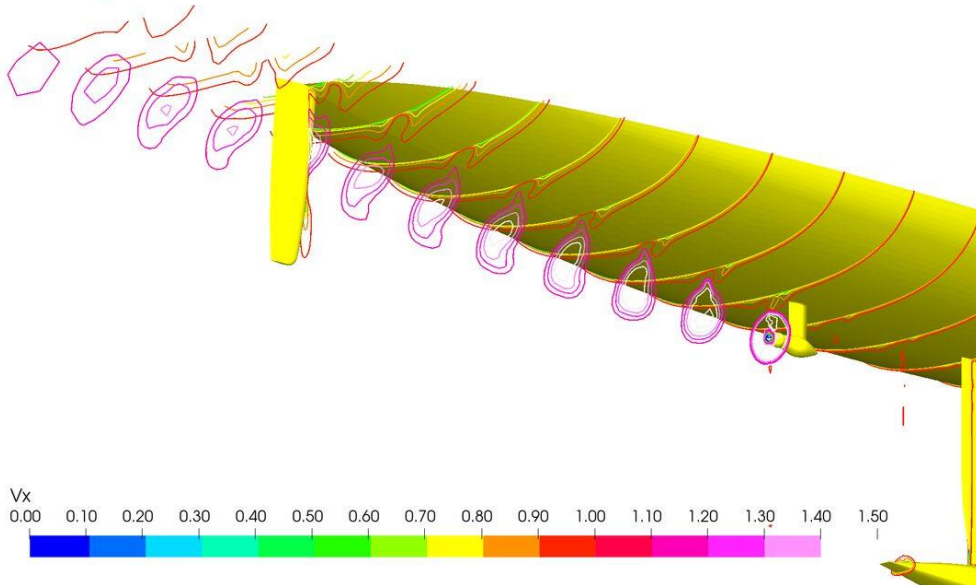
Local skin friction to flat plate friction ratio, oblique underwater view on the stern

SHIP ID	: C2352	Draught Fore (Tf)	: 1.924 m
Water depth	: infinite	Draught Aft (Ta)	: 1.924 m
Thrust coeff	: -ct-	Dyn. sinkage	: 0.000 m
Scale	: 1	Dyn trim	: 0.00 deg
Turb model	: K_OMEGA (SST_2003)	Speed	: 12.00 kn

12 KNOTS, MOTORING, FRONT PROPELLER FEATHERED



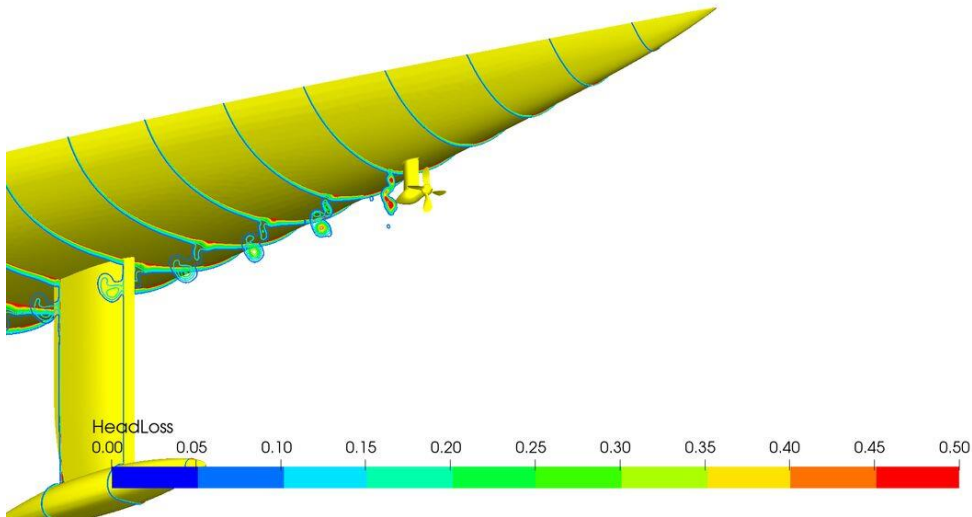
Slices of axial velocity, oblique underwater view on the bow



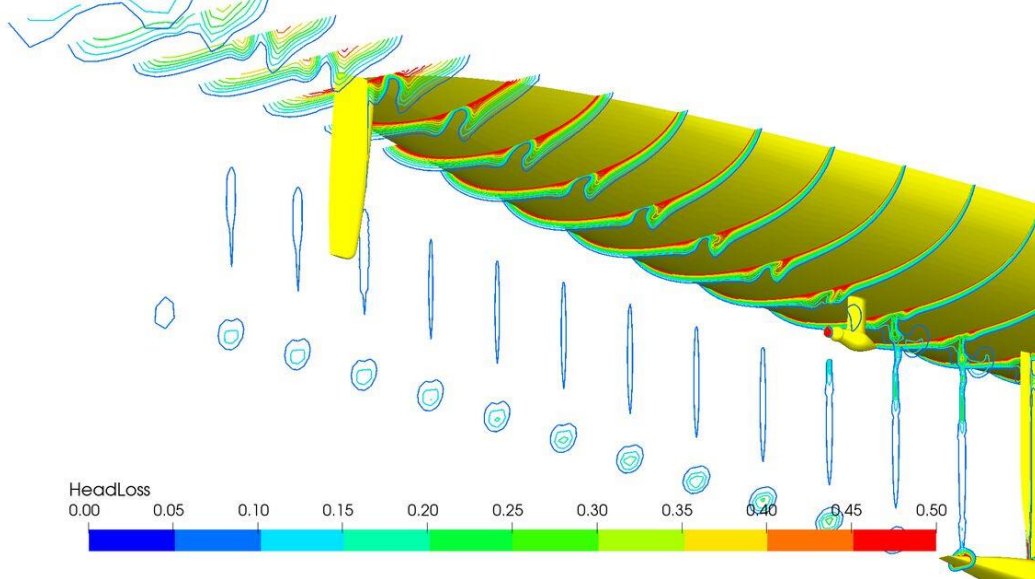
Slices of axial velocity, oblique underwater view on the stern

SHIP ID	: C2352	Draught Fore (Tf)	: 1.924 m
Water depth	: infinite	Draught Aft (Ta)	: 1.924 m
Thrust coeff	: -ct-	Dyn. sinkage	: 0.000 m
Scale	: 1	Dyn trim	: 0.00 deg
Turb model	: K_OMEGA (SST_2003)	Speed	: 12.00 kn

12 KNOTS, MOTORING, FRONT PROPELLER FEATHERED



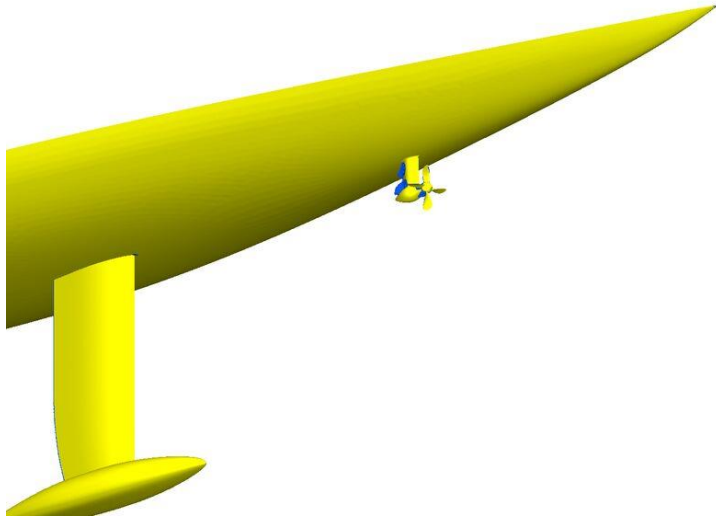
Slices of head loss, oblique underwater view on the bow



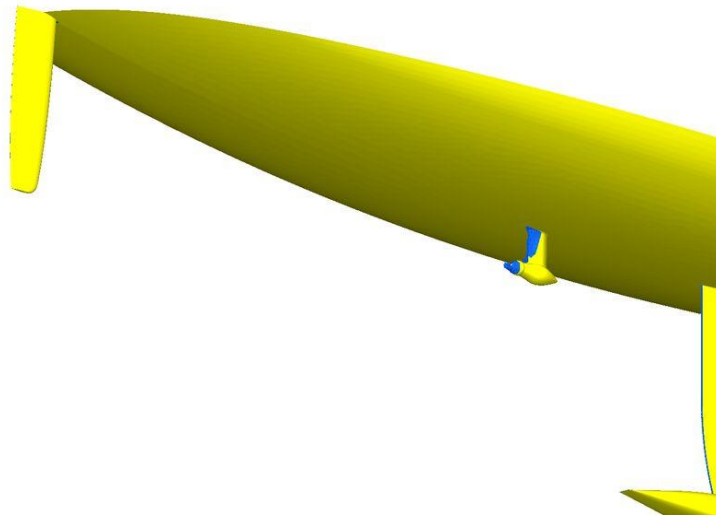
Slices of head loss, oblique underwater view on the stern

SHIP ID	: C2352	Draught Fore (Tf)	: 1.924 m
Water depth	: infinite	Draught Aft (Ta)	: 1.924 m
Thrust coeff	: -ct-	Dyn. sinkage	: 0.000 m
Scale	: 1	Dyn trim	: 0.00 deg
Turb model	: K_OMEGA (SST_2003)	Speed	: 12.00 kn

12 KNOTS, MOTORING, FRONT PROPELLER FEATHERED



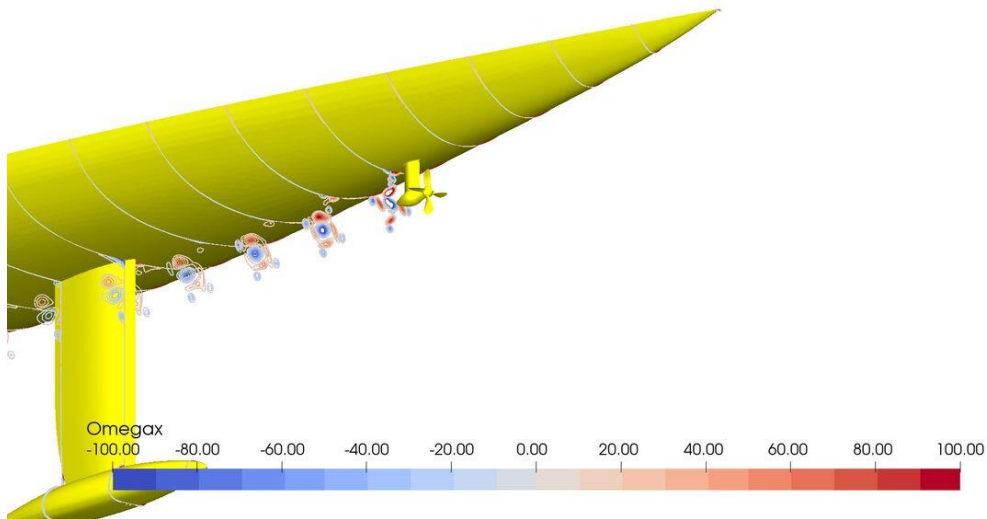
Reversed flow regions, oblique underwater view on the bow



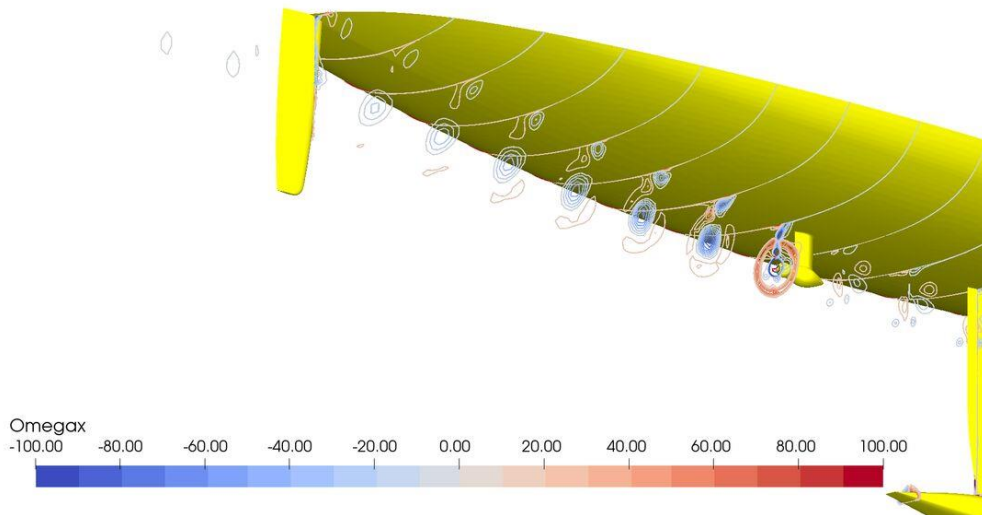
Reversed flow regions, oblique underwater view on the stern

SHIP ID	: C2352	Draught Fore (Tf)	: 1.924 m
Water depth	: infinite	Draught Aft (Ta)	: 1.924 m
Thrust coeff	: -ct-	Dyn. sinkage	: 0.000 m
Scale	: 1	Dyn trim	: 0.00 deg
Turb model	: K_OMEGA (SST_2003)	Speed	: 12.00 kn

12 KNOTS, MOTORING, FRONT PROPELLER FEATHERED



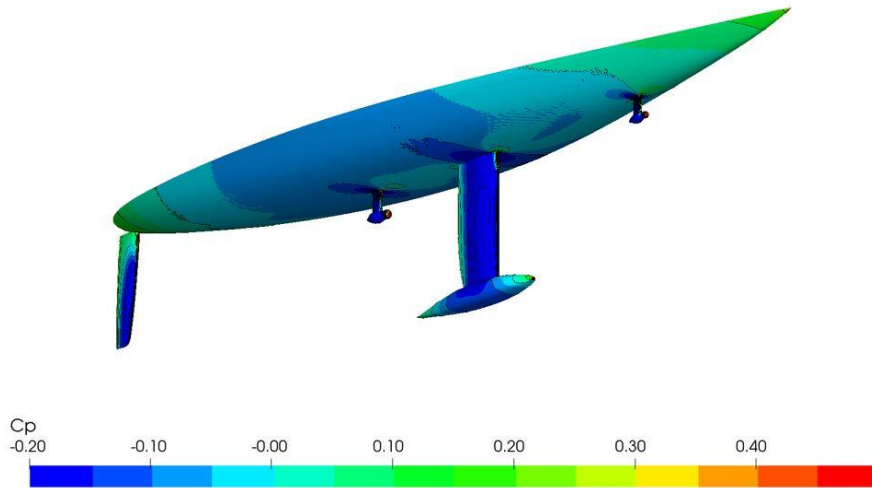
Slices of axial vorticity, oblique underwater view on the bow



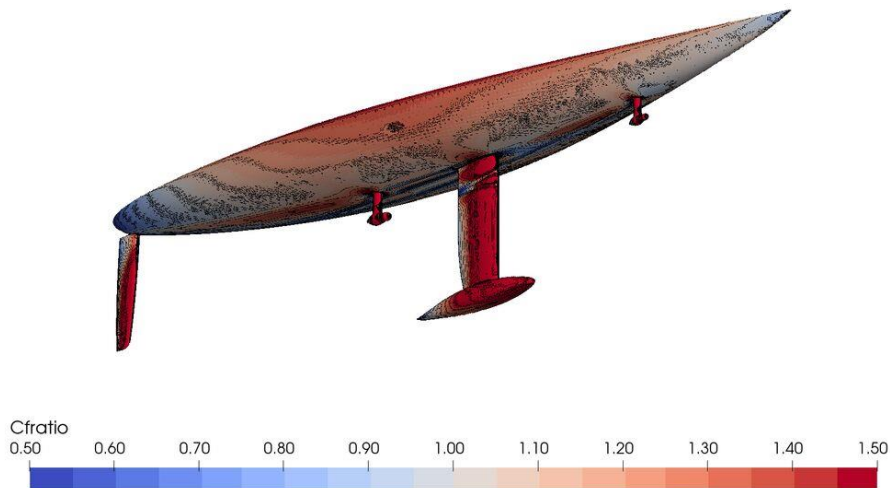
Slices of axial vorticity, oblique underwater view on the stern

SHIP ID	: C2352	Draught Fore (Tf)	: 1.924 m
Water depth	: infinite	Draught Aft (Ta)	: 1.924 m
Thrust coeff	: -ct-	Dyn. sinkage	: 0.000 m
Scale	: 1	Dyn trim	: 0.00 deg
Turb model	: K_OMEGA (SST_2003)	Speed	: 16.00 kn

16 KNOTS, REGENERATING WITH BOTH PROPELLERS



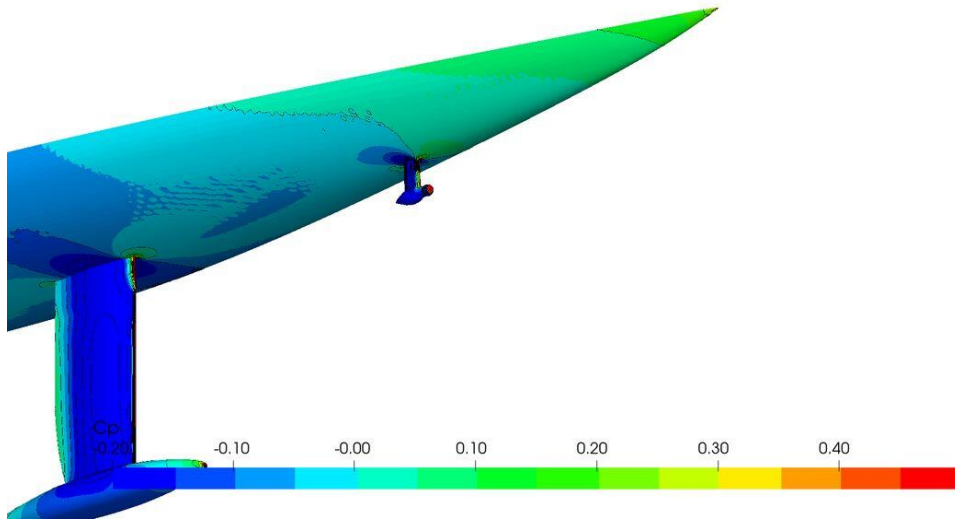
Dynamic pressure coefficient distribution on the hull, oblique underwater view from the bow



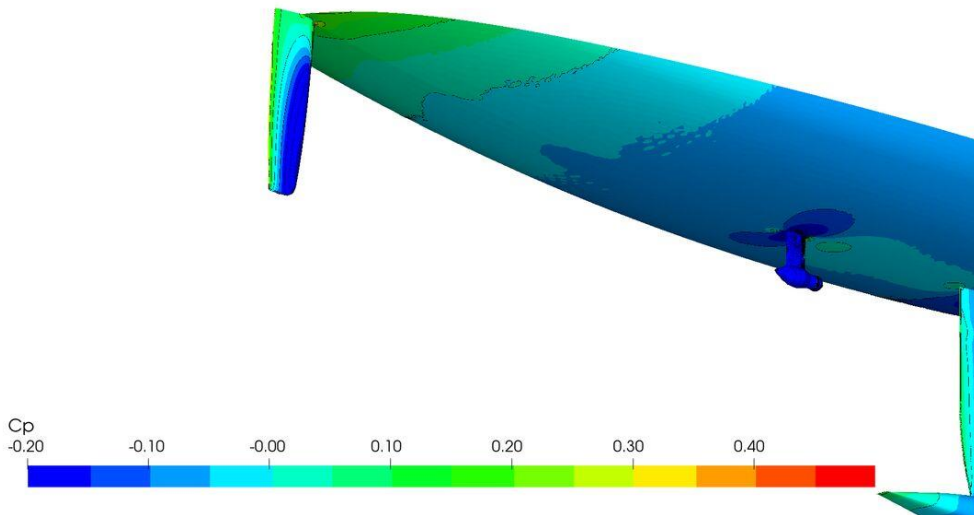
Local skin friction to flat plate friction ratio, oblique underwater view from the bow

SHIP ID	: C2352	Draught Fore (Tf)	: 1.924 m
Water depth	: infinite	Draught Aft (Ta)	: 1.924 m
Thrust coeff	: -ct-	Dyn. sinkage	: 0.000 m
Scale	: 1	Dyn trim	: 0.00 deg
Turb model	: K_OMEGA (SST_2003)	Speed	: 16.00 kn

16 KNOTS, REGENERATING WITH BOTH PROPELLERS



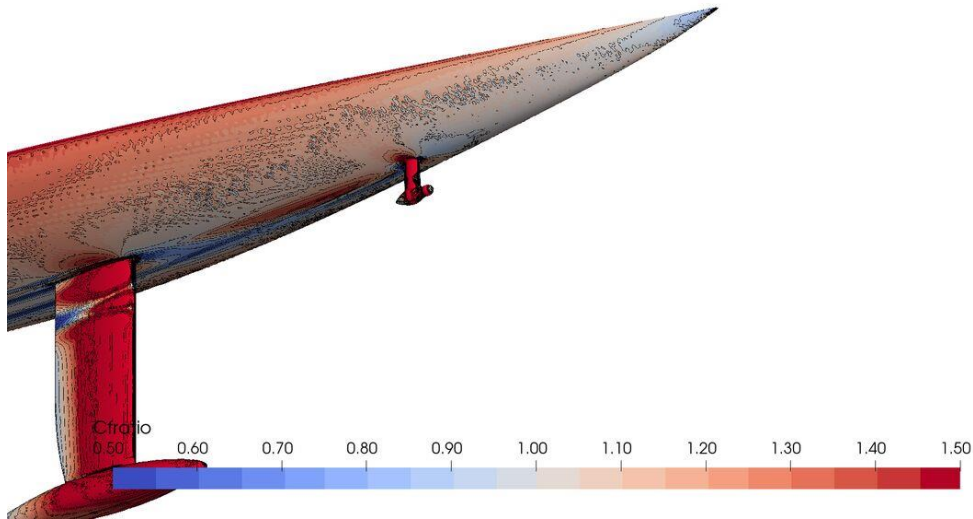
Dynamic pressure coefficient distribution on the hull, oblique underwater view on the bow



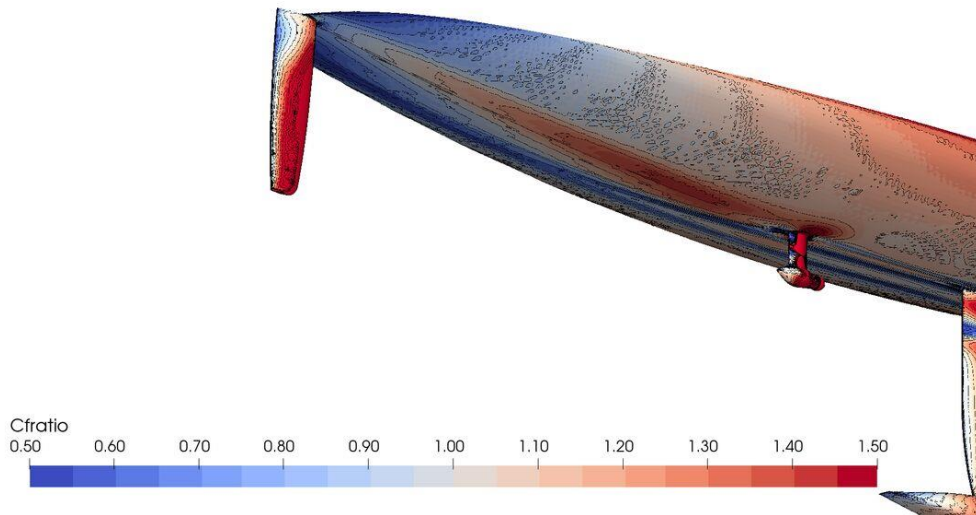
Dynamic pressure coefficient distribution on the hull, oblique underwater view on the stern

SHIP ID	: C2352	Draught Fore (Tf)	: 1.924 m
Water depth	: infinite	Draught Aft (Ta)	: 1.924 m
Thrust coeff	: -ct-	Dyn. sinkage	: 0.000 m
Scale	: 1	Dyn trim	: 0.00 deg
Turb model	: K_OMEGA (SST_2003)	Speed	: 16.00 kn

16 KNOTS, REGENERATING WITH BOTH PROPELLERS



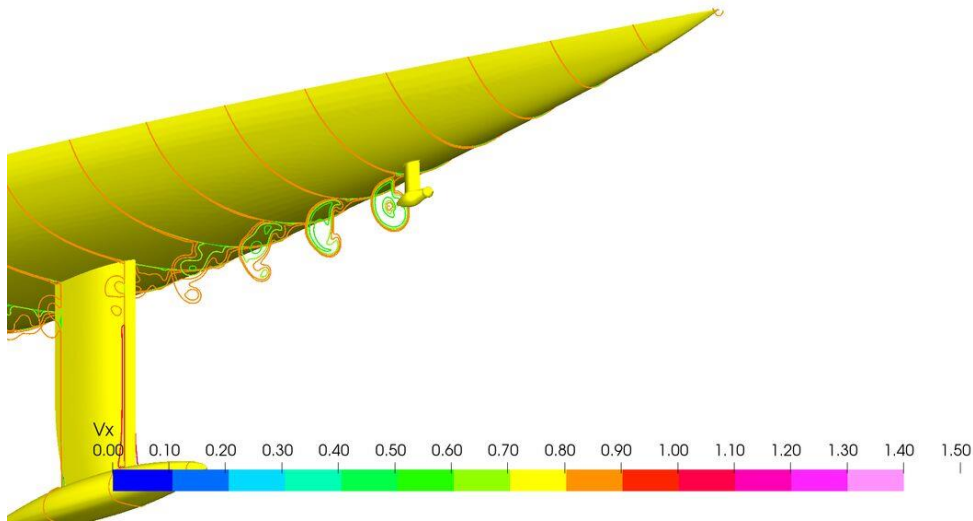
Local skin friction to flat plate friction ratio, oblique underwater view on the bow



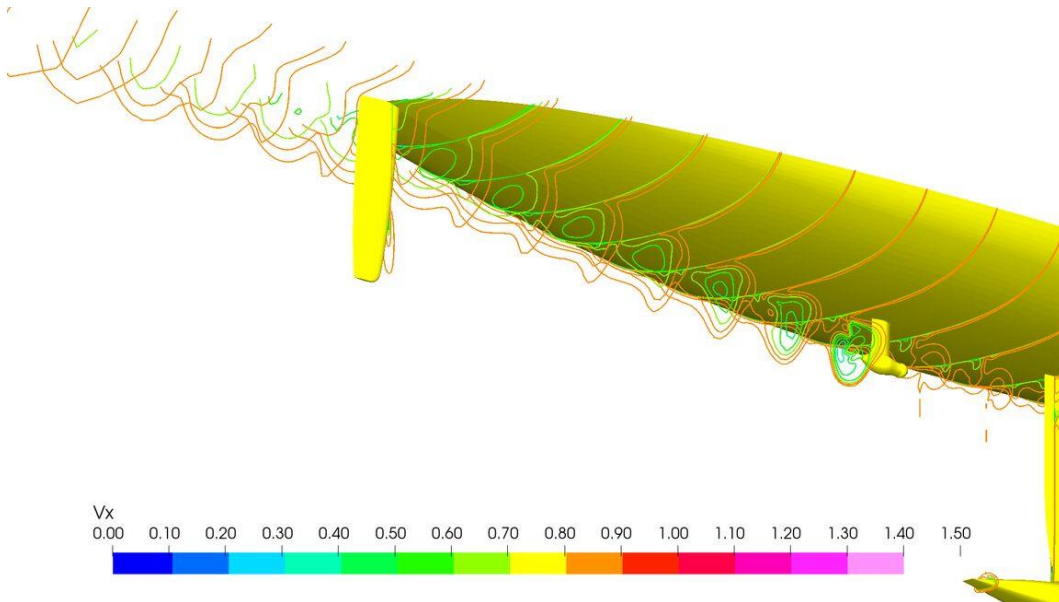
Local skin friction to flat plate friction ratio, oblique underwater view on the stern

SHIP ID	: C2352	Draught Fore (Tf)	: 1.924 m
Water depth	: infinite	Draught Aft (Ta)	: 1.924 m
Thrust coeff	: -ct-	Dyn. sinkage	: 0.000 m
Scale	: 1	Dyn trim	: 0.00 deg
Turb model	: K_OMEGA (SST_2003)	Speed	: 16.00 kn

16 KNOTS, REGENERATING WITH BOTH PROPELLERS



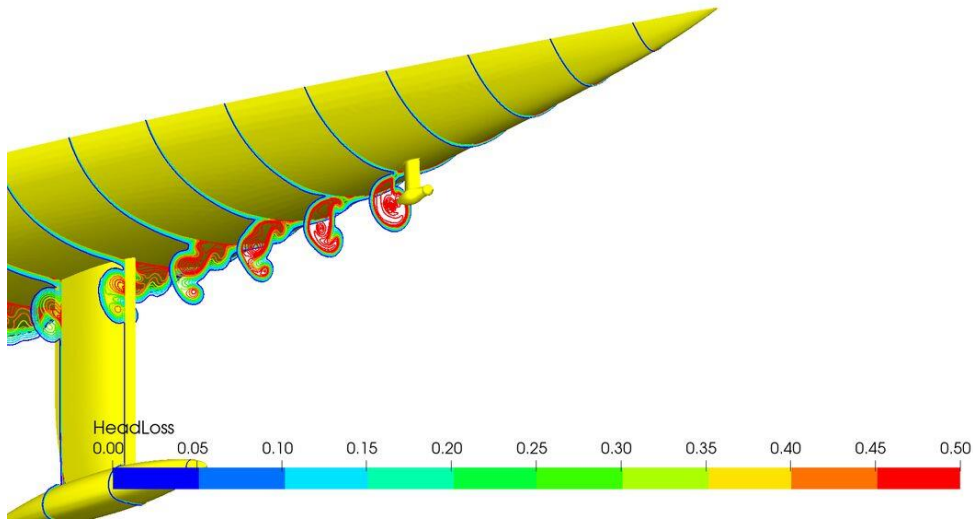
Slices of axial velocity, oblique underwater view on the bow



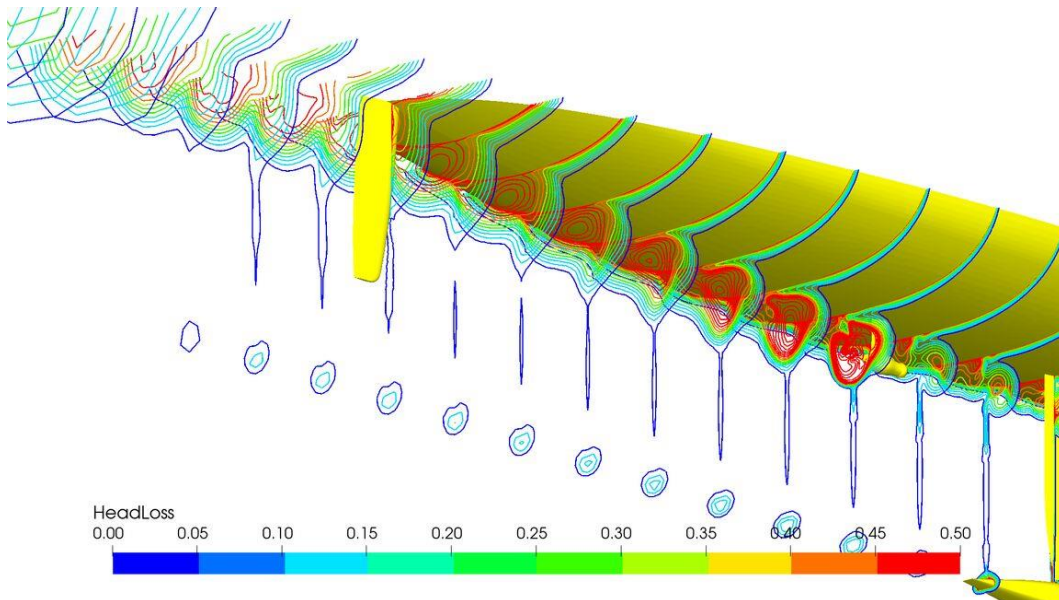
Slices of axial velocity, oblique underwater view on the stern

SHIP ID	: C2352	Draught Fore (Tf)	: 1.924 m
Water depth	: infinite	Draught Aft (Ta)	: 1.924 m
Thrust coeff	: -ct-	Dyn. sinkage	: 0.000 m
Scale	: 1	Dyn trim	: 0.00 deg
Turb model	: K_OMEGA (SST_2003)	Speed	: 16.00 kn

16 KNOTS, REGENERATING WITH BOTH PROPELLERS

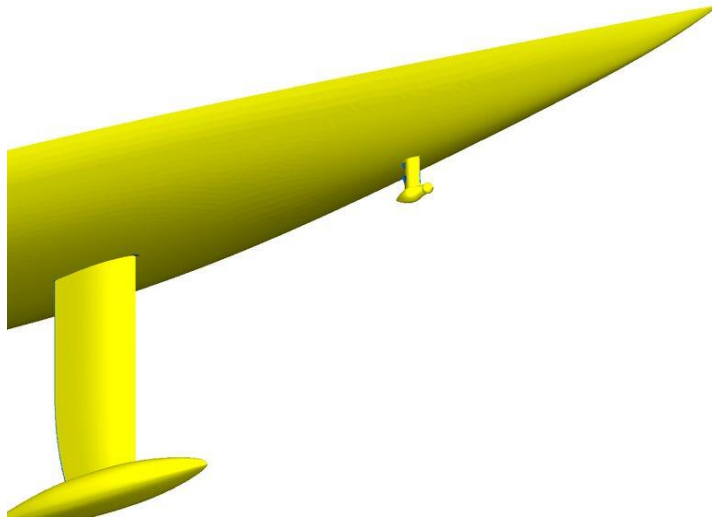


Slices of head loss, oblique underwater view on the bow

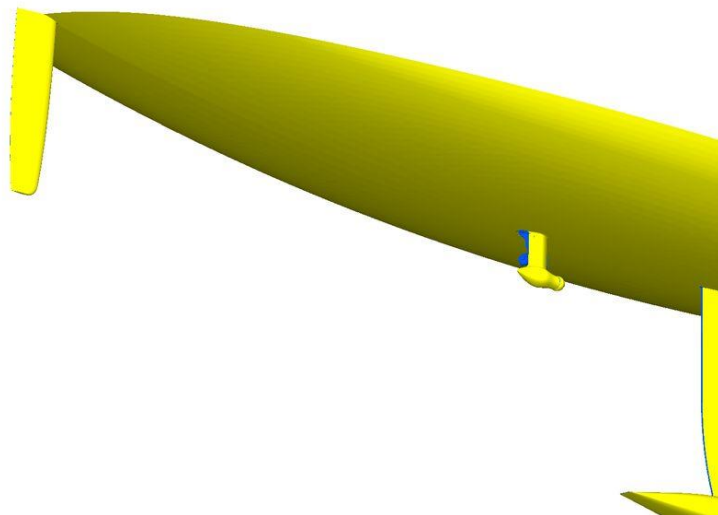


Slices of head loss, oblique underwater view on the stern

SHIP ID	: C2352	Draught Fore (Tf)	: 1.924 m
Water depth	: infinite	Draught Aft (Ta)	: 1.924 m
Thrust coeff	: -ct-	Dyn. sinkage	: 0.000 m
Scale	: 1	Dyn trim	: 0.00 deg
Turb model	: K_OMEGA (SST_2003)	Speed	: 16.00 kn

16 KNOTS, REGENERATING WITH BOTH PROPELLERS

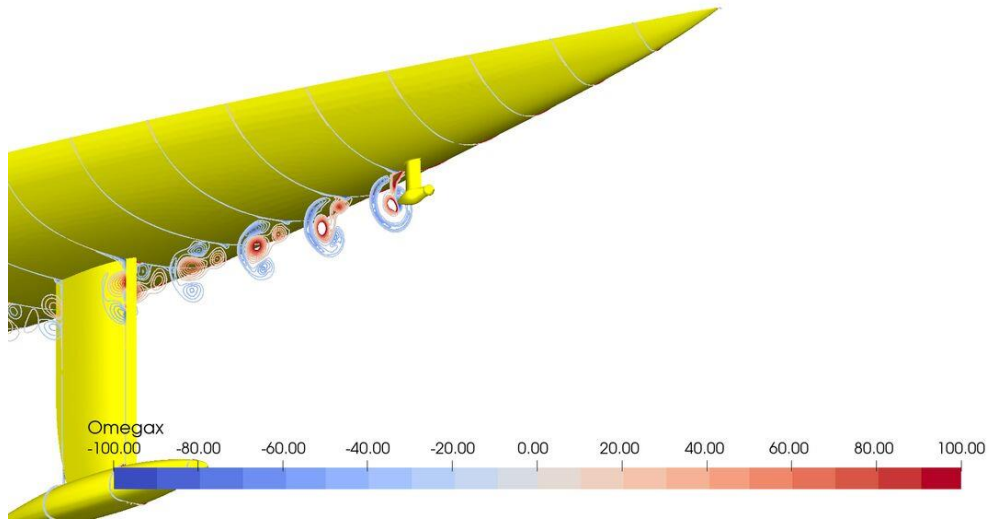
Reversed flow regions, oblique underwater view on the bow



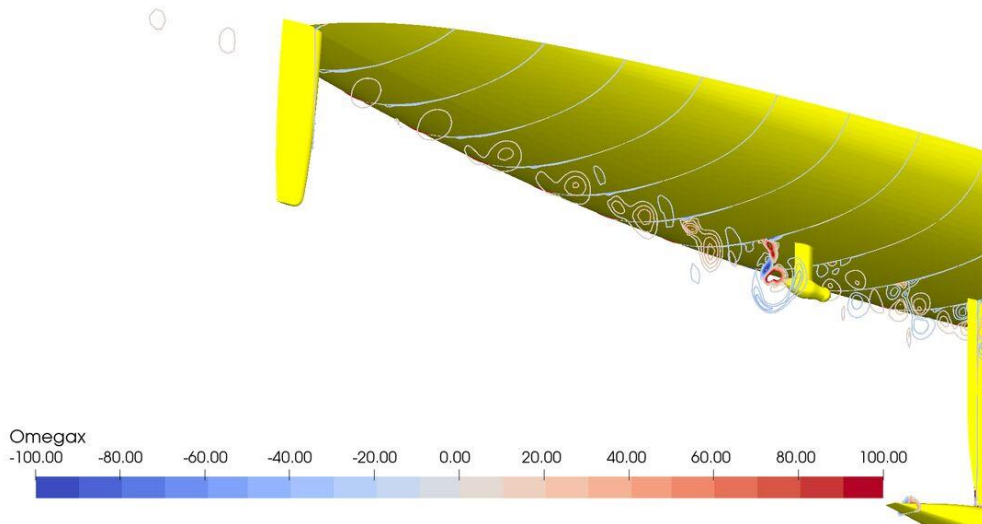
Reversed flow regions, oblique underwater view on the stern

SHIP ID	: C2352	Draught Fore (Tf)	: 1.924 m
Water depth	: infinite	Draught Aft (Ta)	: 1.924 m
Thrust coeff	: -ct-	Dyn. sinkage	: 0.000 m
Scale	: 1	Dyn trim	: 0.00 deg
Turb model	: K_OMEGA (SST_2003)	Speed	: 16.00 kn

16 KNOTS, REGENERATING WITH BOTH PROPELLERS



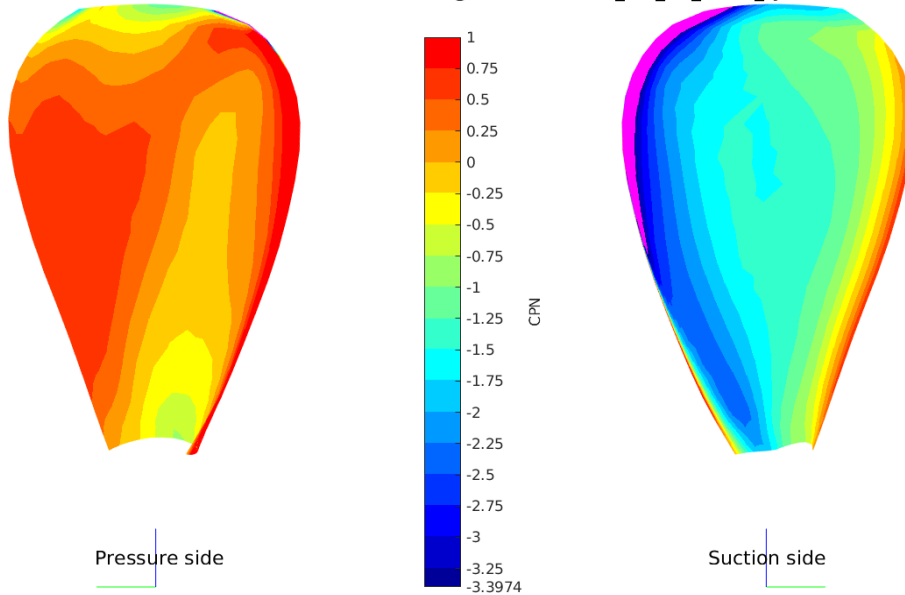
Slices of axial vorticity, oblique underwater view on the bow



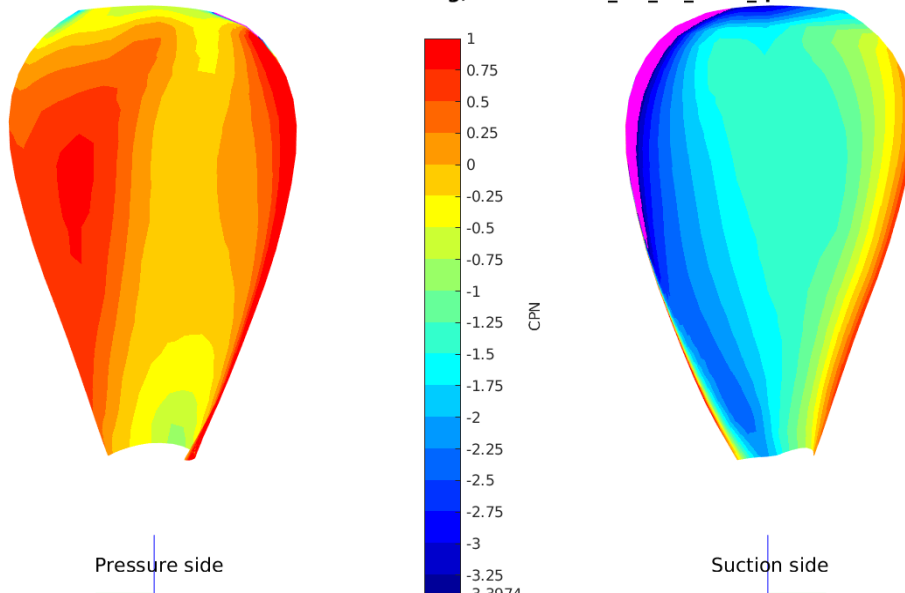
Slices of axial vorticity, oblique underwater view on the stern

PRESSURE CONTOURS ON THE AFT PROPELLER AT 12.00 KNOTS

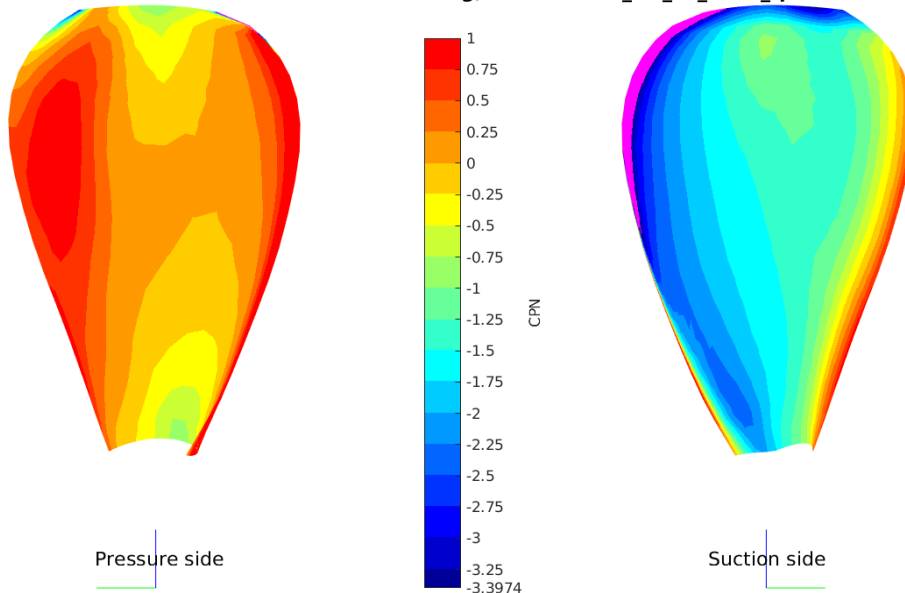
CPN at Theta = 0 deg, HUNDESTED_aft_v1_12kn_fp



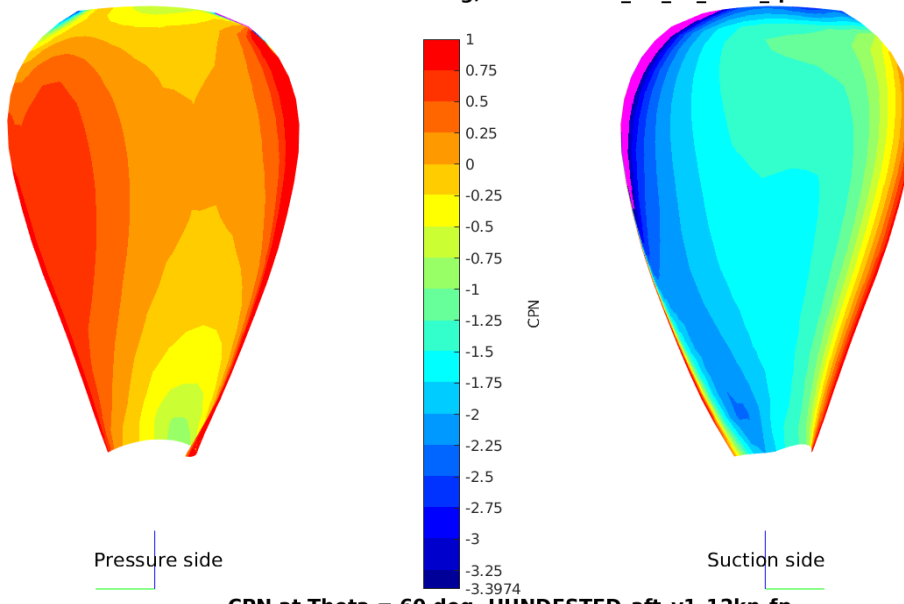
CPN at Theta = 6 deg, HUNDESTED_aft_v1_12kn_fp



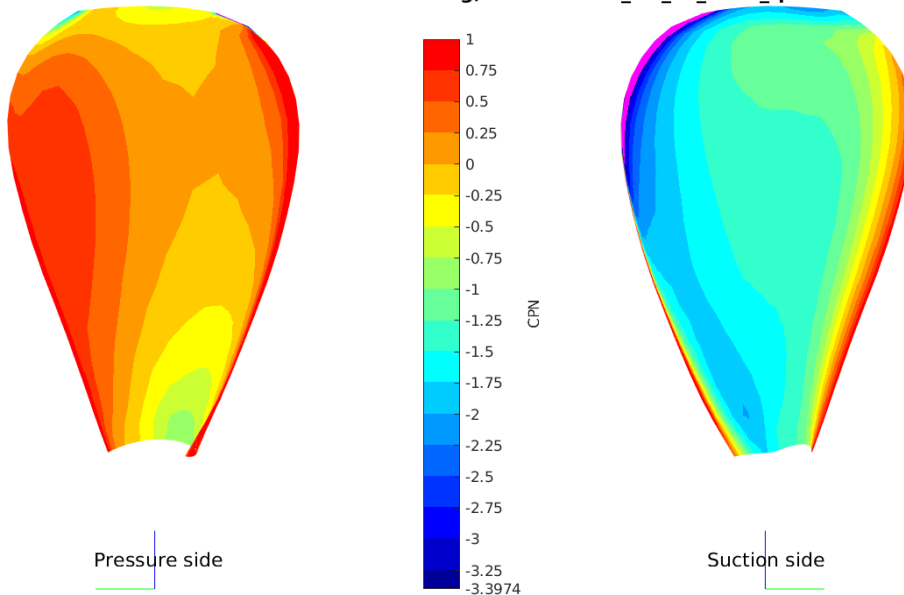
CPN at Theta = 12 deg, HUNDESTED_aft_v1_12kn_fp



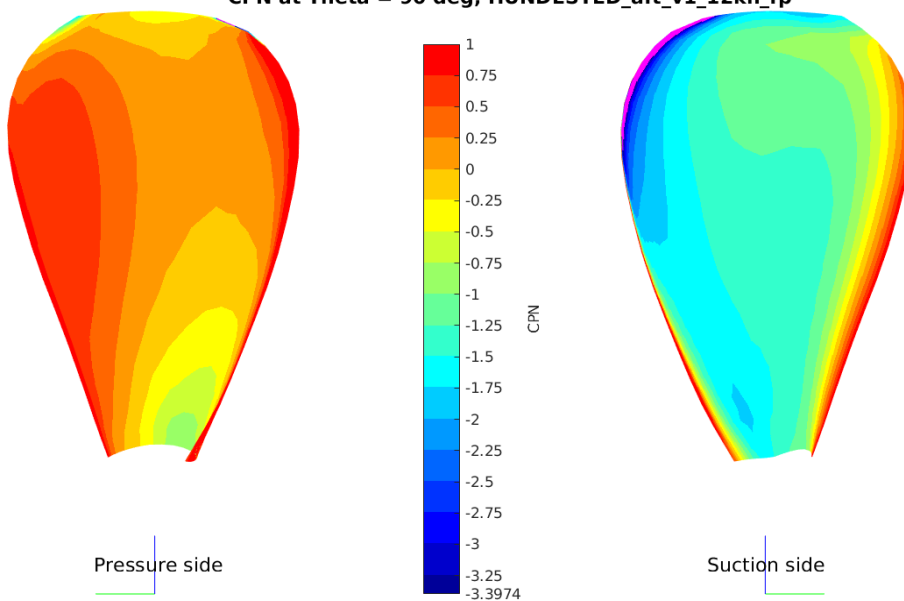
CPN at Theta = 30 deg, HUNDESTED_aft_v1_12kn_fp



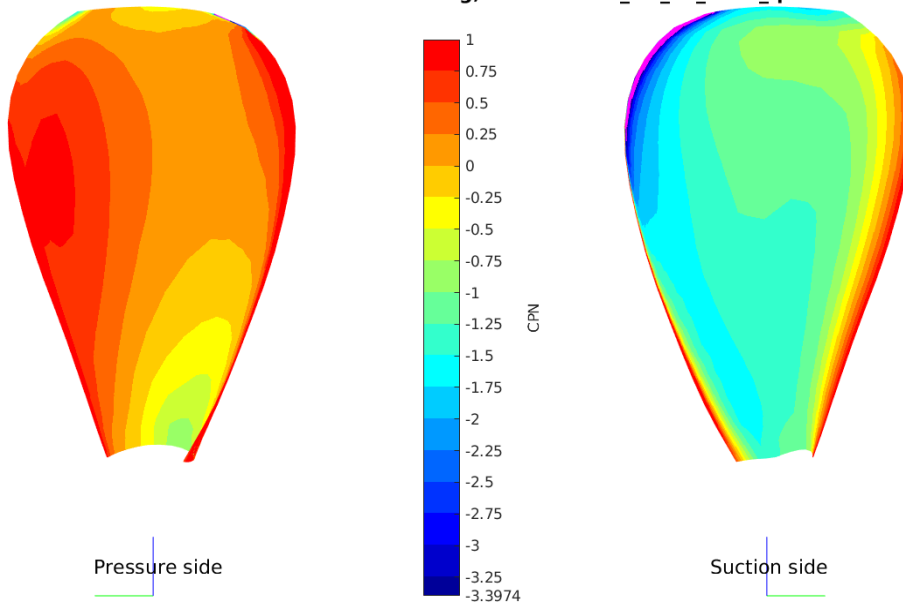
CPN at Theta = 60 deg, HUNDESTED_aft_v1_12kn_fp



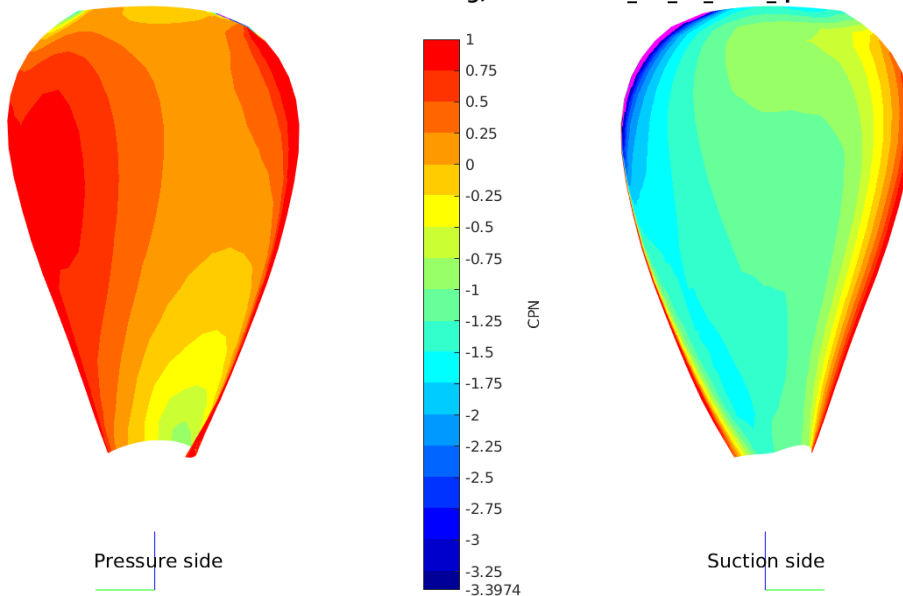
CPN at Theta = 90 deg, HUNDESTED_aft_v1_12kn_fp



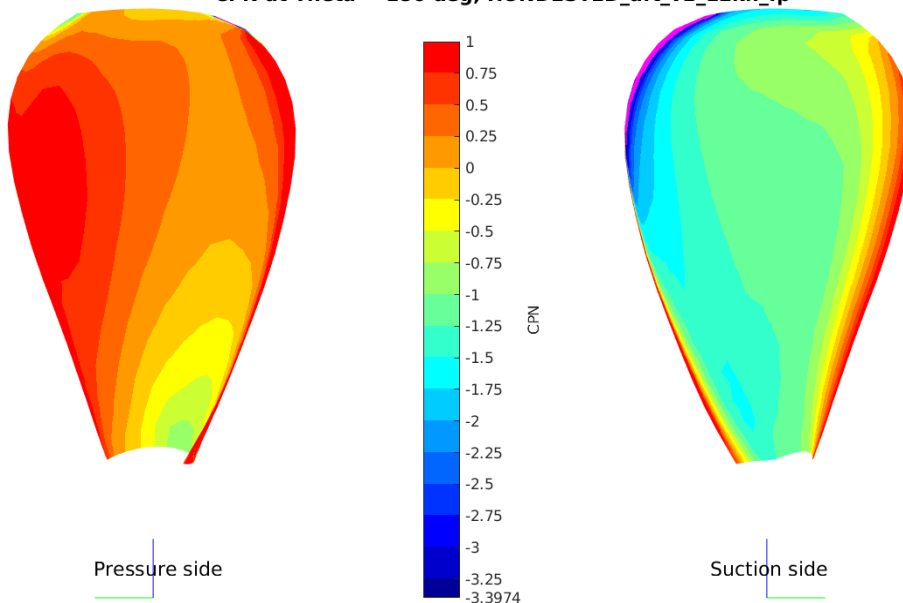
CPN at Theta = 120 deg, HUNDESTED_aft_v1_12kn_fp



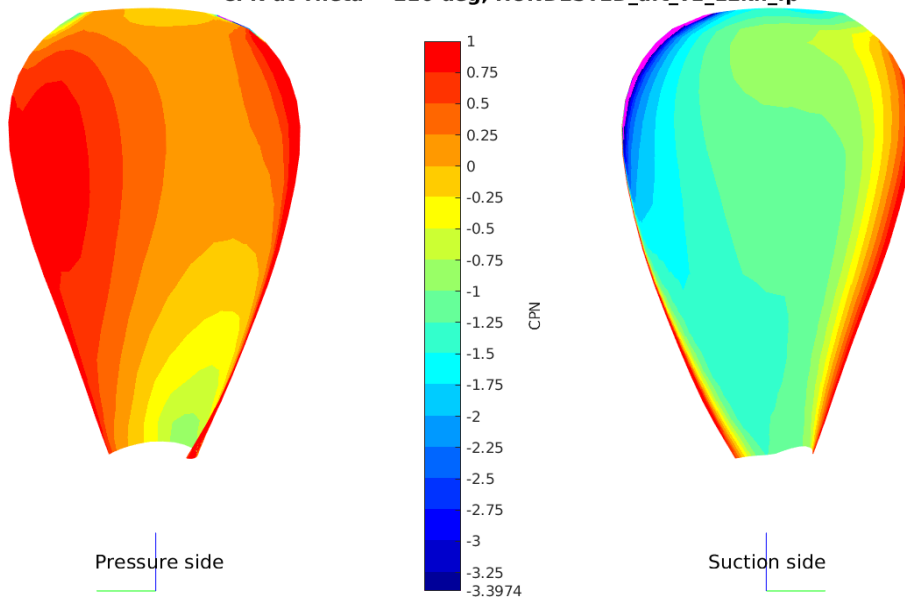
CPN at Theta = 150 deg, HUNDESTED_aft_v1_12kn_fp



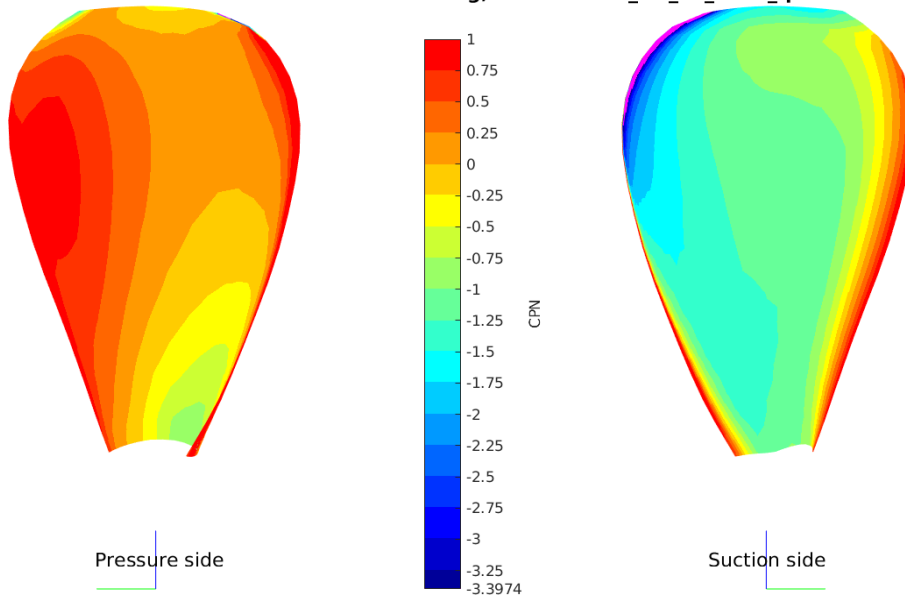
CPN at Theta = 180 deg, HUNDESTED_aft_v1_12kn_fp



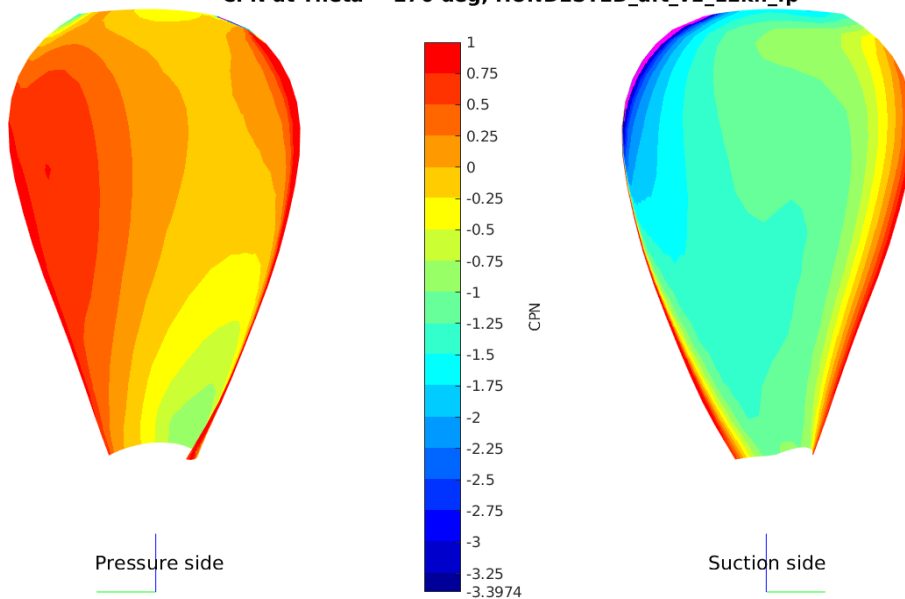
CPN at Theta = 210 deg, HUNDESTED_aft_v1_12kn_fp



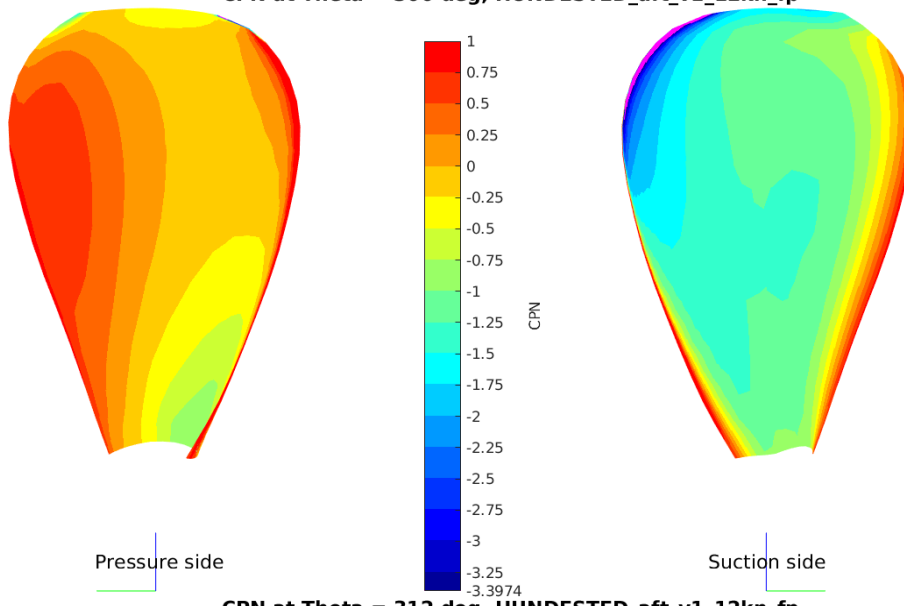
CPN at Theta = 240 deg, HUNDESTED_aft_v1_12kn_fp



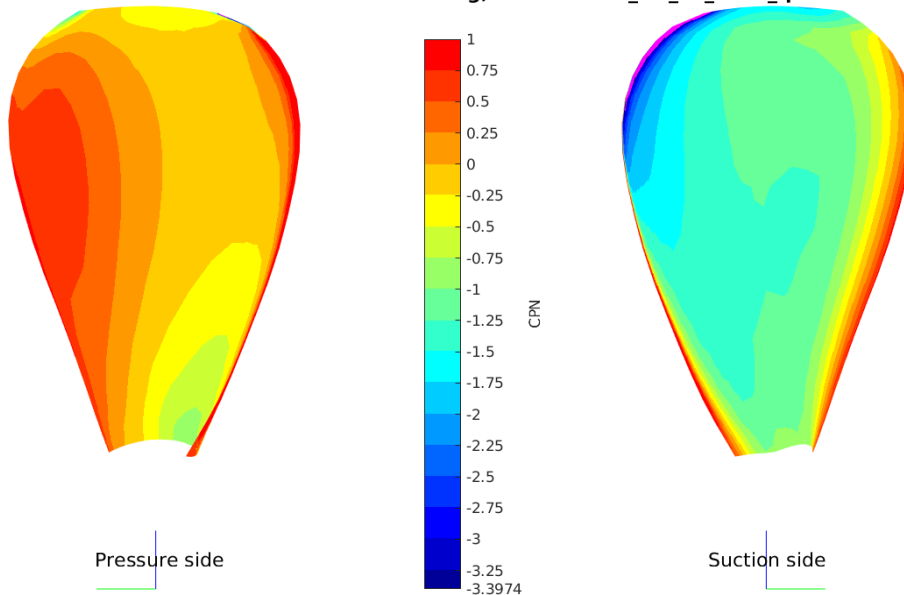
CPN at Theta = 270 deg, HUNDESTED_aft_v1_12kn_fp



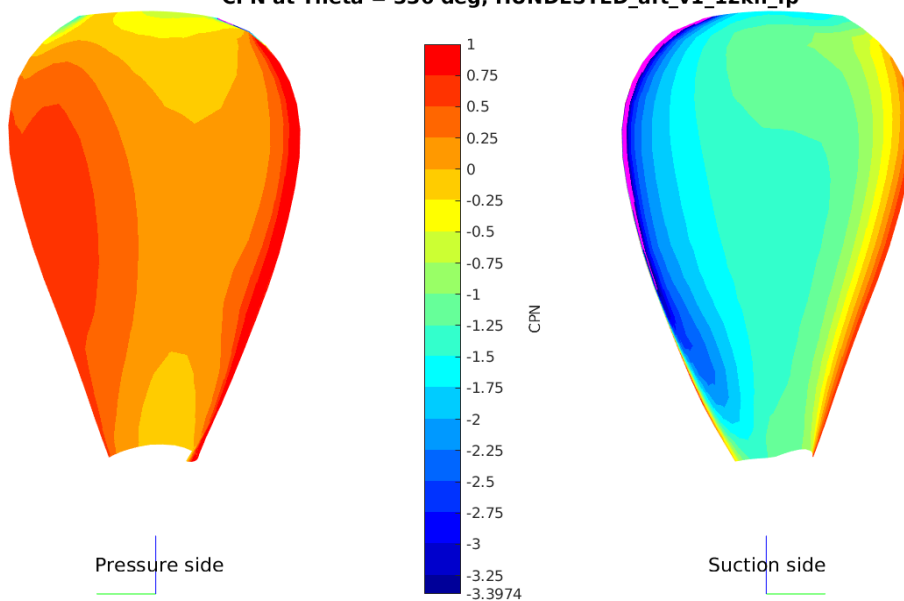
CPN at Theta = 300 deg, HUNDESTED_aft_v1_12kn_fp



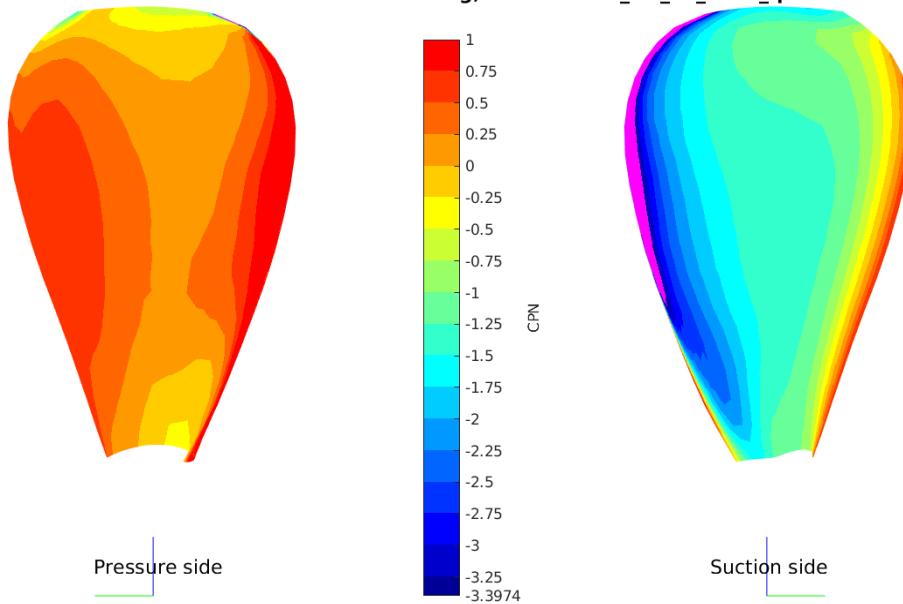
CPN at Theta = 312 deg, HUNDESTED_aft_v1_12kn_fp



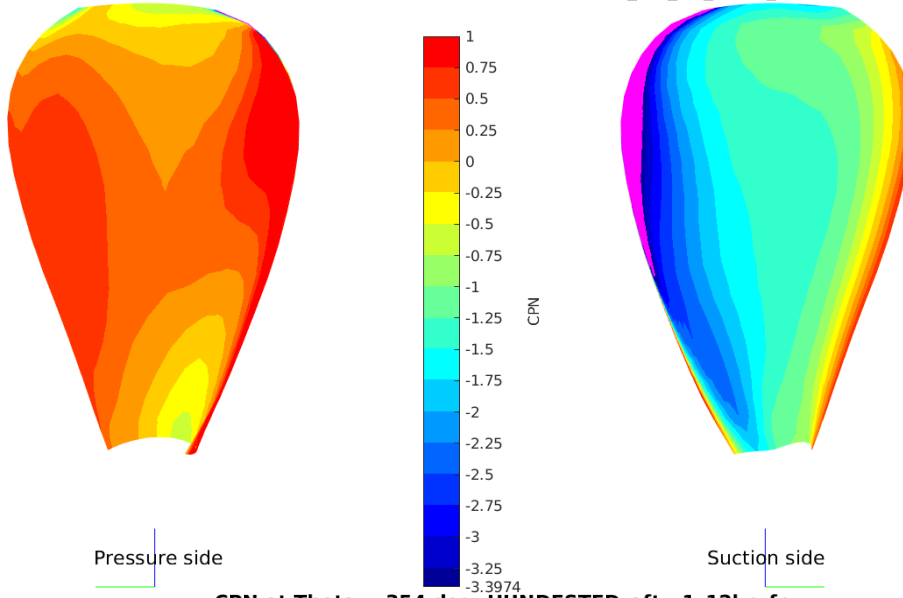
CPN at Theta = 336 deg, HUNDESTED_aft_v1_12kn_fp



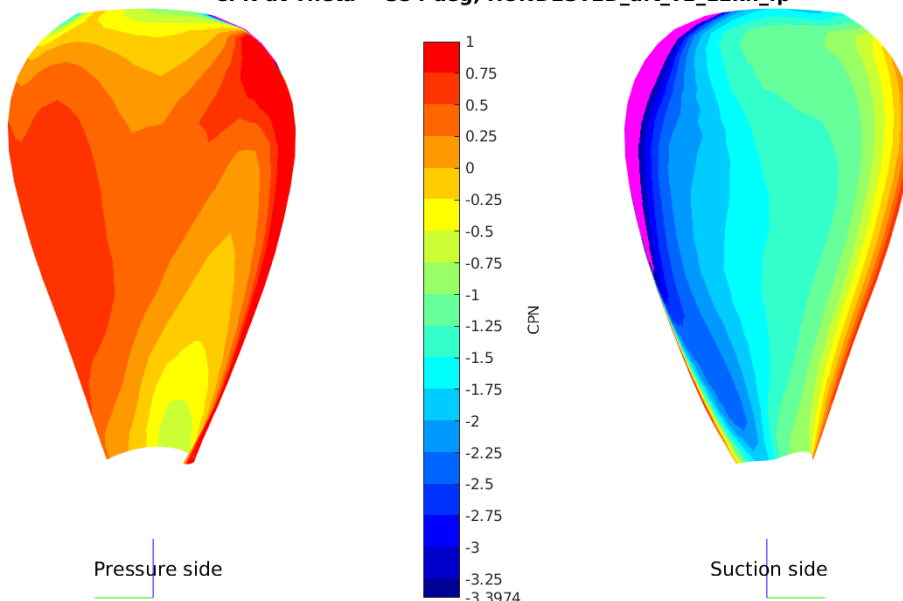
CPN at Theta = 342 deg, HUNDESTED_aft_v1_12kn_fp



CPN at Theta = 348 deg, HUNDESTED_aft_v1_12kn_fp

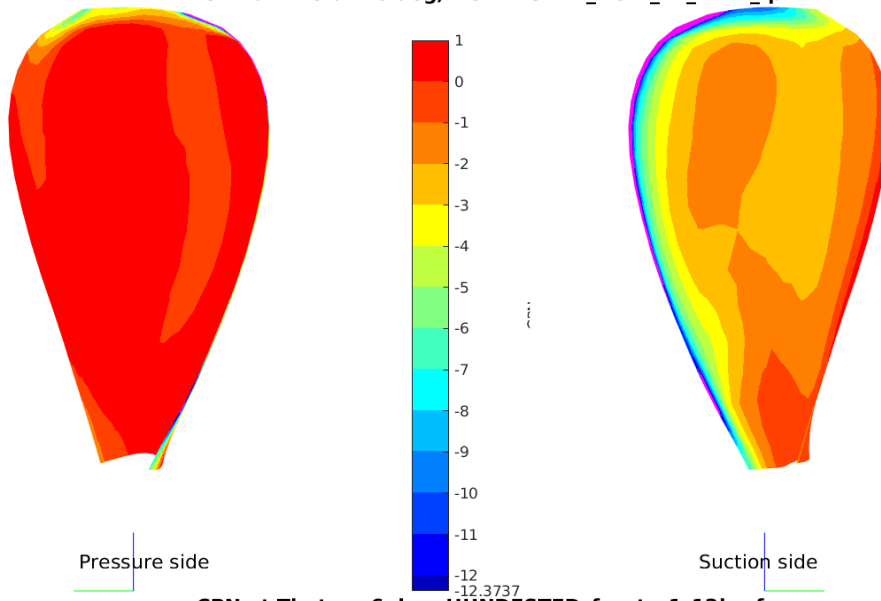


CPN at Theta = 354 deg, HUNDESTED_aft_v1_12kn_fp

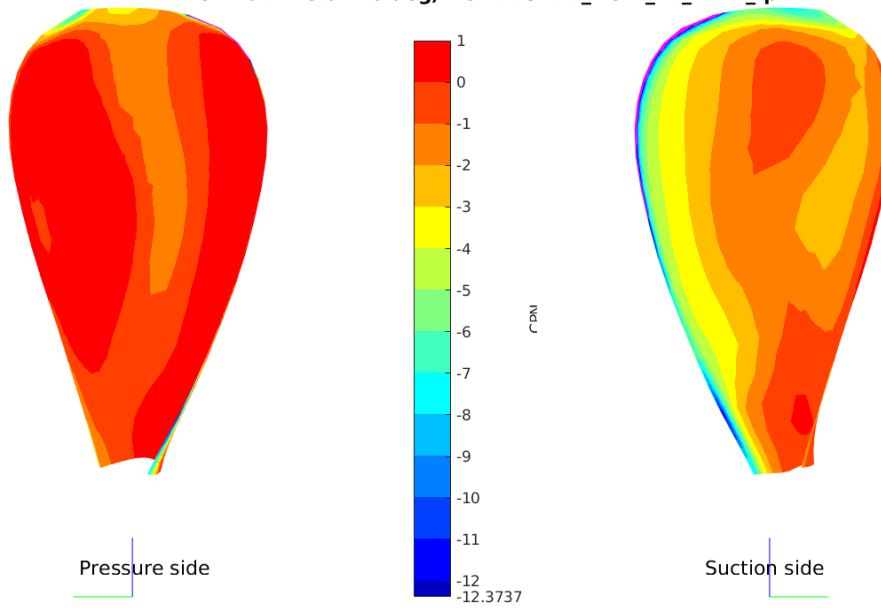


PRESSURE CONTOURS ON THE AFT PROPELLER AT 12.00 KNOTS

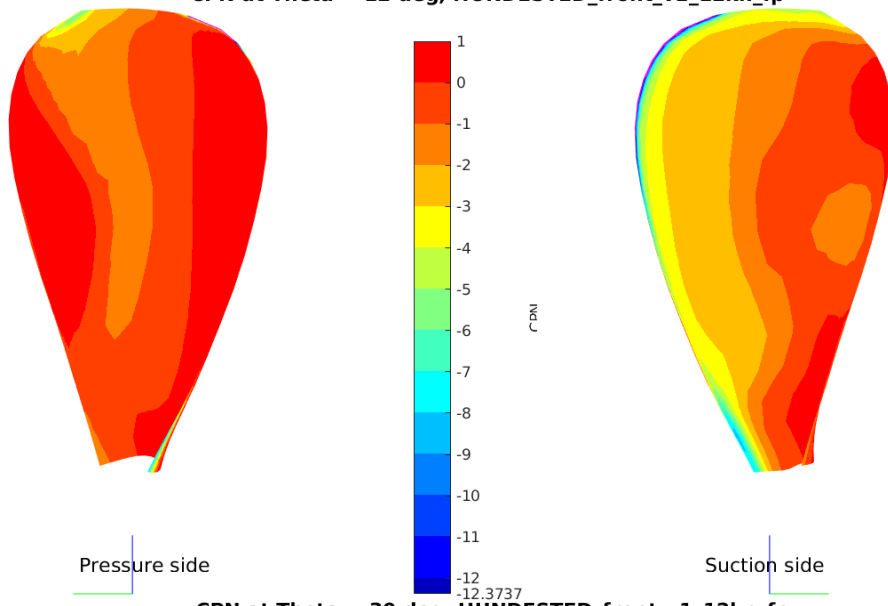
PRESSURE CONTOURS ON THE FRONT PROPELLER AT 12.00 KNOTS
CPN at Theta = 0 deg, HUNDESTED_front_v1_12kn_fp



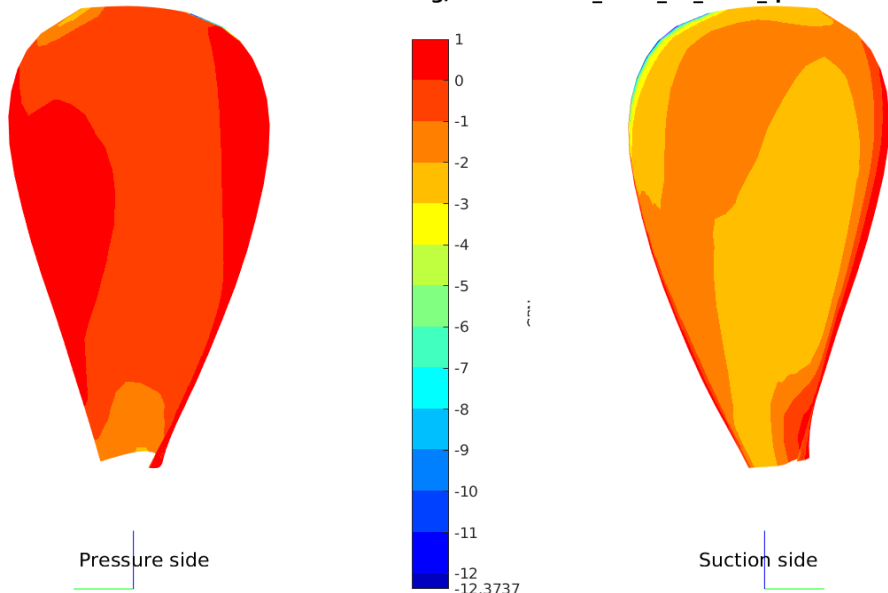
CPN at Theta = 6 deg, HUNDESTED_front_v1_12kn_fp



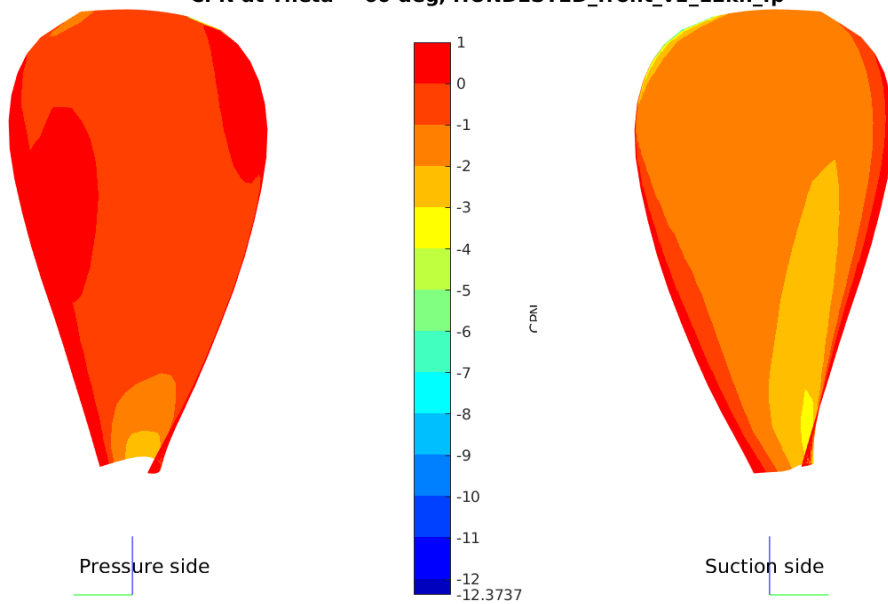
CPN at Theta = 12 deg, HUNDESTED_front_v1_12kn_fp



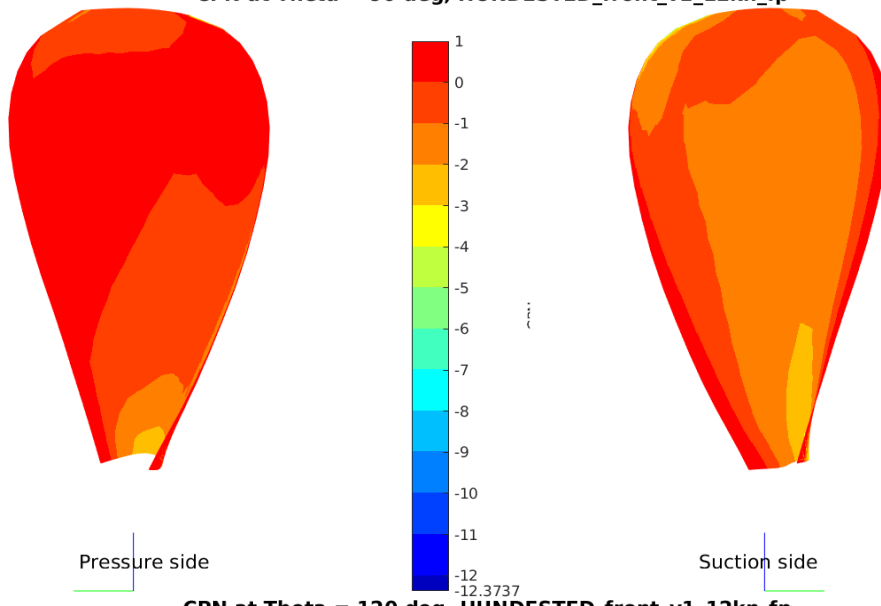
CPN at Theta = 30 deg, HUNDESTED_front_v1_12kn_fp



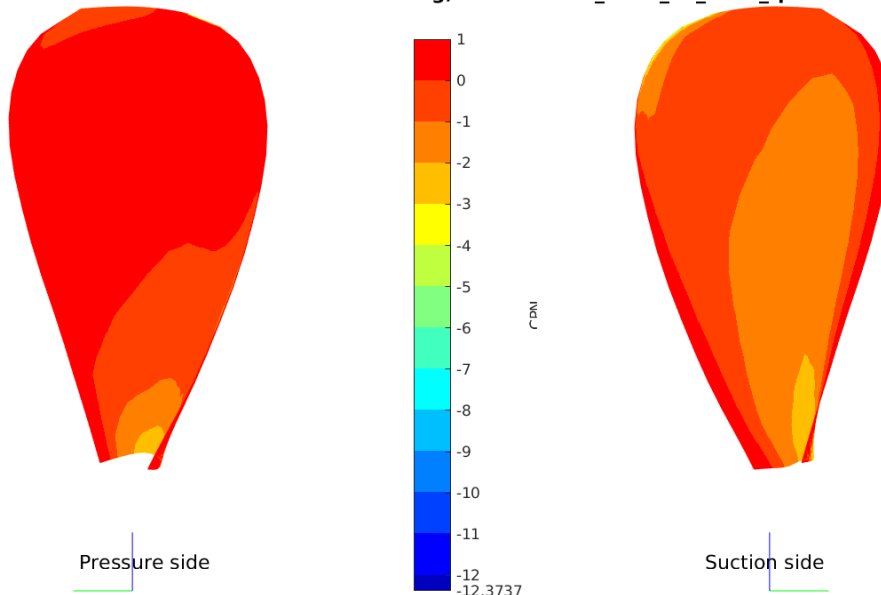
CPN at Theta = 60 deg, HUNDESTED_front_v1_12kn_fp



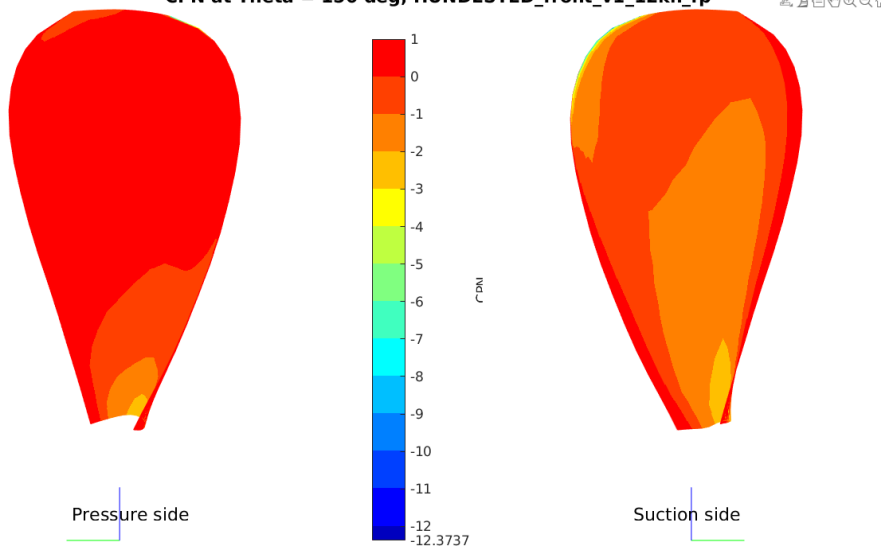
CPN at Theta = 90 deg, HUNDESTED_front_v1_12kn_fp



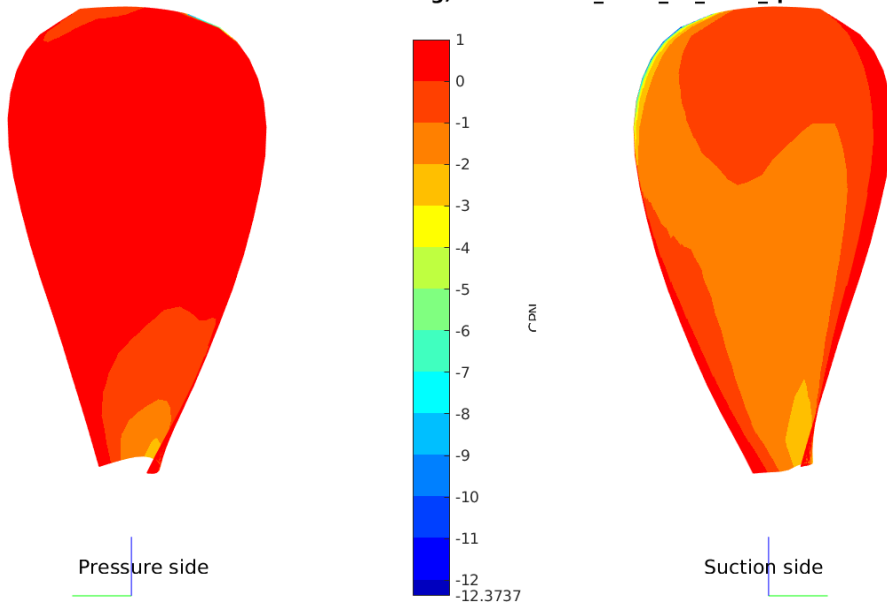
CPN at Theta = 120 deg, HUNDESTED_front_v1_12kn_fp



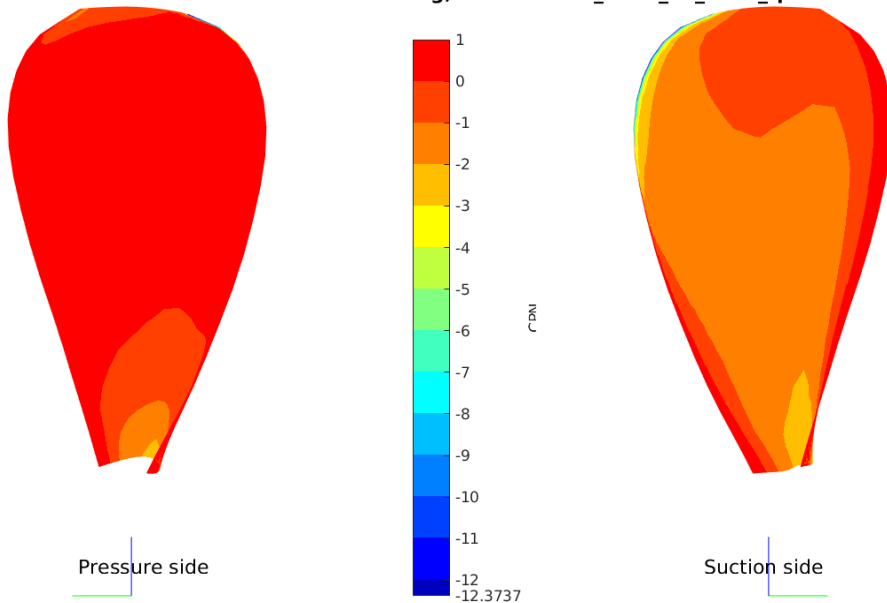
CPN at Theta = 150 deg, HUNDESTED_front_v1_12kn_fp



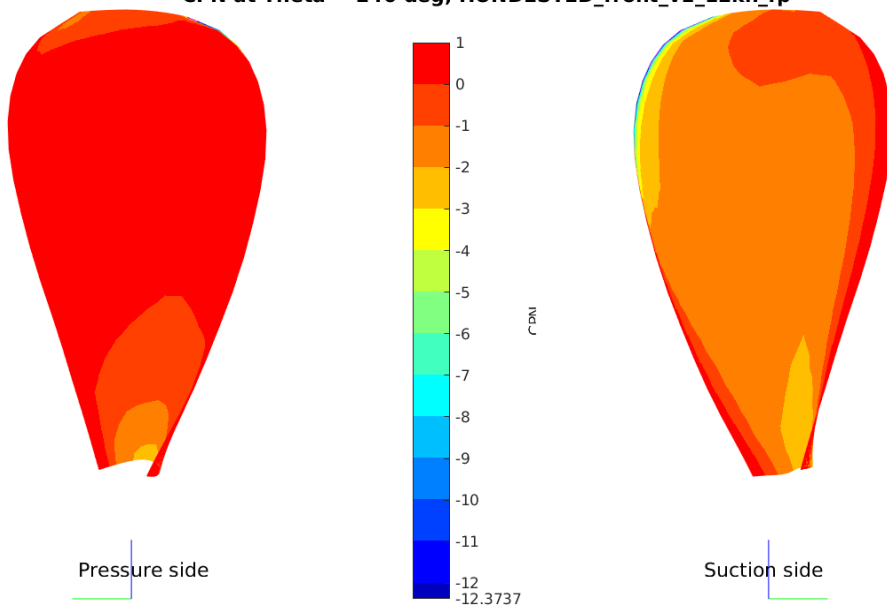
CPN at Theta = 180 deg, HUNDESTED_front_v1_12kn_fp



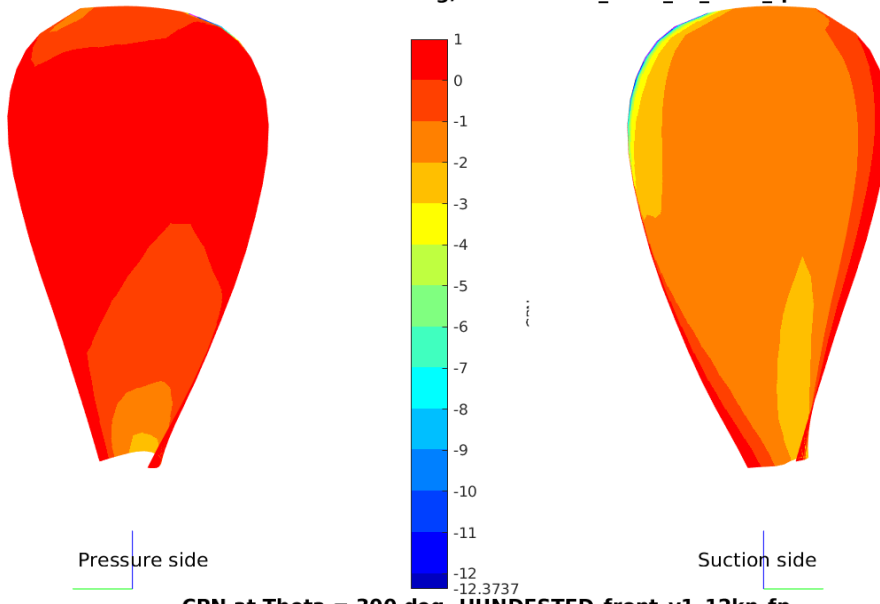
CPN at Theta = 210 deg, HUNDESTED_front_v1_12kn_fp



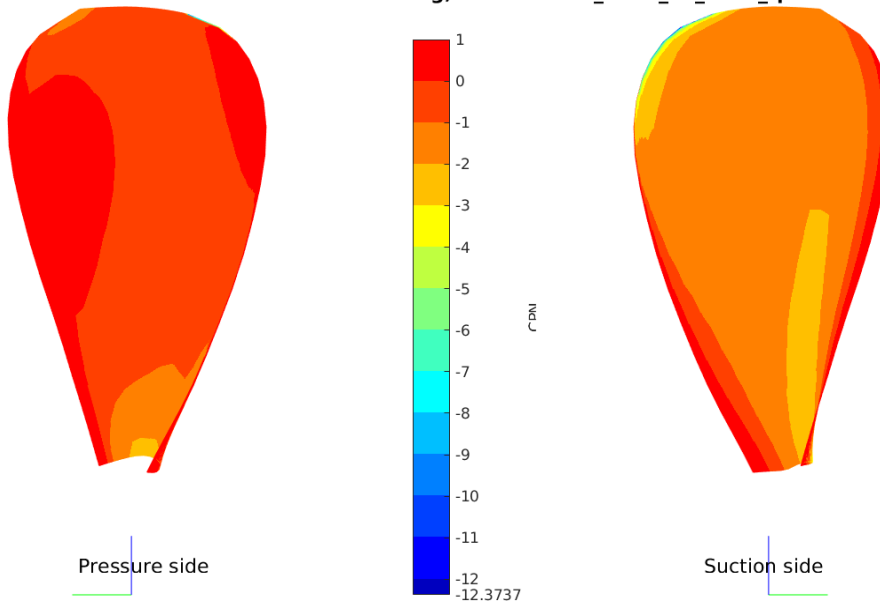
CPN at Theta = 240 deg, HUNDESTED_front_v1_12kn_fp



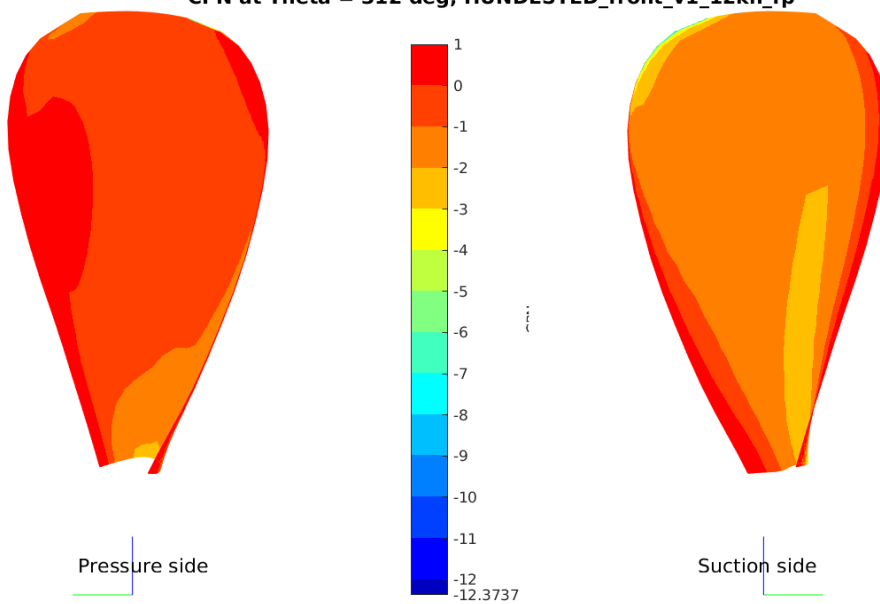
CPN at Theta = 270 deg, HUNDESTED_front_v1_12kn_fp



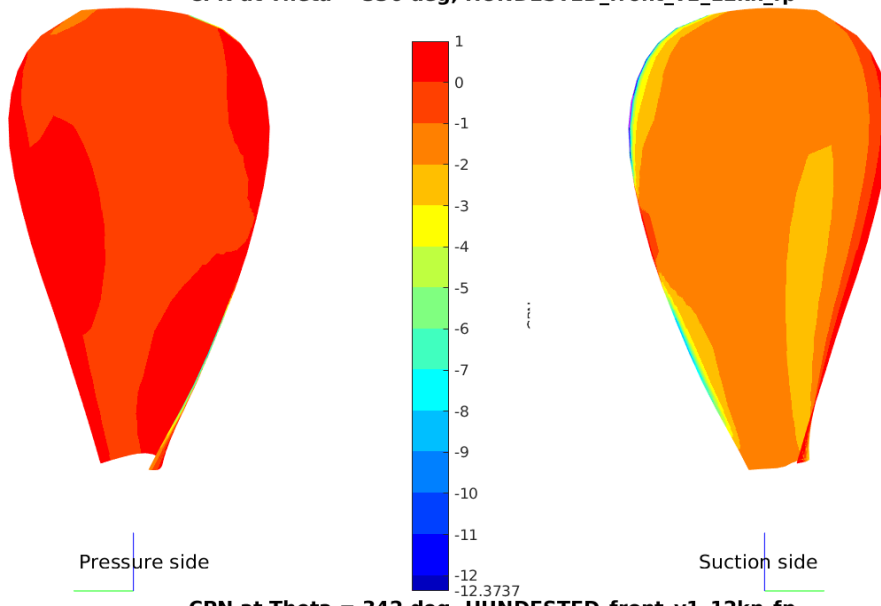
CPN at Theta = 300 deg, HUNDESTED_front_v1_12kn_fp



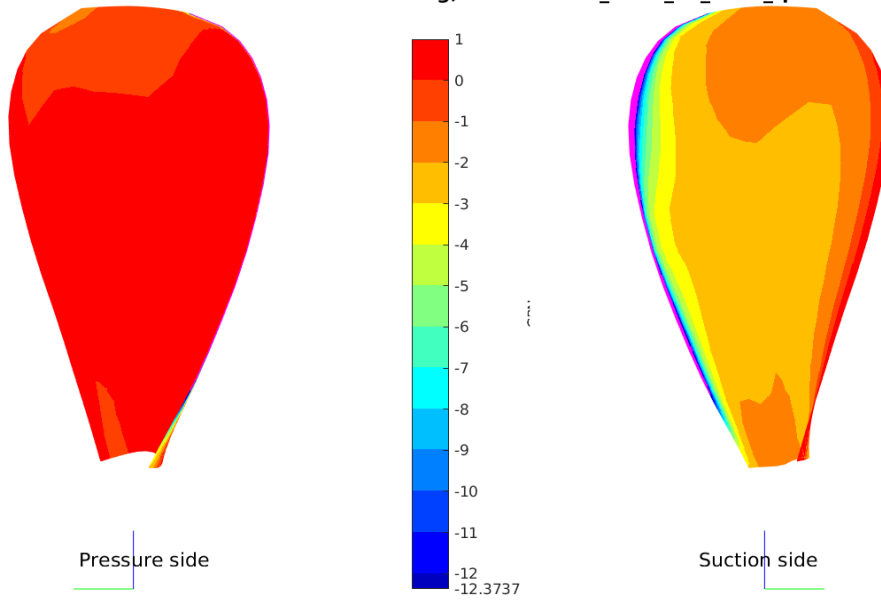
CPN at Theta = 312 deg, HUNDESTED_front_v1_12kn_fp



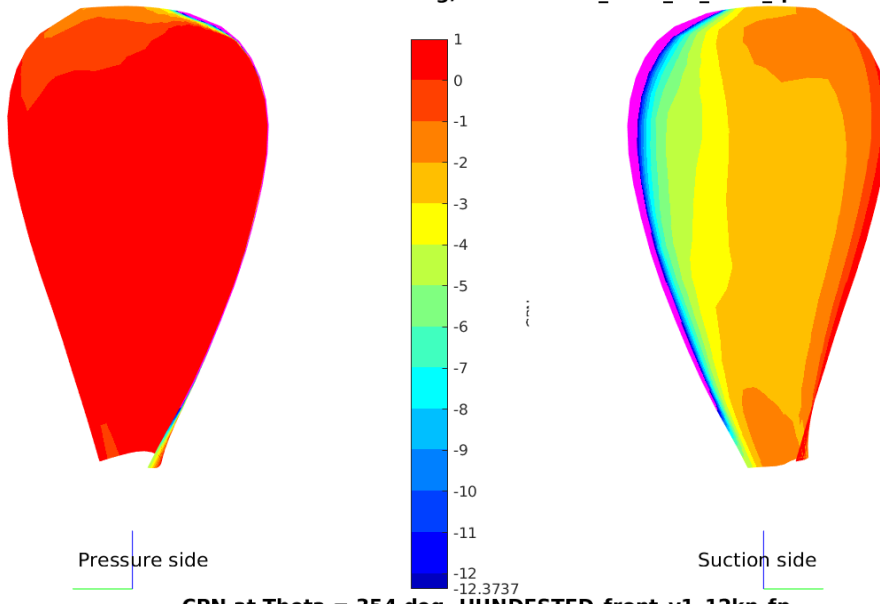
CPN at Theta = 336 deg, HUNDESTED_front_v1_12kn_fp



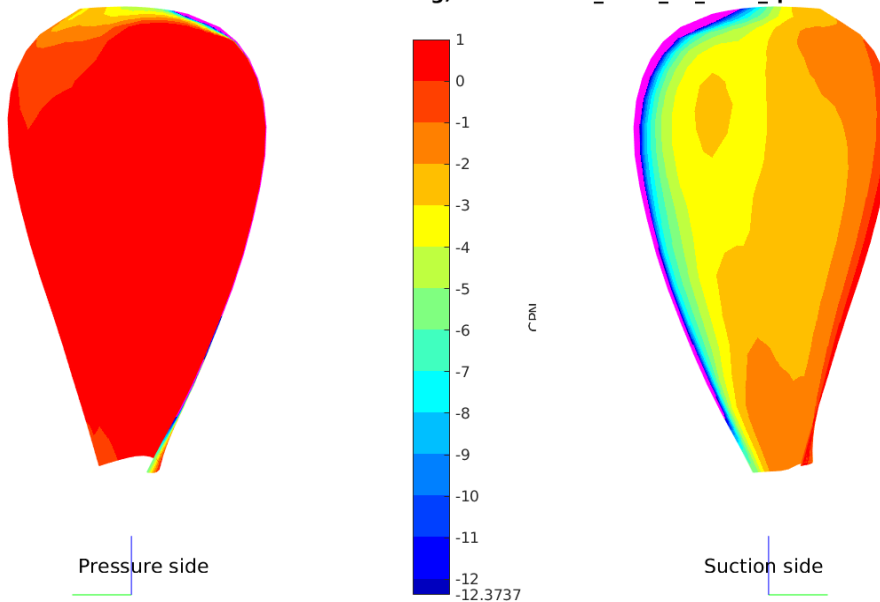
CPN at Theta = 342 deg, HUNDESTED_front_v1_12kn_fp



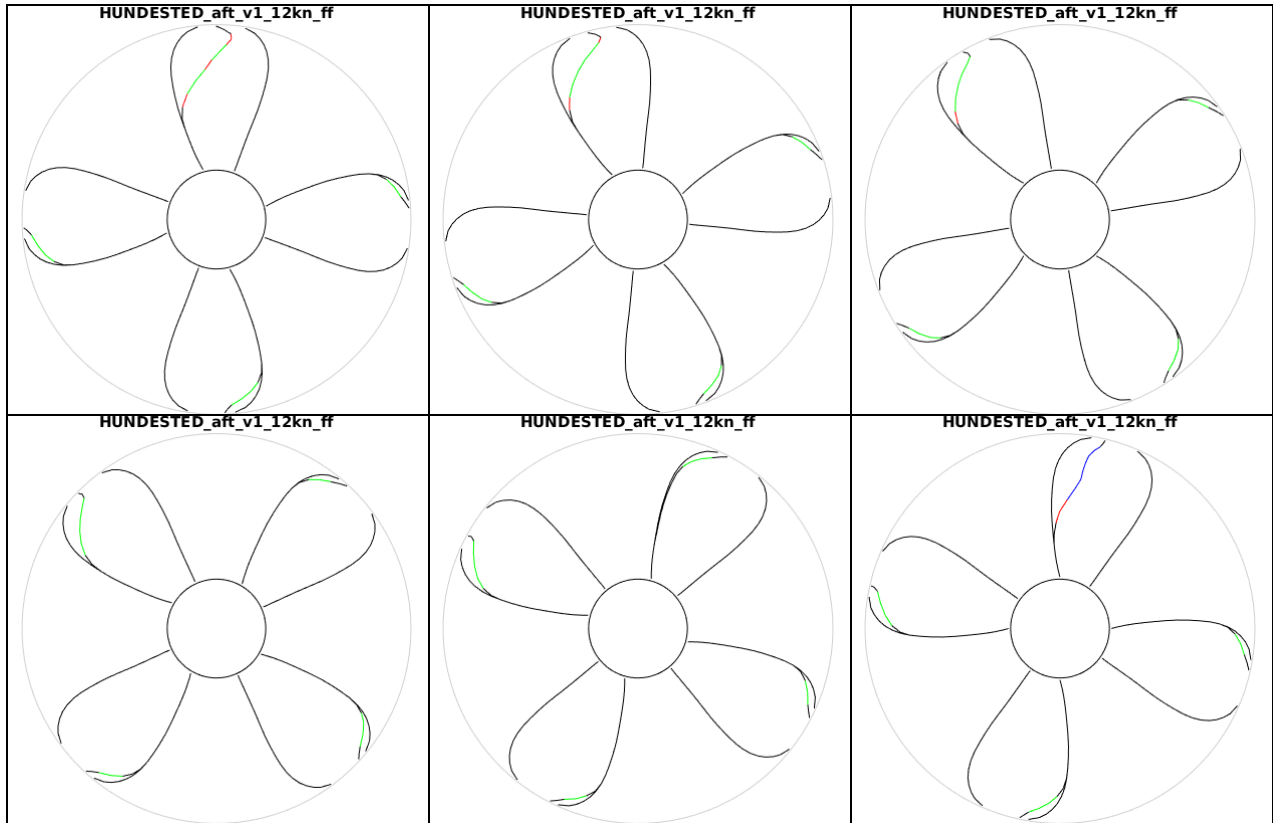
CPN at Theta = 348 deg, HUNDESTED_front_v1_12kn_fp



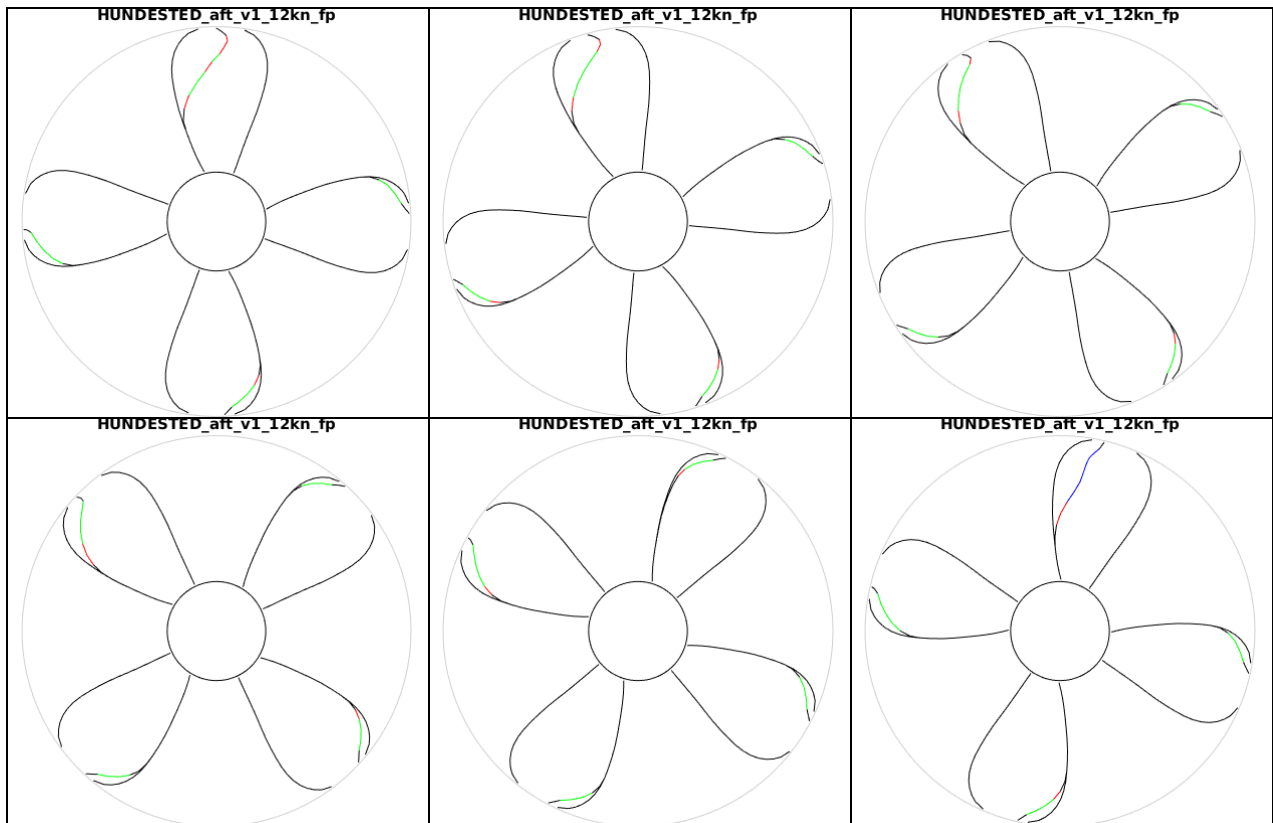
CPN at Theta = 354 deg, HUNDESTED_front_v1_12kn_fp



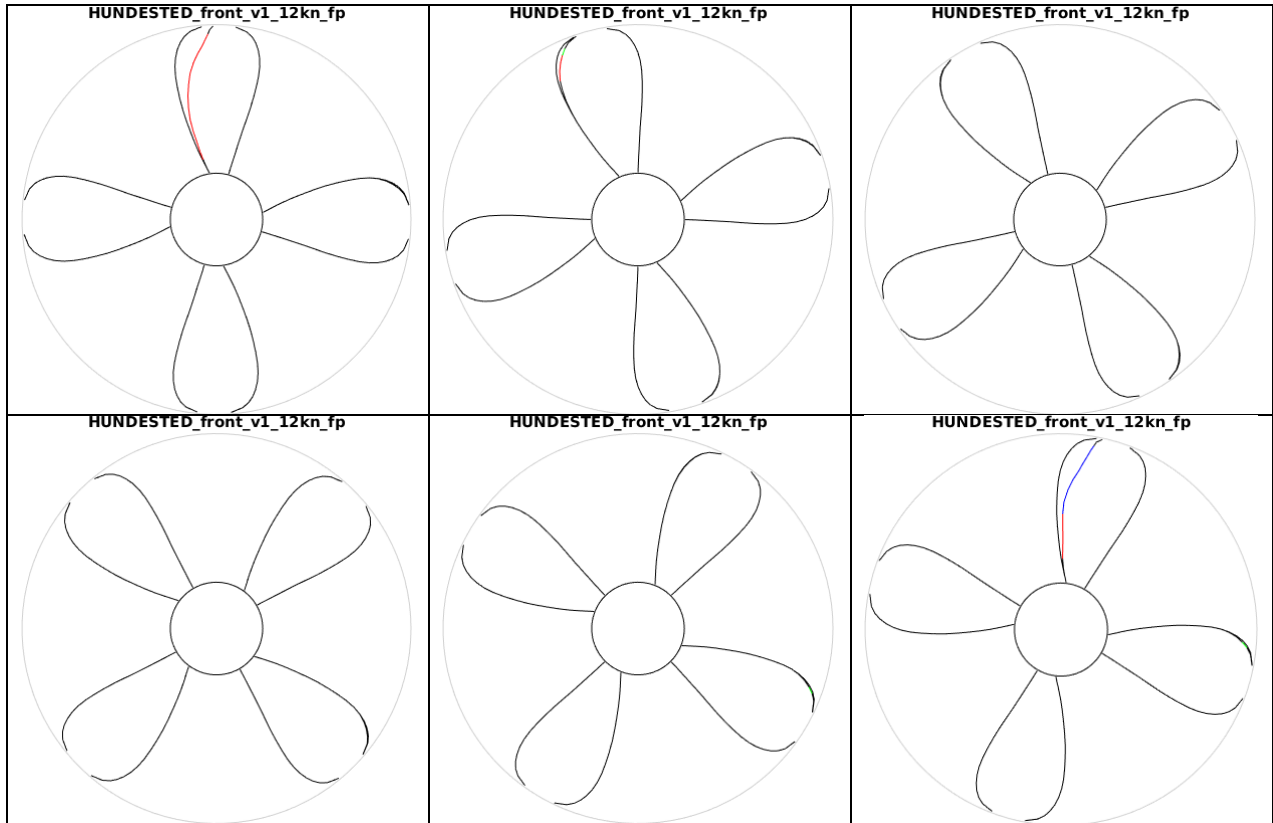
PRESSURE CONTOURS ON THE FRONT PROPELLER AT 12.00 KNOTS



CAVITATION BEHAVIOUR OF AFT PROPELLER, WITH FRONT PROPELLER FEATHERED DURING PROPULSION AT 12 KNOTS



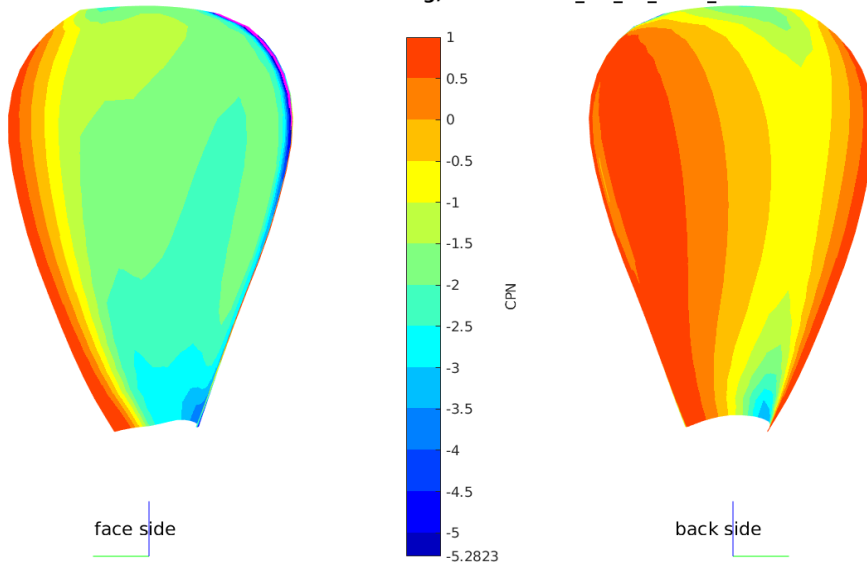
CAVITATION BEHAVIOUR OF AFT PROPELLER, WITH FRONT PROPELLER IN PROPULSION DURING PROPULSION AT 12 KNOTS



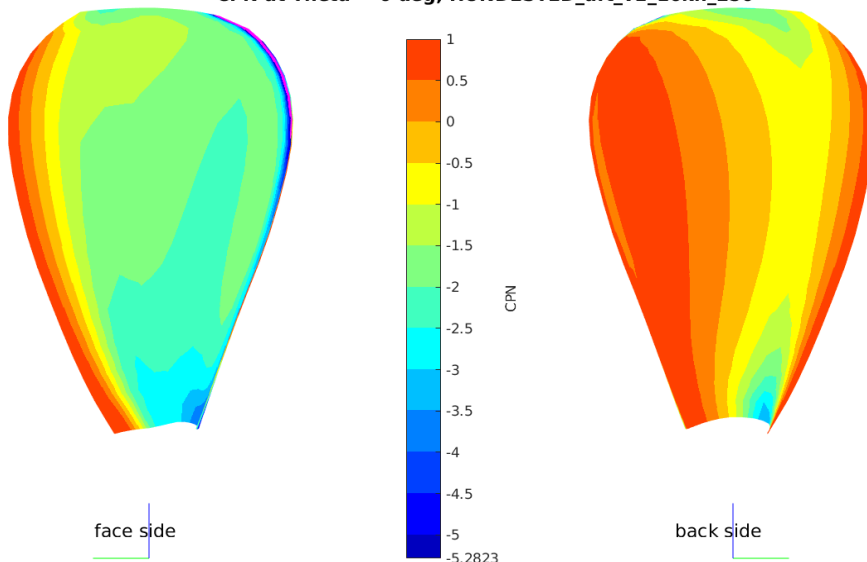
CAVITATION BEHAVIOUR OF FRONT PROPELLER DURING PROPULSION AT 12 KNOTS

PRESSURE CONTOURS ON THE AFT PROPELLER AT 16 KNOTS,
REGENERATING 250 KW MODE

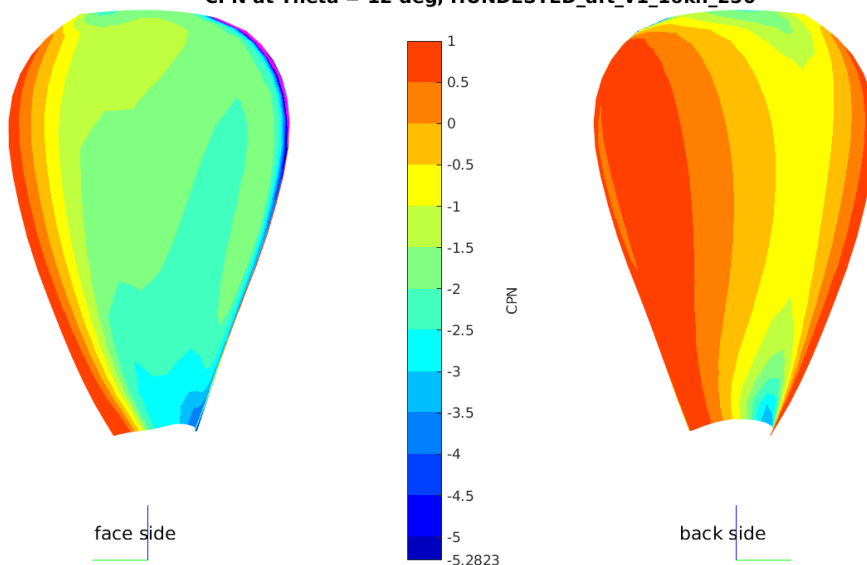
CPN at Theta = 0 deg, HUNDESTED_aft_v1_16kn_250



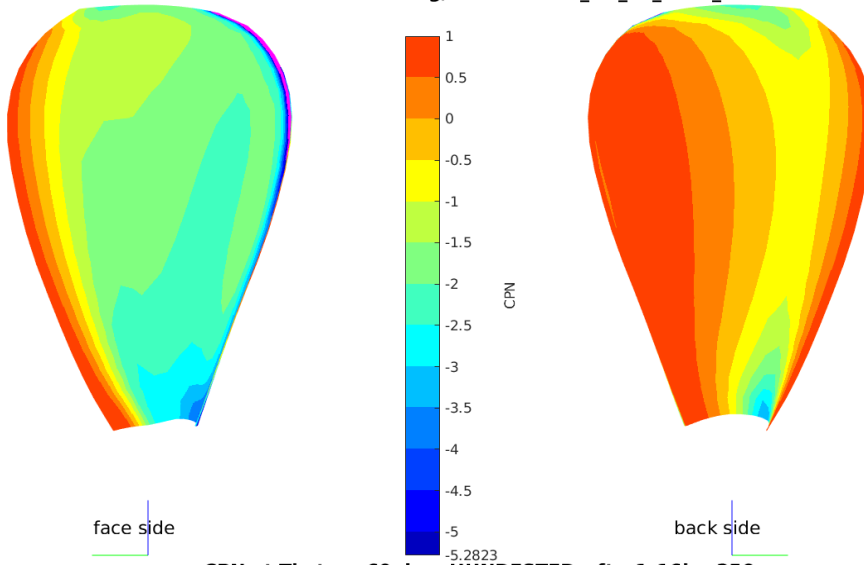
CPN at Theta = 6 deg, HUNDESTED_aft_v1_16kn_250



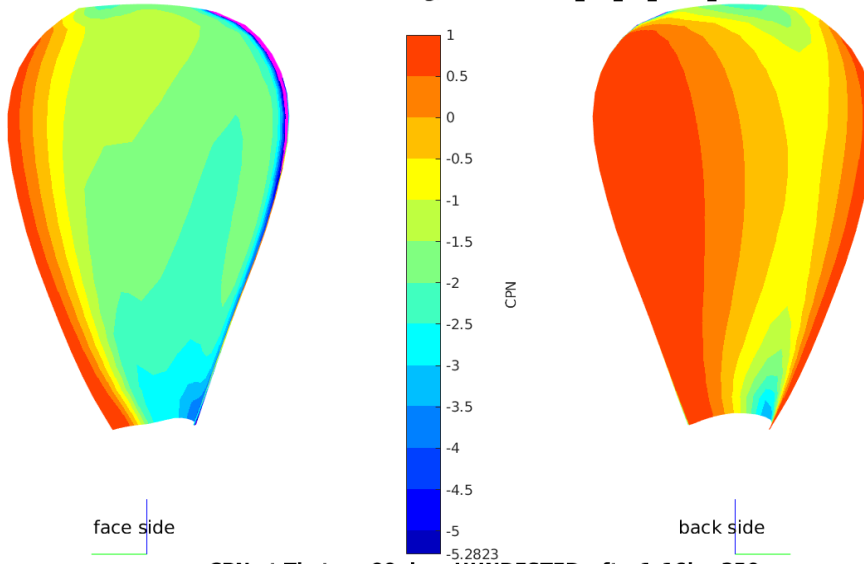
CPN at Theta = 12 deg, HUNDESTED_aft_v1_16kn_250



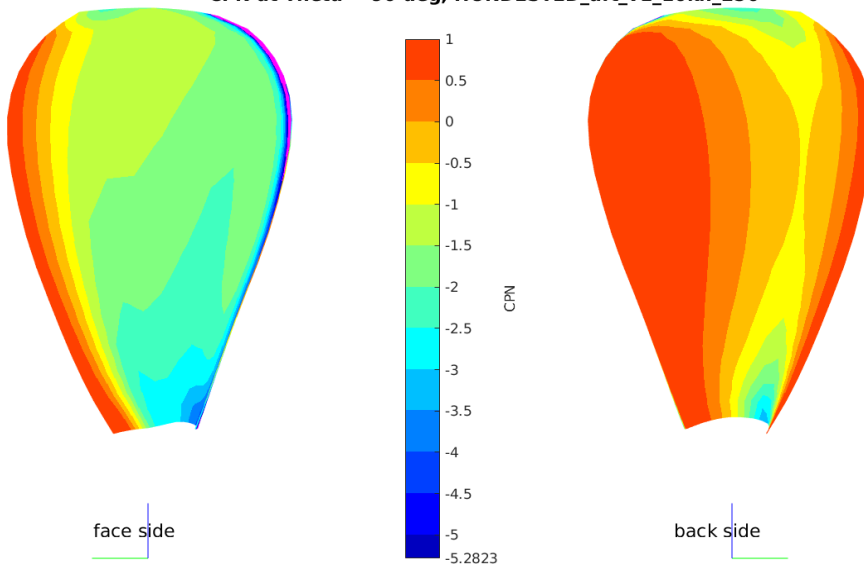
CPN at Theta = 30 deg, HUNDESTED_aft_v1_16kn_250



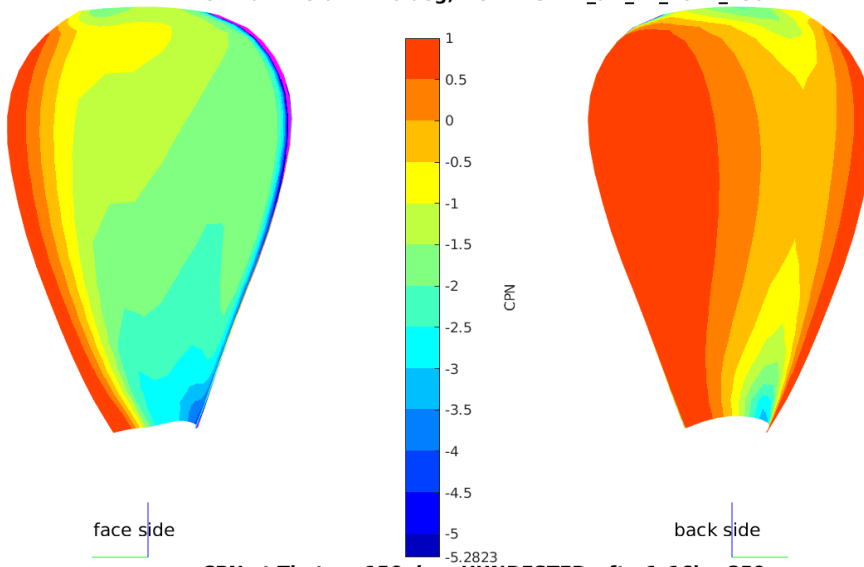
CPN at Theta = 60 deg, HUNDESTED_aft_v1_16kn_250



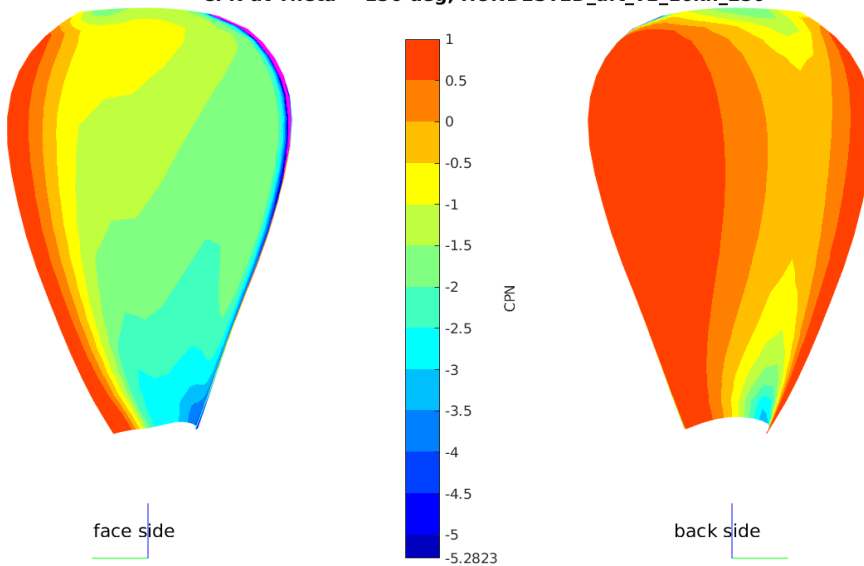
CPN at Theta = 90 deg, HUNDESTED_aft_v1_16kn_250



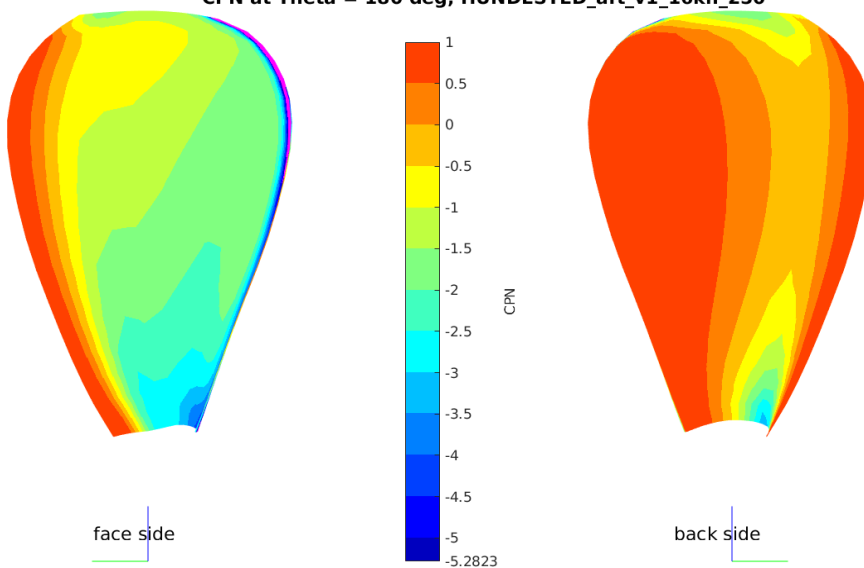
CPN at Theta = 120 deg, HUNDESTED_aft_v1_16kn_250



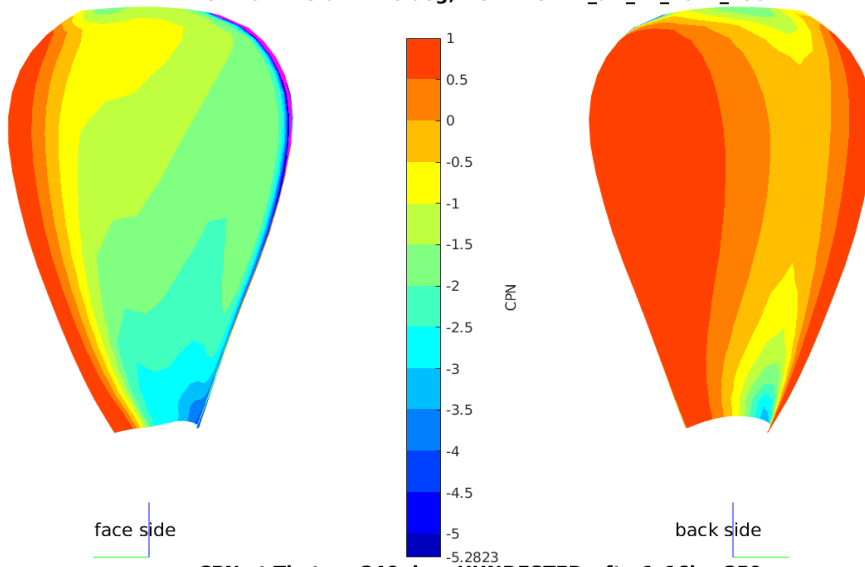
CPN at Theta = 150 deg, HUNDESTED_aft_v1_16kn_250



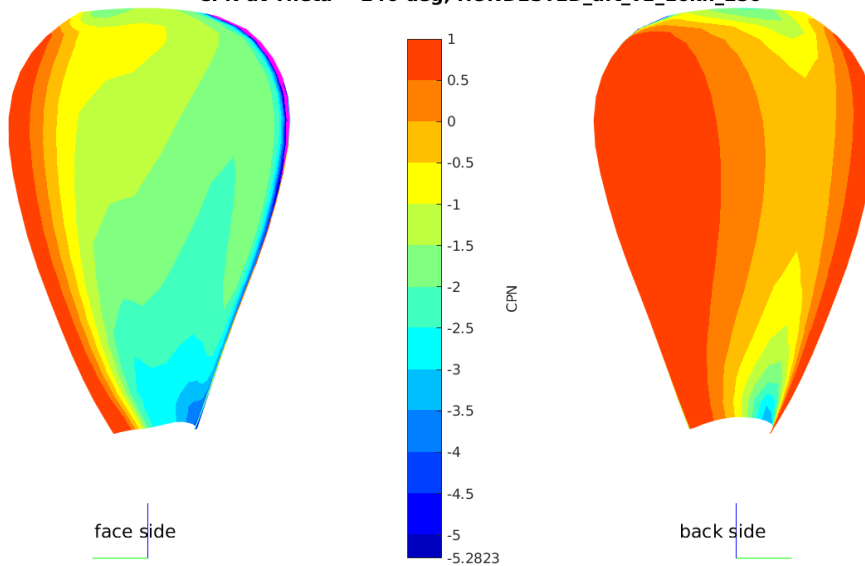
CPN at Theta = 180 deg, HUNDESTED_aft_v1_16kn_250



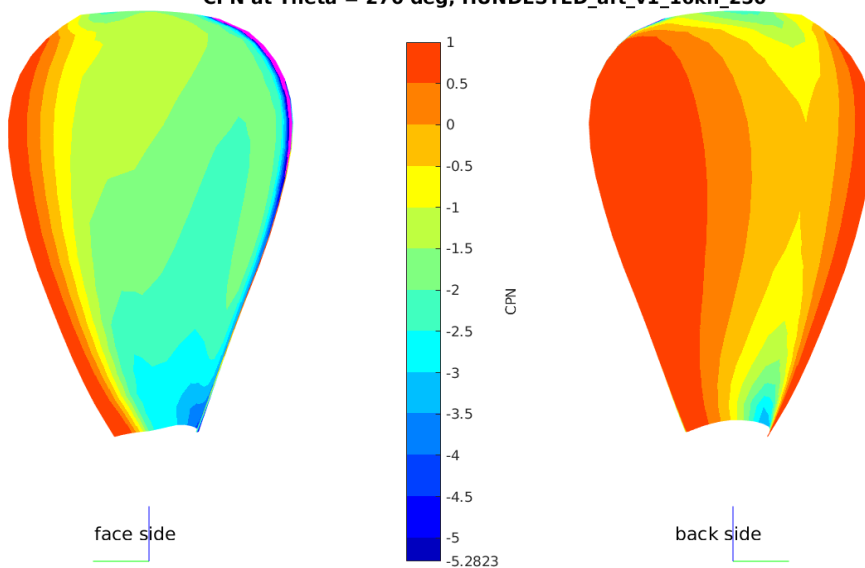
CPN at Theta = 210 deg, HUNDESTED_aft_v1_16kn_250



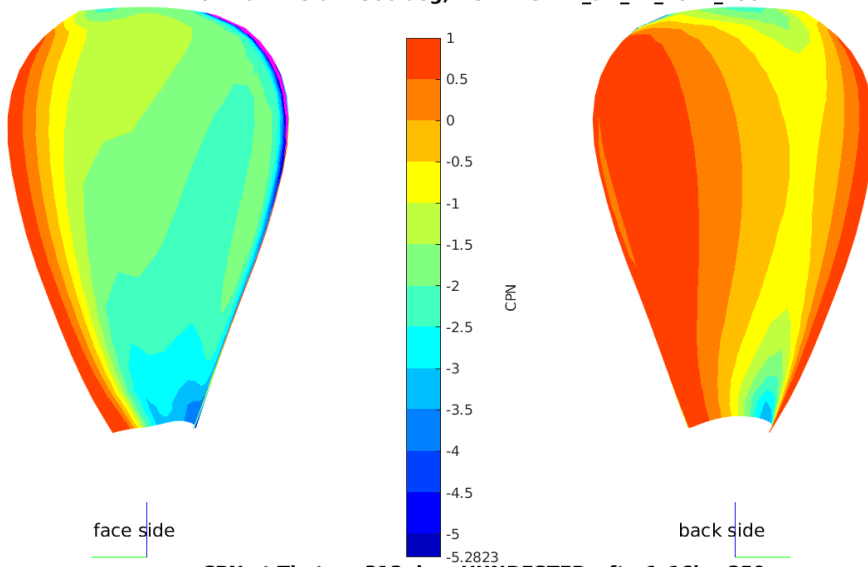
CPN at Theta = 240 deg, HUNDESTED_aft_v1_16kn_250



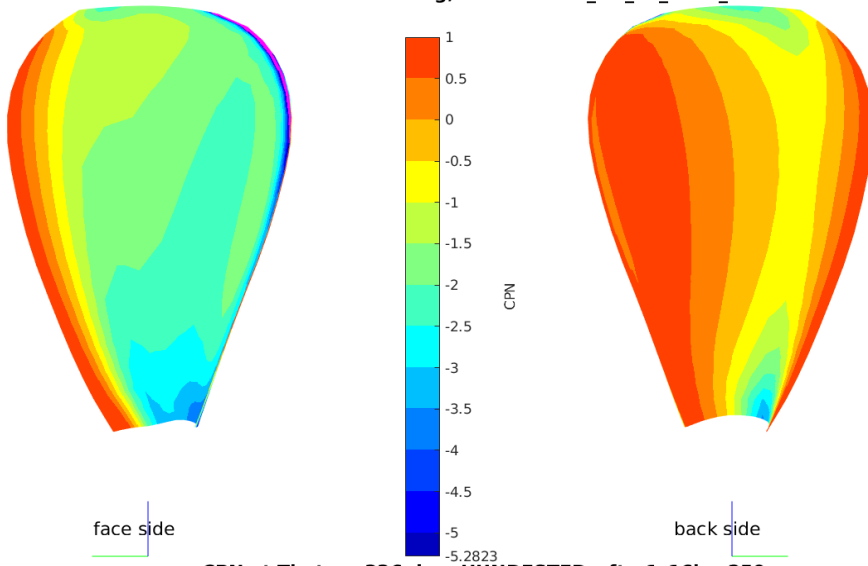
CPN at Theta = 270 deg, HUNDESTED_aft_v1_16kn_250



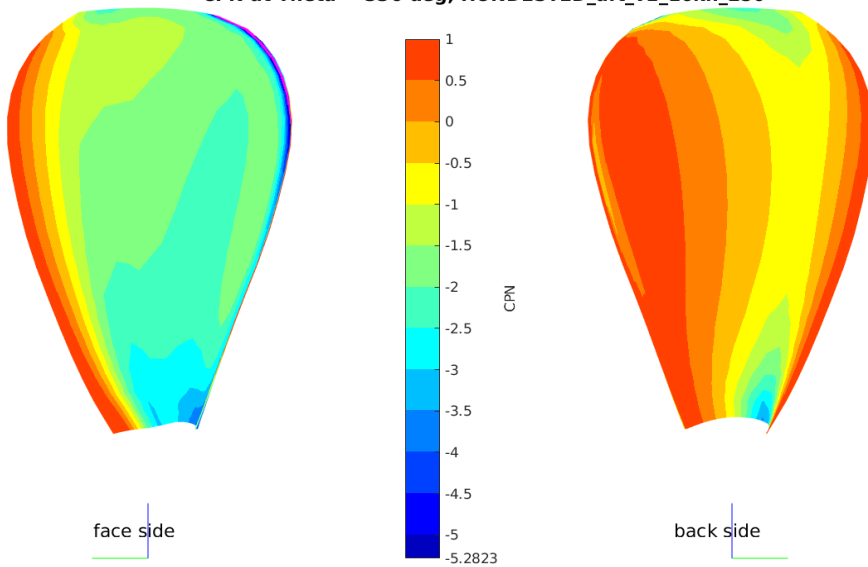
CPN at Theta = 300 deg, HUNDESTED_aft_v1_16kn_250



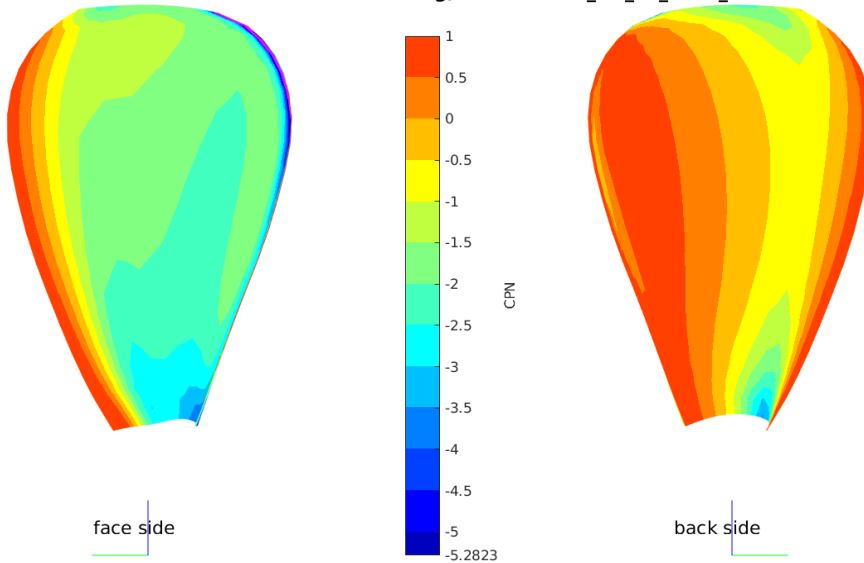
CPN at Theta = 312 deg, HUNDESTED_aft_v1_16kn_250



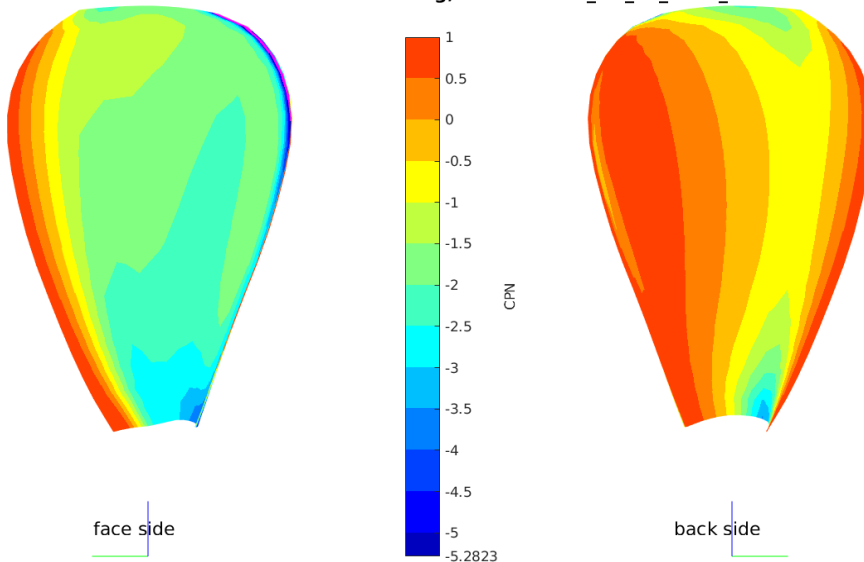
CPN at Theta = 336 deg, HUNDESTED_aft_v1_16kn_250



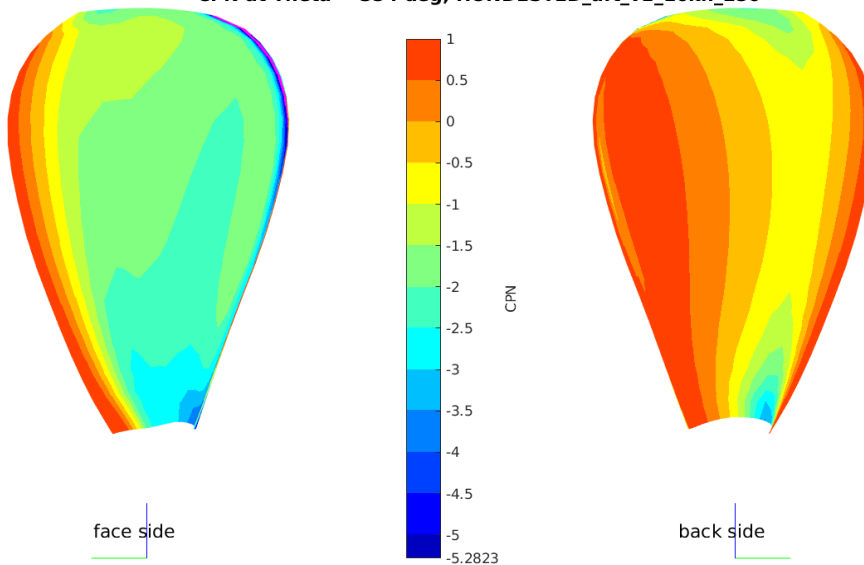
CPN at Theta = 342 deg, HUNDESTED_aft_v1_16kn_250



CPN at Theta = 348 deg, HUNDESTED_aft_v1_16kn_250



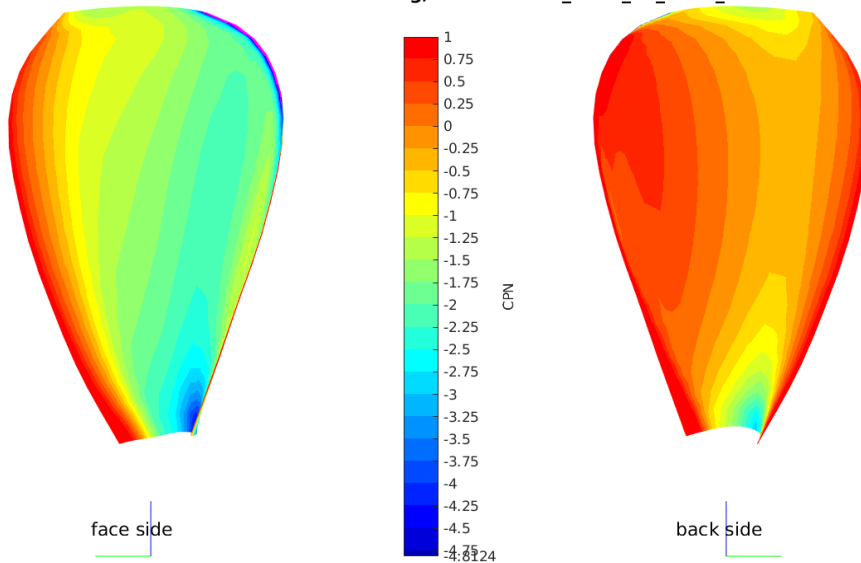
CPN at Theta = 354 deg, HUNDESTED_aft_v1_16kn_250



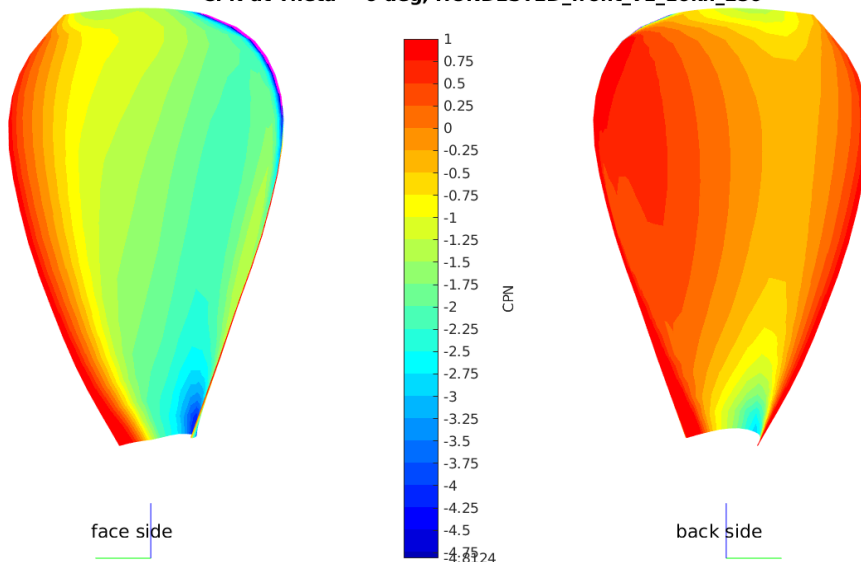
PRESSURE CONTOURS ON THE AFT PROPELLER AT 16 KNOTS, REGENERATING 250 KW MODE

PRESSURE CONTOURS ON THE FRONT PROPELLER AT 16 KNOTS, REGENERATING 250 KW MODE

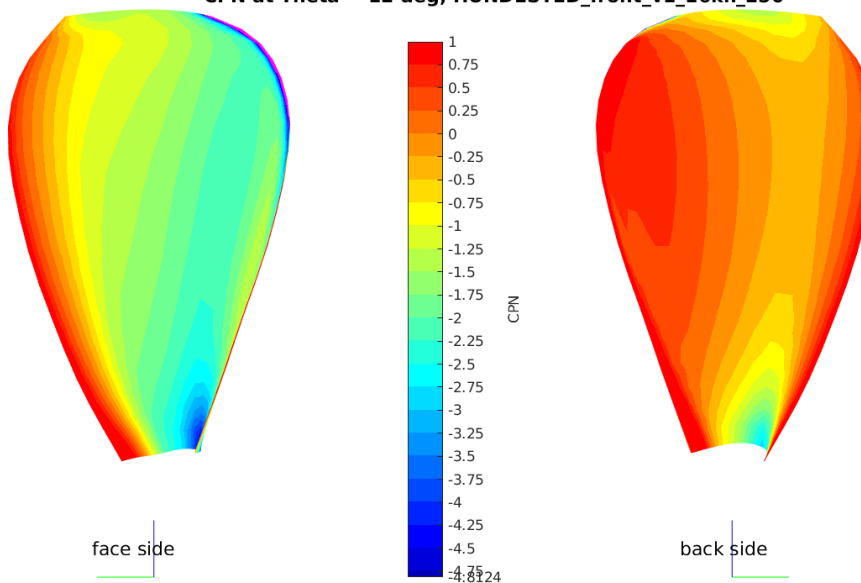
CPN at Theta = 0 deg, HUNDESTED_front_v1_16kn_250



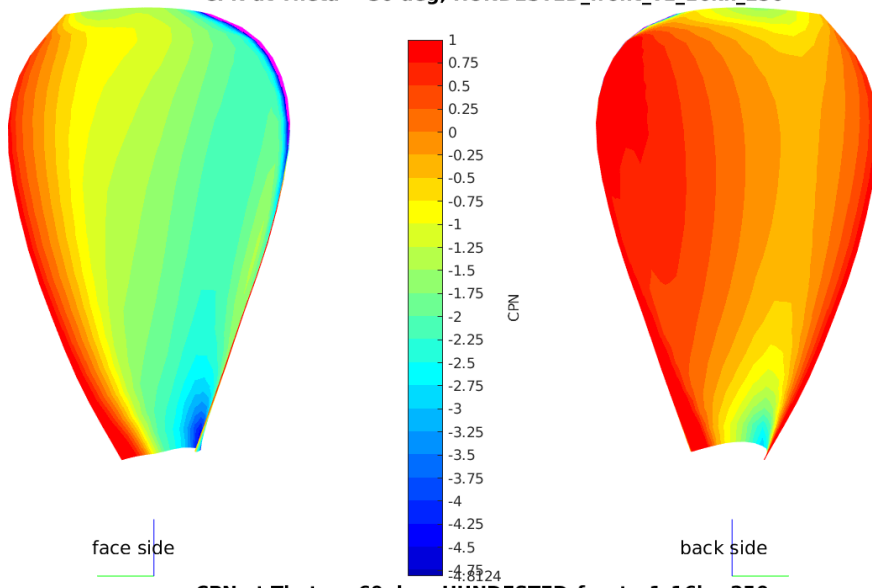
CPN at Theta = 6 deg, HUNDESTED_front_v1_16kn_250



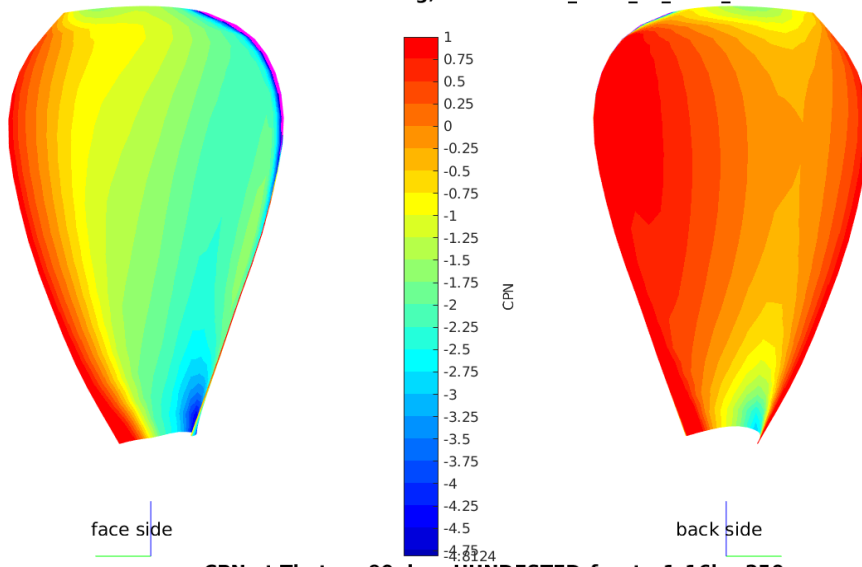
CPN at Theta = 12 deg, HUNDESTED_front_v1_16kn_250



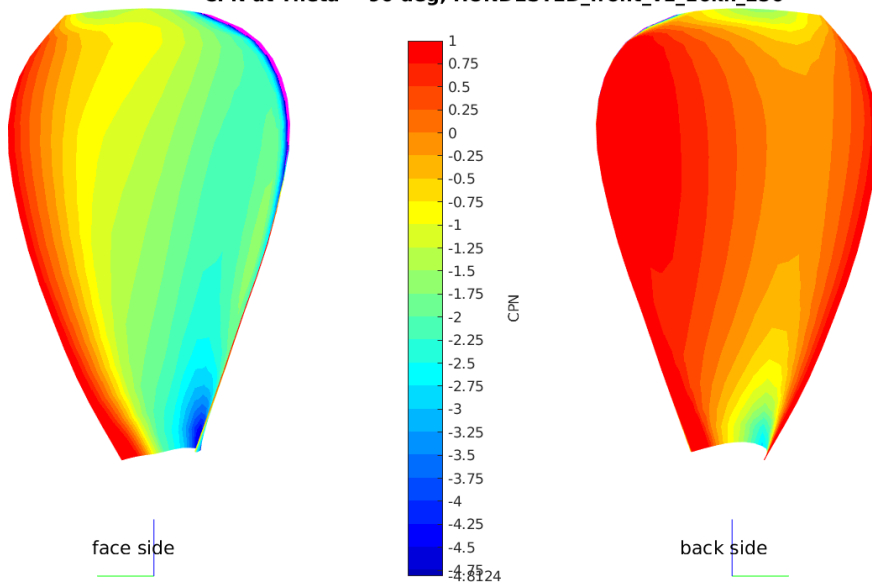
CPN at Theta = 30 deg, HUNDESTED_front_v1_16kn_250



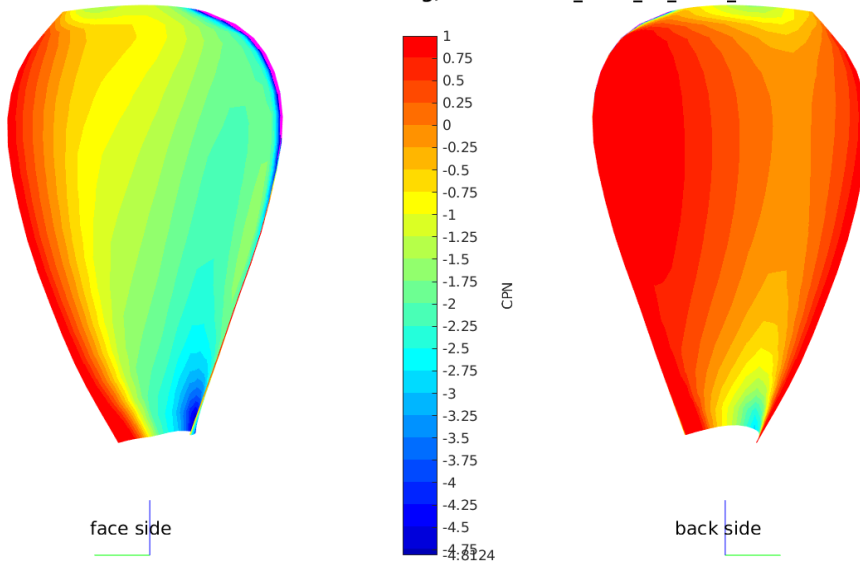
CPN at Theta = 60 deg, HUNDESTED_front_v1_16kn_250



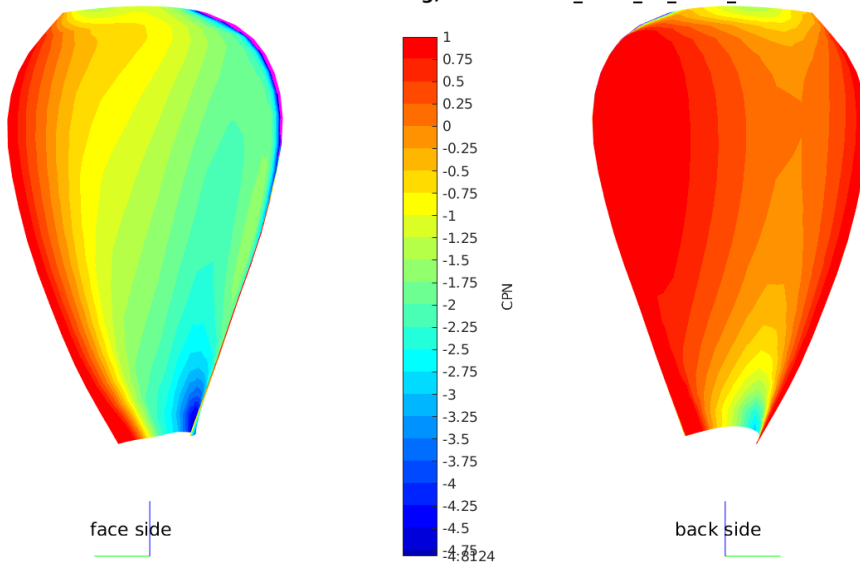
CPN at Theta = 90 deg, HUNDESTED_front_v1_16kn_250



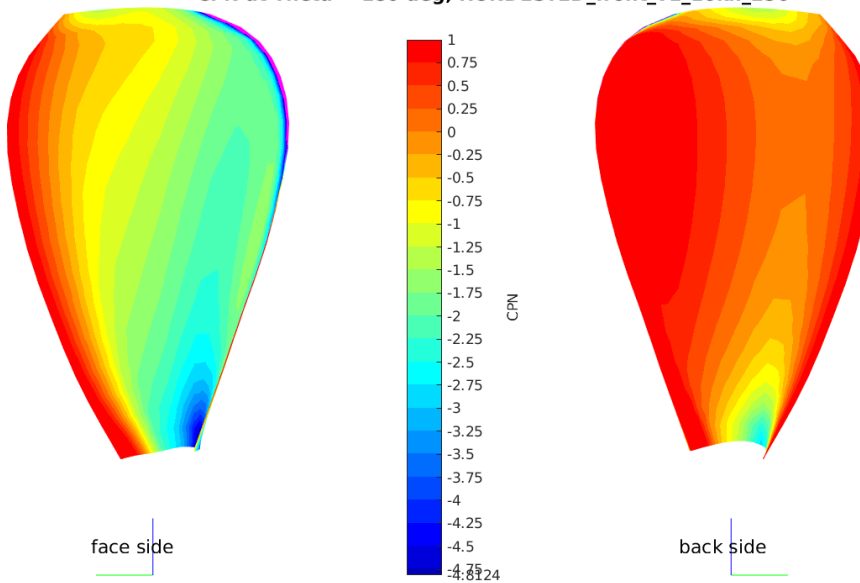
CPN at Theta = 120 deg, HUNDESTED_front_v1_16kn_250



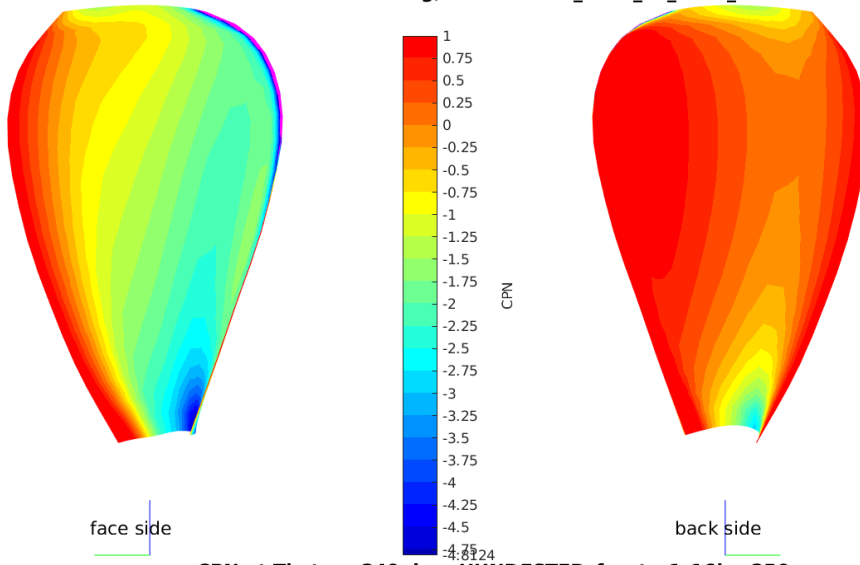
CPN at Theta = 150 deg, HUNDESTED_front_v1_16kn_250



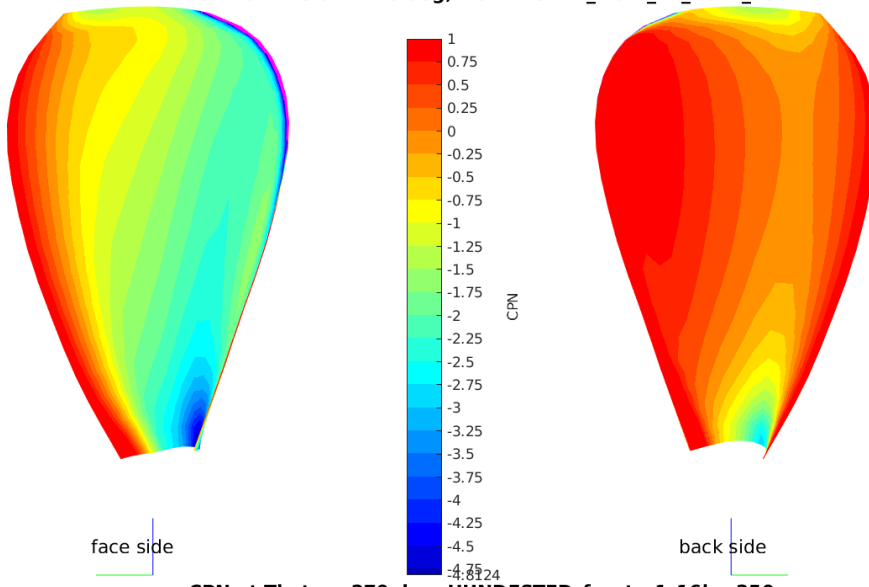
CPN at Theta = 180 deg, HUNDESTED_front_v1_16kn_250



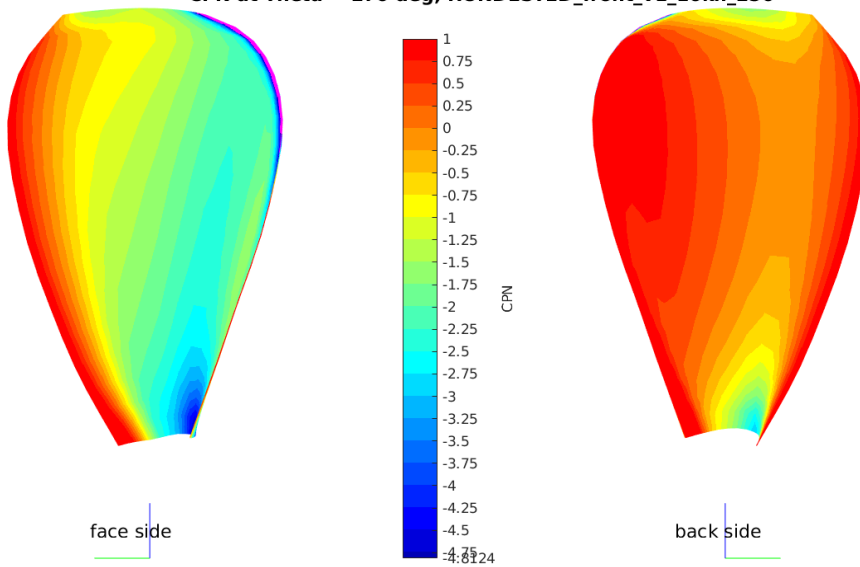
CPN at Theta = 210 deg, HUNDESTED_front_v1_16kn_250



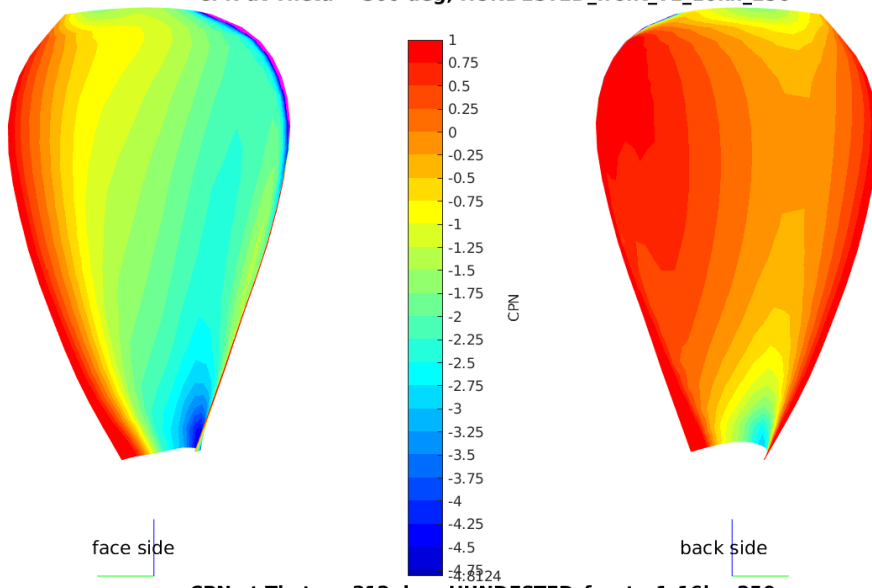
CPN at Theta = 240 deg, HUNDESTED_front_v1_16kn_250



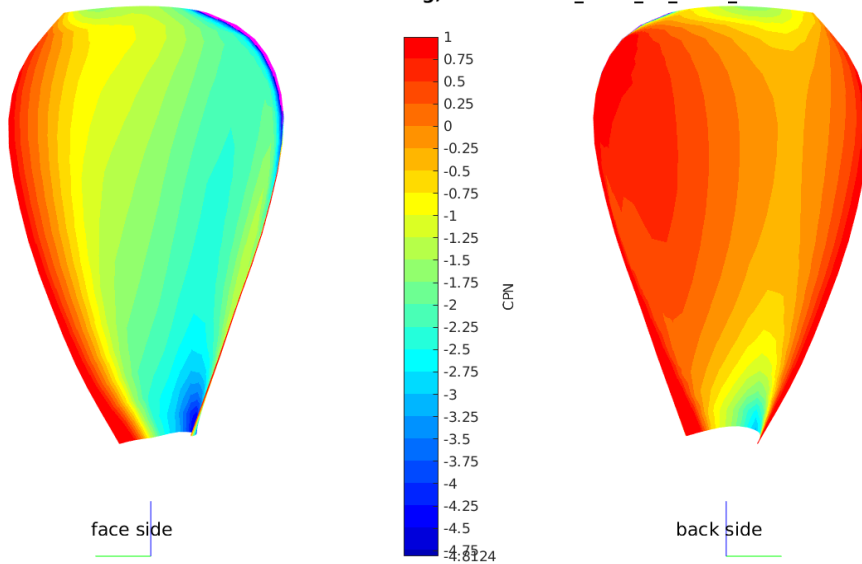
CPN at Theta = 270 deg, HUNDESTED_front_v1_16kn_250



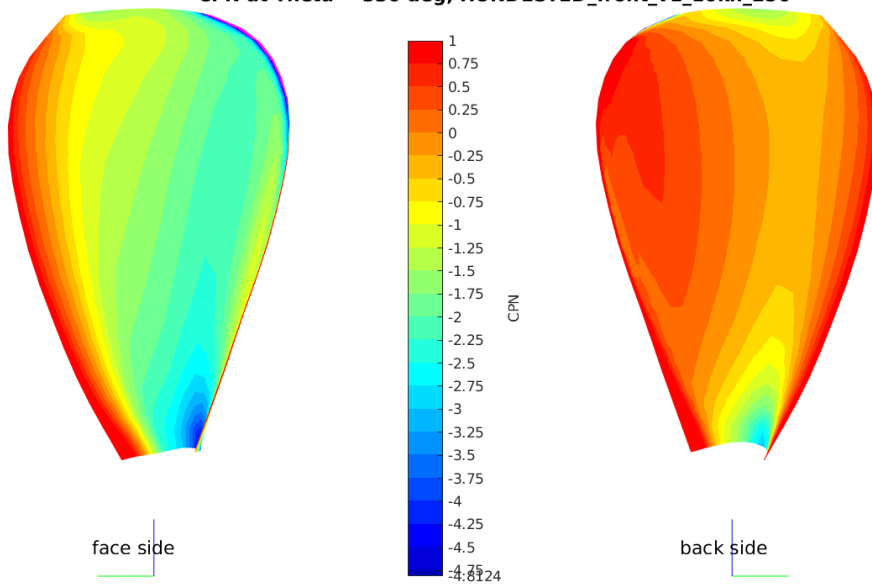
CPN at Theta = 300 deg, HUNDESTED_front_v1_16kn_250



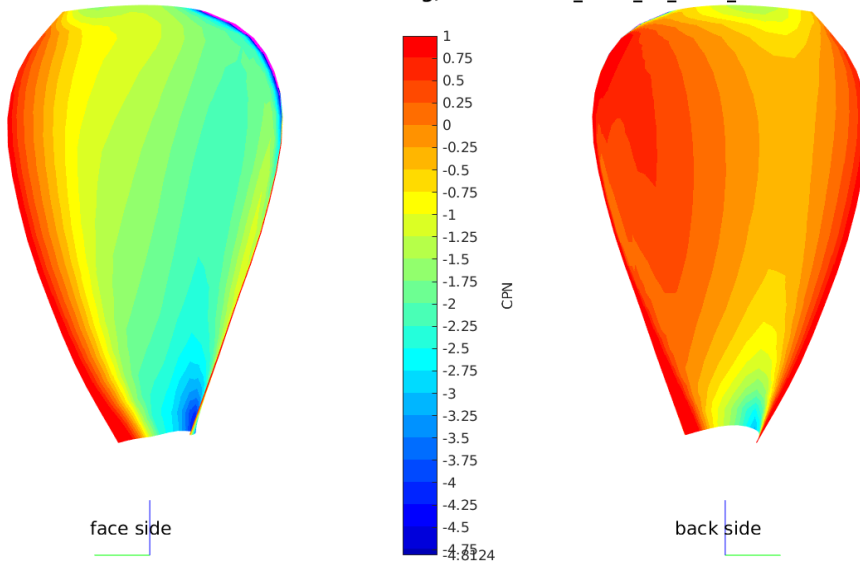
CPN at Theta = 312 deg, HUNDESTED_front_v1_16kn_250



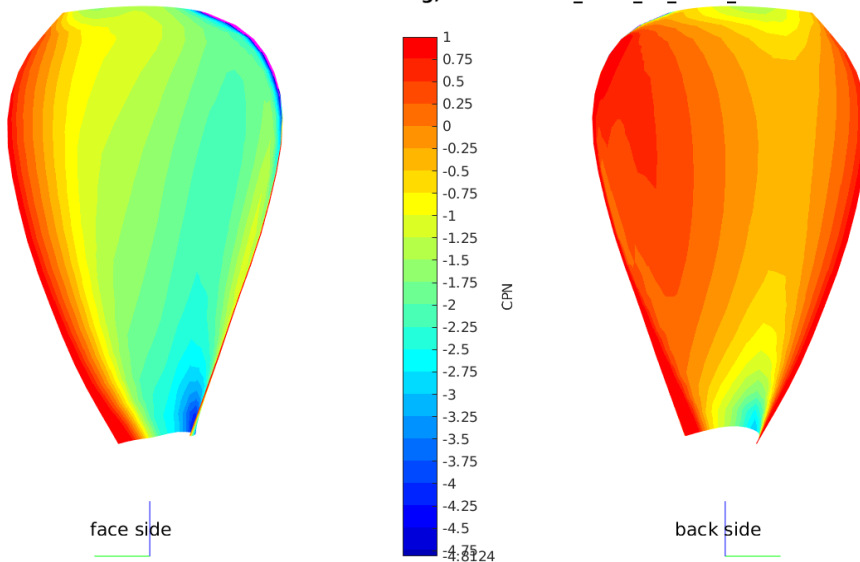
CPN at Theta = 336 deg, HUNDESTED_front_v1_16kn_250



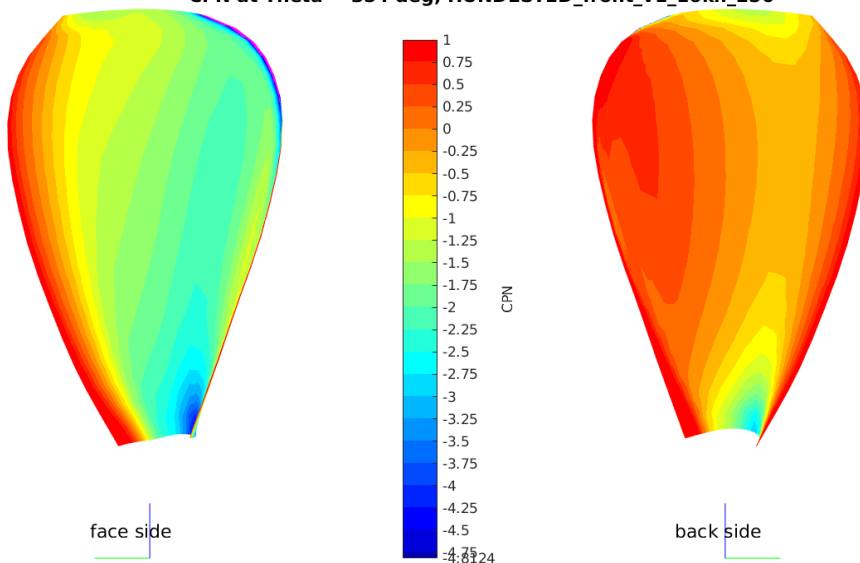
CPN at Theta = 342 deg, HUNDESTED_front_v1_16kn_250



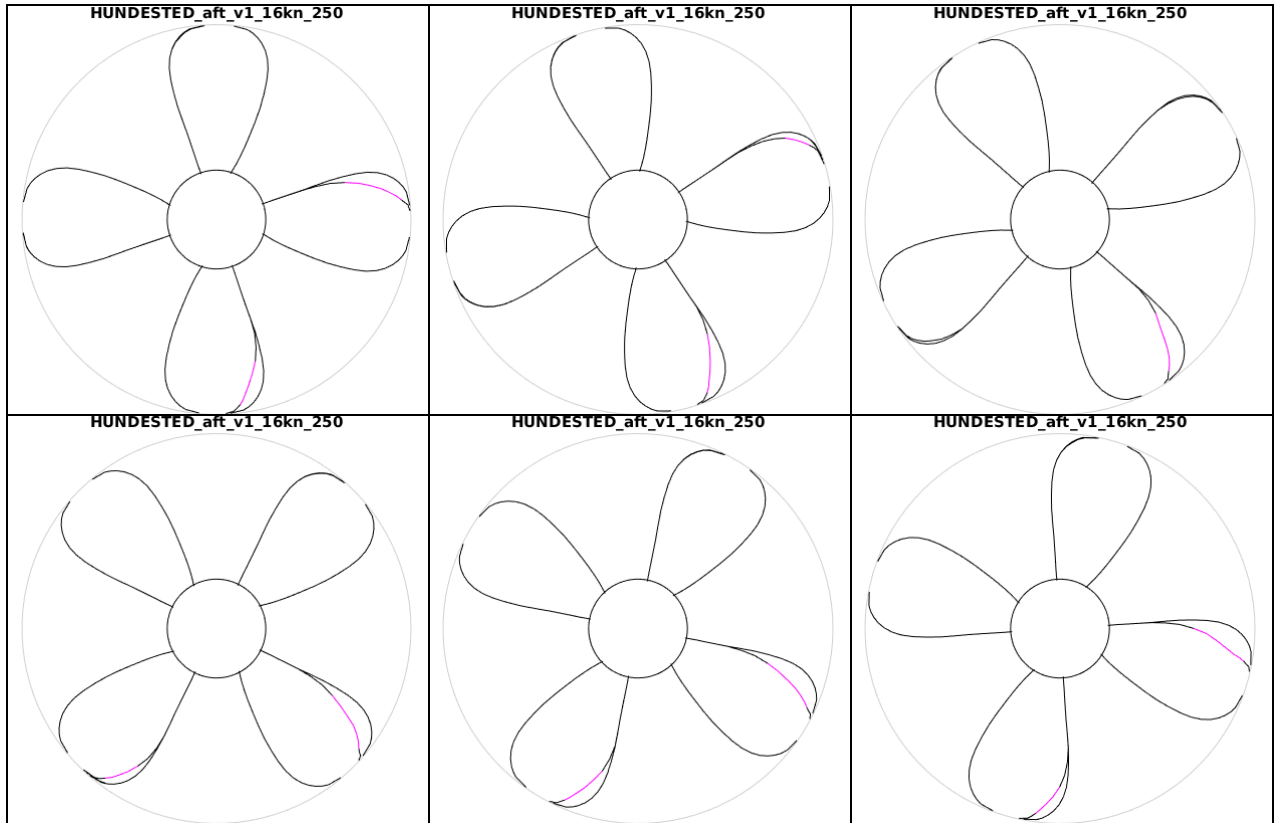
CPN at Theta = 348 deg, HUNDESTED_front_v1_16kn_250



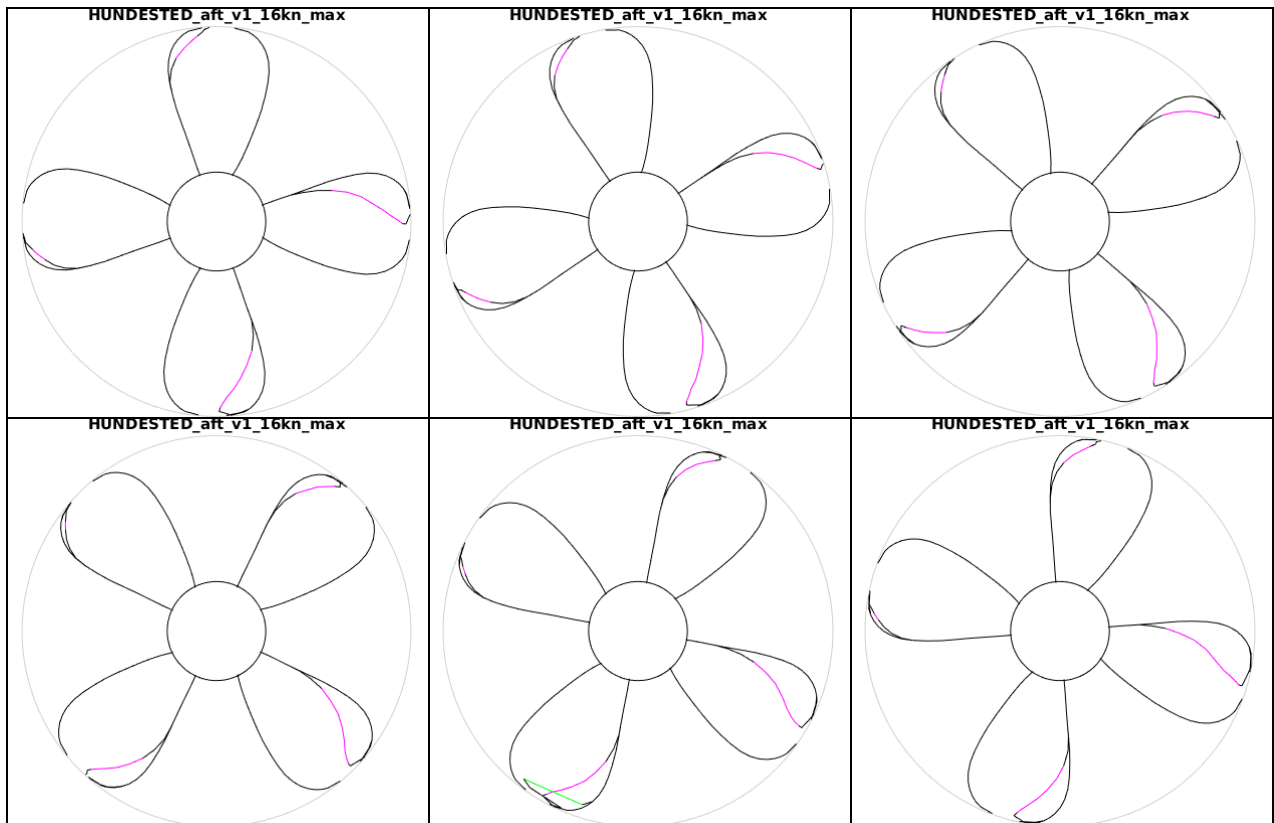
CPN at Theta = 354 deg, HUNDESTED_front_v1_16kn_250



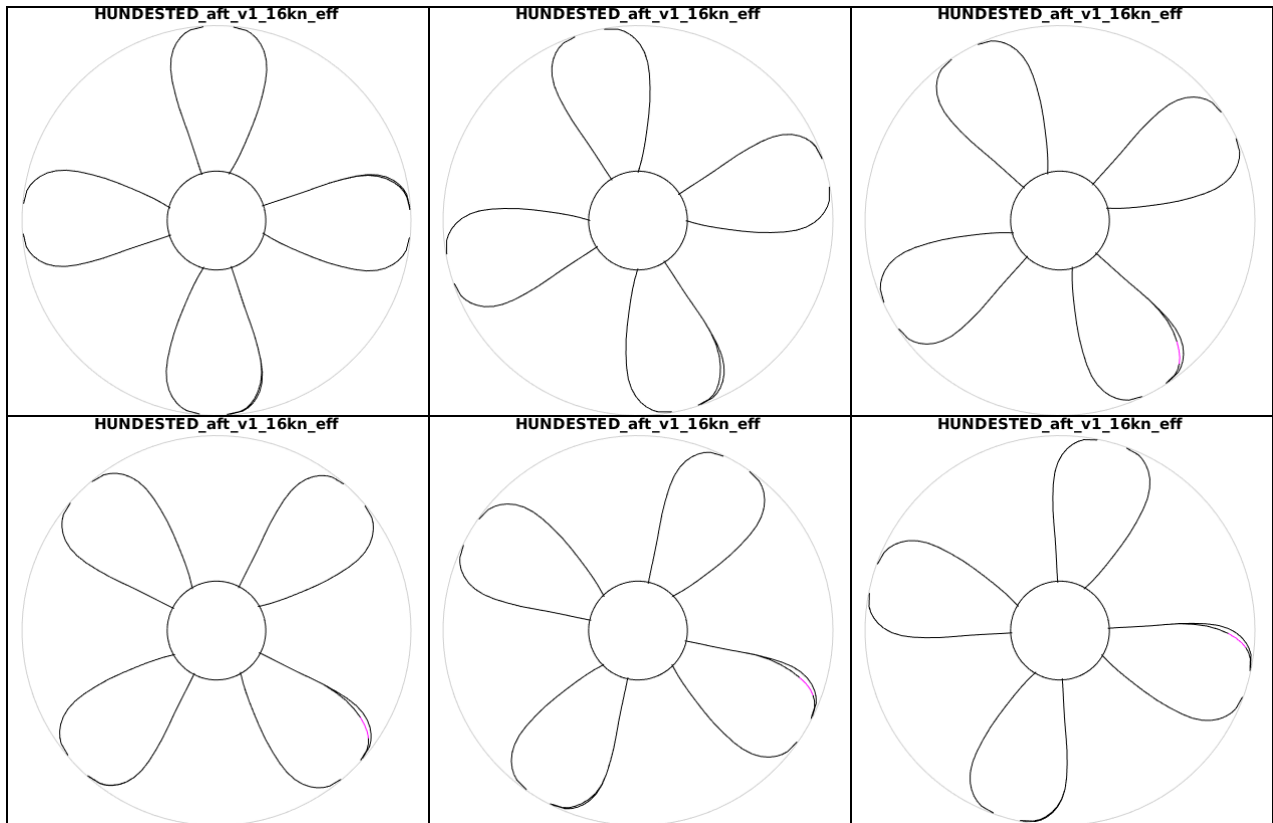
PRESSURE CONTOURS ON THE FRONT PROPELLER AT 16 KNOTS, REGENERATING 250 KW MODE



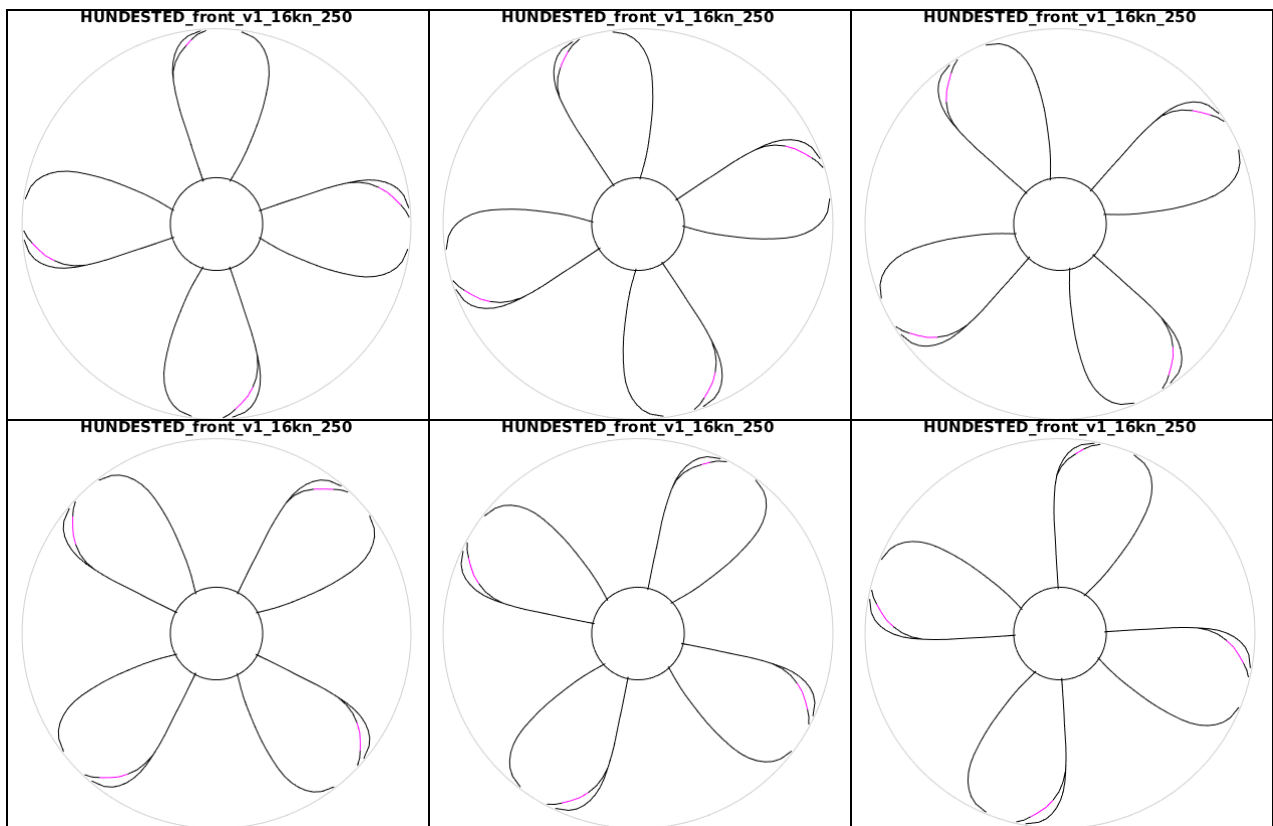
CAVITATING BEHAVIOUR AFT PROPELLER, REGENERATING, 250 KW TOTAL



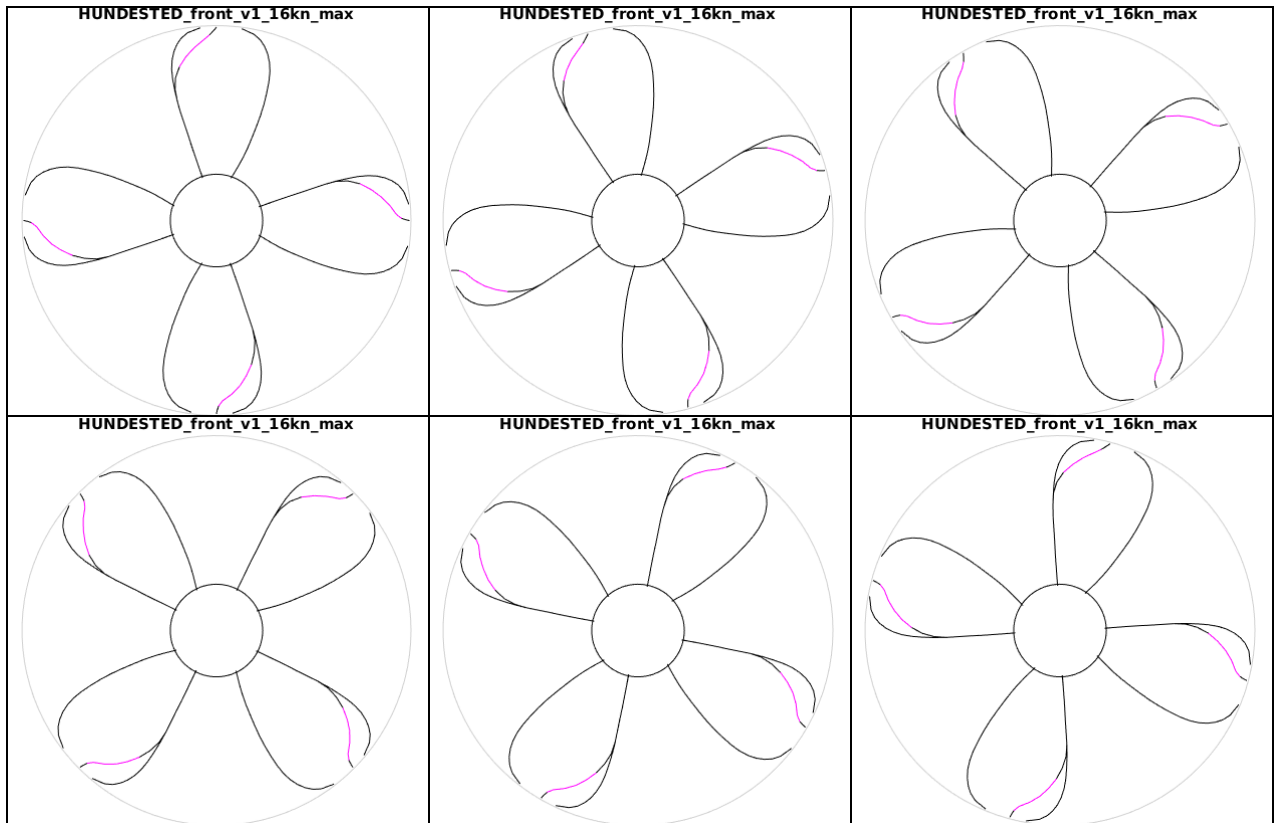
CAVITATING BEHAVIOUR AFT PROPELLER, MAXIMUM REGENERATION



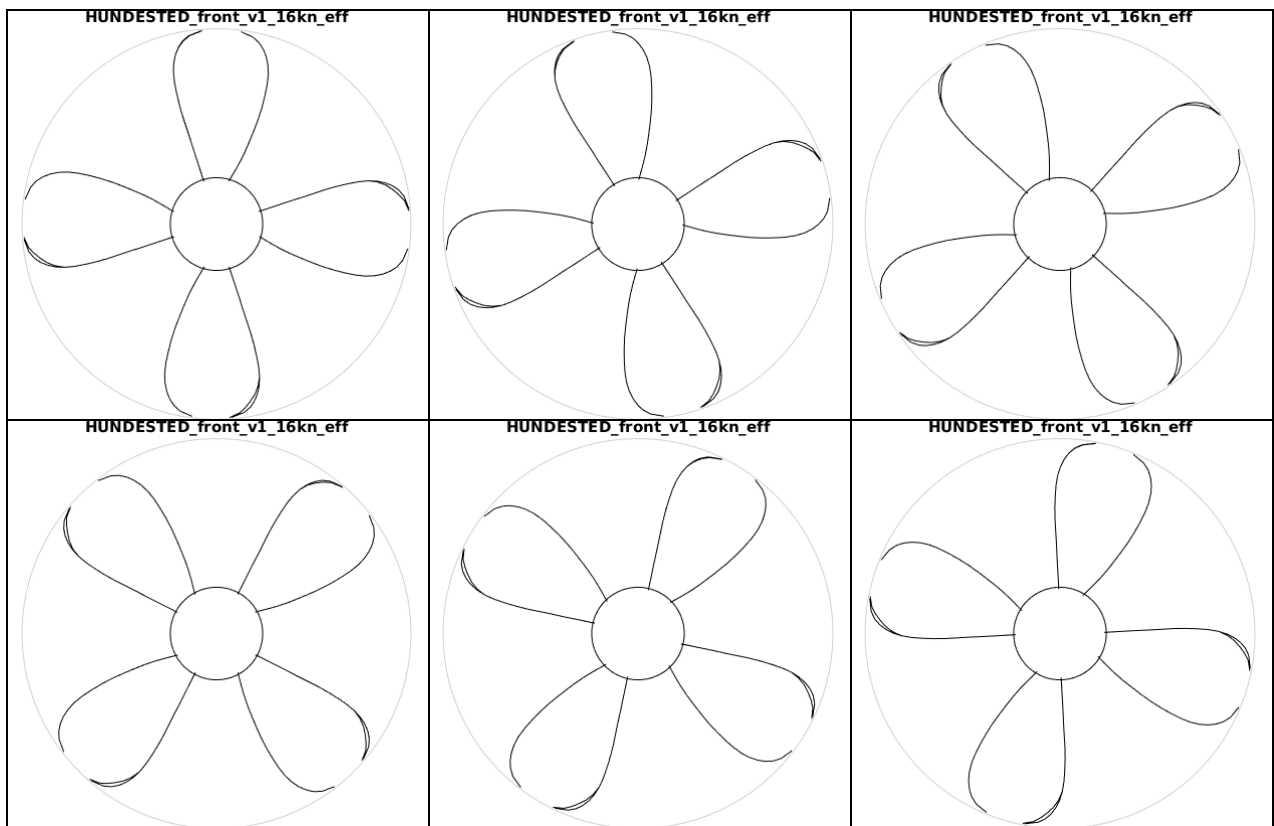
CAVITATING BEHAVIOUR AFT PROPELLER, MOST EFFICIENT REGENERATION



CAVITATING BEHAVIOUR FRONT PROPELLER, REGENERATING, 250 KW TOTAL

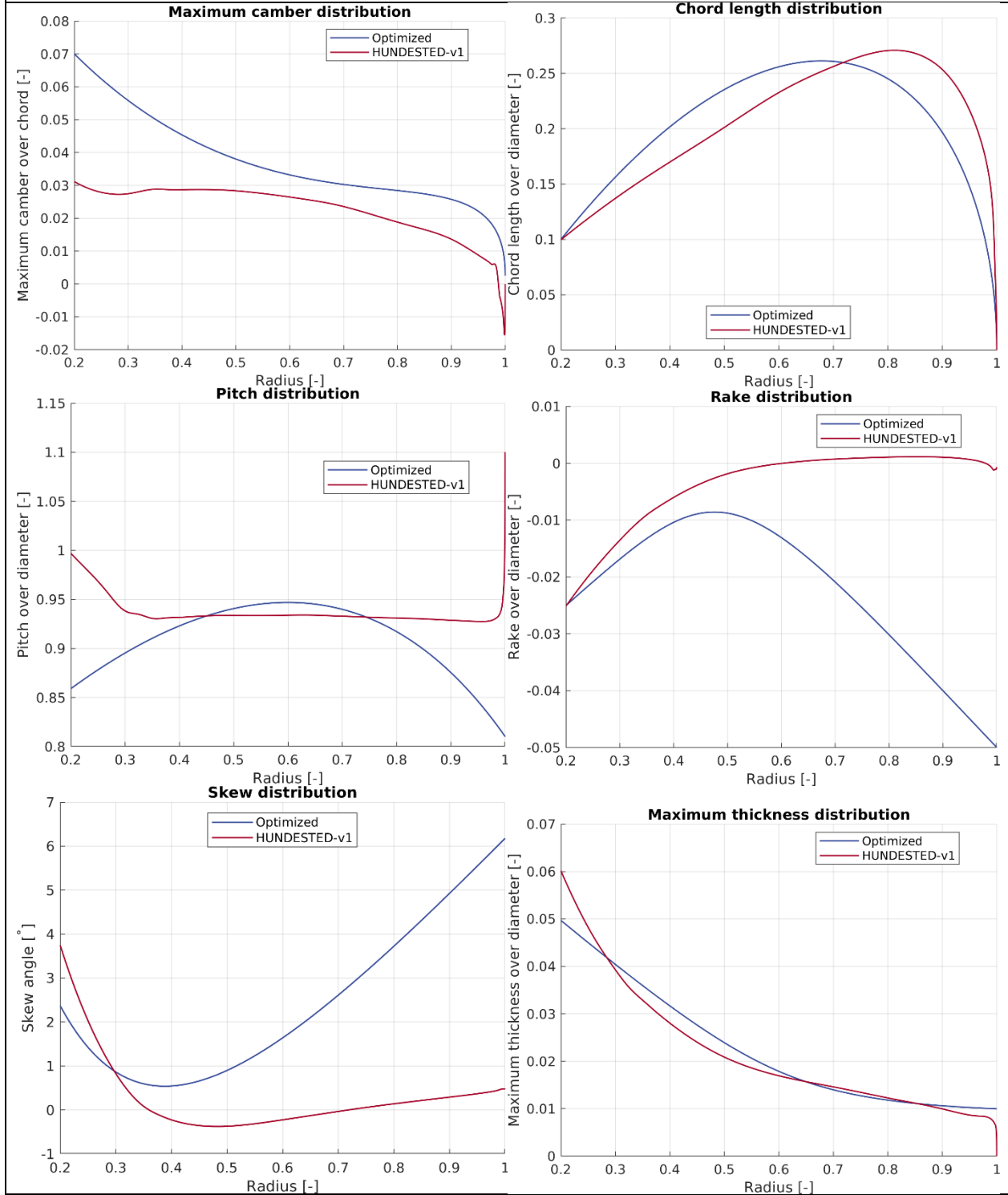


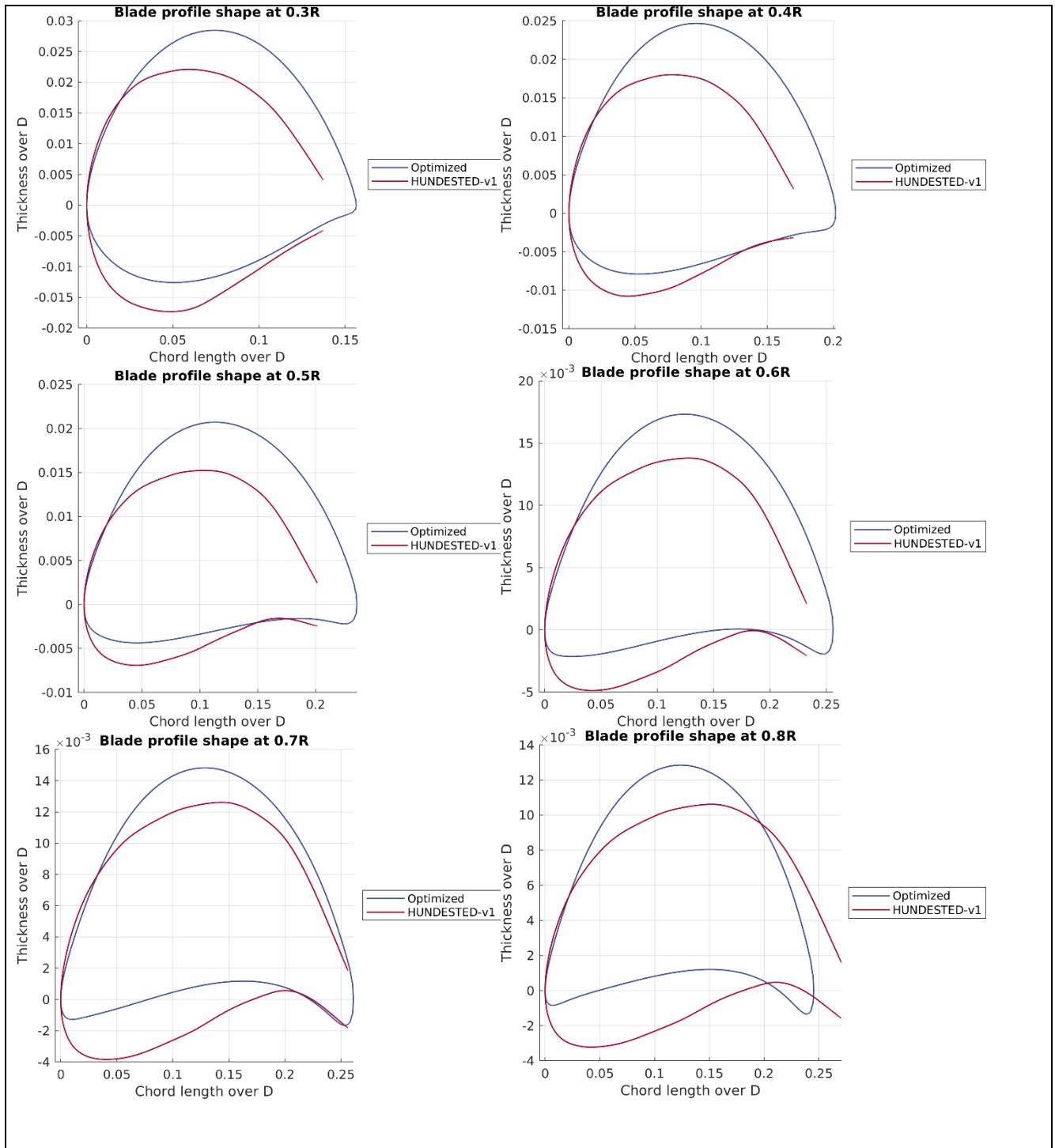
CAVITATING BEHAVIOUR FRONT PROPELLER, MAXIMUM REGENERATION

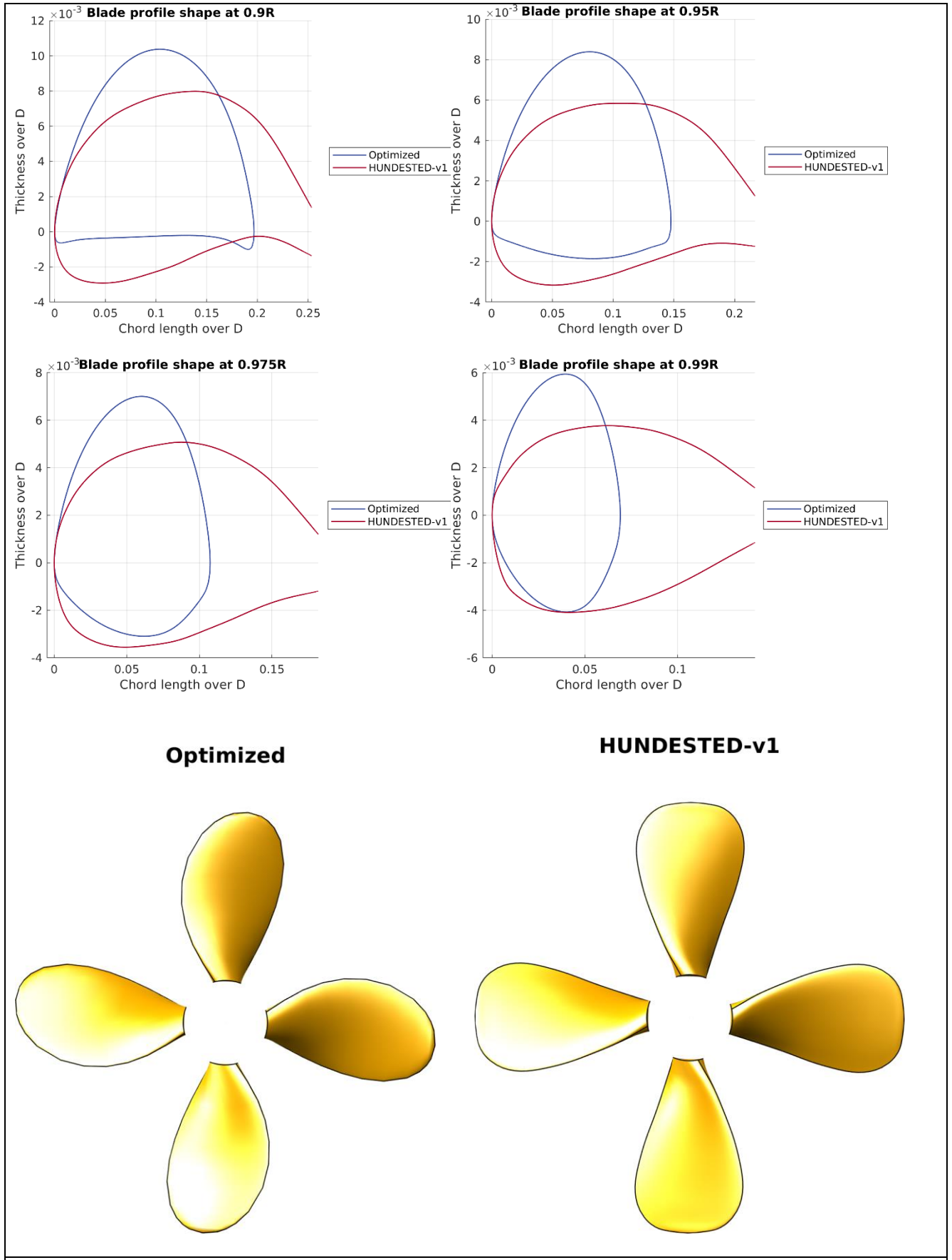


CAVITATING BEHAVIOUR FRONT PROPELLER, MOST EFFICIENT REGENERATION

GEOMETRY COMPARISON OF AFT PROPELLER

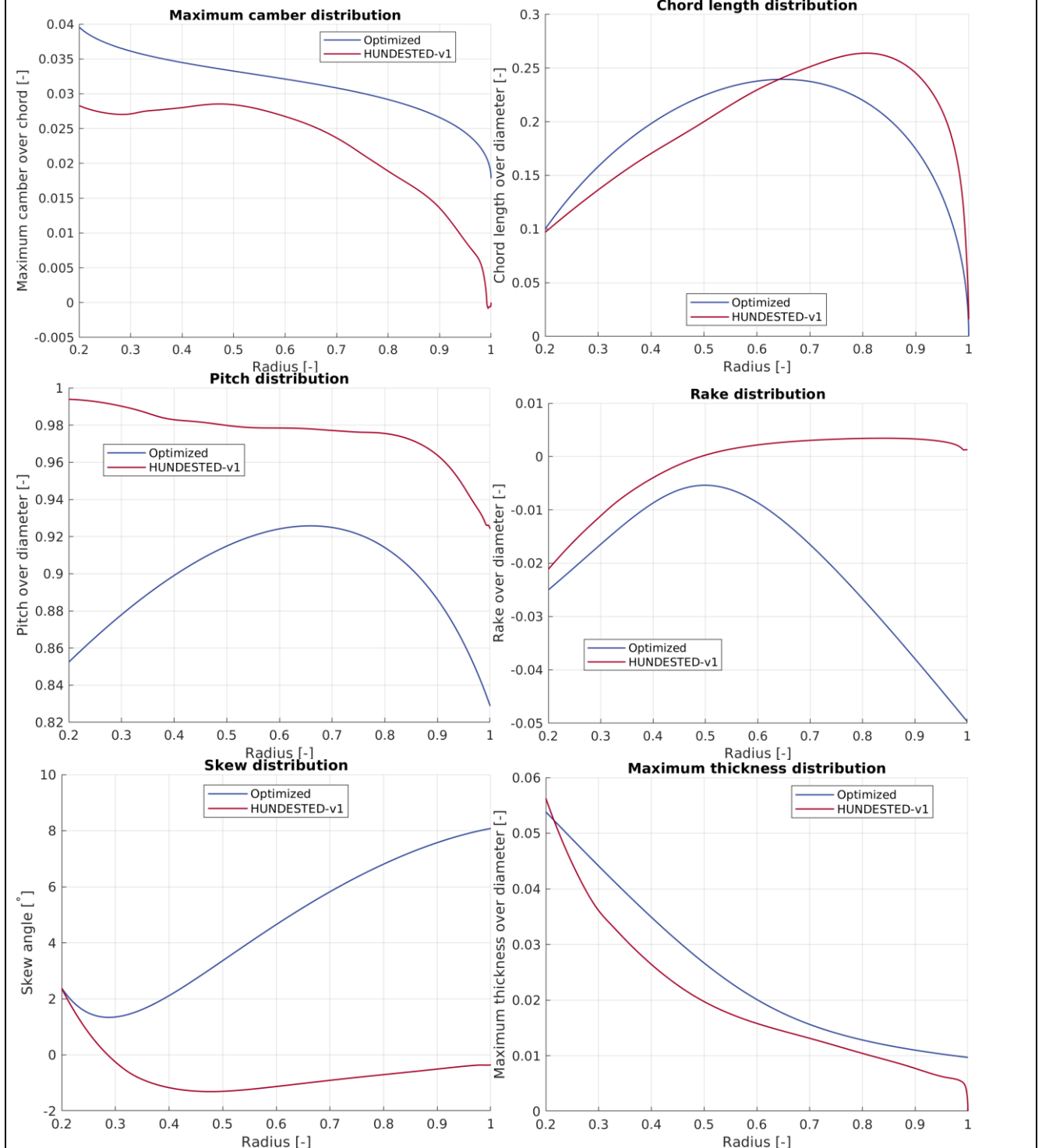


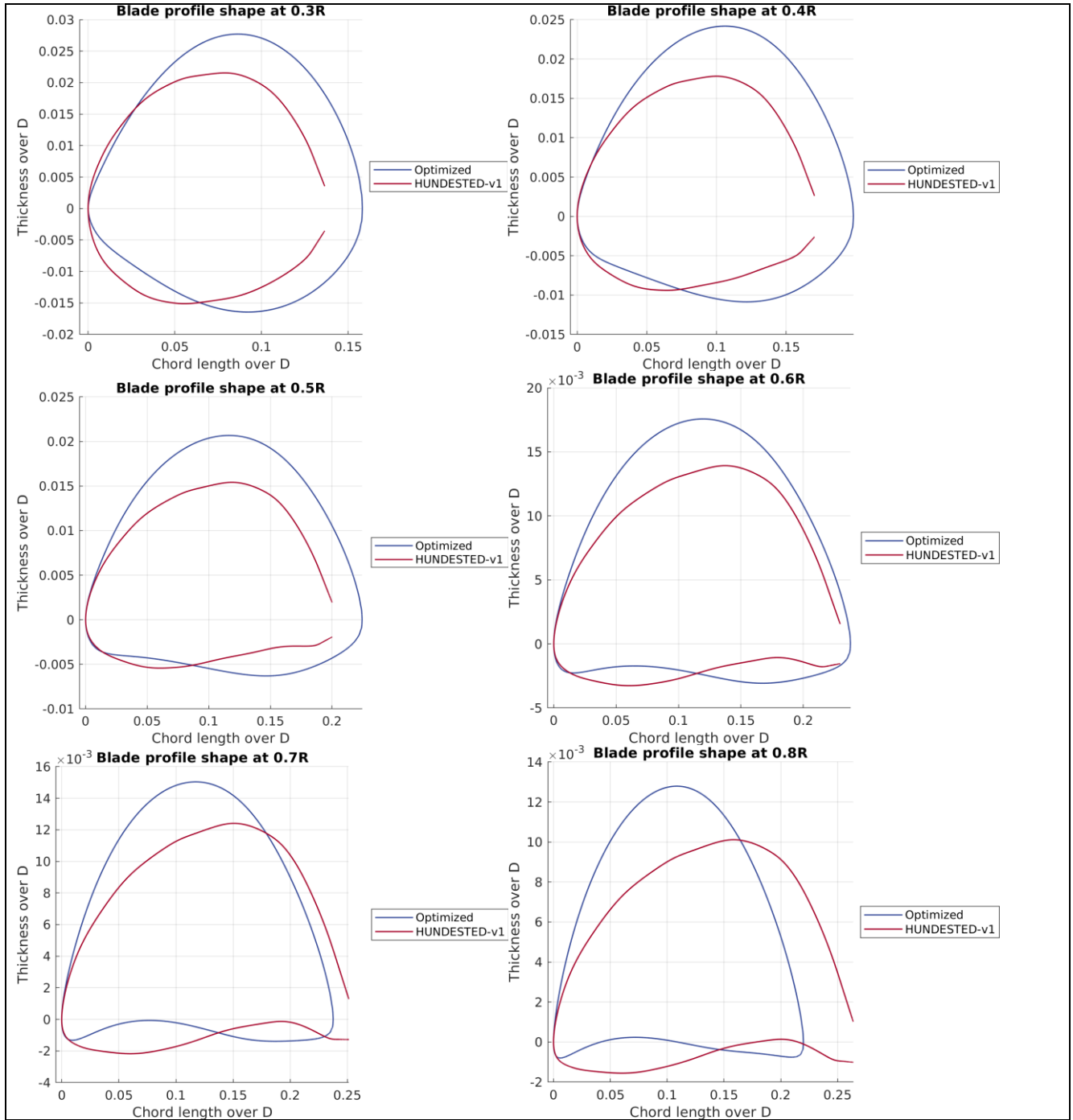


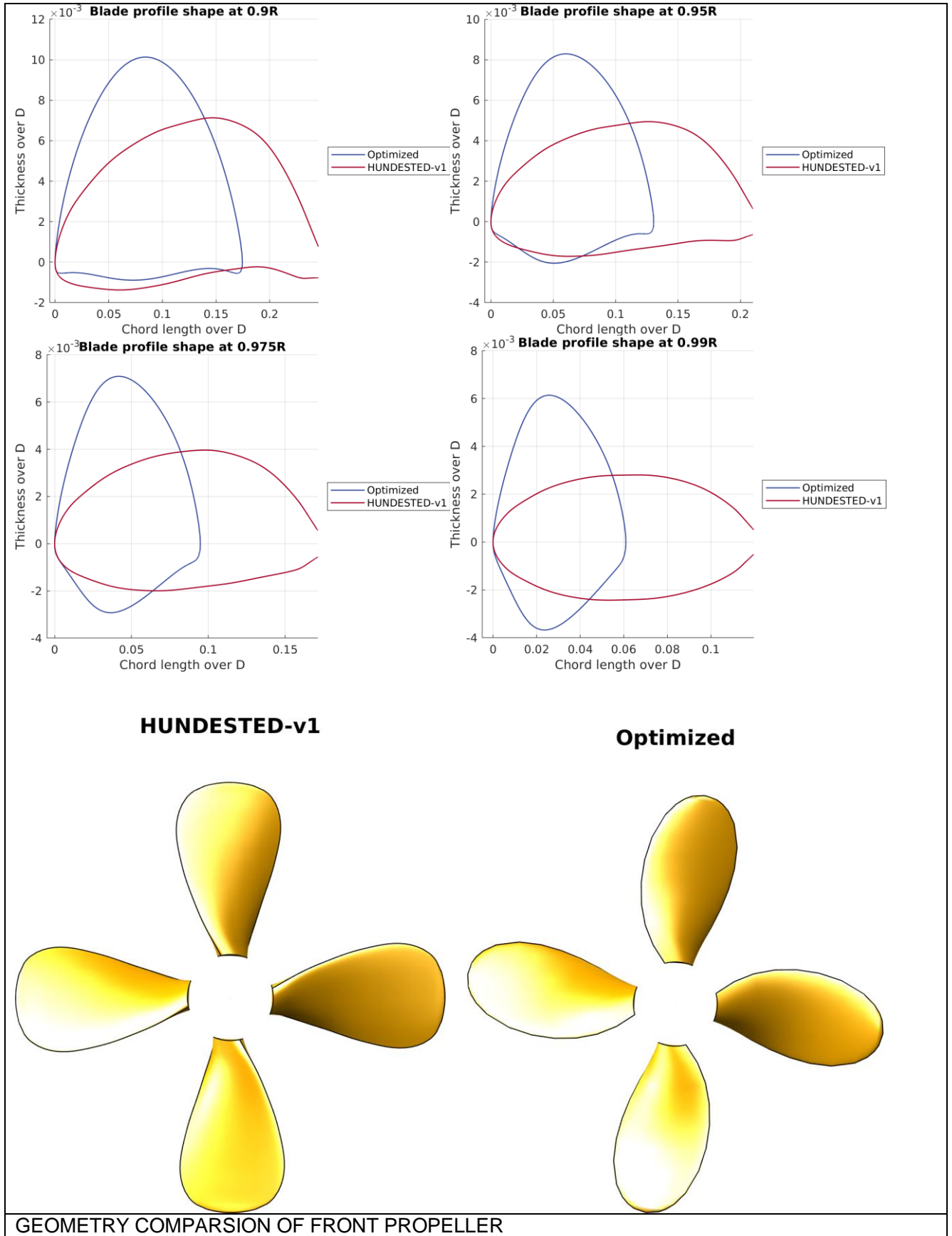


GEOMETRY COMPARISON OF AFT PROPELLER

GEOMETRY COMPARISON OF FRONT PROPELLER







APPENDICES

APPENDIX I

LIST OF SYMBOLS

Symbol	Symbol in computer print	Title
GEOMETRY OF SHIP AND PROPELLER		
A_{BT}		Transverse cross-section area of bulbous bow
A_E		Expanded propeller blade area
A_E/A_O		Expanded propeller blade area ratio
A_M		Midship sectional area below still waterline
A_O		Propeller disc area
A_T		Transom area below still waterline
A_T/A_M		Transom area ratio
A_W		Waterplane area
A_X		Maximum transverse sectional area below still waterline
A_V	AV	Area of portion of ship above waterline projected normally to the direction of relative wind
B		Maximum breadth moulded at or below still waterline
B_M		Maximum breadth moulded at midship
B_{WL}		Maximum breadth moulded at still waterline
c		Chord length of propeller blade section
c/D		Chord length-diameter ratio
C_{REF}		Chord length between reference line and leading edge
C_t		Chord length between maximum thickness point and leading edge
C_B		Block coefficient
C_M		Midship section coefficient
C_P		Longitudinal prismatic coefficient
C_{WP}		Waterplane area coefficient
d		Hub diameter
d/D		Hub-diameter ratio
D		Propeller diameter
FB		Position of centre of buoyancy aft of FP
f		Camber of propeller blade section
h_o		Submergence of propeller shaft axis measured from still water-plane
h_B		Height of centroid of A_{BT} above keel
i_E		Half angle of entrance
LOA		Length overall
LOS		Length overall submerged
LPP		Length between perpendiculars
L_{WL}		Length on still waterline
LCB		Longitudinal position of centre of buoyancy

Symbol	Symbol in computer print	Title
P		Propeller pitch
P/D		Pitch-diameter ratio
r		Radius of propeller blade section
R		Radius of propeller
S, S_{HULL}		Projected wetted surface bare hull
S_{APP}		Wetted surface area appendages
S_1, S_{TOT}		Total wetted surface area
t		Maximum thickness of propeller blade section
t/c		Maximum thickness-chord length ratio
T		Mean draught moulded
T_A		Moulded draught at aft perpendicular
T_F		Moulded draught at forward perpendicular
dTA	dTA	Dynamic draught change at aft perpendicular
dTF	dTF	Dynamic draught change at forward perpendicular
Z		Number of blades
λ		Scale ratio
Φ		Pitch angle of propeller section
∇	DISV	Displacement volume moulded
-m	-M	Subscript for model
-s	-S	Subscript for ship

Symbol	Symbol in computer print	Title
RESISTANCE, OPEN WATER AND PROPULSION		
AC_{Res}		Ship resistance admiralty coefficient
AC_{Prop}		Ship propulsive power admiralty coefficient
C_A	CA	Total Incremental resistance coefficient for model-ship correlation
C_{A0}	CA_0	C_A basic
C_{Arough}	Crough	C_A roughness
C_{Aas}	Caas	C_A air resistance
C_{Abk}	Cbk	C_A bilge keels
$C_{Aballast}$	Cballast	C_A small draught
C_{AD}	CAD	Admiralty coefficient for propulsion
C_D		Drag coefficient
$C_{D\bar{V}}$		Power-displacement coefficient
C_E	CE	Admiralty coefficient for resistance
C_F	CF	Specific frictional resistance coefficient
ΔC_F		Roughness allowance coefficient
C_L	CL	Lift coefficient
C_P		Power loading coefficient
C_Q	CQ	Propeller torque coefficient
C_{QBL}	CQBL	Propeller blade spindle torque coefficient
C_R	CRES	Specific residual resistance coefficient
C_T	CT	Specific total resistance coefficient
C_{Th}		Thrust loading coefficient
C_{TP}	CTP	Propeller thrust coefficient
C_{TD}	CTD	Duct thrust coefficient
C_V	CV	Specific total viscous resistance coefficient
C_W	CW	Specific wavemaking resistance coefficient
C_X	CX	Specific air resistance coefficient
Ⓒ	CIRCC	R.E. Froude's resistance coefficient
F	F	Towing force in propulsion test
F_D	FD	Viscous scale effect on resistance
F_n	FN	Froude number
F_P	PULL	Pull of ship
F_{PO}	PULL	Pull of ship in bollard condition
Ⓕ	CIRCF	R.E. Froude's frictional resistance coefficient
g		Acceleration due to gravity
J	J	Advance coefficient
J_V	JV	Apparent advance coefficient
1+k	1+K	Three-dimensional form factor on flat plate friction

Symbol	Symbol in computer print	Title
K_p		Equivalent sandroughness of propeller blade surface
K_s		Roughness height of hull surface
K_{SiP}	K_{SiP}	Dependency of propulsive efficiency with resistance increase
K_{SiN}	K_{SiN}	Dependency of propeller shaft speed with power increase
K_{SiV}	K_{SiV}	Dependency of propeller shaft speed with speed change
K_Q	K_Q	Torque coefficient
K_T	K_T	Thrust coefficient
K_{TD}	K_{T-D}	Duct thrust coefficient
K_{TP}	K_{T-P}	Propeller thrust coefficient
K_{TS}	K_{T-S}	Stator thrust coefficient
\textcircled{K}	CIRCK	R.E. Froude's speed-displacement coefficient
MCR		Maximum continuous rating
SMCR		Specified maximum continuous rating
NCR		Normal continuous rating
n	N	Rate of revolutions
P_B		Brake power
P_D	PD	Power delivered to the propeller(s)
P_E	PE	Effective power
P_I		Indicated power
P_S	PS	Shaft power
Q	Q	Torque
R	R	Resistance in general
R_n	RN	Reynolds number
R_A		Model-ship correlation resistance
R_F	RF	Frictional resistance
R_V	RV	Total viscous resistance
R_W	RW	Wavemaking resistance
s_A		Apparent slip ratio
s_R		Real slip ratio
t	$THDF$	Thrust deduction fraction
t^*		Thrust deduction fraction from load variation test
T	TH	Thrust
T_D	$TH-D$	Duct thrust
T_P	$TH-P$	Propeller thrust
T_S	$TH-S$	Stator thrust
T_U	$TH-U$	Azimuthing thruster unit thrust
t_v	TV	Running trim

Symbol	Symbol in computer print	Title
V	V	Speed of ship or ship model
V_r	V_r	Radial flow velocity component in the direction of the z-axis of the Pitot tube, and is positive if directed down for strut orientation tests or outward in a wake survey
V_t	V_t	Tangential flow velocity component in the direction of the y-axis of the Pitot tube, and is positive if directed to port for strut orientation tests or in clockwise direction in a wake survey
V_x	V_x	Longitudinal flow velocity component in the direction of the x-axis of the Pitot tube, and is positive if directed aft
V_A	V_A	Advance speed of propeller relative to water flow
w_T	WT	Effective wake fraction on thrust identity
w_Q	WQ	Effective wake fraction on torque identity
β		Advance angle of propeller blade section
β_h		Angle of the flow in the x-y plane of the Pitot tube co-ordinate system, and is positive if the flow is directed to port for strut orientation tests
β_v		Angle of the flow in the x-z plane of the Pitot tube co-ordinate system, and is positive if the flow is directed to the hub for strut orientation tests
η_B		Propeller efficiency behind ship
η_D	ETA-D	Propulsive efficiency
η_ε	ETA- ε	Merit coefficient
η_G		Gearing efficiency
η_H	ETA-H	Hull efficiency
η_M		Mechanical efficiency
η_o	ETA-O	Propeller efficiency in open water
η_R	ETA-R	Relative-rotative efficiency on thrust or torque identity
η_S		Shafting efficiency

Symbol	Symbol in computer print	Title
ν		Coefficient of kinematic viscosity
ρ		Mass density
τ		Ratio propeller thrust and total thrust of ducted propeller system
τ_w		Wall shear stress

m	M	Subscript for model
o	O	Subscript for open water
s	S	Subscript for ship

Symbol	Symbol in computer print	Title
CAVITATION, HULL PRESSURES, SHAFT FORCES AND NOISE		
$a_{x0.8}$		Longitudinal clearance from propeller clearance curve to stern frame at a height of 0.8 R above propeller shaft axis
a_z		Vertical clearance of propeller tip in top position to the hull
A_i		Single amplitude of i-th harmonic component of periodic pressure signal
B_s		Waterline beam at station at most forward point of screw aperture
c		Speed of sound
C		Empirical constant
C_p		Pressure coefficient
D_M		Depth moulded
$E_{H,V}$		Thrust eccentricity
f		Frequency in general
f_1		Blade passage frequency
$f(\Theta)$		Function of mean periodic pressure signal
$F_{H,V}$		Propeller induced dynamic force acting on the shaft
$F_{x,y,z}$	FX,FY,FZ	Propeller induced dynamic force acting on the hull
$F_{z\ eq}$		Equivalent vertical excitation force
g		Acceleration due to gravity
h		Immersion in general
J	J	Advance coefficient
$M_{H,V}$		Propeller induced dynamic moment acting on the shaft
$M_{x,y,z}$	MX,MY,MZ	Propeller induced dynamic moment acting on the hull
n	N	Rate of revolutions
p		Sound pressure
p_o		Ambient pressure
p_v		Vapour pressure of water
r		Distance to cavitating propeller
R_n	RN	Reynolds number
V	V	Speed of ship or model
V_A	VA	Advance speed of propeller relative to water flow
α_i		Phase angle of i-th component in harmonic function
Θ		Angular propeller blade position
ρ		Mass density of water

Symbol	Symbol in computer print	Title
σ_f		Non-dimensional parameter for frequency
σ_n		Cavitation number related to rotation rate
σ_p		Non-dimensional parameter for sound pressure
σ_v		Cavitation number related to flow velocity

-H	-H	Subscript for horizontal
-m	-M	Subscript for model
-s	-S	Subscript for ship
-v	-V	Subscript for vertical

APPENDIX II

PROCEDURES OF MODEL TESTS

Procedure of open water tests

Single propeller

The propeller model is fitted on a horizontal driving shaft, and is moved through the water at an immersion of the shaft axis of at least the diameter of the propeller. The thrust and torque are measured in the hub of the propeller model.

In the test the loading of the propeller is normally varied by varying the speed of advance and keeping the rate of revolutions constant. When limitations in the measuring range (for J-values close to zero) and/or carriage speed (for high J-values) are reached, the rate of revolutions is varied too.

The measured thrust values are corrected for the resistance of the hub and streamlined cap experienced in the test. This correction is determined experimentally in a test with the hub only.

The torque and (corrected) thrust are expressed in non-dimensional coefficients K_{T_0} and K_{Q_0} . Together with the open water efficiency η_0 they are presented as a function of the advance coefficient J.

The non-dimensional thrust and torque coefficients are defined as:

$$K_{T_0} = T/(\rho n^2 D^4) \quad \text{and} \quad K_{Q_0} = Q/(\rho n^2 D^5)$$

The open water efficiency and advance coefficient are defined as:

$$\eta_0 = J K_{T_0} / (2\pi K_{Q_0}) \quad \text{and} \quad J = V/(nD)$$

The open water characteristics are not corrected for scale effects, unless stated otherwise.

Propeller with nozzle

In the case a nozzle is used in the propulsion system the nozzle thrust can be measured as well. In this case the non-dimensional nozzle thrust is defined as:

$$K_{TD_0} = T_D/(\rho n^2 D^4)$$

in which the rotation rate n and diameter D are those from the propeller.

Complex propulsor

In the case of an azimuthing thruster or pod unit the thrust of the complete unit can be measured as well. Also in this case the non-dimensional unit thrust is defined as:

$$K_{TU_0} = T_U/(\rho n^2 D^4)$$

In this case the propeller cap is not replaced by a special streamlined cap as for open or ducted propellers and no correction is applied to the propeller thrust.

On the measured results of pod or thruster open water tests, scale effect corrections are made which are explained in a separate appendix to this report.

Procedure of propulsion tests

In the model propulsion tests the same turbulence tripping on the hull and appendages is applied as in the resistance tests. The propulsion tests are carried out in two parts:

- a) The first part consists of a load-variation test at one or sometimes more than one constant speed.
- b) The second part consists of a speed-variation test at constant apparent advance coefficient J_v (= constant propeller load) or at the self-propulsion point of ship ($F = F_D$).

In the propulsion test the propeller thrust T_m , the propeller torque Q_m and the longitudinal towing force F acting on the model is recorded for each tested combination of model speed V_m and propeller rotation rate n_m . Thrust and torque are measured inside the propeller hub.

During the propulsion test the ship model is free to heave and pitch.

The results of the propulsion tests are analysed in the following way.

The required thrust at the self-propulsion point of ship is determined from:

$$T_s = \left(T_m + (F_D - F) \frac{\partial T_m}{\partial F} \right) \lambda^3 \frac{\rho_s}{\rho_m}$$

in which:

T_m	=	measured propeller thrust
F	=	measured longitudinal model towing force
F_D	=	scale effect correction on viscous resistance

The quantity $\partial T_m / \partial F$ is determined from the load-variation test.

In a similar manner, by interpolation in the measured data using the results of the load-variation test, the required torque and propeller rotation rate at self-propulsion point of ship are determined.

In the extrapolation to full-scale values scale effects are considered:

- On the resistance (F_D).
- On the propulsor entrance velocity (wake).
- On the propeller blade friction.

Procedure of cavitation observation tests

The test conditions for cavitation tests are chosen such that the average propeller thrust loading (expressed by K_T and J-identity) is equal on model and full scale.

In addition the pressure is lowered to such a level that model and full-size cavitation numbers are equal at corresponding points in the propeller disc.

For an arbitrary point at an immersion h_m the propeller cavitation number is:

$$\sigma_{nm} = \frac{p_{om} - p_{vm} + \rho_m g h_m}{0.5 \rho_m n_m^2 D_m^2}$$

in which p_{om} is the surface pressure on model scale and p_{vm} is the vapour pressure of the water. For the ship, which is geometrically similar at a length scale λ , the cavitation number is:

$$\sigma_{ns} = \frac{p_{os} - p_{vs} + \rho_s g \lambda h_m}{0.5 \rho_s n_s^2 \lambda^2 D_m^2}$$

The cavitation numbers for model and ship are equal, provided:

$$p_{om} - p_{vm} = \frac{(p_{os} - p_{vs})(\rho_m n_m^2)}{(\rho_s \lambda^2 n_s^2) + \rho_m g h_m (n_m^2 / (\lambda n_s^2) - 1)}$$

This condition is fulfilled for all values of h_m if $n_m = n_s \lambda^{0.5}$ and $p_{om} - p_{vm} = (\rho_m / \rho_s)(p_{os} - p_{vs}) / \lambda$ (Froude scaling for propeller revolutions and pressure). Substitution of $\rho_s / \rho_m = 1.025$ and $p_{os} - p_{vs} = 99.05$ kPa gives:

$$p_{om} - p_{vm} = 96.64 / \lambda \quad [\text{kPa}]$$

This, in fact, can only be realised in a depressurised towing tank or a tunnel with free surface. For a cavitation tunnel without a free surface a rate of rotation for model scale is chosen within practical limits related to the tunnel capacity, the particular test set-up and the ranges of static pressure to be adjusted. Requiring equal cavitation numbers on model and full scale then leads to the pressure to be adjusted in the tunnel. Obviously, at only one horizontal level the condition of equal cavitation numbers can be fulfilled.

Apart from equal cavitation numbers in the model test facility and on the full scale the propeller loadings have to correspond.

As a measure for the propeller load the advance coefficient of the full-scale propeller is used with:

$$J = V_A / (nD)$$

With Froude scaling of the rotation rate of the propeller and the pressure in a depressurised towing tank the model speed then becomes:

$$V_m = (V_s / \lambda^{0.5})(V_A / V)_s / (V_A / V)_m$$

in which $(V_A / V)_s / (V_A / V)_m$ is the scale effect on the entrance velocity of the propeller.

In the cavitation tunnel it is common practice to acquire the correct propeller load by adjusting the water velocity to arrive at K_T -identity. At K_T -identity the J-identity is almost fulfilled. It should be noticed that the dynamometer is adjusted for the pressure difference inside and outside the cavitation tunnel.

In addition to the adjustment of the correct propeller load and cavitation numbers additional measures are taken to minimise the scale effect on the inception of propeller cavitation. To compensate for the difference in number of cavitation nuclei on model scale (in general only necessary in the Depressurised Wave Basin), a cloud of tiny gas bubbles is generated upstream of the propeller by means of electrolysis of the tank water. To this purpose a cathode and an anode are glued to the ship model in the form of metal strips of 0.5 mm thickness and 3.5 mm wide. In addition to electrolysis, leading edge roughness is used in the test for tripping the flow over the propeller blades to turbulence, because in laminar flow cavitation inception is subject to severe scale effects. The roughness consists of carborundum grains glued in a distributed form in a strip at the leading edges of the blades. Not only the effect on transition from a laminar to a turbulent boundary layer is considered important, also the generation of additional small nuclei at the roughness elements in the direct vicinity of the blade surface is regarded an important factor in suppressing the scale effects on cavitation inception.

The Reynolds number and number of nuclei on model scale determine the required grain size. In the Depressurised Wave Basin mostly a grain size of 60 μm is used. In the cavitation tunnels sandblasting of the leading edges is sometimes applied to achieve the required roughness, and due to testing at higher Reynolds numbers smaller roughness elements are needed in general.

In addition to the observation of the propeller cavitation in predefined conditions the margin against pressure side cavitation is established in the cavitation experiment. In the cavitation tunnel the water velocity is varied and at the point of inception the thrust coefficient is measured.

In the Depressurised Wave Basin the rotation rate is varied during a few measuring runs at constant speed of the ship model. The thrust coefficient K_T is established from the load variation test in the propulsion experiment. From the relationship between K_T and σ_n for the inception of pressure side cavitation the margin expressed in K_T of the predicted full-scale operation point is then found.

Procedure of propeller cavitation inception tests in the Depressurised Wave Basin

A complete propeller cavitation inception diagram is established in the Depressurised Wave Basin by means of visual detection.

During the tests electrolysis of the tank water ahead of the propeller(s) is applied in order to supply the flow through the propeller disc(s) with a sufficiently large number of cavitation nuclei. Moreover, carborundum grains of 60 μm are applied to the leading edges of the blades of the observed propeller model in order to reduce the scale effect on cavitation inception to a minimum by inducing turbulent flow over the blades and by generating additional nuclei close to the blade surface.

In addition, a strip of carborundum grains is applied at the forward end of the propeller hub in order to generate locally additional nuclei to stimulate inception of blade-root cavitation and hub-vortex cavitation.

The visual determination of cavitation inception is done by means of a video camera. First, the camera is installed forward of the propeller inside or outside the ship model. With the camera in this position the back of the propeller can be observed. Secondly, the camera is installed behind the ship model, where it is used to observe the face of the propeller. The propeller is illuminated by a stroboscopic light source, which is located above the propeller model behind a perspex window or outside the ship model.

For each type of cavitation the difference between the distinct propeller blades as regards their cavitation behaviour is investigated first. The blade, which shows the "average" cavitation behaviour for a certain type of cavitation, is selected for the eventual cavitation inception test. Prior to the actual test the radius and angular blade position are determined at which inception occurs for each distinct type of cavitation.

The inception conditions of a particular type of cavitation are then determined by a variation of the rotation rate of the propeller model at a constant speed of the ship model. Next, the rotation rate at which the cavitation disappears is established similarly during the same run. The average of these two rotation rates is called the inception rotation rate. This procedure is repeated for a number of speeds of the ship model and for each particular type of cavitation.

During the cavitation inception tests the air pressure in the towing tank is lowered to the Froude scaled level:

$$p_{om} = p_{vm} + 96.64 / \lambda \text{ [kPa]}$$

Model speeds are constant during the measuring run but the propeller rotation rates are slowly varied with an almost constant rotation rate at the inception point. From the measured inception conditions (p_o , V_m , n_m) the cavitation number σ_n and the thrust coefficient K_T are determined using the results of the load-variation test in the propulsion experiment and taking into account the influence of the leading edge roughness on the thrust coefficient as determined experimentally in a few supplementary measuring runs in the inception test.

In the inception diagram the model inception points are shown in combination with the predicted full-scale K_T - σ_n relationship (operation curve). If there would be no scale effects on cavitation inception the model inception curves are valid for the full scale as well. When effective leading edge roughness and nuclei seeding is applied in the model test, scale effects are supposed to be absent as far as sheet and bubbly types of cavitation are concerned. It is generally accepted that important viscous scale effects are present on the inception of free vortex cavitation.

According to McCormick: "On cavitation produced by a vortex trailing from a lifting surface", Journal of Basic Engineering, Trans. ASME, September 1962, there is a direct relation between the cavitation inception number and the Reynolds number. For equal angles of attack (equal loading) the cavitation inception number σ_{ni} scales with:

$$\frac{\sigma_{nis}}{\sigma_{nim}} = \left(\frac{R_{ns}}{R_{nm}} \right)^{0.35}$$

where R_n is the Reynolds number of the propeller, which is proportional to nD^2/ν , where n is rotation rate, ν is kinematic viscosity and D is diameter.

Hence,

$$\frac{\sigma_{nis}}{\sigma_{nim}} = \left(\frac{n_{is} D_s^2 \nu_m}{n_{im} D_m^2 \nu_s} \right)^{0.35}$$

Writing for the inception rotation rate:

$$n_i = \sqrt{\frac{p_o - p_v + \rho gh}{0.5 \rho \sigma_{ni} D^2}}$$

Because the tank pressure scales by Froude's law of similitude:

$$(p_o - p_v + \rho gh)_m = (p_o - p_v + \rho gh)_s \frac{\rho_m}{\rho_s} \frac{1}{\lambda}$$

we find by substitution:

$$\frac{\sigma_{nis}}{\sigma_{nim}} = \left(\frac{n_{nim}}{n_{nis}} \right)^{0.175} \left(\frac{v_m}{v_s} \right)^{0.35} \lambda^{0.525}$$

Hence,

$$\frac{\sigma_{nis}}{\sigma_{nim}} = \left(\frac{v_m}{v_s} \right)^{0.298} \lambda^{0.447}$$

Tip-vortex cavitation inception is assumed to follow McCormick's scaling rule.

Regarding hub-vortex cavitation it is noted that there are some indications that the scaling rule of McCormick is not the proper rule to be applied. Data from ships on which viewing trials were carried out indicate that the scale effect on hub-vortex cavitation inception is probably smaller than according to McCormick's rule.

Since no proper alternative rule has been formulated yet, the method of McCormick is still applied to the cavitation numbers of hub-vortex cavitation inception determined in the present tests.

Procedure for hull pressure fluctuation measurements

Conditions for the pressure fluctuation measurements are determined using the results of the propulsion test and applying Froude scaling. Similarity of the thrust coefficient K_T and the cavitation number σ_n between model scale and full scale are adopted. This determines the required ambient pressure in the Depressurized Wave Basin. In the following, the subscript s indicates the full-scale value and the subscript m indicates the model-scale value. From Froude similarity:

$$n_m = n_s \sqrt{\lambda}$$

resulting in:

$$p_{0m} - p_{vm} = (\rho_m / \rho_s)(p_{0s} - p_{vs}) / \lambda = 96640 / \lambda$$

where n is the rotation rate in Hz, p_0 and p_v are the ambient and vapour pressures respectively in Pa, ρ the density of water in kg/m^3 and λ the geometric scale ratio of the ship model.

Model speed is also determined based on Froude scaling, although a correction is needed for the scale effect on the ship's wake. The propeller is, on average, too heavily loaded on model scale. In order to correct for this, the model speed is increased slightly. Some ship types (mostly slender vessels such as container ships) exhibit a stronger scale effect on the wake peak in the upper part of the propeller disk. In this area the velocity deficit on model scale is larger than on full scale. Since this is typically also the area where most of the cavitation occurs, the model speed is further increased in order to have the correct propeller loading and thus cavitation pattern in this part of the propeller disk.

To reduce scale effects on cavitation inception, a strip of carborundum grains is applied to the leading edges of the propeller blades on both suction and pressure side. This roughness helps to increase the extent of turbulent flow over the propeller blades such that the flow is more similar to full scale. Electrolysis is used to generate small bubbles to ensure that there are sufficient nuclei for proper cavitation inception.

The hull pressure fluctuations are measured by, typically, 21 charge mode pressure transducers. They are mounted flush in the hull of the ship model above the propeller as shown in the figure below.



The signals from the pressure transducers are sampled and digitised. In order to remove the influence of small changes in the propeller rotation rate, the measurements are resampled to 360 samples per revolution, based on the measured blade angular position. These resampled signals are equidistant with respect to blade position, but not necessarily with respect to time. In order to ensure that the blade passage frequency (BPF) is well captured, only complete revolutions are considered.

This means that only the signal between the first and the last time that blade number 1 is in the top position (blade angular position 0°) is selected. The measured signals are then transformed to the frequency domain as a harmonic series according to:

$$f(\theta) = A_0 + \sum_{i=1}^{\infty} A_i \sin(iZ\theta + \alpha_i),$$

where:

$f(\theta)$	=	function of the mean periodic pressure signal
A_0	=	static value of the function
A_i	=	amplitude of i-th harmonic component
α_i	=	phase angle of i-th harmonic component
θ	=	angular propeller position with $\theta = 0^\circ$ corresponding with blade number 1 in top position
Z	=	number of blades

In this expression the frequency for $i = 1$ is equal to the blade passage frequency (BPF), which is the fundamental frequency of the pressure fluctuations. A_i and α_i are calculated for $i = 1, 2, 3$ and 4. The amplitudes are given as zero-to-peak values.

Correction for vibrations of the ship model

Additionally, acceleration transducers are fitted in the aft body of the model to measure the vibrations of the ship model. The ship model vibrates due to the pressure fluctuations from the propeller as well as vibrations from the drivetrain. Because of these vibrations, the hull of the ship also radiates pressure fluctuations, which are also measured by the pressure sensors. Since this influence is not representative of the full-scale ship, it should be corrected for. This is done by processing the measured vibration signals and using them to compute the part of the radiated pressure fluctuations due to hull vibration. These are then subtracted from the measured pressures (taking both the amplitude and the phase into account) to obtain the pressure fluctuations for an infinitely rigid ship.

Converting the results to full scale

The corrected model-scale pressure amplitudes (in Pa) are converted to full-scale values according to:

$$(A_i)_s = (A_i)_m \frac{\rho_s \lambda}{\rho_m},$$

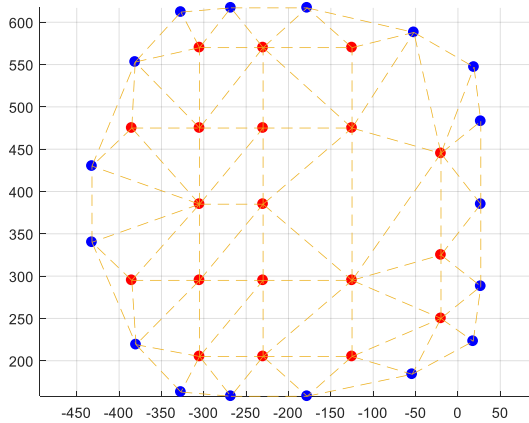
where the subscript s denotes full scale, m denotes model scale.

Only the amplitudes of the pressure fluctuations are scaled. The full-scale phase angles are taken equal to the model values, thus ignoring the small effect of the finite propagation velocity of the radiated pressure waves.

The results of the hull pressure fluctuation measurements are also presented graphically in a narrowband spectrum. These graphs are currently only presented on model scale (both the frequency and the amplitude values). They can therefore not be directly compared to the values in the table or to graphs of other vessels. However, the spectral plots can be used to determine whether broadband excitation occurs, which would indicate a risk of resonance.

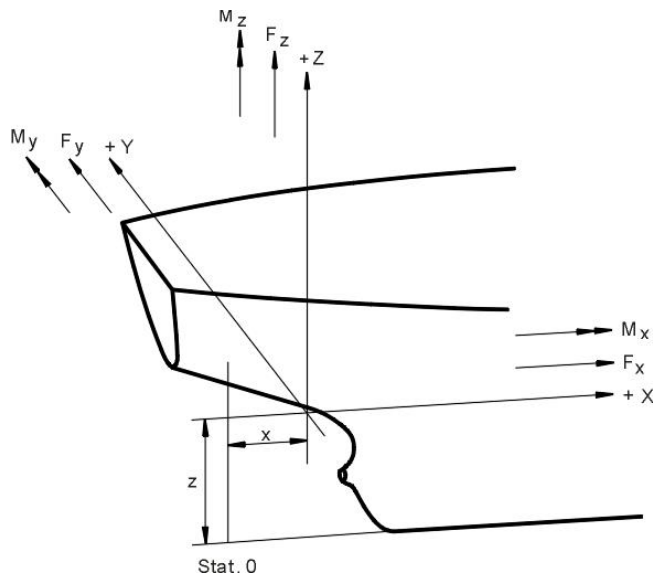
Computation of excitation forces

In order to judge the risk of onboard vibrations, the pressure distribution over the hull is integrated to obtain excitation forces. This integration is done by defining triangles between the pressure sensors as illustrated in the figure below, which shows a top view of typical pressure sensor locations (orange dots) in a ship model. The blue dots indicate the so-called 'zero points' at which the pressure fluctuations are assumed to have decayed to zero, and which are included for interpolation purposes.



Note that this figure is a top view; the positions of the sensors and zero points are defined in three dimensions, thus taking the shape of the ship's hull into account. The pressure amplitude of the three corner points is interpolated to the centroid of each triangle while taking the phase information into account. This pressure value at the centroid is then multiplied by the surface area of the triangle to obtain the force per triangle. This is then decomposed into the components x , y and z using the normal of the triangle. Thereafter the contributions of all triangles are summed (taking the phase into account) to obtain the total excitation forces. This is done for each of the four harmonics of the BPF. The amplitude and phase of the corresponding moments with respect to a given point (usually the propeller centre) are also computed.

The resulting forces and moments are related to the co-ordinate system shown below.



in which:

x	= longitudinal distance from station 0
z	= vertical distance from baseline
F _x	= longitudinal force, positive in forward direction
F _y	= transverse force, positive in port direction
F _z	= vertical force, positive in upward direction
M _x	= longitudinal moment, vector positive in forward direction
M _y	= transverse moment, vector positive in port direction
M _z	= vertical moment, vector positive in upward direction

The input for the integration of the forces (i.e. the pressure amplitudes and phases and the location of the pressure sensors) is on full scale. This means that the computed forces are also given as full-scale values without the need for further scaling.

If the measurements are carried out on a ship fitted with two propellers, both propellers will be operating during the measurement. Therefore, the pressure fluctuations take the contribution of both propellers into account. The integration, however, is only carried out for the area above one single propeller. For a ship equipped with two propellers, the forces will be given for a combination of two propellers rotating in phase with each other. The force amplitudes can then be added directly without an influence of the phase but mirrored around the ship centre line. As a result, the vertical excitation force F_z and the longitudinal force F_x double while the transverse force F_y is zero. This is a worst case scenario; if the actual propellers do not rotate in phase, the combined F_z and F_x will be lower.

Assessment of excitation forces

In order to give a first estimate of the risk of vibrations, the results are compared to the 'van der Kooij criterion'. An equivalent vertical excitation force (F_{Zeq}) is determined based on the four harmonics of F_z (in kN):

$$F_{Zeq} = \sqrt{\sum_{i=1}^4 i \cdot F_{z,i}^2}$$

The number of the harmonic, i, is also used as a weighting factor, which accounts for the fact that vibrations at higher harmonics contribute more strongly in the perception of vibration nuisance. This equivalent force should be smaller than the van der Kooij criterion:

$$F_{Zeq} < c \nabla (0.75 + 75 / L)$$

where:

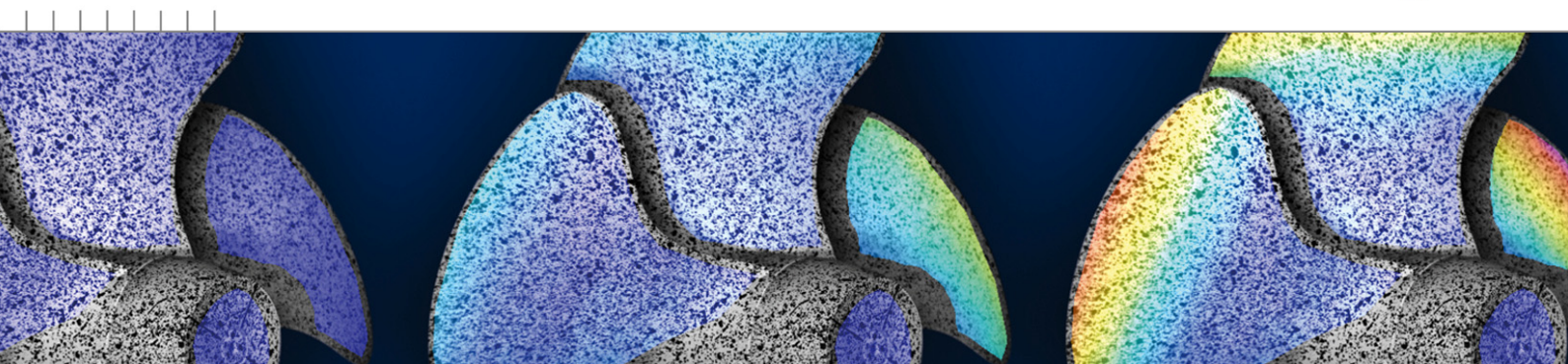
∇	= displacement of the vessel in m ³
L	= length between perpendiculars in m
c	= constant, dependent on ship type

Typical values for the constant c are:

c	= 7 for VLCCs and container ships with the bridge forward
c	= 5 for product tankers and container ships with the bridge aft
c	= 3 for ferries, cruise ships and yachts

Should the equivalent force F_{Zeq} be above the criterion a strong risk of vibration-related nuisance aboard the vessel is expected. This is, however, also dependent on the structural response of the vessel. If resonance occurs, vibration nuisance may be a problem even when the force is below the criterion.

DOCUMENTATION SHEETS

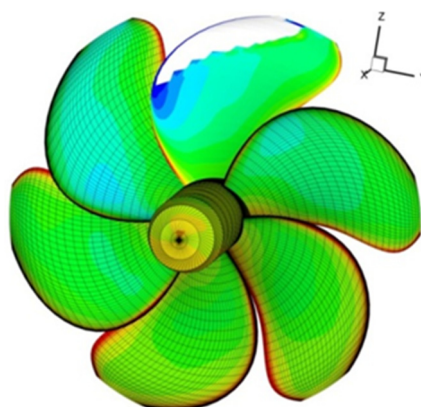


PROCAL

Calculating propeller performance in potential flow

MARIN internal use only

The computer program PROCAL calculates the unsteady inviscid flow including sheet cavitation around a propeller geometry using a boundary element method. It is used for the analysis of the propeller performance operating in open water or in a wake field of a ship hull. For the analysis of the hull pressure fluctuations of the non-cavitating and cavitating propeller, a coupling is made with the boundary element method EXCALIBUR, which solves the acoustic wave equation and takes the diffraction of the ship hull and the free surface into account. PROCAL has been developed in the period 2003-2008 within the Cooperative Research Ships organisation (CRS). Extensive use has been made of MARIN's experience in the implementation and application of boundary element methods for propeller analysis.



Applications

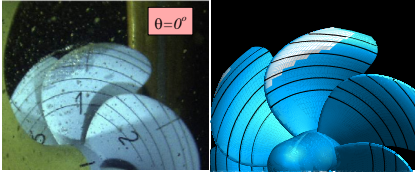
The PROCAL code has been applied to a wide variety of propeller geometries to analyse:

- Open water performance (shaft thrust and torque)
- Behind-hull performance (blade and shaft forces and moments)
- Sheet cavitation inception, extent and volume
- Field velocities and propeller-induced pressure fluctuations

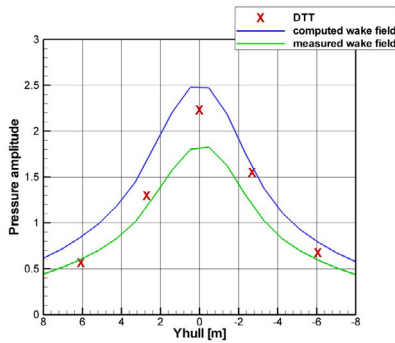
The code is capable of analysing multi-component propulsors and its application for podded propellers, propeller-rudder combinations and ducted propellers is currently being investigated. The code has also been applied for the analysis of wings at varying angles of attack.

Accuracy

The code has been validated for a large number of different propeller geometries and it gives, in general, good results. The accuracy depends somewhat on the propeller geometry and the operating point, but PROCAL results are very consistent making it a reliable propeller analysis tool for a wide range of propeller geometries. The sheet cavitation model shows very realistic patterns and good correlation with model scale and full-scale observations while predicting only a small phase lead in the growth of the cavity compared to experiments. An acceptable prediction of the pressure pulses on the hull for the first blade passage frequency is obtained.



Comparison between cavitation extents observed during experiments in the Depressurised Towing Tank (DTT) and computed by PROCAL.



Variation of pressure fluctuations on the hull in the propeller plane. PROCAL results are shown using a measured wake field and a PARNASSOS computed ship wake and compared with model scale measurements in the DTT.

References

- Vaz, G. and Bosschers, J.; “Modelling Three-dimensional Sheet Cavitation on Marine Propellers Using a Boundary Element Method”, Sixth international symposium on Cavitation, CAV2006, Wageningen, 2006.
- Bosschers, J., Vaz, G., Starke, A.R., Wijngaarden, E. van; “Computational Analysis of Propeller Sheet Cavitation and Propeller-ship interaction”, RINA conference MARINE CFD2008, Southampton, 2008.

For more information contact MARIN:
 SOSC
 T +31 317 49 32 37
 E sosc@marin.nl

Input

The graphical user interface PROWISE, developed by DRDC Atlantic within the CRS, helps to generate and visualise the panel distribution for the propeller and the hub, to generate the other input files and to analyse the results. The propeller geometry needs to be described by a propeller description file using tabular offset data for the foil sections and radial distribution data of pitch, chord, skew and rake. A hub geometry of arbitrary shape can be generated in PROWISE. The propeller inflow velocity field, representing the effective wake field of the hull, is specified in a ship wake file. Finally, the coordinates where field point velocities and pressures are to be calculated need to be selected. The wake field of the ship hull can be obtained from model tests or from computations using MARIN's RANS solvers PARNASSOS and REFRESCO. These computations can be made for model scale and full-scale conditions. Several methods are available for obtaining effective wake fields from nominal or total wake fields.

Output

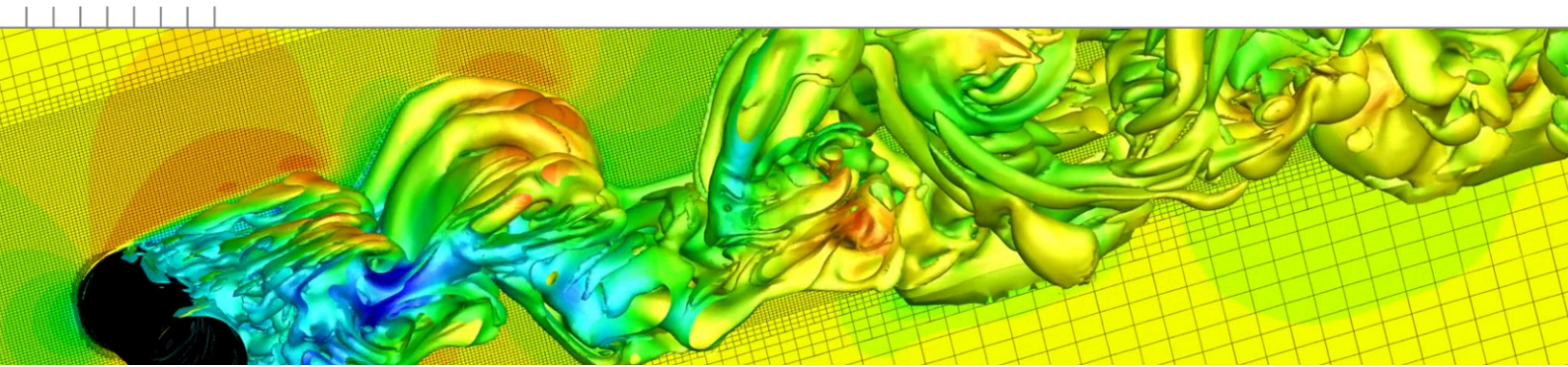
A large variety of output files are generated, showing pressure, cavity thickness and velocity distributions on the propeller and hub geometry, pressure and velocities in field points and hull points, radial distribution of loading, cavity length and volume on the propeller blade, and the integrated forces and moments for each blade and as transmitted to the propeller shaft. All results can easily be visualised using PROWISE.

Computational approach

PROCAL uses the Morino formulation to solve for the velocity potential. The geometry of the propeller wake is modelled by either an empirical formulation or by an iterative approach computing the wake pitch and tip vortex roll-up. An iterative procedure is applied to satisfy the pressure Kutta condition at the propeller blade trailing edge. The cavitation model iteratively solves the non-linear boundary conditions assuming that the cavity thickness remains small. The analysis of the propeller in a wake field is performed in the time domain for a number of shaft revolutions until the change in propeller wake strength and blade loading between subsequent revolutions is sufficiently small.

Restrictions

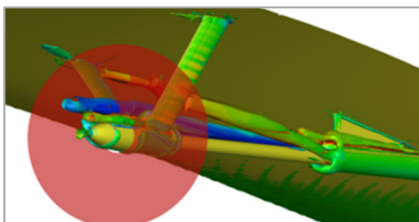
As the code is based on inviscid flow theory, the influence of boundary layers, flow separation and vortex formation is not included. These effects may become important for the analysis of high skew propellers and propellers operating in off-design conditions. The cavitation model is restricted to sheet cavitation and therefore does not include vortex cavitation and cloud cavitation that can be generated from the aft end of the sheet.



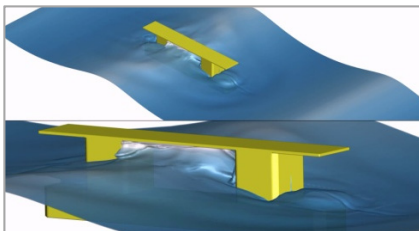
ReFRESKO

A community-based open-usage and open-source CFD code for the Maritime World

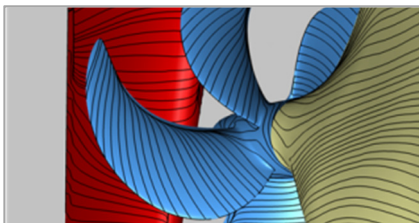
The CFD code ReFRESKO has been under development since 2005. It is based on state-of-the-art numerical algorithms and software features, and on the long-standing experience of MARIN in CFD. ReFRESKO stands for **Reliable&Fast Rans Equations (code for) Ships (and) Constructions Offshore**. In several respects it resembles a general-purpose CFD commercial code, although it has been verified, validated and optimised specifically for numerous maritime industry applications.



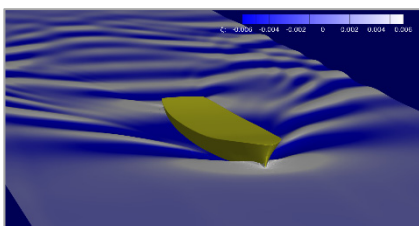
Fully-appended ships



Impacts



Cavitation



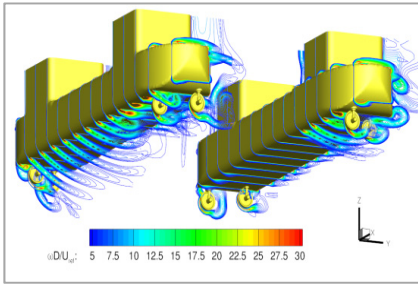
Free surface & waves

Computational method

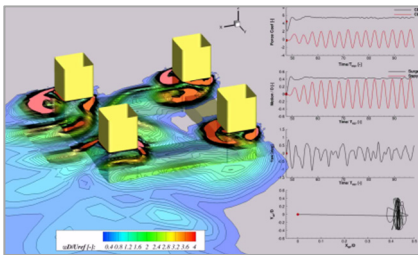
ReFRESKO is a viscous-flow CFD code that solves multiphase (unsteady) flows using the incompressible Navier-Stokes equations, complemented with turbulence and cavitation models [1]. The equations are discretised using a finite-volume approach and in strong-conservation form. A pressure-correction equation based on the SIMPLE algorithm is used to ensure mass conservation [2]. At each implicit time step, the non-linear system for velocity and pressure is linearised using Picard's method. A segregated or coupled approach may be used. The code is parallelised using MPI and runs on Linux workstations and HPC clusters.

CFD features

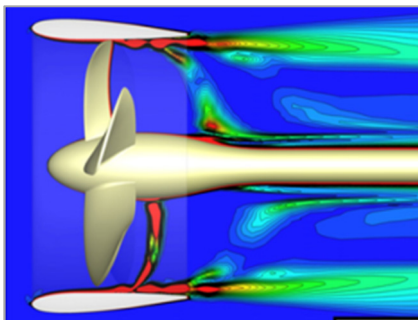
Due to specific numerical schemes, ReFRESKO can deal robustly with low up to high (full-scale) Reynolds numbers, permitting the accurate estimation of scale effects. The face-based implementation permits the handling of grids from several different grid-generation packages. State-of-the-art CFD features such as moving, sliding and deforming grids, as well automatic grid adaptation (refinement and/or coarsening) are also available. Both 6DOF rigid-body, and flexible-body (fluid-structure interaction) simulations, can be performed. For turbulence modelling, both traditional RANS and Scale-Resolving Simulations (SRS) models such as SAS/DES/IDDES/XLES, PANS and LES can be used. Noise predictions can be made using an acoustic analogy module. Couplings with propeller models (RANS-BEM coupling), fast-time simulation tools (XMF) and wave generation potential flow codes (OceanWave3D, SWASH) are implemented.



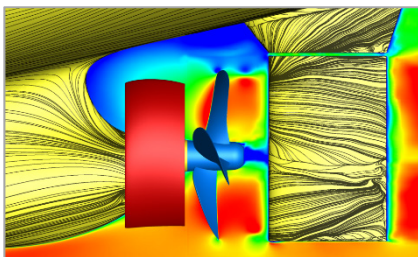
Current loads



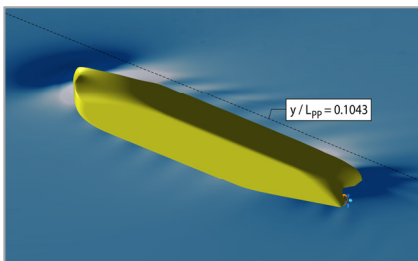
VIV & VIM



Propellers



Energy Saving Devices (ESDs)



Propulsion

For more information contact MARIN:
the ReFRESKO YouTube channel or
contact the MARIN CFD group

T + 31 317 49 39 11

E refresco@marin.nl

W www.refresco.org

Development and applications

ReFRESKO is currently being developed, verified and validated at MARIN in collaboration with several other worldwide non-profit organisations (universities and research institutes). Modern verification & validation (V&V) techniques and tools are used in the development and application of ReFRESKO. ReFRESKO has been applied, verified and validated for the following range of applications:

- Resistance and propulsion of fully-appended ship hull forms;
- Submarines, including manoeuvres and geometry optimisation;
- Propeller and complex propulsor flows, including cavitation;
- Energy-saving devices;
- Marine current and floating wind turbines;
- Current and wind loads on offshore structures;
- VIV and VIM of offshore structures and renewable energy devices;
- Thruster-hull and thruster-thruster interaction problems;
- Free-surface flows, wave loads and wave impacts;
- Seakeeping problems such as loads and motions for free-floating structures.

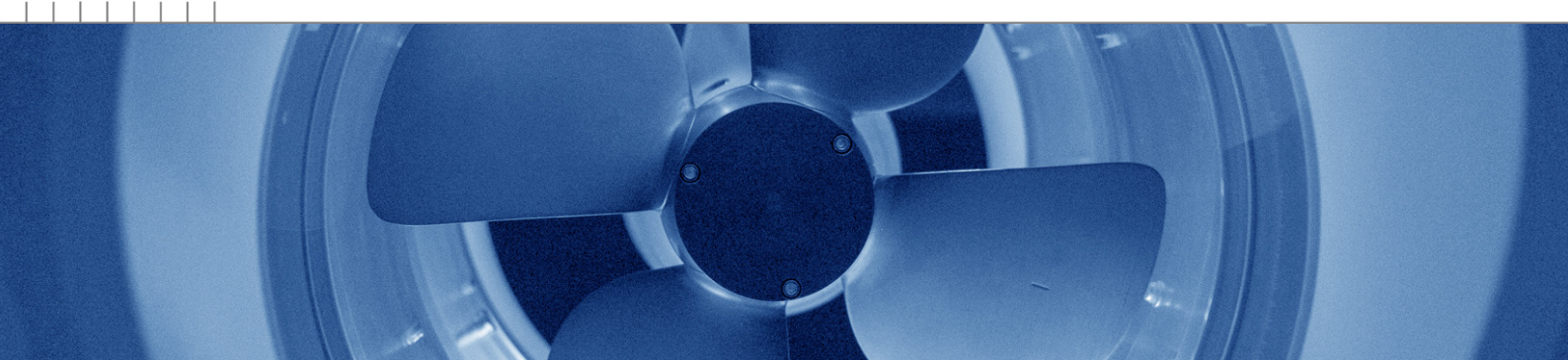
ReFRESKO-Operation and ReFRESKO-ReSearch

Two types of partnership are available to companies and institutes wishing to use ReFRESKO. The ReFRESKO-ReSearch partnership focuses on sharing the code for collaborative research, without any fees but common open development, testing, verification and validation. Tight quality control is enforced by MARIN and there is only one ReFRESKO source repository for all partners. ReFRESKO-Operation extends the ReFRESKO-ReSearch partnership by allowing commercial application of ReFRESKO (a membership fee is required). In addition, the user gains access to ReFRESKO support services, as well as MARIN's CFD best practice guidelines.

Bibliography

- [1] Vaz, G., Jaouen, F. and Hoekstra, M.; "Free-Surface Viscous Flow Computations. Validation of URANS code FreSCO", OMAE2009, Hawaii, Honolulu, USA. 2009.
- [2] Klaij, C. M., and Vuik, C.; "Simple-type Preconditioners for Cell-centered, Colocated Finite Volume Discretization of Incompressible Reynolds-averaged Navier-stokes Equations", International Journal for Numerical Methods in Fluids, 71(7), pp. 830–849. 2013.

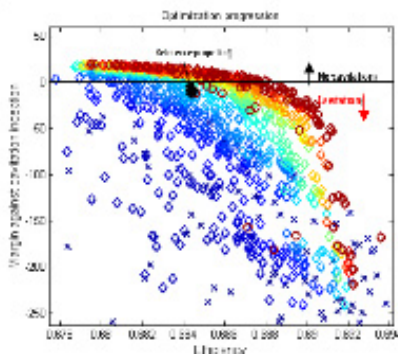




Propeller Design Support & Evaluation

MARIN offers its propulsor services to ship yards, operators, propeller manufacturers and suppliers of marine propulsion components. These services include an independent prediction of the performance of propellers and design support. Propeller design involves finding the right balance between conflicting objectives, for instance between propulsive efficiency and cavitation related nuisances like propeller induced pressure pulses on the ship hull and underwater noise. The hydrodynamic performance is evaluated by computational methods, often followed by model experiments or full scale observations.

MARIN focuses on a wide-range of propeller designs, e.g. high-end “low-noise” propellers for yachts, naval, research and cruise ships with delayed cavitation inception, propellers with low vibration-excitation and ducted propellers for special purpose vessels such as dredgers, tugs and fishing vessels. Also for merchant ships, MARIN can for instance provide insight into whether the best possible compromise between the propulsive efficiency and cavitation related pressure pulses is achieved or further improvements can be made.



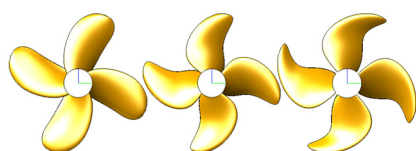
Example of optimization case with final Pareto front in red. Both the margin against cavitation and efficiency should be maximized.

Throughout the years, MARIN developed substantial knowledge of propulsors by means of calculations, model tests and full scale tests. This experience is virtually indispensable for a good propeller design.

Evaluation

An independent second opinion on a propeller design may for instance be required:

- to provide good understanding of the best possible efficiency within given boundaries;
- before proceeding to more expensive model test experiments or propeller manufacturing;
- after the vessel’s commissioning as trouble shooting, when there are, for example, problems including cavitation erosion or onboard vibrations and noise.

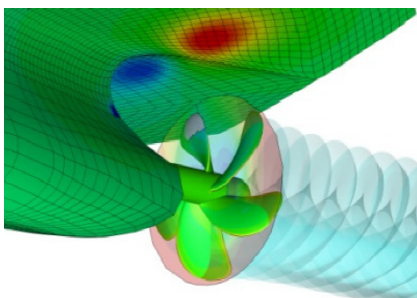
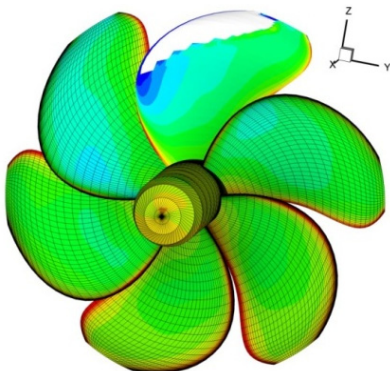
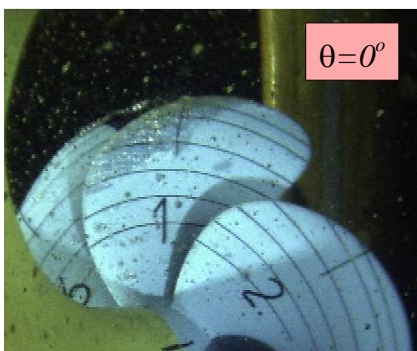


Example of propeller candidates within an optimization study

A propeller evaluation will always be tuned to the specific project at hand. MARIN will give expert advice on the performance and draw recommendations to solve possible issues.

Design

By using the latest design techniques and experience within the whole chain of design, model tests and full scale observations, MARIN is able to make a best suited independent propeller design based on the specifications provided by the customer. The MARIN propeller blade design often acts as a reference or counter design for third parties.



For more information contact MARIN:
department Ships
T +31 317 49 34 72
E ships@marin.nl

Optimization

Multi-objective optimisation techniques allow propeller designers to perform design studies. An optimization gives insight in the different trade-offs between conflicting objectives and indicates the influence of design constraints on the attainable objectives. Possible objectives or constraints are for instance efficiency, avoidance of pressure side cavitation, cavitation volume, pressure pulses, tip vortex nuisance, material stress or weight. The propeller is fully parameterized to allow large design freedom. The optimization either serves as a preliminary investigation of feasible objectives in conceptual design studies or as a choice support tool for the best possible compromise which serves as starting point for further detailed design.

Model experiments

Verification of propulsive performance and cavitation behaviour by model experiments is often desired by ship owners to check whether the design fulfils the expectations and is likely to reach its targets at full scale. Cavitation observations, pressure pulse measurements and noise recordings are performed daily in MARIN's Depressurised Wave Basin (DWB).

Full scale observations

Full scale cavitation observations are indispensable as feedback for propeller design and interpretation and correlation of model tests. MARIN offers a full scale consulting and monitoring service, and has gained considerable experience in a broad field of ship types over the years. Each time, MARIN carefully analyses the propulsor performance which is used to further improve propeller design methodology and model experiments.

Design conditions

For each propeller design study the design conditions such as shaft power, thrust, RPM and ship speed are necessary. Either model tests with stock propellers, CFD studies or empirical methods could be used to determine the design conditions, all of which are offered by MARIN. Furthermore, the wake field in which the propeller operates should be known, preferably the effective wake field at full scale.

Tools

Throughout the years, several systematic series such as the Wageningen B, C & D series were generated and computational tools were developed. Detailed propeller design and prediction of pressure distributions and cavitation patterns are possible with the Boundary Element Method (BEM) PROCAL. Pressure pulses on the hull due to cavitation will be analysed with the BEM code EXCALIBUR. Optimization can be performed using a genetic algorithm which is coupled to a geometry generator and PROCAL. Effective wake fields could be computed with MARIN's RANS codes PARNASSOS or REFRESCO on either model or full scale by coupling them to PROCAL. Nowadays, state of the art full RANS propeller computations are becoming more and more the standard.

MARIN
P.O. Box 28

6700 AA Wageningen
The Netherlands

T +31 317 49 39 11
E info@marin.nl

I www.marin.nl
   